The collision risk of migrating birds at wind farms

Final report VolZug project

Version 3.0

Dr. Jannis Liedtke
Dr. Matthieu Bruneaux
Dr. Antje Girndt
Dr. Jorg Welcker

Husum, November 2025

Prepared for

Baltic Eagle GmbH, DanTysk Sandbank Offshore Wind GmbH & Co. KO, EnBW Energie Baden-Württemberg AG, Ørsted Wind Power A/S, OWP Gennaker GmbH, RWE Offshore Wind GmbH, Vattenfall Europe Windkraft GmbH, Windanker GmbH, WindMW GmbH

BioConsult SH GmbH & Co. KG
Schobüller Str. 36
25813 Husum

Tel. 04841 77937-10
Fax 04841 77937-19

info@bioconsult-sh.de
www.bioconsult-sh.de

Project name	**VolZug**	
Project number	**22_1402**	
Contractor:	BioConsult SH GmbH & Co. KG Schobüller Straße 36 25813 Husum www.bioconsult-sh.de	
Project leader	Dr. Jorg Welcker	+49 (0)4841 77937-39 j.welcker@bioconsult-sh.de
Substitute of the project leader	Dr. Jannis Liedtke	+49 (0)4841 77937-92 j.liedtke@bioconsult-sh.de
Report preparation	Dr. Jannis Liedtke, Dr. Antje Girndt, Dr. Jorg Welcker	
QA / Approval	Date 12/11/2025 Dr. Jorg Welcker	Version: 3.0 j.welcker@bioconsult-sh.de
Cover picture	AVES video screenshots	
Suggested citation	J. Liedtke, M. Bruneaux, A. Girndt, J. Welcker (2025): The collision risk of migrating birds at wind farms. (ed. BioConsult SH). Husum (DEU).	
Client	**Baltic Eagle GmbH,** **DanTysk Sandbank Offshore Wind GmbH & Co. KO,** **EnBW Energie Baden-Württemberg AG,** **Ørsted Wind Power A/S,** **OWP Gennaker GmbH,** **RWE Offshore Wind GmbH,** **Vattenfall Europe Windkraft GmbH,** **Windanker GmbH,** **WindMW GmbH** Supported by: **Federal Association of Offshore Wind Energy eV (BWO)**	

CONTENTS

List of figures

List of tables

1 SUMMARY

A substantial part of the nocturnal bird migration in Europe passes through the North and the Baltic Sea. These migrating birds are increasingly confronted with development of offshore wind farms, which pose a risk of collision with these anthropogenic structures. It is commonly assumed that the number of collisions increases with the number of birds flying at rotor height. This assumption would mean that collision fatalities peak during periods of peak migration traffic rates (MTR). However, due to lack of suitable methods at sea, empirical data are lacking.

The main aim of the present study was to quantify the collision risk of migrating birds and to test the hypothesis of a strong positive relationship between collision rate and MTR. Alternatively, a bird's collision risk may depend on other factors, foremost weather conditions. For example, adverse weather may reduce the ability of a bird to perceive the rotor in time to avoid it.

With a combination of innovative and established methods, we recorded the MTR of birds at a coastal onshore wind farm using a specialised bird radar system (BirdScan MR1 by Swiss Birdradar Solution AG) and recorded the number of rotor transits, defined as birds crossing the rotor plane, using AI-supported camera systems (AVES Offshore HPC by ProTecBird GmbH) during more than three complete migration periods. This enabled us to analyse the relationship between the number of collisions and MTR. Using these data, we determined the avoidance rates of nocturnal and diurnal migrants - a parameter of paramount importance in collision risk models (CRM) that captures the proportion of birds avoiding the rotors when approaching the wind farm. Applying stochastic Band CRMs, along the exact MTR at rotor height and empirically estimated avoidance rates, we then calculated the expected number of collisions for the whole study period (including both day and night activity).

Finally, to validate the theoretically calculated number of collision fatalities, we employed an independent and well-established empirical method. Using thorough Post Construction Fatality Monitoring (PCFM), we searched for bird carcasses at the turbines at a 5-day interval and estimated the total number of fatalities while correcting for search area, searcher efficiency and carcass persistence.

In general, the number of rotor transits was very low when the turbines were operational. During night, on average one transit was recorded every 132 hours when the rotation speed was ≥2 rounds per minute. However, there was a remarkable difference in rotor transit rates depending on the operational status of the rotors. When turbines were inactive, transit rates were about 20 times higher than when rotors were operating, suggesting a reduced avoidance response at idle turbines. Furthermore, our results did not show a strong positive relationship between rotor transit rates and MTR. In other words, even during nights of high migration intensities, the probability of collisions to occur did not increase. However, contrary to our expectation, weather parameters also explained only a small part of the probability of rotor transits and therefore collision risk. These results indicate that collision risk may depend mostly on other factors, which remain to be investigated.

Avoidance rates, calculated by comparing the number of observed rotor transits with the expected number based on MTR at rotor height, were found to be high: 0.9987 during the night and 0.9986 during the day when the turbines were operating. This means, an estimated 99.87 and 99.86

percent of birds, approaching the wind farm at rotor height while turbines were operating, avoided the rotor plane during night and day, respectively. Also, the overall estimated collision risk for birds flying through the wind farm area at 25–1025 m altitude was very low: for nocturnal migrants only 0.0016 percent of flights were expected to result in a collision, for daytime movements the risk was similarly low at 0.0020 percent.

Comparison of the theoretically calculated number of collisions with the empirically determined fatalities using PCFM, showed a high overall agreement for the period of this study (Band CRM: 76.6 fatalities [95%CI: 57.3-97.6] and PCFM: 99.7 [95%CI: 55.0-168.0]). In addition, collision victims found during the main bird migration seasons did not contain species known to constitute the bulk of nocturnal migration at the study site. This i) confirms the overall low collision risk for migrating birds, ii) validates estimated rotor transits and avoidance rates and iii) highlights the usefulness of applying CRMs to estimate collision risk when fed with realistic avoidance rates and appropriate site-specific turbine and bird flux rate data.

These results have important implications for potential measures to mitigate the risk of collision for migrating birds, such as turbine curtailment during periods of high migration intensity. Such curtailment measures imply a strong positive relationship between the probability of bird collisions and migration intensity, which could not be confirmed by our findings. Therefore, turbine curtailment during periods of high migration intensity is likely to be ineffective.

2 INTRODUCTION

Billions of birds migrate long distances each year between breeding and wintering grounds (NEWTON 2023). In Europe, a substantial proportion of these migratory birds pass through regions with an increasing expansion of renewable energy—particularly offshore wind power. A major part of the European offshore wind farm (OWF) developments is located in the North Sea[1]. While each spring and autumn, an estimated 1.0 – 1.3 million seabirds migrate through the Southern North Sea (DE LUCAS ET AL. 2007; BRABANT ET AL. 2015), non-seabird migration is substantially larger, with seasonal estimates ranging from 85 million to several hundred million individuals (BOURNE 1980; ALERSTAM 1990; HÜPPOP ET AL. 2006; KRIJGSVELD ET AL. 2011; BSH 2025).

While the development of offshore wind energy plays a key role in reducing greenhouse gas emissions, it may also pose risks to migratory bird species. One of the central areas of conflict is the risk of collision with the rotor blades of offshore wind turbines (OWT). The majority of migratory birds, particularly passerines, migrate at night (HÜPPOP ET AL. 2009; NEWTON 2023) and nocturnally migrating birds are often considered particularly vulnerable to collision with wind turbines. However, knowledge on the collision risk of birds at night and the question whether and how collision risks differ between daytime and nocturnal migration is still scarce (KRIJGSVELD ET AL. 2009; WELCKER ET AL. 2017; WELCKER & VILELA 2019, 2020).

The collision risk of migratory birds is also regarded in the area development planning in the German Exclusive Economic Zone (EEZ) and current approval procedures for offshore wind farms[2,3]. One proposed mitigation measure is the temporary shutdown of OWTs during periods of intense bird migration. This discussion is characterised by the uncertainty regarding the number of birds colliding with OWT and their avoidance behaviour (AVITEC RESEARCH GBR 2014; WELCKER & VILELA 2019; CROLL ET AL. 2022). Onshore, well-established methods exist for empirically quantifying collision rates, such as systematic searches around the infrastructures, for example post-construction fatality monitoring (PCFM). At offshore wind farms, PCFM is impossible, as carcasses are lost from the collision area due to sinking, scavenging and dispersal by wind or waves. Moreover, access limitations and safety risks impede the inspection of foundation structure platforms, which could potentially retain a portion of bird carcasses. On the other hand, it remains unclear whether available information on collisions at other offshore infrastructures such as platforms is representative for OWT (AUMÜLLER ET AL. 2011; SCHULZ ET AL. 2013; HÜPPOP ET AL. 2016). Hence, empirical data on the actual risk of birds colliding with OWT remains limited (but for seabirds see for example SKOV et al. 2018).

With the idea to minimise collision risk, the Federal Agency for Nature Conservation (BfN) has called for temporary nighttime shutdowns of OWT if nocturnal bird migration intensity in the 0–200 m

[1] https://map.4coffshore.com/offshorewind, last accessed 26.05.2025

[2] https://www.bmwsb.bund.de/SharedDocs/gesetzgebungsverfahren/Webs/BMWSB/DE/Downloads/stellungnahmen/verordnung-raumordnung-deutsche-wirtschaftszone-in-nordsee-und-ostsee/bundesamt-fur-naturschutz.pdf?__blob=publicationFile&v=2, last accessed 26.05.2025

[3] https://www.bsh.de/DE/THEMEN/Offshore/Flaechenvoruntersuchung/_Anlagen/Downloads/AJ2021_Entwurf_Eignungsfeststellung_Ergaenzung.pdf?__blob=publicationFile&v=2#:~:text=Die%20Vorgabe%20dient%20der%20Vermeidung%20der%20Realisierung%20des,verboten%2C%20europäische%20Vogelarten%20zu%20töten%20oder%20zu%20verletzen, last accessed 26.05.2025

altitude range exceeds a threshold of 250 MTR (migration traffic rate, i.e. birds per hour crossing a virtual 1 km line; (SCHMALJOHANN ET AL. 2008))[4]. Furthermore, a similar mitigation measure has already been implemented in the Dutch North Sea. There, the mitigation process begins with the prediction of nocturnal bird migration intensity at rotor height 48 hours in advance, using a forecasting model developed specifically for this purpose. If the forecast in unison with an expert team indicates that a predefined MTR threshold (500 MTR) will be exceeded, various stakeholders are automatically notified with the aim of implementing turbine curtailment if it can be accomplished without compromising grid stability. Currently, this mitigation measure is not tied to any additional factors, such as weather conditions.

The BfN recommendation and Dutch mitigation measure imply that the collision risk for nocturnally migrating birds at sea depends primarily on their migration intensity at rotor height. However, a simple direct proportional relationship, for example that doubling the number of nocturnally migrating birds would result in twice as many collisions, is questionable for several reasons. For example, several studies in coastal onshore areas found that nocturnally migrating birds were detected only in very low numbers during carcass searches, despite high migration intensities being recorded within the relevant altitude range (KRIJGSVELD ET AL. 2009; GRÜNKORN ET AL. 2016; WELCKER ET AL. 2017). Strong bird migration predominantly occurs under favourable weather conditions (VAN BELLE ET AL. 2007; VAN DOREN & HORTON 2018; NILSSON ET AL. 2019; WELCKER & VILELA 2019; ROY ET AL. 2025), and it seems plausible that favourable weather conditions (e.g. good visibility, supporting wind conditions, no precipitation) do not impair the capability of nocturnally migrating birds to perceive and avoid OWT in the dark.

However, substantial bird migration, particularly in offshore areas, occasionally occurs even under unfavourable weather conditions (AUMÜLLER ET AL. 2011; WELCKER & VILELA 2019). Under such conditions, the birds' reaction thresholds may be reduced—poor visibility may result in a closer approach to structures before avoidance responses are triggered (AVITEC RESEARCH GBR 2014). At night, this risk may be further amplified by the potential attraction of nocturnally migrating birds to artificial light sources, especially during fog, rain, or dense cloud cover (AVITEC RESEARCH GBR 2014). This light effect has long been documented and can lead to significant accumulations of birds, particularly passerines, near illuminated structures (e.g. see summary in AVITEC RESEARCH GBR 2014). Such situations — high migration intensities occurring under unfavourable weather conditions — may result in increased collision events. (e.g. AUMÜLLER ET AL. 2011). Offshore wind energy installations equipped with safety lighting, are also considered potential attractants or light traps (DREWITT & LANGSTON 2008) under these conditions.

Due to the lack of direct data on bird collisions at offshore wind farms, estimates of fatalities have so far been derived based on collision risk models (CRM), predominantly by application of the so-called Band model (BAND 2012). In addition to the fact that for obvious reasons these models cannot be validated in the offshore environment, several caveats impair the reliability of model outcomes (CHAMBERLAIN ET AL. 2006; MASDEN 2015; MASDEN & COOK 2016; WELCKER & VILELA 2019). Most importantly, the number of estimated collisions depends tremendously on the assumed avoidance rate of the birds. Already small changes in the avoidance response incorporated in the model, and consequently the estimated number of birds passing through the rotor plane (rotor transits), results

[4] Same as note 2

in large differences in model outcome. For instance, assuming an avoidance rate of 98 % instead of 99 % will double the number of predicted collision fatalities. As up to now very little information is available with respect to the avoidance response of nocturnally migrating birds (KRIJGSVELD ET AL. 2011; SCHULZ ET AL. 2014), the validity of modelled collision risk at OWT is unknown.

In the absence of robust empirical collision data at OWT, the magnitude of the collision risk as well as the nature of the relationship between migration intensity and the number of collision fatalities remains uncertain. Information on the timing of collisions, the conditions under which collisions occur, and their absolute number in relation to the total number of birds migrating through offshore wind farms is urgently needed. Such data are essential for implementing targeted mitigation measures or for re-evaluating the necessity of such measures altogether.

The main aim of this study was to collect data on the collision risk of migrating birds, particularly nocturnal bird migration, at near-shore wind turbines to contribute to closing existing knowledge gaps. We tested whether the probability of birds flying through the rotor plane and thus the number of collisions is proportionally related to the intensity of bird migration or influenced by weather conditions. Moreover, we empirically determined avoidance rates and performed intensive fatality searches to validate collision models. This will support improved estimations of bird collision risk in offshore areas and help evaluating current approaches to mitigation measures.

We applied a combination of well-established and innovative methods to reach that aim. Using a specialized bird radar, we collected data on overall MTRs at rotor height and altitudes up to 1000 m at the study site. Complementing these measures, we installed a bird call recorder, to derive information on the main species involved in nocturnal bird migration. Novel AI-driven stereo-vision camera systems were applied to record the number of bird rotor transits during both day and night, allowing for precise estimation of avoidance rates in relation to MTR. Finally, we conducted intensive carcass searches to derive an independent measure of collision risk.

2.1 Goals

The overall goal of this study was to specify the collision risk of migratory species, with a focus on nocturnal migrants and to investigate whether this risk depends on environmental conditions. More specifically, with the data collected we aimed to answer the following questions about the interplay of migration intensity, collision risk and number of actual fatalities:

- Is there an association between migration intensity at rotor height and the number of rotor transits?
- Does the relationship between migration intensity at rotor height and the number of rotor transits differ between daytime and nighttime migration?
- To what extent are both parameters (MTR at rotor height and number of rotor transits) influenced by weather conditions?
- Does the number of rotor transits vary depending on wind turbine operational status (i.e.: below or above 2 rpm)?

- What is the relationship between the number of birds passing through the wind farm (25 -1025 m) and the estimated number of collisions?
- How many actual collision victims can be found at the wind farm based on systematic carcass search protocols?

Furthermore, the routinely used 'Band model' (SCOTTISH NATURAL HERITAGE 2000; BAND 2012) to estimate collision risk was validated for nocturnally migrating birds, based on data collected on migration intensity, observed flight behaviour within the rotor area (rotor transits), and estimated collision fatalities. This involved the following:

- Determination of avoidance rates of nocturnal migrants based on radar and camera data. The avoidance rate is a key parameter of the Band model.
- Comparison of collision risk between daytime and nighttime migration.
- Validation of the model by comparing its results derived by empirically determined avoidance rates with the estimated number of collisions determined through carcass searches.

3 METHODS

3.1 Overview

The study was conducted at the coastal wind farm 'Windtestfeld Nord' between 23 February 2023 and 30 November 2024, covering four migration seasons: two springs and two autumns. Camera data was recorded during more than three migration seasons, from 15 May 2023 to 30 November 2024. The 'Windtestfeld Nord' is a test site for wind turbines and hosted five different prototype turbines, spaced 600 to 1350 m apart (see chapter 3.2 for details and Table 3-1 for turbine specifications).

A detailed description of all employed methods is provided in the respective chapters below. Owing to varying logistical requirements, the methods were initiated at different times, allowing each to be implemented under optimal conditions.

Camera systems (see chapter 3.4 and Table 3-1) were installed on two of these turbines. The systems recorded all bird (and bat) passages through the rotor plane, both during the day and at night. Nocturnal activity was captured using infrared cameras in combination with infrared emitters. We applied AVES Offshore HPC systems from ProTecBird GmbH that were specifically developed for this purpose.

To assess general migration intensity in the area, we used a specialized bird radar, the BirdScan MR1 system from Swiss-Birdradar Solution AG (see also chapter 3.3) and an acoustic bird call recorder, both positioned close the wind farm (see chapter 3.5).

In addition, at all five turbines we conducted so-called post construction fatality monitoring (PCFM) at a five-day interval throughout the study period to detect potential collision victims (see chapter 3.6).

Data on weather conditions were obtained from various data sources. Wind speed, wind direction, and temperature were measured directly at the turbines at rotor height. For other parameters—such as precipitation, barometric pressure, and visibility—we used data from a local weather station and mean values derived from publicly available data provided by the German Meteorological Service (Deutscher Wetterdienst, DWD) from multiple locations surrounding the wind farm. Correlation matrices indicated a strong agreement between these mean values and the corresponding parameters recorded within the wind farm itself (see chapter 3.7.1 for details).

3.2 Study site `Windtestfeld Nord´

The fieldwork was conducted at `Windtestfeld Nord´[5] near Husum, Germany (54.449°N, 9.035°E, Figure 3-1). The site is located close (~2.3 km) to the coast of the Schleswig-Holstein Wadden Sea

[5] https://www.windtestfeld-nord.de/de, last accessed 27.06.2025

National Park and the North Sea, and encompasses a variety of habitats, most notably agricultural fields, channels, ditches, small roads, trees and shrubs.

The wind farm area spans approximately 150 ha and the maximum width of the site perpendicular to the main migration direction is about 1.2 km (East-Southeast to West-Northwest). Common bird species in this area include geese, ducks, gulls, waders and songbirds. Within this area, five operating wind turbines of varying types and sizes (see Table 3-1) were used for this study. These turbines are still operating.

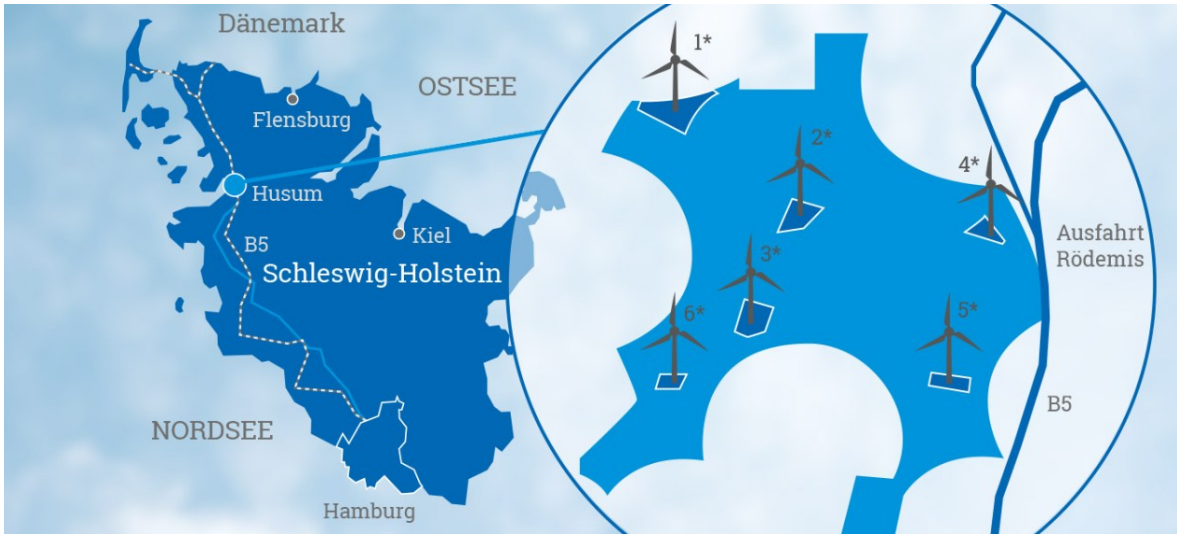

Figure 3-1 *Map providing an overview of the `Windtestfield Nord' at Südermarsch, near Husum, including details of the five prototype turbines and their IDs, corresponding to those listed in Table 2-1 (e.g. 2 = A2, and so on). Please note, that A1 was decommissioned shortly before the start of this study. Source: https://www.windtestfeld-nord.de/de/testanlagen.php.*

Table 3-1 *Technical specifications of the five prototype turbines at `Windtestfeld Nord', and AVES camera system installation status (yes/no).*

Producer	Turbine ID	Model type	MW	Rotor radius [m]	Hub height [m]	Total turbine height [m]	Lower rotor tip height [m]	Camera system
Senvion GmbH	A2	EBC	3.6	70	110	180	40	yes
Siemens Wind Power	A3	SWT-3.6-130	3.6	65	85	150	20	no
Nordex (GP Joule)	A4	N 131 3600	3.6	65.5	98	164.8	32.5	yes
GE Renewable Energy	A5	GE 3.2	3.2	65	85	150	20	no
Enercon	A6	E 126 EP 4	4.2	63	100	163.5	37	no

3.3 Radar

A BirdScan MR1 ornithological radar, developed by Swiss Birdradar Solution, was operated continuously throughout the entire study period (23/02/2023 – 01/12/2024), with minimal downtime due to maintenance or local power outages. The MR1 is a vertical-looking radar system designed for real-time monitoring of bird movements[6]. It is a 25 kW pulsed X-band radar (9.4 GHz) with a maximum range for large birds of approx. 2000 m and 1000 m for smaller birds, like passerines. The vertical cone-shaped detection range of the radar is illustrated in Figure 3-2.

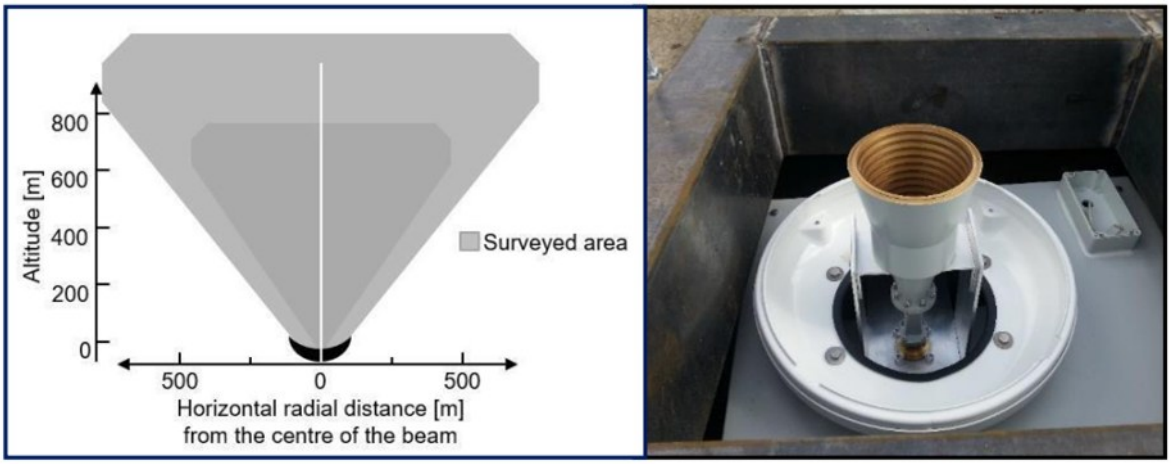

Figure 3-2 *Left: Illustration of the monitored radar volume of the horn antenna of the MR1 radar after reduction of noise and sidelobes. Right: Horn antenna of the MR1.*

Using echo signature characteristics, the MR1 is unique in classifying detected tracks as bird or non-bird (e.g. bats, and insects). It further distinguishes birds into groups based on wing-beat patterns, such as waders, passerines, swifts and large birds. This distinction enables the use of species-specific MTRs and flight height distributions (FHDs). Small birds, such as passerines, can be reliably detected up to a height of 1025 m. It has been shown that the BirdScan MR1 radar can robustly monitor both absolute and relative bird migration intensity (NILSSON ET AL. 2018).

The radar was installed about 650 m from the nearest wind turbines of the study site (Figure 3-3 and Figure 3-4, turbine A2 and A4, both of which were equipped with a camera system, see chapter 3.4). The radar data on MTRs and FHDs can therefore be regarded as representative of the wind farm area.

[6] https://swiss-birdradar.com/systems/radar-birdscan-mr1/#:~:text=BirdScan%20MR1%20is%20a%20compact%20radar%20system%20for,a%20rich%20set%20of%20information%20for%20each%20target%3A, last accessed 27.06.2025

Figure 3-3 The MR1 radar installation site close to the wind farm 'Windtestfeld Nord' (in the background).

Figure 3-4 Study site with location of radar (yellow), wind turbines equipped with AVES camera systems, and additional turbine locations used for fatality monitoring.

3.4 Camera system

To systematically collect data on rotor transits of birds (defined *sensu* BAND (2012) further details below), we employed innovative camera systems at two turbine locations (see Figure 3-4). We used

the AVES Offshore HPC system, developed by ProTecBird GmbH[7] specifically for the purpose of detecting birds as small as a passerine within the rotor plane and the area immediately leeward of the rotors, both during the day and night (Figure 3-6 and Figure 3-9).

The camera system consists of several high-resolution stereo-vision camera pairs (Figure 3-5), which allow for distance estimation of detected objects and thus for determining whether birds flew within or outside the length of the rotor. The number of cameras, along with the resolution (4k: 3840x2160 pixel) and sensitivity of the sensors and the opening angle of the lenses (45°), was devised to ensure detection of even the smallest nocturnal migrants across the full length of the rotor blades (70 m, see Table 3-1). This was confirmed by a series of tests in which carcasses of small birds were attached to a drone to determine the range of the cameras during both day and night.

For this study, each camera system comprised four camera pairs (Figure 3-5). To facilitate object detection at night, the systems included four active infrared emitters (100 W) designed to sufficiently illuminate the entire field of view within the rotor area (see also Figure 3-6).

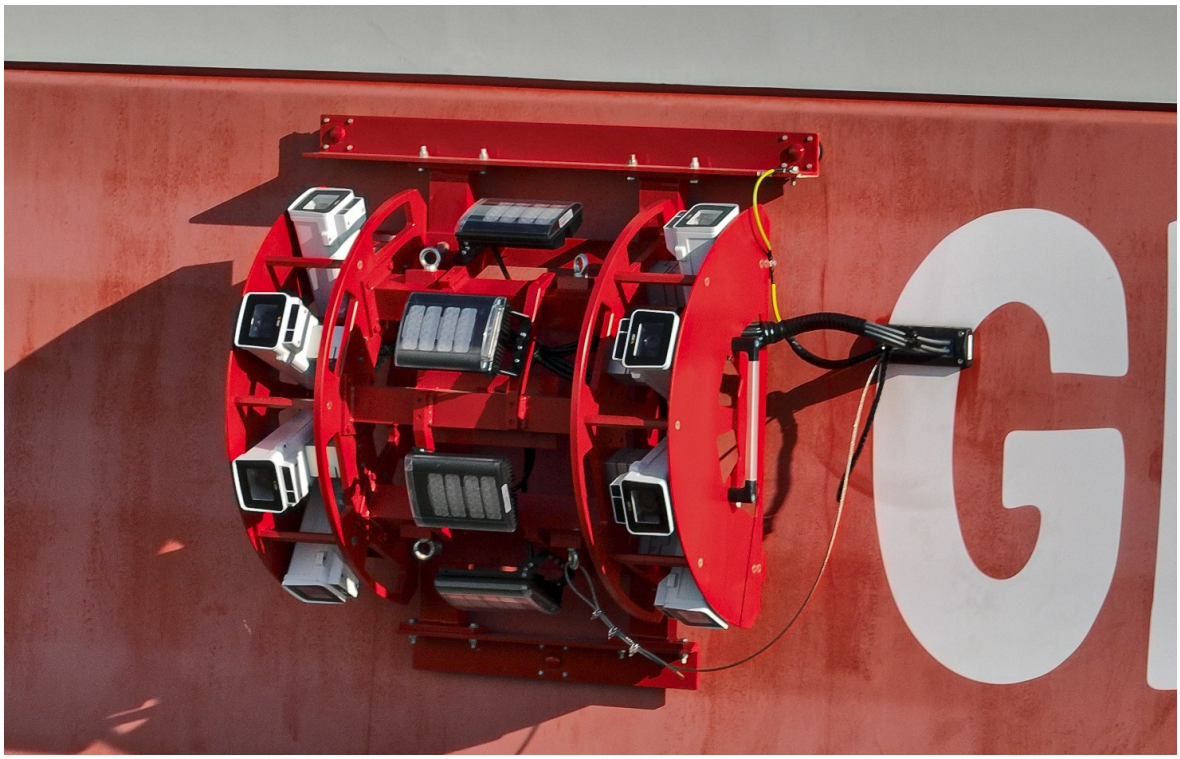

Figure 3-5 The AVES Offshore HPC system, consisting of four stereo-vision camera pairs and infrared light sources to facilitate bird detection at night.

[7] https://protecbird.com/aves-wind-high-precision-counter/, last accessed 18.07.2025

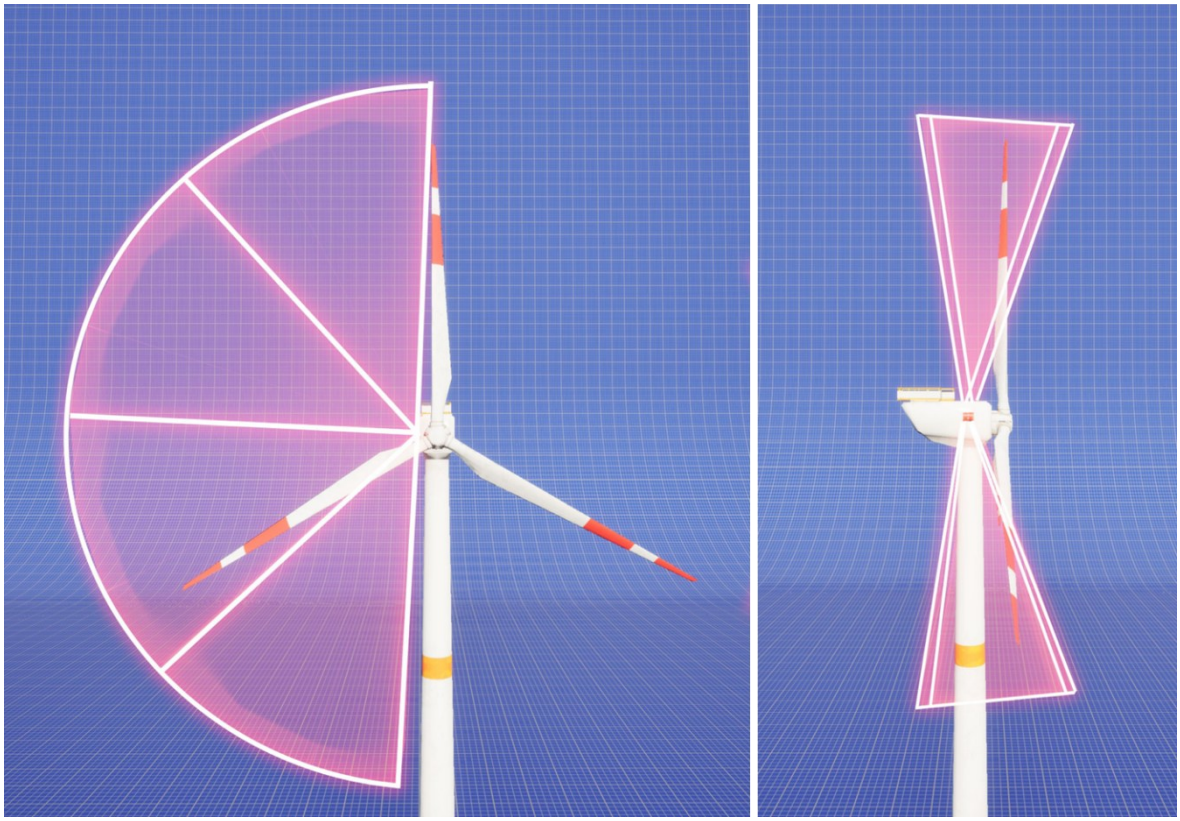

Figure 3-6 Illustration of the field of view of the AVES camera systems.

The camera systems were installed on the nacelles of the turbines (Figure 3-6). Compared to installations at the base of turbines towers, this positioning offers several important advantages:

- the cameras remain perfectly aligned with the rotor plane regardless of wind direction and rotor orientation
- the required detection distance is minimised to the length of the rotor blade, rather than the full rotor diameter
- each camera system can cover one complete half of the rotor plane (180°), capturing areas both above and below the nacelle to the same extent (Figure 3-6); and
- adverse weather conditions such as fog and precipitation have less effect on the camera detection performance due to the reduced observation distance and favourable camera orientation.

Figure 3-7 Installation of an AVES Offshore HPC system at the study site.

Even though collisions can be detected with these camera systems (we recorded two nocturnal bird collisions and one bat collision during the study period), due to the positioning of the cameras and opening angle of the lenses only parts of the rotor blades were within their field of view. Therefore, camera data were not used for direct collision monitoring but rather to precisely record bird movements through the rotor plane as an indirect way of determining collision risk (see also chapter 3.7.10).

For the purpose of this study, and following BAND (2012), rotor transits were defined as events where birds cross the rotor plane of a wind turbine (Figure 3-8). Manual review of the video data from the cameras (see below) was used to determine rotor transits. As the cameras' field of view did not cover the entire rotor blade, rotor transits were partially deducted from the flight paths of the birds (Figure 3-8). For example, this applies to flight path scenario 4, whereas flight path scenario 1 represents a fully recorded rotor transit within the cameras' field of view. Scenario 2 and 3, on the other hand, describe cases where no rotor transit would be recorded. In scenario 2, a micro avoidance is observed with no rotor plane crossing, while in scenario 3, the micro avoidance and no rotor plane crossing remain undetected.

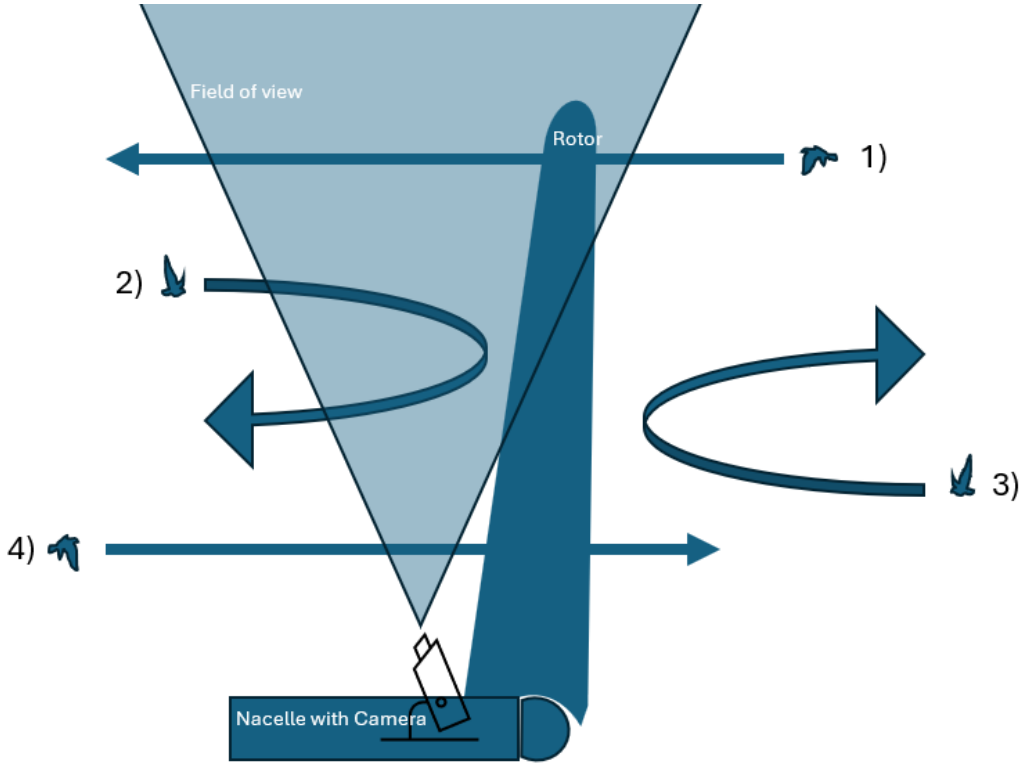

Figure 3-8 *Illustration of rotor transits: four possible flight path scenarios of birds in relation to the cameras' field of view. Scenario 1 and 4 would be scored as rotor transits, whereas scenario 2 would be scored as no rotor transit. Scenario 3 could not be detected by the cameras and would not qualify as a rotor transit.*

Bespoke AI-models for detecting birds (and bats) were developed and applied. Different AI-models were required for daytime (RGB videos) and nighttime (greyscale footage), as well as for two different background categories: sky and landscape/vegetation. Pre-existing models were fine-tuned and validated during the initial months of the study and subsequently implemented at different points in time until mid-November 2023.

During the early stages of camera data collection, continuous (24/7) video footage was recorded and stored. This data was later analysed offline using the finalised AI-models. From mid-November 2023 onwards, the AI-models for bird detection were deployed online in real time, and only video sequences with positive detections were stored for later reference.

The performance of the AI-models was validated manually by experienced reviewers using test datasets that were not part of the AI training material. The confidence level of the final AI-models for detections was set to ensure 100 % recall of all manually identified birds. This approach was deemed necessary because rotor transits can be regarded as relatively rare events, and underestimating transit rates could potentially have a large impact on the results.

As a consequence, this approach resulted in a high number of false positive detections (instances where the AI incorrectly identified non-bird objects as birds), which were manually reviewed and filtered. Due to this manual review effort, combined with the fact that AI detection could not be implemented at the start of the data collection period, resulting in high computational demands

and extended processing times for stored video footage analysed offline, not all available video data was analysed.

In general, video data analysis was restricted to the main bird migration periods (01 March until 31 May and 15 July until 30 November) as defined by StUK4 (BSH 2013), which are applied to all offshore bird migration surveys in German waters within the context of offshore wind developments. These periods encompassed a total of 387 days. As cameras were installed on two wind turbines this resulted in 774 turbine-days, where one turbine-day refers to one turbine being monitored for a single day (24 h including the night).

Data were successfully recorded on 722 of these turbine-days. The remaining 52 turbine-days lacked data due to turbine maintenance activities, power outages, or other reasons that caused long-term camera system downtime. From the 722 turbine-days (and nights), we selected 547 nights (76 %) and 305 days (42 %) for data analysis. A monthly overview of the selected days and nights is provided in Table A-5.

Days and nights were selected based on MTR values derived from bird radar data and information on weather conditions (specifically visibility), with the aim of choosing days/nights that represented similar proportions of low, medium and high migration intensities. At the same time, care was taken to ensure that time periods with reduced visibility were also included. The aim was to ensure a balanced dataset for analysing the relationship between rotor transits with migration intensities, as well as the effects of unfavourable weather conditions.

Overall, the operational availability of the camera systems during the analysed time periods (i.e., 547 night- and 305 day-periods) was 89 %. The main causes of camera downtime were short-term power outages, as well as server maintenance and failures. Periods of camera downtime were accounted for in subsequent data analyses.

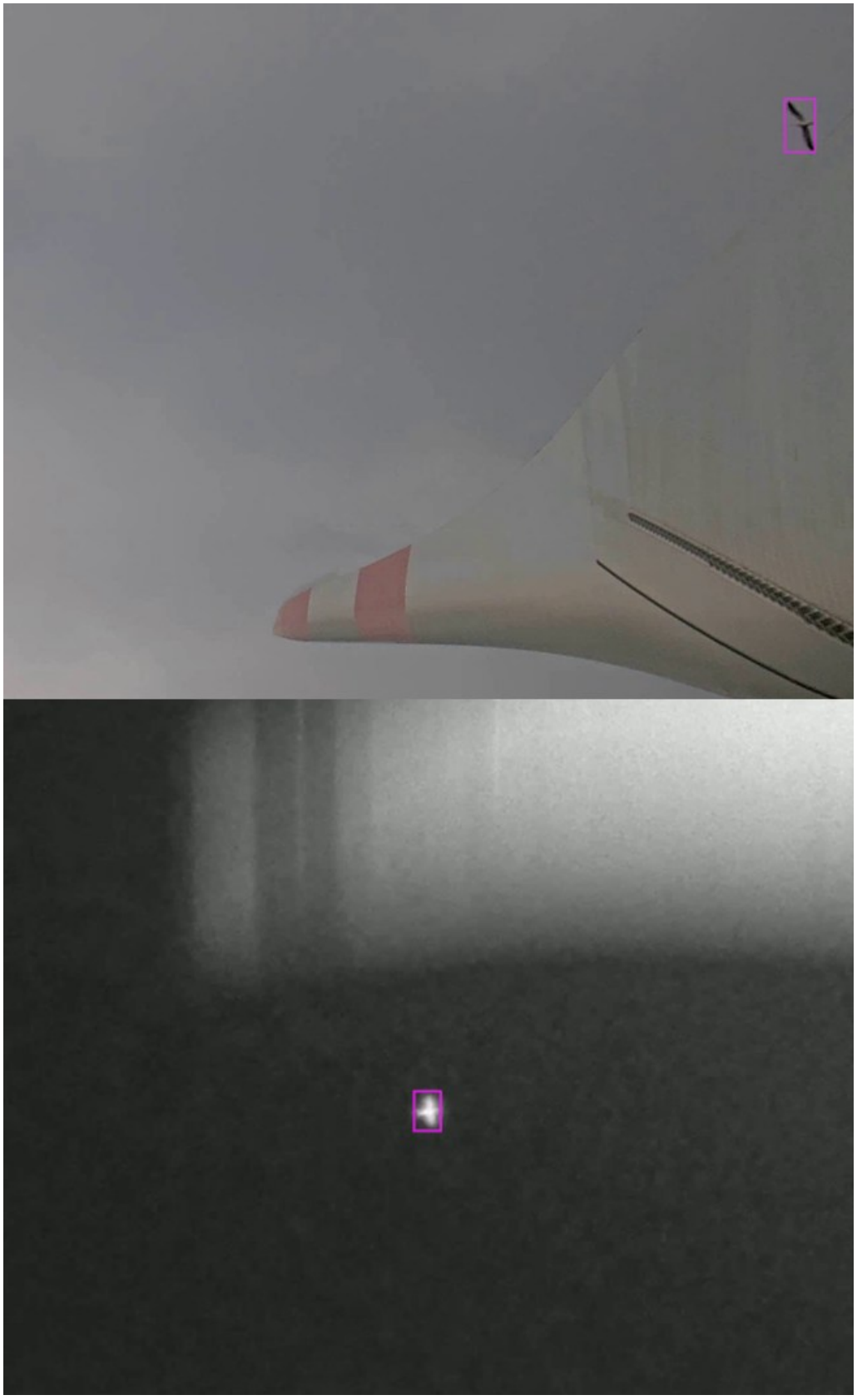

Figure 3-9 Screenshots of birds detected by the AVES camera system during the day (above) and the night (below).

3.5 Bird call recordings

To record bird calls we used an acoustic recorder called `Song Meter' (SM4, Wildlife Acoustics[8]). The Song Meter was placed next the study area in close vicinity to the radar (see Figure 3-4). It was powered with a solar panel. The Song Meter was programmed to record continuously from 12 May 2023 until 30 November 2024, with a sampling rate of 24000 kHz, gain of 16.0 dB, preamp of 26 dB, and a resolution of 16 bits per sample. The detection range of the `Song Meter' varies depending on the call amplitude (species-specific differences) and environmental conditions such as wind and precipitation. Under optimal conditions, loud calls can be detected at distances of several hundred metres, whereas under unfavourable conditions (e.g. strong wind), the effective range may be limited to a few metres for faint calls.

To ensure sufficient available data storage, SD cards were replaced regularly every three to four weeks. Unfortunately, on three occasions (between 26/10/2023 – 17/11/2023; 12/12/2023 – 01/02/2024, and 08/06/2024 – 15/07/2024) data recording was interrupted due to technical failure of data storage; water damage and a daredevil sheep. Audio files were stored as uncompressed wav-files and manually inspected to verify that the recorded signals met the requirements and were then analysed for bird species using the algorithms of the software 'Sound ID'[9].

3.6 Post Construction Fatality Monitoring (PCFM)

The aim of the PCFM was to estimate the number of collision fatalities at the five turbines of the wind farm during the study period from 15 May 2023 to 30 November 2024. Throughout this period, designated plots around each turbine were regularly searched for collision victims, depending on visibility conditions (see below). Two of the five turbines monitored during PCFM were non-operational for extended time periods during the study period.

The search area at each turbine was defined as a radius of 120 m around the base of the tower. The area was divided in different plots depending on accessibility and type of vegetation. Plots with permanently high vegetation, shrubs or trees were excluded. Also, to keep search effort within feasible limits, for some uniform plots (e.g. farmland) the search area was restricted to an 80 m radius in which most carcasses were predicted to fall. Visibility conditions for each subarea were recorded on every survey day and categorised as `very good', `good', `sufficient' or `not sufficient' (in which case the area was not searched) depending on the height of the vegetation or other limitations (e.g. farming activities or flooding after periods with high precipitation; see Table 3-2). As the primary focus of the study was on passerine birds, a narrow transect width of 7 m was implemented within search plots. Thus, observers were required to search for carcasses within 3.5 m to either side of each transect line. Transect layouts were optimised for each subarea, and observers navigated the transects using tablets equipped with GPS (Figure 3-10).

[8] https://www.wildlifeacoustics.com/products/song-meter-sm4, last accessed 30.06.2025

[9] https://merlin.allaboutbirds.org, last accessed 01.07.2025

Table 3-2 Visibility conditions of plots for carcass searches.

Visibility Category	Description
1 = Very Good	Freshly ploughed and harrowed field without vegetation (i.e., fine soil)
	Tracks and crane standing areas
	Germinated rapeseed/maize up to 5 cm
	Emerging winter cereals up to 2 cm
2 = Good	Mowed grassland
	Germinated rapeseed up to 10 cm
	Emerging winter cereals up to 10 cm
	Stubble fields without undergrowth
3 = Sufficient	Rapeseed/maize/winter cereals up to 20 cm
	Stubble fields with undergrowth
	Ploughed field
4 = Not sufficient	Not searched due to very poor visibility

Figure 3-10 Overview of test area with all five turbines indicated with orange dots. Red lines show transect design for carcass searches. Inner blue circle indicates 80 m and outer circle indicated 120 m radius around the turbine.

Carcass searches were carried out every five days throughout the study period to minimise the risk of potential carcass removal between visits. However, intervals between surveys in any given sub-area could be extended depending on visibility conditions. The location of carcasses found during the searches were recorded using GPS, and carcasses were identified at species level either in the

field or subsequently in the laboratory by an ornithologist specialised in feather identification. A total of 114 search days were conducted of which the first day (15/05/2023) was the initial search, with the aim of removing all carcasses of collision fatalities that happened before the start of the study period.

In accordance with the PCFM handbook (INTERNATIONAL FINANCE CORPORATION 2023) remains of dead birds were defined as a collision fatality if at least two contiguous primary feathers or at least ten loose smaller feathers were found within a radius of approximately 2.5 m.

Additionally, field trials were conducted to estimate carcass persistence and observer efficiency, enabling appropriate corrections in the final estimates of total collision victims based on carcass records.

3.6.1 Carcass persistence and search efficiency

Carcass persistence

Carcasses can be removed by scavengers or degrade and decompose over time, making them undetectable during subsequent surveys. Carcass persistence trials take account of this limitation by providing empirical data to model a persistence function using survival analysis approaches and thereby improving the accuracy of fatality estimates.

For this study, 80 carcasses from three different body size categories (small: n = 37; medium: n = 30; large: n = 13) were used in four carcass persistence trials. Thus, differences in persistence time with carcass size could be taken into account in subsequent data analyses. These four trials were conducted across different seasons to account for potential seasonal variation in scavenger activity. Only carcasses of species that naturally occur in the study area were used. The condition of each carcass (i.e. `very good', `good', 'sufficient' and 'insufficient'.) was recorded until it was no longer detectable or until the end of the trial period (21 days), whichever occurred first. The start day of the four trials were: 28/02/2024 (19 carcasses), 28/05/2024 (20 carcasses), 05/09/2024 (23 carcasses), and 04/11/2024 (18 carcasses).

Search efficiency

Searcher efficiency trials were used to estimate the probability of detecting a carcass that was present in the field at the time of search. Bird carcasses were placed in the field at various dates and in various visibility conditions during the study without informing observers. We combined persistence and search efficiency trials by using the carcasses of the persistence trials also for the search efficiency. To increase sample size, we placed additional 17 carcasses for the search efficiency analysis. Observers could identify carcasses from search efficiency trials by the small brown string tied to the carcasses' legs. Number of carcasses were carefully balanced such that the three carcass size categories were equally present in the three visibility classes (see Table 3-3). The detection by field observers on their first subsequent search was recorded. Given the success rate of detecting carcasses under different visibility conditions, size and visibility specific efficiency estimates were calculated (see chapter 3.7.9).

Table 3-3 Number of carcasses used in searcher efficiency trial across size categories and visibility levels.

Carcass size	Visibility level		
	Very good	good	sufficient
small	15	17	7
medium	12	11	12
large	8	6	9

3.7 Data Analyses

When scrutinising data, there are often multiple approaches by which the same dataset can be analysed. Given the wide range of modern analytical techniques, it becomes apparent that there is no single best solution, and different technically sound methods can yield varying estimates (GOULD ET AL. 2025). One way to address the challenge of selecting an appropriate statistical technique for a given task is to apply multiple methods of data analysis and assess the extent to which their estimates differ. This approach may offer, on the one hand, the assurance that the results are robust; or, on the other hand, when results are contradictory, it indicates that further investigation is required. In the present study we adopted this strategy by employing different statistical methods to evaluate the most critical hypothesis: that the rotor transit rate is linearly associated with migration intensity at rotor height.

Since the number of rotor transits followed a Poisson rather than a normal distribution, simple linear models were not appropriate. Therefore, we first conducted nonparametric analyses using Kendall's rank correlation, followed by generalized linear models (GLMs) and generalized linear mixed models (GLMMs). Further details are provided in the following chapters.

Next, as we expect that both the overall MTR and its potential association with rotor transits depend on weather conditions, we applied modern Bayesian models incorporating weather parameters as explanatory variables. Since MTRs are also strongly influenced by temporal patterns such as season and time of the day, we included these variables in the models to distinguish the effects of weather conditions from those of temporal variation.

We also used Bayesian statistics, as it enables rigorous error propagation, resulting in precise estimates of effect sizes and associated uncertainty. Moreover, Bayesian statistical modelling allows for control over model assumptions, the underlying data distribution, and the interplay between variables (MCELREATH 2019).

To incorporate weather variables, we obtained the relevant data from appropriate sources and carried out pre-processing. Details are provided in the following chapter 3.7.1.

All statistical analyses were conducted using the R software environment (R version 4.4.1 (2024-06-14 ucrt) R Core Team, 2024).

3.7.1 Pre-processing of weather data

Part of the meteorological data was collected on-site at `Windtestfeld Nord', either by the wind turbines themselves or by a weather station operated by Pavana GmbH (Husum, Germany), which kindly provided the data. However, these measurements were discontinued in August 2024 and are therefore incomplete for the full study period. To ensure consistent meteorological data across all four migration periods analysed, publicly available hourly weather data from the DWD were used[10]. Based on previous studies on nocturnal bird migration, eight weather parameters were selected for analyses (see Table 3-4; for more details see also appendix A.4).

Table 3-4 Meteorological parameters used for the regression analyses and their DWD sources. 'Relative humidity' (in grey) was excluded from further analysis due to its strong correlation with visibility (r ≥ 0.7).

Parameters	Unit	Meteorological stations used
Precipitation	mm	Mean of Hattstedt, Erfde, Leck, Schleswig, SPO
Temperature	°C	Mean of Hattstedt, Erfde, Leck, Schleswig, SPO
Wind speed	m/s	Mean of Leck, Schleswig, SPO
Wind direction	°	Mean of Leck, Schleswig, SPO
Barometric pressure	hPa	Mean of Leck, Schleswig, SPO
Cloudiness	eights	Mean of Leck, Schleswig, SPO
Visibility	m	Mean of Leck, Schleswig, SPO
Relative humidity	%	Mean of Hattstedt, Erfde, Leck, Schleswig, SPO

The nearest DWD station is in Hattstedt (54.527°N, 9.043°E), approximately 9 km from the study area. However, not all required weather parameters were recorded at this site. Therefore, data from five nearby DWD stations were combined. Details are provided in Table 3-5.

Table 3-5 Overview of the five DWD weather stations used in the study. Including station ID, altitude above sea level (a.s.l), geographic coordinates and distance to wind farm in km.

Town	DWD Station ID	Altitude a.s.l. (m)	Coordinates (°N, °E)	Distance [km]
Hattstedt	7298	4	54.527, 9.043	8.84
Erfde	1266	18	54.299, 9.316	24.67
Leck	2907	7	54.7903, 8.9514	38.46
Sankt Peter-Ording (SPO)	4393	5	54.3279, 8.6031	30.88
Schleswig	4466	47	54.528, 9.549	34.48

[10] https://opendata.dwd.de, last accessed for data download 07.01.2025

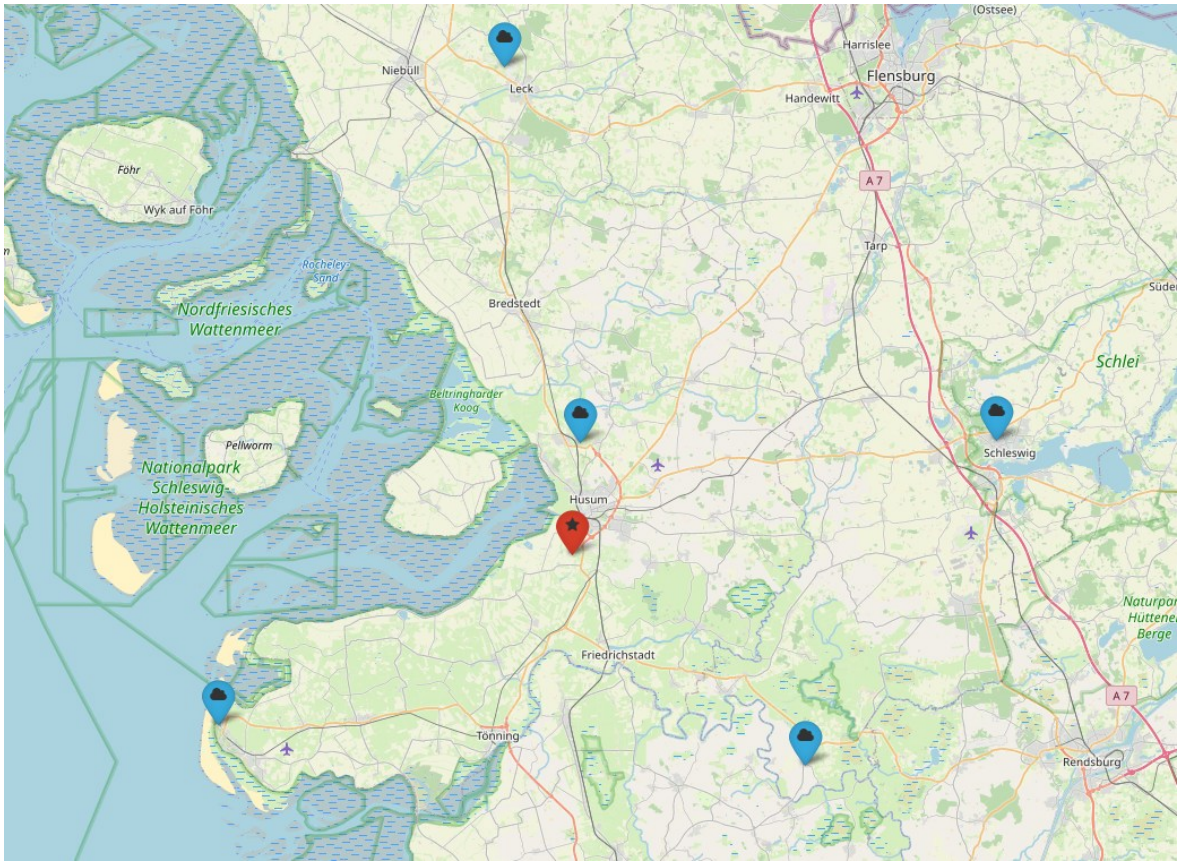

Figure 3-11 Overview of the five DWD weather stations used in the study indicated by blue 'cloud' marker. Location of test wind farm is indicated by red 'star' marker.

To assess the suitability of the DWD data as a substitute for local measurements, Pearson correlations were calculated using the R package `correlation' (v. 0.8.5; MAKOWSKI ET AL. 2022). The aim was to identify the best-matching DWD source for each parameter recorded by the Pavana weather station. For parameters not measured by the Pavana station (relative humidity, cloud cover, visibility), mean values across DWD stations were used (Table 3-5).

To prevent multicollinearity and ensure model stability in subsequent regression analyses, correlations among weather variables were examined. Variables with a correlation coefficient of $r \geq 0.7$ were considered highly correlated, and in such cases, one variable was excluded. Relative humidity and visibility exhibited a strong correlation ($r > 0.7$); since visibility was of particular interest regarding the migratory behaviour of passerines, relative humidity was excluded (see Figure 3-12).

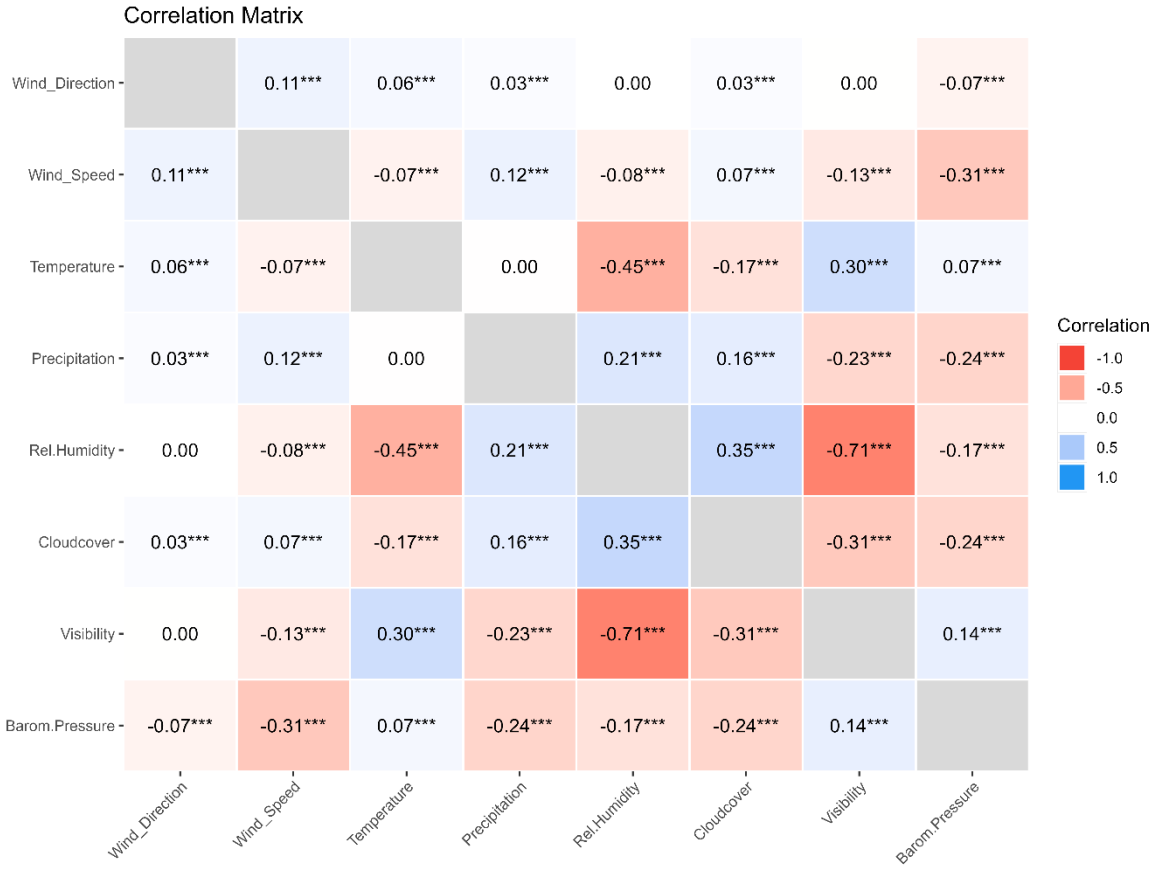

Figure 3-12 *Correlation matrix of weather parameters selected for regression models. Variables with a correlation coefficient of r ≥ 0.7 were considered highly correlated. Variables represent mean of DWD station values; wind variables correspond to the mean of the five turbines in the wind farm.*

Tail- and Crosswinds

One of the most important environmental predictors of migratory behaviour is wind conditions (ERNI ET AL. 2002; WELCKER & VILELA 2019; NUSSBAUMER ET AL. 2022; SCHEKLER ET AL. 2024). For example, Welcker and Vilela (2019) found that migration intensity increases with tailwinds. Tailwinds are defined as winds blowing in the direction of migration and thus supporting the birds' movement, whereas headwinds increase the energetic costs of flight and typically reduce the likelihood of migration. In addition to wind direction, wind speed determines the extent to which wind exerts a supportive or adverse effect on the birds' movement. Therefore, the tailwind component is typically calculated as a function of wind direction and wind speed (e.g.: ZEHNDER ET AL. 2001; HÜPPOP & HILGERLOH 2012). In line with these approaches, we estimated the tailwind component (TWC) as:

$TWC = \cos(OWD - TWD) \cdot WS$ where *OWD* is the `observed wind direction', *TWD* is the `tailwind direction' and *WS* is the `wind speed'.

TWD was calculated from the radar data as the average flight direction per season. In spring, the main flight direction was 25° and in autumn 205°. These directions are more north-south oriented than those reported in other studies (e.g. BRADARIĆ ET AL. 2024b), which typically find a stronger southwest-northeast direction in spring and northeast-southwest direction in autumn. We

attributed the predominantly north-southernly flight directions at our study site to the local geographical conditions.

In addition to tailwinds, also crosswinds are expected to influence migration. Crosswinds are defined as winds blowing perpendicular to the main migration direction, and the `crosswind component' (CWC) is estimated similarly to the TWC:

$$CWC = \sin(OWD - TWD) \cdot WS$$

Where, as above, *OWD* is the `observed wind direction', *TWD* is the `tailwind direction' and *WS* is the `wind speed'.

Positive CWC values indicate winds blowing from the bird's left side relative to its flight direction, while negative values indicate winds from the right. Considering the assumed migration direction, positive CWC values correspond to winds coming from the sea in spring and from the coast in autumn. To facilitate readability, we defined CWCs blowing towards the shore—relative to the season's specific main migration direction—as `shorewinds´, and those blowing towards the sea as `seawinds'.

It has been shown that a change of weather conditions from one day to the next influences the migration behaviour of birds (e.g. NILSSON ET AL. 2019; NEWTON 2023). To capture this in statistical analyses, Δ-values of weather parameters are applied (e.g. BRADARIĆ ET AL. 2024a). Typically, Δ-values represent the difference of the parameter value from the previous day or night to current day or night. In our study, we calculated the difference (i.e. the Δ-values) as the difference of the current hour = $date_i hour_j$ with the average value of the previous night:

$$\frac{1}{n} \sum_{j=1}^{n} date_{i-1}\, hour_j$$

3.7.2 Modelling the relationship between migration intensity and weather conditions

To gain insight into the general pattern of nocturnal migration and its dependency on weather conditions we used generalised additive models (GAMs) in a Bayesian model framework. Specifically, we tested the impact of weather conditions on i) MTR of passerines at flight altitude between 25 and 1025 m and ii) the proportion of these birds flying at rotor height, and iii) MTRs at rotor height (25-180 m).

The preprocessing of weather data and the model on 'the proportion of birds flying at rotor height' as the response variable, were performed as a part of a Master thesis. A detailed method description can be found in the thesis attached the appendix A.4. In deviation to our study, the approach adopted in the Master thesis involved CWC calculation as absolute values not distinguishing from which side the cross wind occurred, and Δ-values were calculated on an hourly base i.e. the weather of $date_i\ hour_j$ was compared to the $date_{i-1}\ hour_j$ instead of the comparison to the average values of the previous night (see chapter 3.7.1).

Bayesian models were fitted using the '*brms*' package (v. 2.22.0; BÜRKNER 2017). The GAMs were separately constructed for three response variables, to determine the effects of temporal, phenological and meteorological explanatory parameter on:

- the nocturnal MTR of passerines throughout the migratory seasons up to 1025 m (absolute migration traffic rate across the full vertical range)
- the nocturnal MTR of passerines throughout the migratory seasons at rotor height (25 – 180 m, absolute migration traffic rate at rotor height)
- the proportion of nocturnal MTR of passerines occurring at rotor height (25 – 180 m, relative migration traffic rate at rotor height).

All GAMs were fitted separately for the two migratory seasons.

For models on MTR up to 1025 m and at rotor height, a negative binomial distribution with a log-link was used to handle over-dispersed count data, providing more flexibility than a Poisson model (LINDÉN & MAENTYNIEMI 2011). For the negative binomial model, a smoothed effect of ydate (k = 30, both seasons) and of ProportionOfNight (k = 5, spring; k = 7, autumn) were applied to the mean μ of the negative binomial response (with a log link). A smoothed effect of ydate (k = 10) was applied to the precision parameter ϕ of the negative binomial response (with a log link).

Models predicting the proportion of birds flying at rotor height used a beta-binomial distribution with a logit-link, suitable for over-dispersed proportion data with an upper limit. For this beta-binomial models, a smoothed effect of ydate (k = 10, both seasons) and of ProportionOfNight (k = 5, spring; k = 7, autumn) were applied to the mean μ of the beta-binomial response (with a logit link). A smoothed effect of ydate (k = 10, spring; k = 5, autumn) was applied to the precision parameter ϕ of the beta-binomial response (with a log link).

Both model types incorporated splines for time-related effects, such as Julian date and proportion of night. Final models were fitted using four MCMC chains (Markov Chain Monte Carlo, i.e. an explicit method for sampling from probability distributions) with 5000 iterations each. To improve convergence and avoid divergences, adapt_delta was set to 0.95 and max_treedepth to 15.

Model performance was assessed using leave-one-out cross-validation (LOO) via the 'loo' R package (VEHTARI ET AL. 2024). Compared models differed only in the k-values (degrees of smoothness) for "ydate" and "ProportionOfNight", while other terms remained fixed. Models with significantly better ELPD scores (difference > 4 × standard error) were preferred (SIVULA ET AL., 2025).

Six models were selected (one per season for the different response variables). To avoid overfitting, the lowest k-values were chosen that did not lead to significant performance loss.

The following smoothing settings were used:

- Negative binomial model (MTR 25-1025 m):
    - 'ydate': k = 30 (both seasons)
    - 'ProportionOfNight': k = 5 (spring), k = 7 (autumn)
    - 'shape': k = 10
- Negative binomial model (MTR 25-180 m):

- ‘ydate’: k = 15 (both seasons)
- ‘ProportionOfNight’: k = 5 (both seasons)
- ‘shape’: k = 5

- Beta-binomial models (proportion at rotor height):
  - ‘ydate’: k = 10
  - ‘ProportionOfNight’: k = 5 (spring), k = 7 (autumn)
  - ‘phi’: k = 10 (spring), k = 5 (autumn)

MCMC sampling for our models was performed with Stan. We relied on Stan’s comprehensive range of built-in diagnostics to check for sampling problems. Stan automatically checks, among other things, for R-hat values, bulk- and tail-ESS, and divergent transitions (https://mc-stan.org/learn-stan/diagnostics-warnings.html). If an MCMC run passed Stan’s automatic checks, we then proceeded to check the model fit using posterior predictive checks (PPC).”

Results are presented in ‘MCMC interval plots’ (see e.g. Figure 4-13) which show the posterior uncertainty intervals (i.e. the Credibility Interval (CI), or, more precisely, a *Central tendency Interval*) of the explanatory variables. The closed symbols depict posterior medians, bold segments show the 50 % credible intervals, while the thin outer lines indicate the 90 % credible intervals. The x-axis is read as the effect size of variables, with negative values indicating negative association between the respective variable and MTR and vice versa. The y-axis lists the explanatory variables. Variables, where the CI values cross the x-intercept, can be regarded as having no significant effect on the response variable according to the model.

3.7.3 Number of rotor transits and its relation to wind turbine operational status

The number of birds flying through the rotor plane (‘rotor transits’, see chapter 3.4) was determined by manual inspection of the AI-detections from the camera systems. Birds that were detected by the cameras but did not cross the rotor plane were excluded from the analysis.

The number of rotor transits was determined for day and night separately. Day and night were defined based on civil twilight at the study site. Furthermore, we compared rotor transits during time periods where rotation speed of rotor blades was ≥2 rpm vs. rotation speed <2 rpm. It is commonly assumed that collision risk is substantially reduced when rotor speed is below 2 rpm, i.e. when turbines are idling or stationary. This threshold is also applied in onshore shutdown on demand procedures as well as in the Dutch start-stop procedure to mitigate collisions of nocturnally migrating birds at offshore wind farms[11]. Following this assumption, we counted rotor transits for collision risk assessment only when the rotor speed was 2 rpm or more.

[11] https://www.noordzeeloket.nl/en/functions-use/offshore-wind-energy/start-stop, last accessed 23.04.2025

To determine whether the number of rotor transits varied depending on wind turbine operational status, we adopted two approaches.

At first, we used descriptive statistics, presenting rotor transit rates by operational status. Transit rates were calculated by dividing the number of transits for each turbine operational status by the corresponding observation time. Although rotor speed data were available in 10-minute intervals, we used video footage to determine the operational status of the rotor at the time of each transit. This provided greater accuracy, as in some cases the average rotation speed for a 10-minute interval exceeded 2 rpm, even though the rotor was clearly stationary during a specific transit event — and vice versa.

In a second step, we included `rotation speed' as an additional continuous explanatory variable in the Bayesian model on the relationship between rotor transits and weather conditions, which is described in a following chapter (chapter 3.7.5).

As turbine A2 was non-operational due to maintenance work for an extended time period in autumn 2024 (25 days and 57 nights of analysed data), sample size for these analyses were high (see chapter 4.2.1).

3.7.4 Modelling the relationship between rotor transits and migration intensity at rotor height

To test the hypothesis that collision risk shows a proportional association with migration intensity at rotor height, we conducted two different analyses:

- Kendall's rank correlation test
- Generalised linear models (GLM) with a binomial distribution

We restricted these analyses to rotor transits during time periods where turbines were active (rotation speed ≥ 2rpm).

The number of rotor transits followed a Poisson distribution. As a first approach, we therefore performed simple non-parametric Kendall's rank correlation tests. We did this analysis separately for day and night hours. Day and night were defined based on civil twilight at the study site.

Furthermore, we implemented regression analyses in which we could include an offset for observation effort and include turbine ID next to MTR at rotor height (i.e. 25 – 180 m) measured by the bird radar as explanatory variables. Although the AVES system generally operated with high reliability, on some occasions one or more of the eight cameras per system failed to function (see chapter 3.4). To account for this variation in sampling effort, we estimated the monitoring effort per date and per camera system and included this effort as an offset term in the regression analyses. Turbine ID was used as an additional factor because the two turbines differed in their height and rotor diameter among others (see Table 3-1), which might influence the number of rotor transits.

However, given the rare event of transits when turbines were active the models ran separately for day and night did not perform well according to standard model diagnostic plots and tests for overdispersion. Model performance was evaluated using diagnostic plots with the R package DHARMa

(HARTIG 2024). We therefore combined the dataset of day and night to increase sample size and included the factorial variable 'DayOrNight' as an explanatory variable and the interaction term between 'DayOrNight' and MTR which allowed us to differentiate any effects of MTR on number of transits between day and night. Since models using Poisson distribution still did not perform well (not shown) and as only in four hours more than one transit occurred, we transformed the number of transits per hour into a binary response variable indicating whether a transit occurred or not within that hour. Accordingly, we used a binomial distribution in the generalized linear model with 'logit' link function (e.g. ZUUR ET AL. 2009). Diagnostic model plots showed that the model fitted well (see Figure A-2).

3.7.5 Weather dependency of rotor transits

For investigating the association between the number of rotor transits and weather conditions we used a generalized additive model (GAM), as we expected non-linear relationships of variables as often observed in biological systems (WOOD 2017). According to Wood (2017), GAMs are particularly well-suited to biological and ecological data, where relationships between variables are often complex and non-linear, and where flexible modelling approaches are needed to avoid overly restrictive assumptions.

Furthermore, we used a Bayesian approach for analysing the association of transits with a multitude of explanatory variables. In addition to producing better error estimates, a strong benefit of Bayesian analysis is that one does not need to account for multiple testing of various explanatory variables or of their interactions. Whilst in NHST, i.e. the standard frequentist approach, the likelihood of getting significant results (e.g. a p-value < 0.05) increases with the number of tests done, this is not the case in Bayesian statistic (KRUSCHKE 2015a).

As above (chapter 3.7.4), the original response (number of observed transits) was converted to a binary response variable (transit occurrence, yes/no). That binary response variable was modelled using a GAM (generalized additive model) with a binomial response and a cloglog (complementary to log-log) link function. We chose to use a cloglog link function because transit events had a very low probability in our datasets.

Explanatory variables included in the model were the day of year, season (spring/autumn), rotor rotation speed, MTR at rotor height and various weather parameters (precipitation, atmospheric pressure, temperature, visibility, cloudiness, TWC, absolute value of CWC). The effect of day of year was modelled as a smooth function, using a cubic B-spline basis of dimension k = 6. Atmospheric pressure and temperature were centred to a mean of 0 and scaled to a standard deviation of 1. MTR, precipitation, visibility, cloudiness, TWC, and CWC were scaled to a standard deviation of 1. Mean sampling effort was taken into account in the model by introducing an offset (log(mean effort)).

The Bayesian model was fitted using the function `stan_gamm4()` of the rstanarm package (CRAINICEANU ET AL. 2005) and its default priors. MCMC sampling of the parameter posteriors was performed using four chains and 4000 iterations per chain, of which the first half was discarded. The expected predictive accuracy of the full model was compared with that of a base model which contained only an intercept and the mean effort offset, based on ELPD (expected log pointwise predictive density) using the `loo` package. The ELPD difference between the full and the base

model was small (compared to its estimated standard error) and thus did not reveal any substantial difference between the expected predictive accuracy of the full model and of the base model. This indicated that adding the explanatory variables contained in the full model did not improve the model performance substantially when predicting transit occurrence probability. Nonetheless, since we were interested in the potential effects of the explanatory variables on transit probability we examined their estimated effects in the full model, but those should be considered as purely indicative of possible associations between the explanatory variables and the transit probability, which could be supported or disproved using larger datasets with more transit events in the future.

Relative effect sizes of the explanatory variables were visualized using credible intervals of the posteriors of the raw coefficients for the centred/scaled variables. However, since the model used a binomial response with a cloglog link function, it might be more informative to examine posterior conditional predictions of the effect of each explanatory variable on its original scale on the transit probability. We calculated those conditional predictions using day of year = 100, season = spring, and the mean values of the other explanatory variables on their original scale.

3.7.6 Estimating the expected number of birds passing through the rotor plane

To estimate the expected number of birds passing through the rotor area assuming no avoidance response, we used the MTR data as the primary input. Expected bird transits form the basis for subsequent empirical estimation of avoidance rates. The estimation process involved the following main steps, which are further explained below:

- calculating MTR at rotor height on a monthly basis per turbine
- estimating theoretical transits through the rotor area using the proportion of the rotor area in relation to the area the MTR was calculated for

For each turbine, the exact MTR was calculated per hour and per metre height band within the rotor area. These values were then averaged for the turbine-specific altitude range and per date, separately for day and night. For two turbines (A3 and A5, Table 3-1) the lower rotor tip extended below the radar's lower detection range (25 m). In these cases, the mean MTR was calculated assuming that MTR at the lower ~5 m of the rotor area was similar to the overall mean of the rotor area. As the lower 5 m of the rotor area represent only a very small proportion of the total rotor area this uncertainty was considered negligible. In summary, two MTR values were derived per turbine and per date: one for daytime and one for nighttime.

Using the calculated MTR values, we estimated the number of expected bird transits per turbine and per date, separately for day and night. Since the MTR is defined as the number of birds per hour per kilometre for a given altitude range, we first calculated the fraction of one kilometre represented by each turbine's rotor diameter (i.e. diameter in metres divided by 1000). Secondly, as the MTR reflects birds crossing an imaginary vertical plane forming a rectangular shape, we applied a correction to account for the circular shape of the actual rotor area. Specifically, we multiplied the number of expected bird transits by the ratio of a circle's area to that of the enclosing rectangle (i.e. the fraction of area the rotor circle occupies within the equivalent square).

Finally, we multiplied the mean MTR per day and night by the number of hours of daylight or darkness per date.

The final equation for daytime or nighttime expected transits estimation is given below:

$$n\_\text{transits\_expected} = \sum_{d}\sum_{t=1}^{5} MTR_{t,d} * fractionKilometre_t * fractionRectangle * n_{hours_d} * diameter_t$$

Where:

- t = turbine ID (1 to 5)
- d = date
- MTR $_{t,d}$ = MTR (birds/hour/km) for turbine *t* on date *d*, either for daytime or nighttime
- *FractionKilometre*$_t$ = turbine *t* rotor diameter (m)/1000
- *fractionRectangle* = area of rotor circle/area of enclosing square
- *n_hours*$_d$= number of daytime/nighttime hours per specific date
- diameter$_t$ = rotor diameter of turbine *t,* in meters

The expected numbers of transits were then summed across all five turbines per month to derive total monthly transit rates, which served as input for the estimation of avoidance rates and subsequent collision risk models (CRMs, see chapter 4.3.2).

3.7.7 Estimation of avoidance rates from expected versus actual rotor transits

To estimate the actual avoidance rates of birds at the study site during daytime and at night, we first calculated the expected number of rotor transits for the two turbines at which AVES systems were installed (A2 and A4) as described in chapter 3.7.6 above.

We then compared these estimates with the actual number of rotor transits recorded by the cameras. As stated above, we included only transits that occurred while the rotor was operating at a rotation speed of ≥ 2 rpm.

Furthermore, we corrected the number of actual transits to account for

- Downtime of cameras: we calculated a correction factor based on the availability of the cameras
- Missed rotor transits due to collisions: we accounted for the fact that the camera systems could not systematically record collisions which would lead to an underestimation of actual rotor transits and consequently to an overestimation of calculated avoidance

rates. To do this, we calculated the number of missed collisions based on actual rotor transits and the 'single transit risk' for nocturnal species (using Redwings (Turdus iliacus) as substitute) and diurnal species (Wood pigeon (Columba palumbus)) for each of the two turbines equipped with camera systems. For this calculation, we used the 'single_transit_risk' function of the Band CRM, provided in the R package stochLab (CANECO ET AL. 2022). These collision estimates (see Table A-1) were subsequently used to adjust the number of rotor transits recorded by the AVES system.

Since only a subset of days from the AVES data was analysed, we selected the corresponding subset of the MTR data. Additionally, we multiplied the number of transits by two, as each camera system monitored only one (vertical) half (180°) of the rotor area.

The final equation for estimating the expected number of transits was as follows:

$$n\_\text{transit\_expected} = \sum_{h}\sum_{t=1}^{2} MTR_{t,h} * \frac{fractionKilometre_t}{2} * fractionRectangle * fractionRadarbin_{25_{180}}$$

Where subscript t denotes the turbine ID and h the hour.

The expected number of transits was then compared with the actual number of transits recorded by the AVES offshore monitoring systems. This analysis was conducted separately for daytime and nighttime periods. To calculate the avoidance rates, we used the following equation:

$$Avoidance\ rate = 1 - \frac{actual}{expected}$$

Please note, that the avoidance rate calculated here represents the parameter by which the number of rotor transits is estimated based on a given mean MTR at rotor height. It does not necessarily imply that all birds that do not pass through the rotor plane exhibited an active avoidance response (see also 'oblique approach' BAND 2012).

3.7.8 Estimation of avoidance rates based on fatality searches and MTR

In addition to calculating avoidance rates based on detected rotor transits, we used a second method using estimated fatality numbers (by PCFM) and data on MTR as originally suggested by BAND (2012). This method is independent of the calculated number of rotor transits and can therefore also be used to evaluate the plausibility of the camera data. We applied the simple equation as given in BAND (2012 p 26, § 79):

$$A_{\text{overall}} = 1 - \frac{\text{actual collision rate}}{\text{predicted collision rate if preconstruction levels of flight activity were maintained}}$$

Where 'actual collision rate' is the estimated number of collision victims found during PCFM. 'Predicted collision rate if pre-construction levels of flight activity were maintained' is equal to results of the CRM when avoidance rate is set to zero.

As we cannot determine the exact time collisions took place, with this method we cannot distinguish between day and night with regard to the avoidance rate, and we therefor calculated avoidance rate combined for day and night.

3.7.9 Number of collision victims identified through carcass searches

Field data processing before modelling

The field data used in this analysis comprised:

- the locations of the turbines, as well as the location and shape of the searched subareas around each turbine
- a visibility dataset recording the visibility level for each subarea on each field search date; and
- a carcass dataset containing the date, location, species and size class of each carcass found in the field.

In addition to these core design and carcass data, datasets from (i) carcass persistence trials and (ii) searcher efficiency trials were also used. Hourly rotor speed measurements were provided for each turbine.

Carcass data

The carcass dataset was processed as follows to ensure the highest possible reliability of the data used in the fatality model. First, carcasses identified as body parts from the same individual were merged into a single record. The assigned location for each merged carcass was calculated as the average of the recorded locations of the body parts. Second, minor location adjustments were made for a few carcasses that had been recorded very close to the searched subareas. These adjustments placed the carcasses within the nearest subarea, under the assumption that the discrepancy was due to GPS inaccuracy (typically ± 5 m). Carcasses found more than 10 m outside a searched subarea were considered off-plot finds and, following the recommendations of the *International Finance Corporation good practice handbook and decision support tool* (INTERNATIONAL FINANCE CORPORATION 2023), were excluded from fatality estimation. Third, another three carcasses were excluded as they were considered unlikely to be true collision victims. They were found during a period in which the nearest turbine had been inactive for at least more than three weeks, based on rotor speed data.

Rotor rotation speed data

Rotor rotation speed was used to determine whether a given turbine was operating or non-operating during each hour, using a threshold of 2 rpm. In rare events (1.2 %), for some turbines, hourly rotor speed measurements were missing. The missing values were replaced by the proportion of available records indicating the turbine was active.

Fatality model

Overview

The fatality model estimated the total number of collision victims over the study period, accounting for the imperfect detection of carcasses found in the field. The mathematical framework used in this analysis is based on the work of Dalthorp, HUSO AND DAIL (2017), DALTHORP ET AL. (2018), and DALTHORP ET AL. (2023a), and on the documentation from the corresponding R packages (DALTHORP ET AL. 2017, 2023b; DALTHORP & HUSO 2023).

In essence, the model estimates the true number of collision victims from the carcasses found in the field by accounting for:

- the size, shape, and location of each searched subarea in relation to its associated turbine mast
- the expected carcass dispersion as a function of distance from turbine masts
- the visibility conditions of each subarea at the time of search, along with searcher efficiency under these conditions
- the persistence time of carcasses in the field before disappearance (e.g., due to scavenging or decomposition)
- the operational schedule of each turbine, based on measured rotor rotation speed

Bird size is accounted for by conducting the fatality analysis separately for small, medium-sized, and large birds. To achieve this, the carcass dataset was divided into these three size categories, which were also applied consistently in the carcass persistence trials and searcher efficiency trials.

Due to the limited number of carcasses found, a single dispersion analysis was performed using all carcasses pooled across size categories. The resulting dispersion pattern was then applied uniformly across all size classes.

The mathematical formulation of the fatality model is provided below. The model was implemented in R using Stan, which applies a Hamiltonian Monte Carlo algorithm to sample from the Bayesian posterior distribution via MCMC.

Core model

The core model defines a base fatality rate λ_0 (also referred to as the base carcass arrival rate), for the wind farm over the study period. This rate represents the average number of birds killed per turbine per day (unit: birds/turbine/day) for an operating turbine and is estimated by the model. It is assumed to be constant over the study period and identical across all turbines at the site.

For each turbine U_i, an effective fatality rate $\lambda_i(t)$ is defined by multiplying λ_0 by 1 or by 0, depending on whether the turbine is operating at time t, as determined by its rotor rotation speed.

Then, for a given subarea E_{ij}located near turbine U_i, the fundamental relationship between $\lambda_i(t)$ and the number of observed carcasses Y_{ij} in that subarea is given by:

$$\lambda_{ij} = dwp_{ij} \times \int_{t_0}^{t_f} \lambda_i(t)dt$$

$$M_{ij} \sim Poisson(\lambda_{ij})$$

$$Y_{ij} \sim Binomial(M_{ij}, g_{ij})$$

where:

- λ_{ij} is the expected number of carcasses in subarea E_{ij} during the study period
- dwp_{ij} is the proportion of birds killed by turbine U_i that are expected to fall within subarea E_{ij} associated with that turbine. This corresponds to the *density-weighted proportion* value as described by DALTHORP AND HUSO (2023). Its value depends on the geometry of the subarea relative to the location of the turbine mast on the dispersion function used to model carcass fall distances. The dispersion function is estimated from the observed distances between turbine masts and detected carcasses, using the dwp R package (DALTHORP & HUSO 2023)
- $\lambda_i(t)$ is the effective fatality rate for turbine U_i, as defined previously, accounting for variation in turbine operation over time
- M_{ij} is the true (but unobserved) number of bird fatalities that fell into subarea E_{ij} during the study period
- g_{ij} is the probability of detecting a carcass that fell into subarea E_{ij} during the study period. In other words, given that a carcass fell into the subarea, g_{ij} is the probability that it was detected at some point during the study. The value of g_{ij} depends on the timing of fatality events, carcass persistence, the search schedule, visibility conditions during searches, and searcher efficiency.

A crucial part of the model is the estimation of dwp_{ij} and g_{ij}.

Estimating carcass dispersion

The value of dwp_{ij} depends on the shape and location of the subarea E_{ij} and on the distribution of carcass distances from the turbine masts. This distribution is estimated outside of the Stan model, using the dwp package. The dwp package takes the turbines and subareas shapefiles, the location of all the carcasses found, as well as the search schedule and visibility information, and fits several candidate distributions to the data. Since we were unable to directly incorporate temporal variation in subarea visibility into the model, we accounted for changes in search status by duplicating each subarea geometry, once for each search date. Each duplicated subarea instance was assigned the visibility conditions present on its corresponding search date. Detected carcasses were then associated with the appropriate subarea instance based on their observation date.

Distribution models fitted with dwp on the carcass, and subarea data were scored using the dwp::modelFilter() function. The models were selected based on whether they fulfilled at least four out of five model selection criteria: (i) extensibility (predicted number of carcasses outside of searched subareas must be finite), (ii) left and (iii) right tail plausibility (thresholds applied on the predicted proportions of carcasses falling too close or too far from the turbine), (iv) absence of high influence points and (v) ΔAICc value <10 compared to the model with the lowest AICc value (DALTHORP & HUSO 2023) Among those selected candidates, the best model was chosen based on visual inspection of the candidate pdfs and consideration of which criteria were fulfilled/missed by each model.

In this project, we selected a Maxwell-Boltzmann (MB) distribution as it provided the most satisfactory fit to the observed carcass distances. Using the dwp::ddSim() function, we generated a large number of plausible values for its characteristic parameter based on the fit obtained with the dwp package. These values were then used to define a reference prior distribution for the carcass dispersion function, which was incorporated into the Bayesian fatality estimation model.

We further imposed an upper limit on the radius within which 95 % of the carcasses were expected to fall, based on the turbine heights in this study and on dispersion patterns estimated in a comparable study conducted by BioConsult SH. For the present analysis, we used a threshold of 156.7 m, assuming that 95 % of carcasses must fall within this radius. This assumption is consistent with the mean turbine height of 161.7 m for the five turbines at the wind farm.

Estimating probability of carcass detection

The calculation of g_{ij} , the probability of detecting a carcass that fell into subarea E_{ij} during the study period, involves decomposing this probability by integrating over all possible carcass arrival times within the study period and all potential detection times during the scheduled field searches.

For all possible pairs of arrival times and detection times, the resulting probability of detection is calculated based on (i) the probability that the carcass could persist until detection time (based on the carcass persistence trials) and (ii) the probability that the carcass was detected by field searchers in the current visibility conditions (and undetected at previous searches, if any) based on the searcher efficiency trials. Once those probabilities are calculated, they are weighted by the relative arrival rate of carcasses for that particular turbine, depending on the considered arrival times and on the turbine activity schedule (based on measured rotor speed).

Carcass persistence

We used a survival analysis approach as given in the GenEst R package (DALTHORP ET AL. 2023b) to estimate carcass persistence. The candidate persistence functions included the exponential, Weibull, log-normal and log-logistic distributions. Size class was incorporated as a covariate for both the location and scale parameters of these distributions (except the exponential distribution, which only includes a location parameter).

The model selected for downstream analyses was chosen from among those retaining an effect of the size class covariate on either the location or scale parameter, based on differences in AICc and the relative simplicity of the distribution. The exponential distribution, being the simplest of the four distributions, as it only includes a location parameter.

Once the final model was selected, we used the GenEst::rcp() function to generate a range of plausible values for its parameter(s). These were then used to define a reference prior distribution for the carcass persistence function, which was subsequently incorporated into the Bayesian model for fatality estimation.

Estimating searcher efficiency

Based on the carcass persistence trials, we used the GenEst package to estimate searcher efficiency as the probability $p_{size,vis}$, representing the likelihood that a carcass of a given size class would be detected during the first search following its fall, under specified visibility conditions. We estimated $p_{size,vis}$ separately for each carcass size category and for each visibility level and used the distributions of parameter estimates provided by GenEst as priors to the Stan model.

The fatality model also defines a k parameter ($0 \leq k \leq 1$), which is applied as a multiplicative factor to correct $p_{size,vis}$ for each subsequent search as long as a carcass remains undetected. Since we could not estimate k from field trials (because undetected trial carcasses were not left for subsequent searches), we used a beta prior with mean of 0.5 and standard deviation (SD) 0.1.

Estimating total numbers of fatalities

Once the model produced a posterior for the λ_0 parameter, we generated the predicted number of fatalities occurring over the study period by sampling the number of missed (i.e. undetected) carcasses for each turbine and adding it to the number of actual observations.

We ran the model and obtained estimated fatalities for each size class. We then summed up the predicted fatalities for the three size classes to obtain an overall number of bird fatalities predicted over the study period.

Validating the model

Validation of the Stan model was performed by simulating data: many datasets were generated by drawing parameter values from the model priors, and the Stan model was run on those simulated datasets. The true values for λ_0 and for the fatality numbers in those datasets were then compared to the model posteriors. This allowed us to assess the absence of bias in the point estimates and to evaluate the calibration of the credible intervals derived from the posterior distributions, based on the frequency with which they contained the true parameter values.

3.7.10 Validation of the Band Collision risk models

We validated the outcome of the Band model by comparing the model results with the determined number of collisions based on the collision victim searches. We implemented the stochastic Band model using the R package `stochLab' (CANECO ET AL. 2022) to estimate the expected number of collisions for the entire wind farm.

Since the model produces monthly fatality estimates, we ran it using the monthly averages of MTR. The MTR values were calculated from radar data collected between 15 May 2023 and 30 November 2024, covering the same period as the collision victim searches.

As the study site held five different turbines, each with unique attributes such as size and rotor speed (Table 3-1), we run CRMs separately for each turbine and combined the estimates to obtain the overall collision estimate for the entire windfarm.

For each turbine, we calculated the monthly non-operating time, defined as periods when rotor speed was below 2 rpm, separately for day and night. We also computed the mean and standard deviation of rotor speed during operation, as well as the mean and standard deviation of pitch angle. Since pitch data for one turbine was missing, we used the average pitch values from the other four turbines as substitute data. Together with the exact rotor size, hub height, and lower rotor tip height of each turbine, this information was used to inform CRMs. Because blade profiles for the turbines were unavailable, we used the default profile for a 5 MW offshore turbine built into the stochLAB package (CANECO ET AL. 2022).

Using the actual MTR for each month, and FHD values separately for day and night (see below for details), we ran one daytime and one nighttime CRM for each turbine covering the entire study period. For each scenario, we performed 10.000 iterations to obtain a precise estimate of the variance.

To validate the Band model, we estimated the total number of collisions summed across all five turbines and compared these results with the PCFM estimates. We ran the CRMs using three different avoidance rates: i) a 'standard' avoidance rate for nocturnal migration, set at 0.98, which also aligns with the higher rate reported by SCHULZ ET AL. (2014), ii) a rate of 0.9662 representing the lower value reported for nocturnal migration by Schulz et al. (2014), and the avoidance rates estimated in the present study: 0.9987 during nighttime and 0.9986 during daytime (see chapter 4.3).

FHD for day and night was calculated from radar data provided in 1 m altitude bins. To smooth out minor inaccuracies in the original data, we summed the MTR values from 1 m bins into 3 m bins. This resulted in MTR values per 3 m bins spanning from 25 m to 1025 m in altitude (with the final bin consisting of only one 1 m bin). Since two turbines had a lower rotor tip height (LRTH) of 20 m, we lacked MTR data for the lowest 5 m. We substituted this missing data by using the values for the lowest 3 m bin (25-27 m).

We further smoothed the FHD data by fitting local polynomial regressions using the `loess' function from the `stats' package (R CORE TEAM 2022). The resulting FHD values were then normalized to sum to 1, as required by the `stoch_crm' function in the `stochLab package' (CANECO ET AL. 2022). Please note that during the smoothing process, the values of the lowest two bins (19 m to 21 m and 22 m to 24 m) were also smoothed based on the polynomial regression, resulting in values slightly different from the 25 m to 27 m bin values originally used as substitute data.

We compared the FHD across seasons and years, as well as for day and night, to identify any notable differences in the distribution shape. Visual inspection revealed considerable differences between day and night (see Figure 3-13), while seasonal and yearly differences were less pronounced. Therefore, we used two separate FHDs in the CRMs: one for day and one for night. Consequently, the CRMs for the five turbines were run twice each to obtain separate estimates for daytime and nighttime. These estimates were then summed to produce the overall collision estimate for the wind farm.

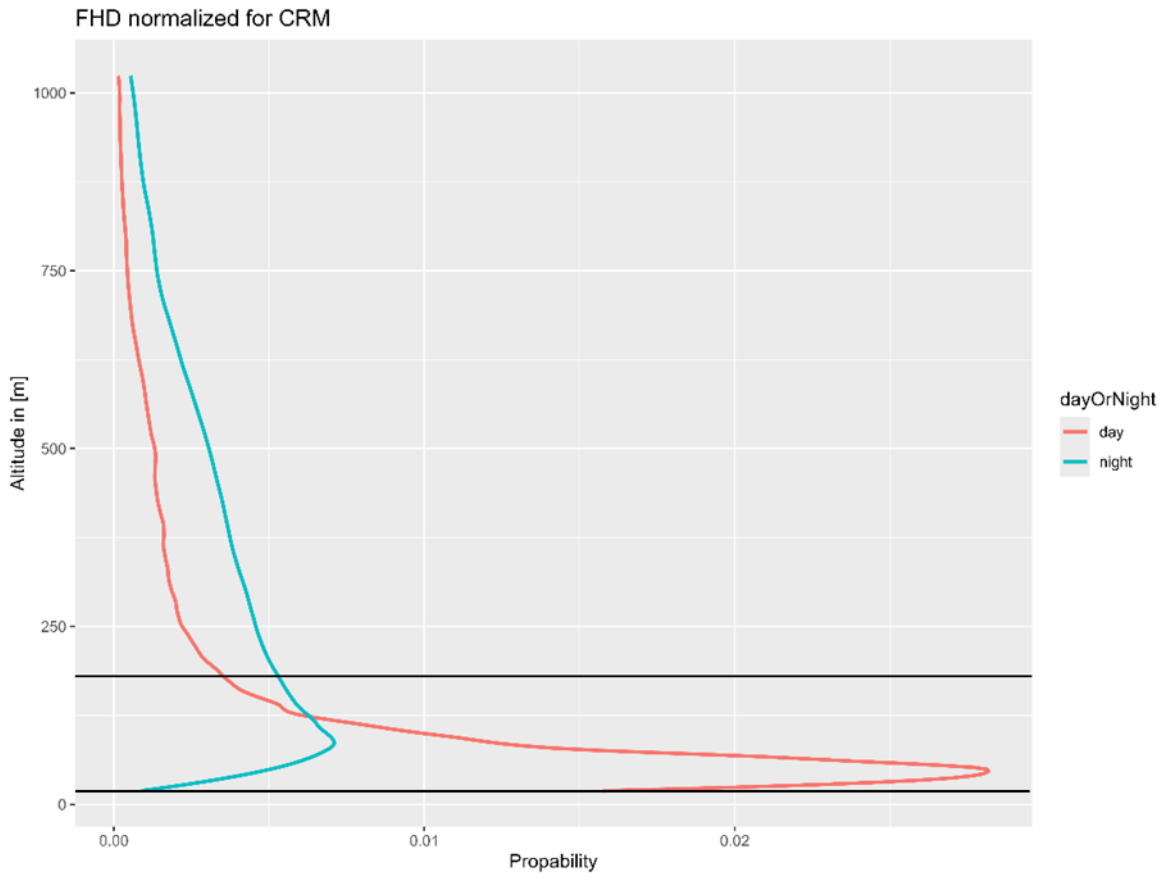

Figure 3-13 Flight height distribution for day (red line) and nighttime (blue line) based on MTR measured by bird radar. Values were normalized so that the sum of day and nighttime is 1 each. Horizontal black lines indicate the lower and upper limit of the rotor zone at the wind farm (20-180 m).

In the CRM, we used body size and flight speed data from two different bird species as proxies for daytime and nighttime species. For daytime, we selected the Wood pigeon (*Columba palumbus*), as, on average, larger birds were flying during the day (mtr.large_bird = 11.95 during day versus 5.23 at night; see Figure 4-5 and Figure 4-6) in that area, for nighttime, we used the body size and flight speed data from Redwings (*Turdus iliacus*) which is a typical passerine nocturnal migrant.

3.7.11 Bird calls

Due to the high sensitivity of the acoustic recorder, a vast number of sounds were recorded, resulting in a dataset comprising multiple million recordings. To manage this big dataset, we utilised the openly available AI tool Merlin from the Cornell Lab of Ornithology, USA[12]. The algorithm analyses recorded sounds and assigns a bird species label along with information on confidence level ranging from 0 to 1 for each detected sound. Most sounds received very low confidence scores, often indicating background noise. Therefore, the first step in our data processing was to filter out all sounds with confidence levels below 0.15. Even after this filtering, the dataset still contained mainly

[12] https://merlin.allaboutbirds.org/ last accessed 18.07.2025

background noise. To improve the reliability of the dataset, we subsequently assessed the accuracy of the AI's species-level identification performance as described below.

To verify the accuracy of the AI identification, we randomly selected a subset of the nighttime data for analysis by human bird call experts. A total of 29 nights were reviewed by the experts without any prior knowledge of the AI bird identification.

By comparing the expert's results with the AI labels, we classified each sound into one of three categories:

- True Positive (TP): e.g., a Redwing call correctly identified by the AI as a Redwing
- False Positive (FP): e.g., a sound incorrectly identified by the AI as a Redwing call, but actually belonging to another species or background noise
- False Negative (FN): e.g., a Redwing call present in the recording that the AI failed to detect or misclassified as another species.

Given these results, we determined, for each species, the minimum confidence level at which the AI model achieved a specified accuracy threshold. Accuracy was calculated as follows:

$$A = TP_c \,/\, (TotalCalls + FP_c)$$

Where TP_c and FP_c are the numbers of true positives and false negatives at a given confidence level c; TotalCalls is the sum of all $TP + FN$. TotalCalls was summed for all calls regardless of the confidence level. As the confidence level increases, both FN and TP were progressively filtered while $TotalCall$ remained constant. When TP were filtered out by a given confidence level, they were counted as FN.

The AI performance varied markedly between species (see chapter 4.6). To reliably estimate accuracy, a minimum number of calls per species is required. We therefore selected a subset of species for which the experts identified at least 10 positive calls (see Table A-8). We then visually inspected diagnostic plots showing accuracy by confidence level for each species and chose a species-specific confidence threshold that balanced accuracy and loss of true positives. Since not all species reached a sufficiently high accuracy level, only a subset of species was included in further analyses (see Table A-8).

4 RESULTS

4.1 Radar data

4.1.1 Migration intensity at the study site

Migration intensity followed the expected seasonal pattern for this location (Figure 4-1). Peak MTR values during autumn migration were substantially higher than those observed in spring, especially at night. The duration of migration also appeared to be longer in autumn compared to spring. Table 4-1 gives the mean MTR values for day and night separately (25 – 1025 m altitude), over the whole study period and as expected, shows higher mean MTRs during the nighttime than during the day-time (day = 208.1, night = 322.7).

In contrast, mean MTRs at rotor height (25 - 180 m) were higher during the day than during the night (Figure 4-2). This pattern is likely caused by local breeding and primarily resting birds which are common at the study site and tend to fly lower than migrating birds.

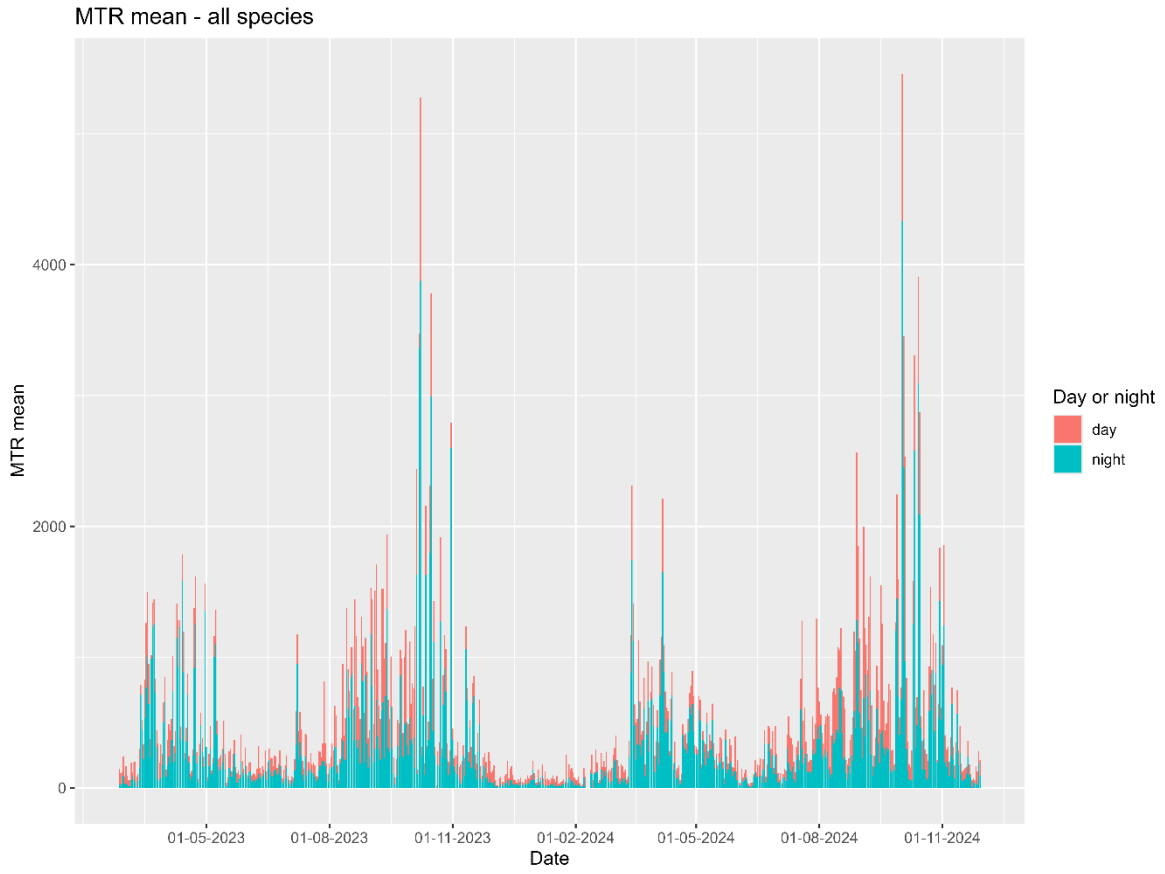

Figure 4-1 *Mean migration traffic rate (MTR), i.e. mean number of birds per hour crossing a virtual 1 km line, for the altitude range 25-1025 m per date across the study period, covering four migration seasons. `Red' indicates mean daytime MTR and `blue' mean nighttime MTR.*

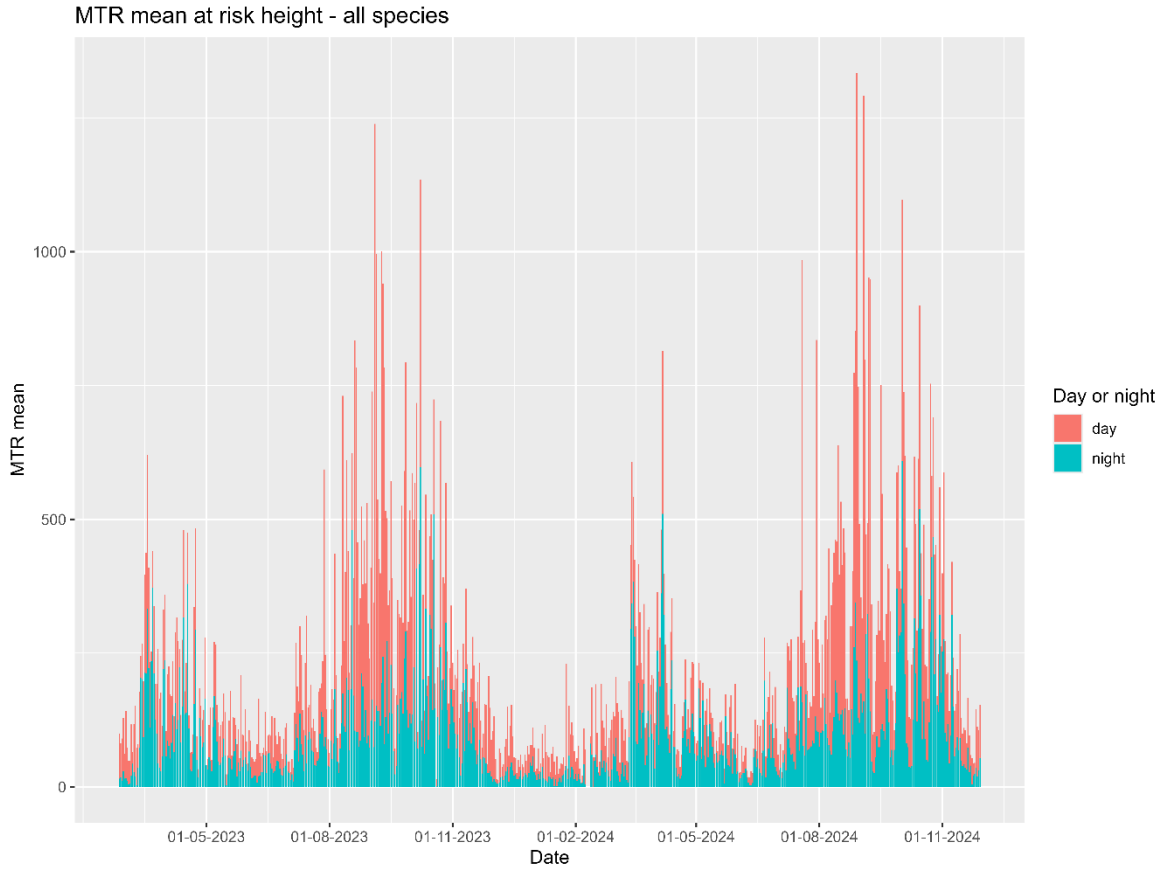

Figure 4-2 *Mean migration traffic rate (MTR) at rotor height only: 25 – 180 m, for details see caption of Figure 4-1.*

Nocturnal mean MTR at rotor height is shown separately in Figure 4-3. Flux rates above 250 MTR occurred regularly during all migration seasons but nights with very high migration intensities above 500 MTR were recorded only five times and almost exclusively during autumn migration (Figure 4-3).

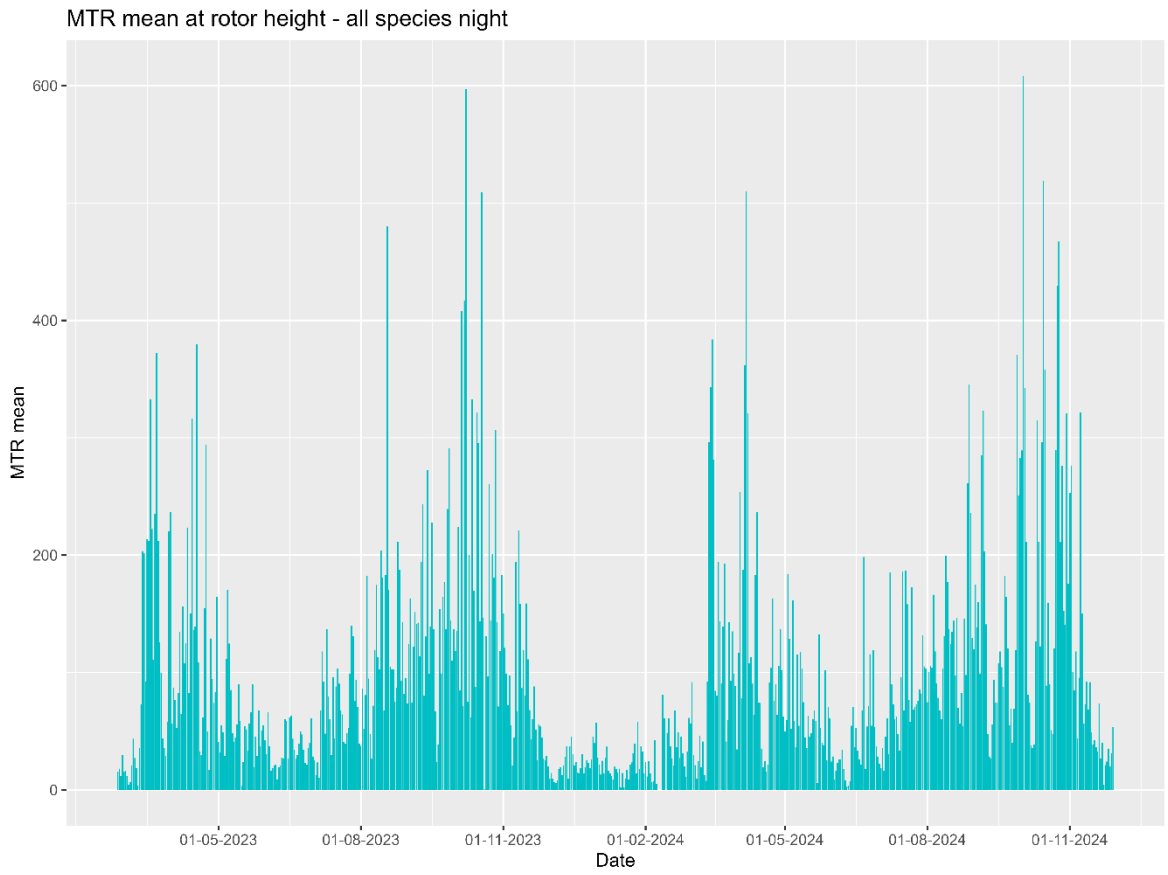

Figure 4-3 *Mean migration traffic rate (MTR) at rotor height during night only: 25 – 180 m, for details see caption of Figure 4-1.*

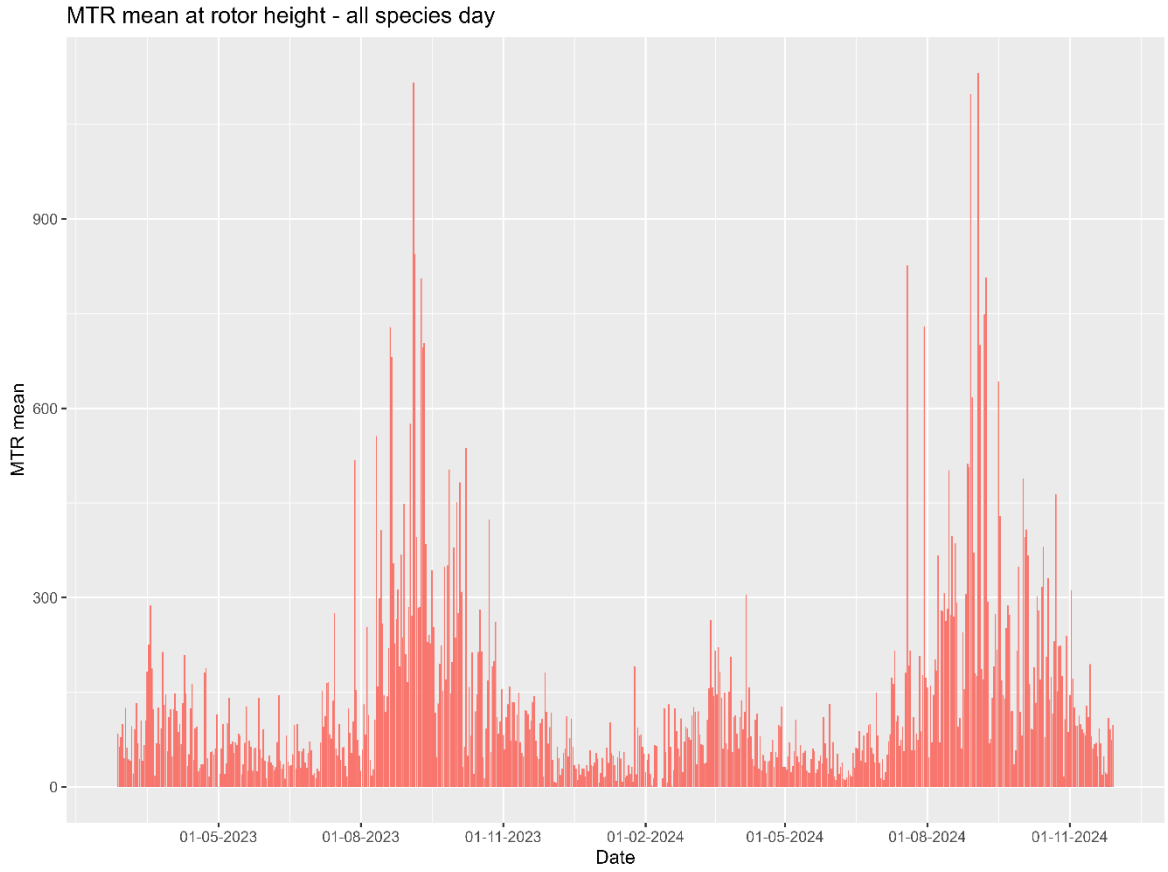

Figure 4-4 *Mean migration traffic rate (MTR) at rotor height during day only: 25 – 180 m, for details see caption of Figure 4-1.*

Summing up all MTR values, it is estimated that more than 3.5 million birds passed over a theoretical 1 km line during the main study period (15 May 2023 to 30 November 2024) at the altitude range up to 1025 m (Table 4-1). About 53 % of these birds were recorded during the night. Extrapolated to the total width of the wind farm, a total of 4.2 million birds passed through and over the wind farm during the study period.

Table 4-1 *MTR of all bird species summed across the entire height distribution covered by the radar (25 - 1025 m). The study period (15 May 2023 to 30 November 2024) corresponded to the period when carcass searches were conducted. The width of the windfarm (WF) perpendicular to the migration direction was 1.2 km.*

Day or Night	MTR sum	MTR mean	MTR sum x WF width (1.2 km)	MTR mean x WF width (1.2 km)
day	1673772	208.1	2008526	249.7
night	1856930	322.7	2228316	387.2
Total	**3530701**	**265.4**	**4236841**	**318.5**

The percentage composition of bird groups identified by the radar (i.e.: 'large bird', 'bird flock', 'swift type', 'passerine type', 'wader type', and 'unidentified bird') varied between diurnal and nocturnal migration (Figure 4-5 and Figure 4-6). Both during day and night, the by far most frequently detected bird group was the 'passerine type' followed by 'swift type'. However, as expected, the

proportion of `passerine type' birds were substantially higher at night than during day (72 % versus 41 %). At the same time, 'swift type' and 'large birds' constituted considerably higher proportions during daytime.

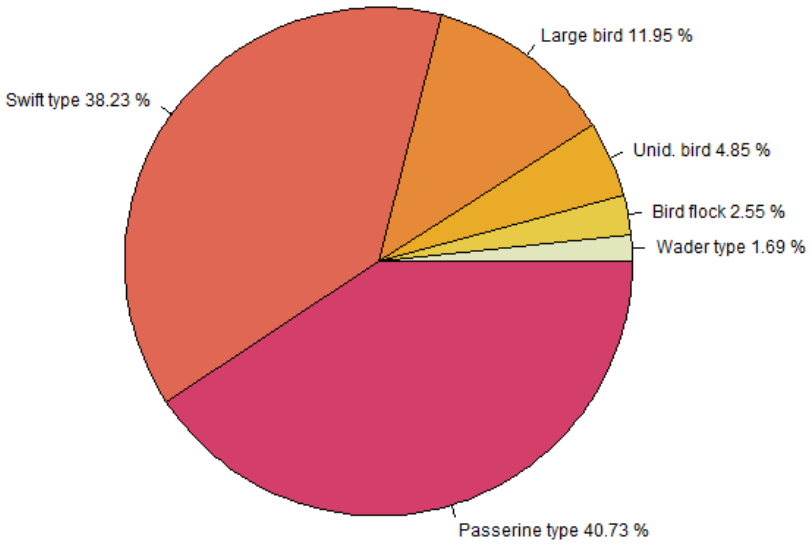

Figure 4-5 *Percentages of `bird type' groups identified by the radar during the daytime across the entire study period. The pie chart displays the relative composition of six bird group categories based on radar detections during the day.*

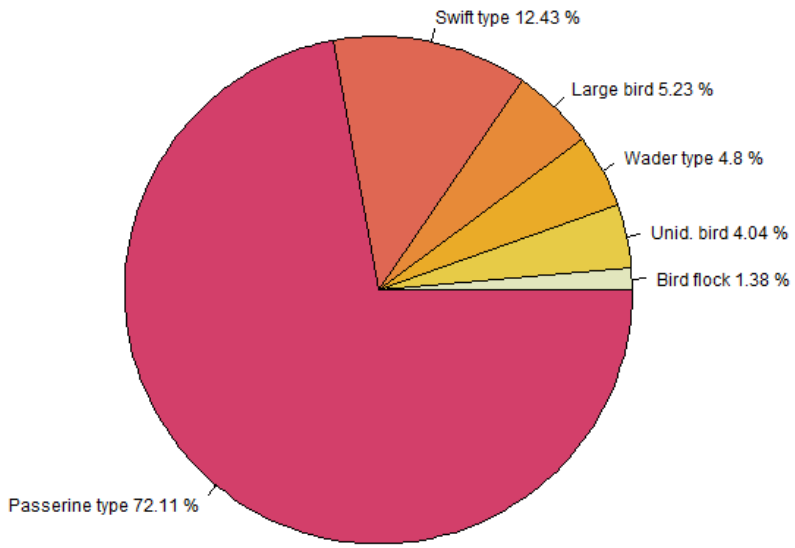

Figure 4-6 *Percentages of `bird type' groups identified by the radar during the nighttime across the entire study period. The pie chart displays the relative composition of six bird group categories based on radar detections during the night.*

4.1.2 Flight height distribution (FHD)

The flight height distribution, combined across all bird groups identified by the radar did not show notable differences between the years (Figure 4-7), but clear differences were observed between day and night (Figure 4-8), and to some degree between seasons (Figure 4-11 and Figure 4-12) and bird classes identified by the radar (Table 4-2).

In general, similar patterns are apparent and have been repeatedly shown at offshore sites in German waters of the EEZ. Diurnal migration concentrated to a higher degree within the lowest 200 m compared to nocturnal migration. Similarly, the proportion of birds flying low was reduced during spring compared to autumn, particularly during the night.

Table 4-2 Percent flying at rotor height (25-180 m). N = 4036477. Please note that in 'All bird classes' the radar signal category of 'unidentified bird' is included.

Period	All bird classes	Passerine	Non-Passerine
Total	45.3	43.9	71.1
Total day	70.3	70.0	84.4
Total night	30.9	34.9	45.3
Spring	37.2	39.2	55.3
Autumn	47.0	44.2	76.0
Spring day	60.5	61.5	72.5
Spring night	28.4	33.0	35.5
Autumn day	72.8	71.8	87.6
Autumn night	30.6	34.1	47.9
Year 2023	44.6	42.7	71.3
Year 2024	46.0	45.1	71.0

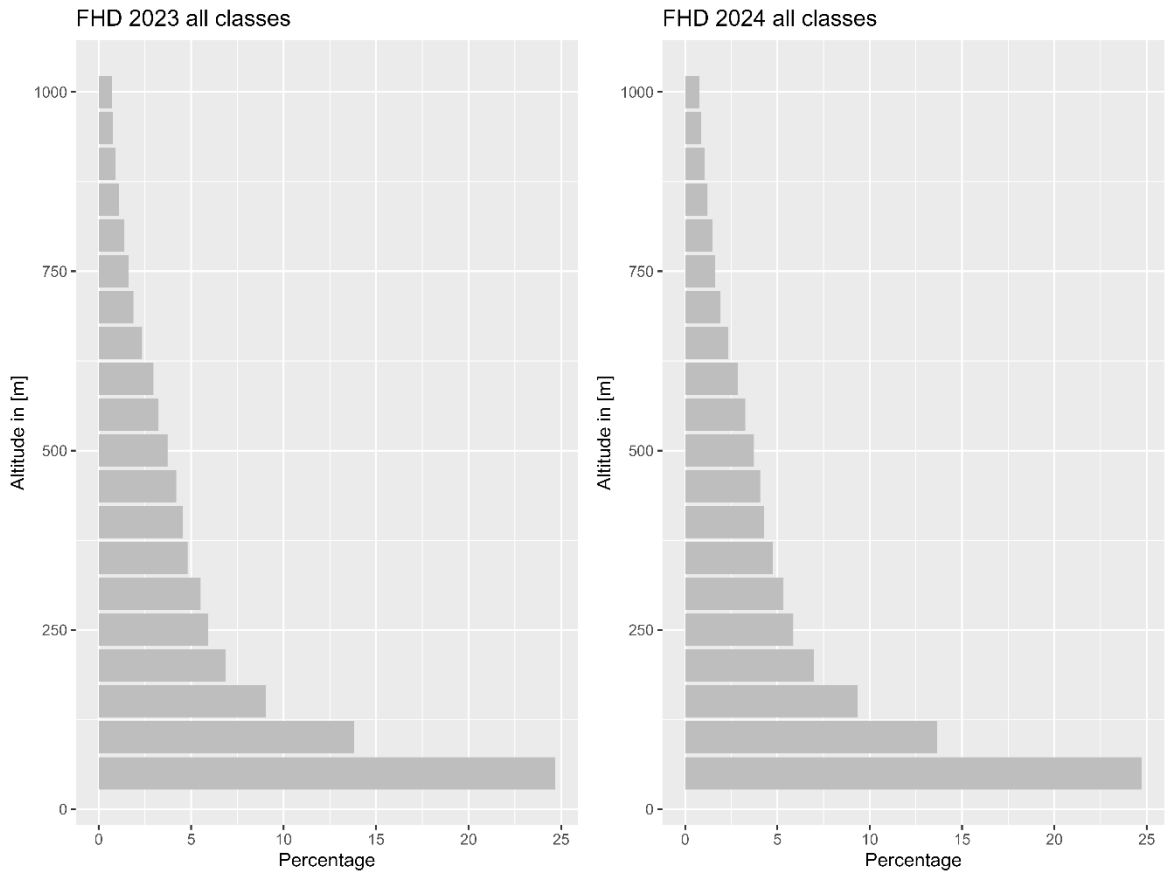

Figure 4-7 Flight height distribution combined for all bird species in percent for the years 2023 (left) and 2024 (right), including both daytime and nighttime data.

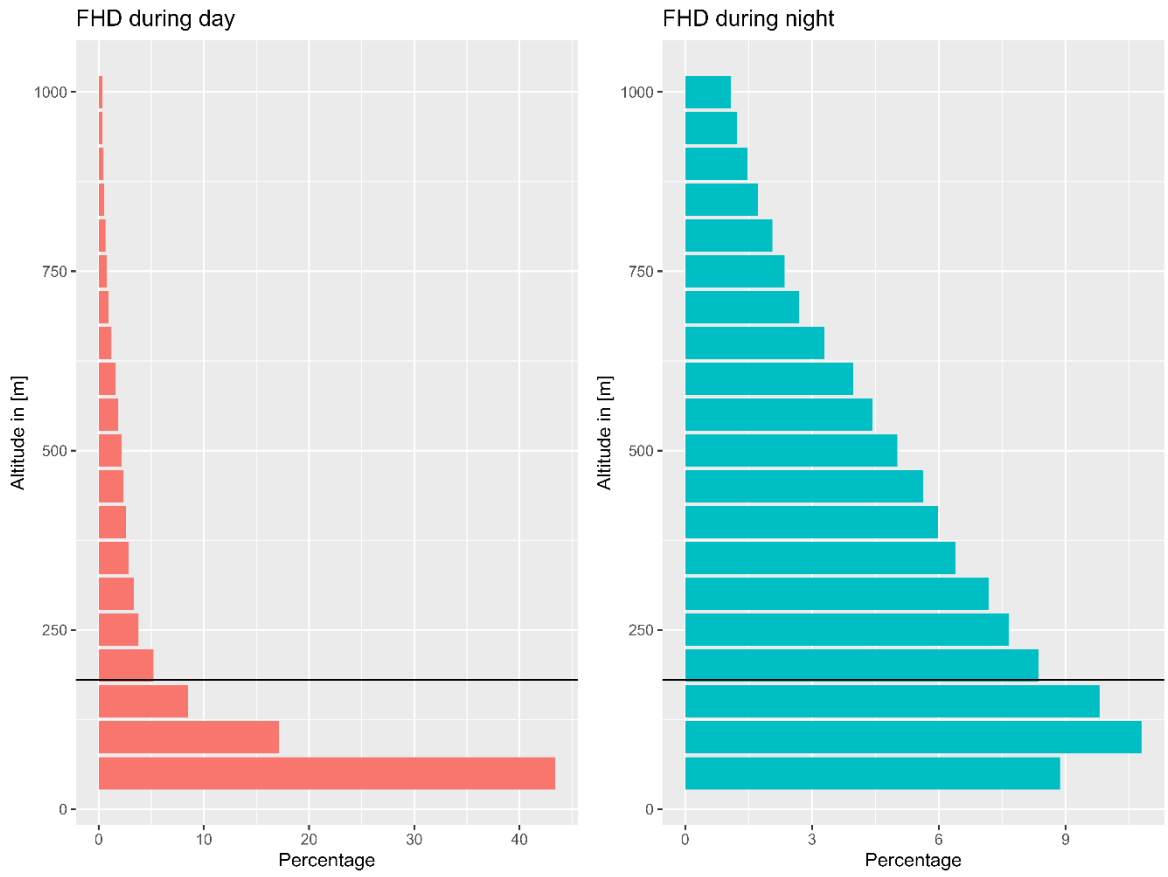

Figure 4-8 *Flight height distribution combined for all bird species in percent and separated by day (left) and night (right) across the entire study period. The horizontal black line indicates the upper rotor height (180°m) within the wind farm.*

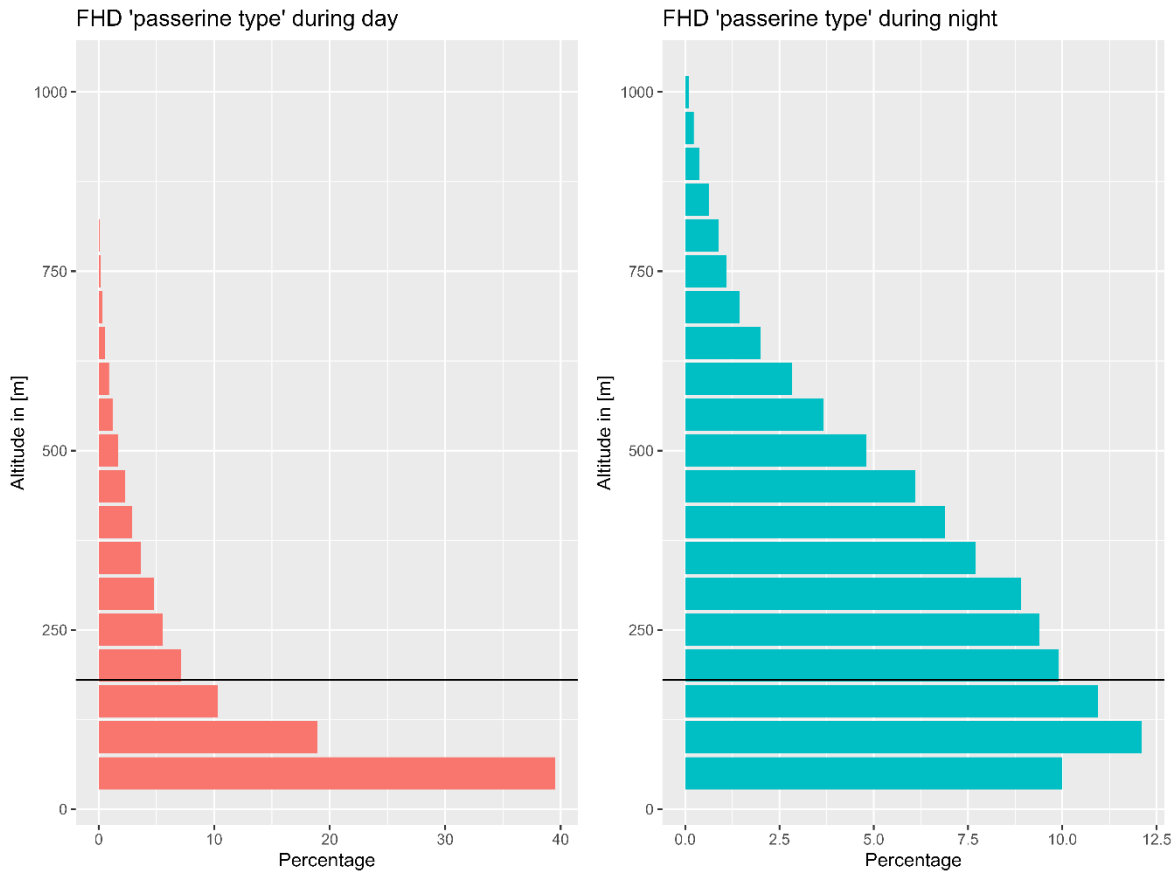

Figure 4-9 *Flight height distribution for 'passerine type' in percent and separated by day (left) and night (right) across the entire study period. The horizontal black line indicates the upper rotor height (180°m) within the wind farm.*

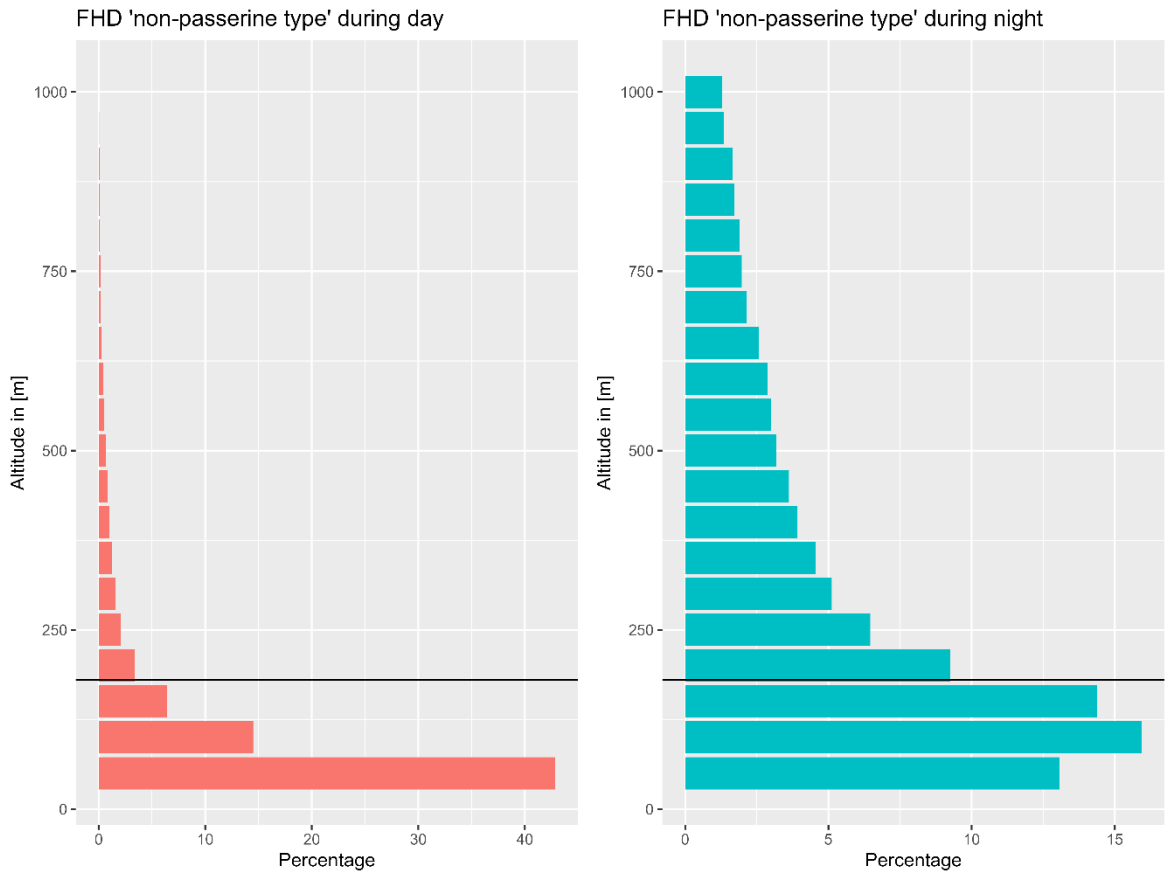

Figure 4-10 Flight height distribution combined for all 'non-passerine type' bird species in percent and separated by day (left) and night (right) across the entire study period. The horizontal black line indicates the upper rotor height (180°m) within the wind farm.

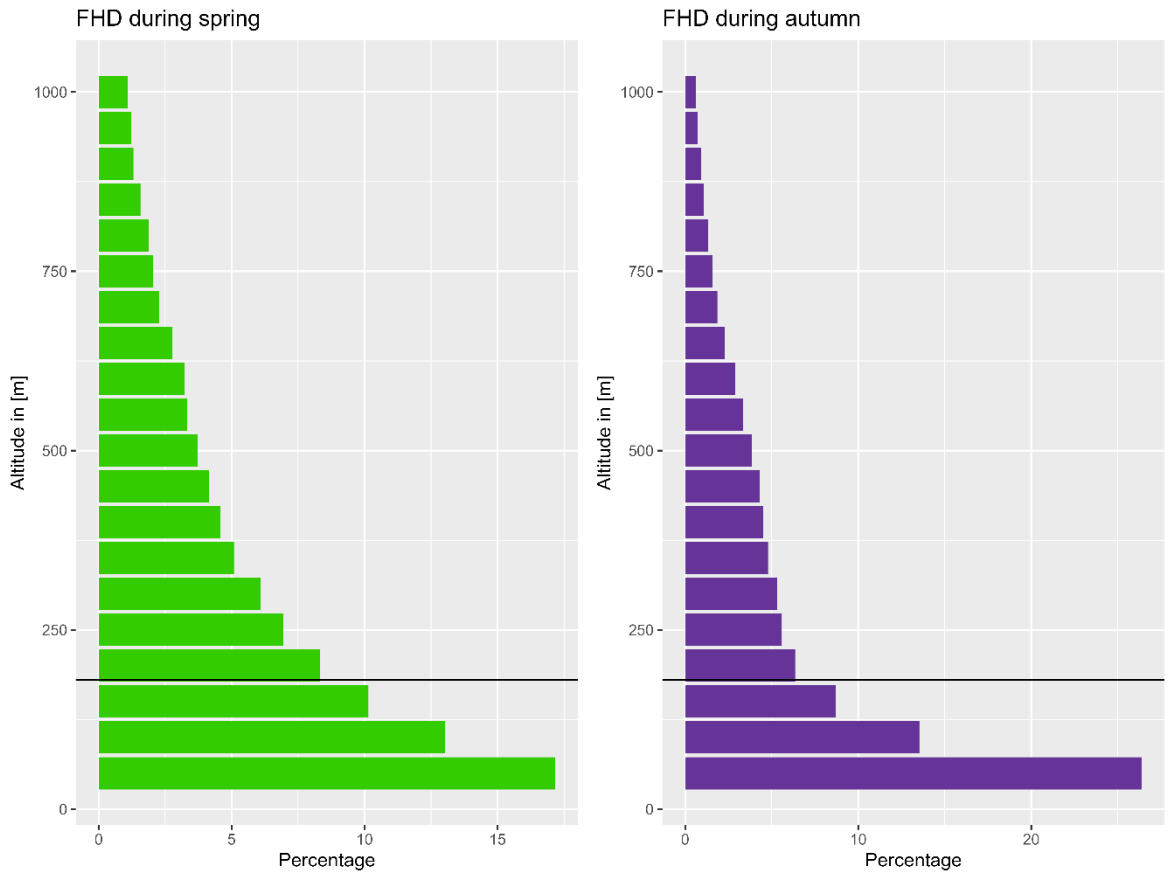

Figure 4-11 Flight height distribution combined for all bird species in percent and separated by spring (left) and autumn (right) across the entire study period. The horizontal black line indicates the upper rotor height (180°m) within the wind farm.

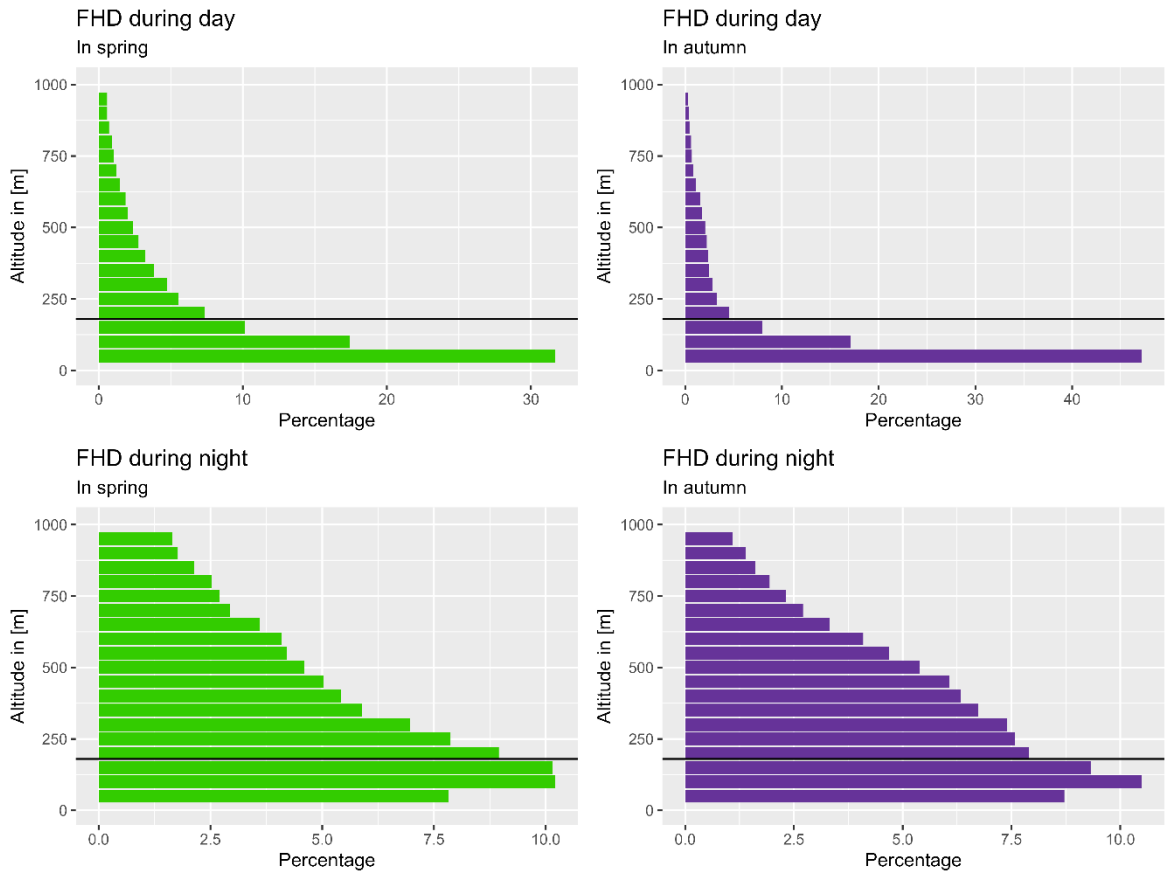

Figure 4-12 Flight height distribution combined for all bird species in percent. Flight height distribution is separated by spring (upper and bottom left) and autumn (upper and bottom right) and day (top left and top right) and night (bottom left and bottom right) across the entire study period. The horizontal black line indicates the upper rotor height (180°m) within the wind farm.

4.1.3 Weather dependency of nocturnal migration intensities of passerines only

MTR whole altitude range (25 - 1025 m)

The results of the models examining the effect of weather on migration intensities of passerines at the altitude range 25 - 1025 m are summarized in Figure 4-13 and Figure 4-14. The overall variance explained by the model was about 69.0 % for spring and 66.2 % in autumn according to the Bayesian R^2-values. To estimate the R^2-value for these Bayesian models, we followed the approach introduced by Gelman and colleagues (GELMAN ET AL. 2019), which can be interpreted similarly to the R^2 in frequentists approaches, that is, as the proportion of variance in the response variable that is explained by the predictors (marginal R^2) or predictors and random effects (conditional R^2). As found in other studies (e.g. BRUDERER & LIECHTI 1998; VAN DOREN & HORTON 2018; WELCKER & VILELA 2019; BRADARIĆ ET AL. 2020, 2024a; NUSSBAUMER ET AL. 2021; BRADARIĆ 2022), diverse weather variables affected the mean MTR.

In spring, variables with positive association with passerine MTR (listed from most influential to least, i.e. from right to left) were delta temperature, temperature, and delta TWC (Figure 4-13). Increases in both temperature and tailwind components compared to the previous night (delta values) were estimated to result in rising migration traffic rates. Furthermore, the analysis showed

that the only variable negatively affecting passerine MTR in spring was CWC, so when CWC increased the passerine MTR decreased and vice versa.

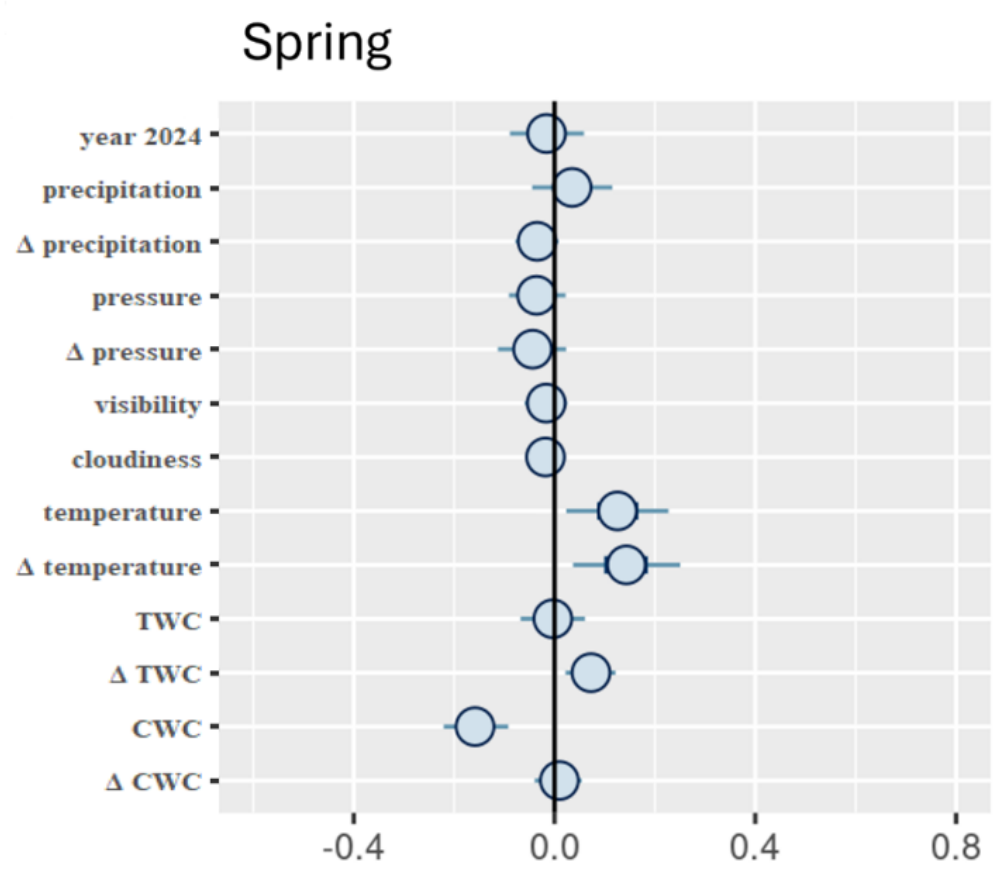

Figure 4-13 *Bayesian MCMC posterior model estimates for spring with MTR from passerines only (n/km/h) (for altitude range 25 - 1025 m) as the response variable. Posterior medians are depicted as open symbols. Thin segments indicate 90 % CI. Positive values on the x-axis correspond to positive associations with the MTR and vice versa. Variables, where CI values cross the x-intercept have no significant effect on the response variable according to the model output.*

In autumn variables positively associated with passerine MTR were (from right to left) TWC, delta pressure, temperature, visibility, delta CWC and delta TWC (Figure 4-14). Variables negatively impacting MTR in autumn were (from left to right) delta temperature, CWC and year 2024.

Overall, both precipitation and cloudiness did not seem to significantly impact passerine migration during both migratory seasons.

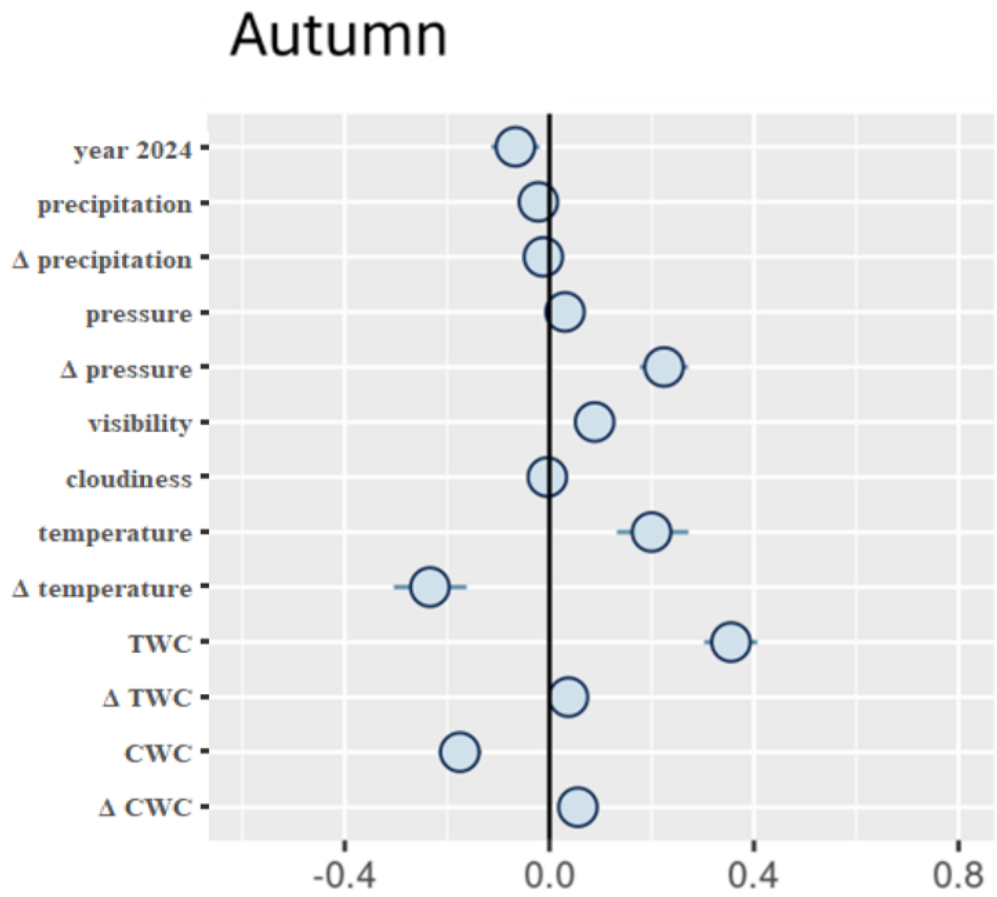

Figure 4-14 Bayesian MCMC posterior model estimates for autumn with MTR from passerines only (n/km/h) (for altitude range 25-1025 m) as the response variable. For details please see Figure 4-13.

MTR at rotor height (25 – 180 m)

Similar to the MTR over the whole altitude range, the MTR of passerines at rotor height was influenced by weather conditions (Bayesian R^2-values: 0.624 for spring and 0.631 for autumn) with supportive tail wind conditions increasing the MTR (Figure 4-15 and Figure 4-16), although the effect size tended to be smaller. Next to wind, temperature seemed to be the strongest positive predictor variable in both spring and autumn models.

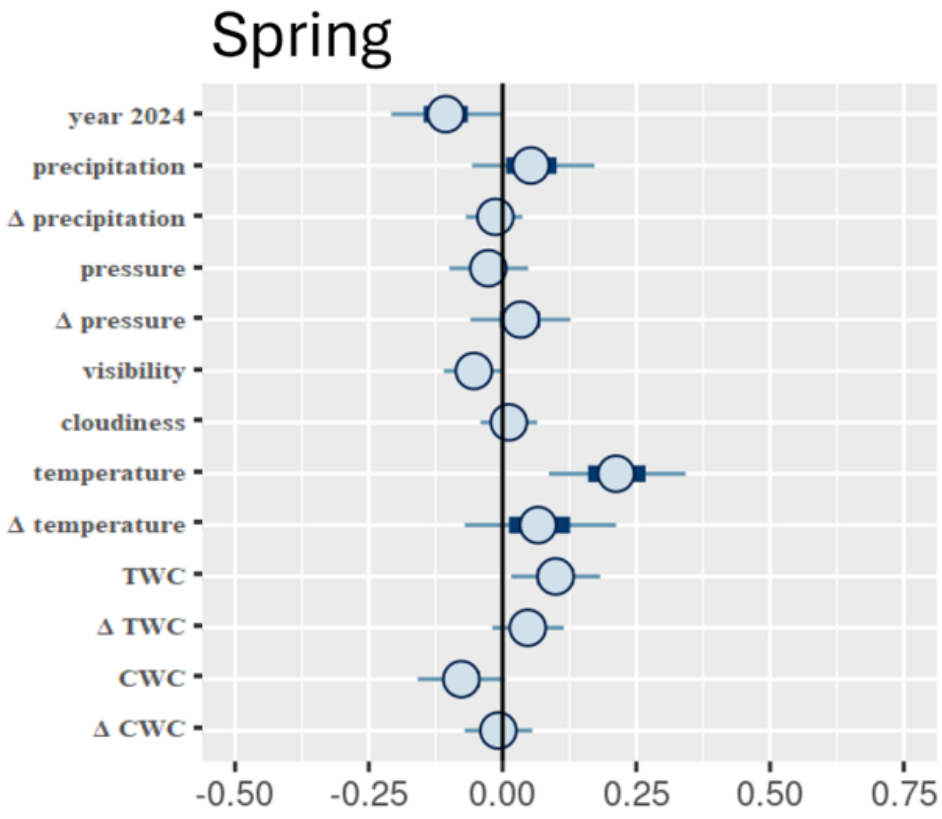

Figure 4-15 Bayesian MCMC posterior model estimates for spring with MTR from passerines only (n/km/h) (for altitude range 25 - 180 m) as the response variable. For details please see Figure 4-13.

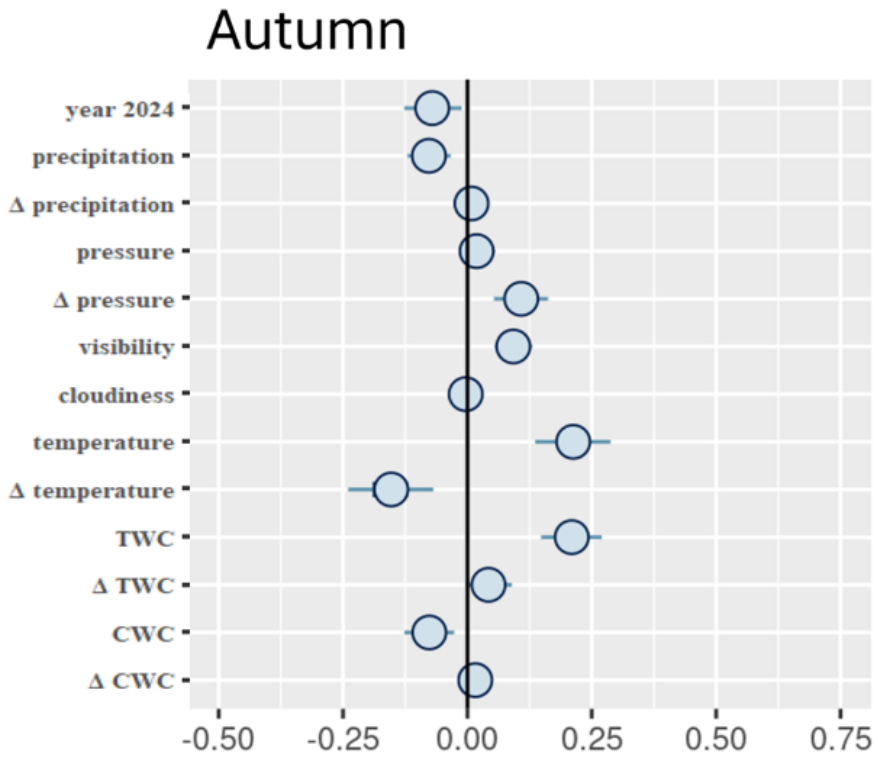

Figure 4-16 Bayesian MCMC posterior model estimates for autumn with MTR from passerines only (n/km/h) (for altitude range 25 - 180 m) as the response variable. For details please see Figure 4-13.

Proportion flying at rotor height (25 – 180 m)

This model, fitted within the Master thesis by Mehnert (see appendix A.4), investigated the effect of weather conditions on the proportion of passerines flying at rotor height. Like in the models for migration intensity (MRT at rotor height and MTR over the whole altitude range), weather conditions had a significant influence (Figure 4-17) and overall weather variables seems to explain more variation in autumn compared to spring. Interestingly, in spring an increase in precipitation, TWC, and CWC increased the likelihood of flying at rotor height, whereas in autumn increased precipitation and TWC led to a reduced likelihood of flying at rotor height while CWC increased this likelihood.

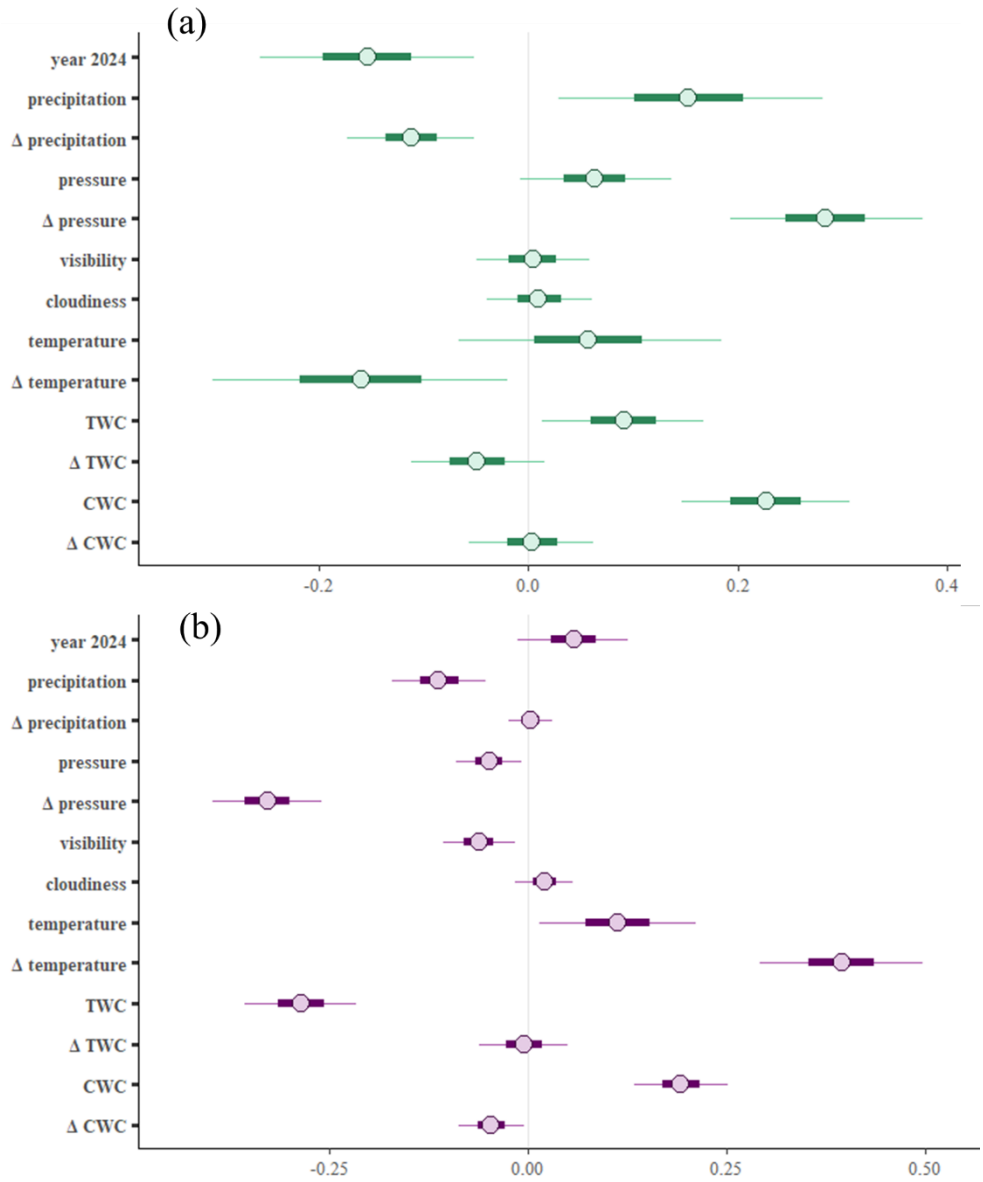

Figure 4-17 *MCMC intervals for (a) spring and (b) autumn models with the probability of passerines flying in the risk zone as the response variable. Posterior medians are depicted as open symbols. Bold segments indicate 50 % CIs, thin segments indicate 90 % CIs. Positive values on the x-axis correspond to positive associations with the probability of flying at rotor height and vice versa. Figure taken from the Master thesis by F. Mehnert, caption adapted; see appendix A.4.*

4.2 Number of rotor transits

In total, 1026 transits through the monitored rotor area (50 % of the rotor plane from turbines A2 and A4) were recorded by the camera systems during the analysed dates (Table A-5). Of these, 399 transits occurred within two hours on the morning of 17 September 2023, when several barn swallows (*Hirundo rustica*) were repeatedly flying through the rotor area while the rotor was stationary. For a while, some swallows were even observed resting on the blades. This event was clearly exceptional and constitutes a significant outlier in the data. Therefore, we report two daytime results: one including the `barn swallow event' and one excluding it.

Furthermore, since the number of analysed hours differed between day and night (4279 and 5379) respectively, see Table 4-3), a simple comparison of absolute transit counts is not appropriate. Instead, we calculated the mean number of rotor transits per hour and the corresponding day-to-night ratios. For reference, a table with the absolute number of rotor transits per turbine and operational status for both day and night is included in the appendix (Table A-2).

Without the `barn swallow event' we found 193 transits during day and 434 during night, in relation to observation effort (i.e. hour) the mean transits rate per hour was approximately twice as high during night than during day (see Table 4-3).

Table 4-3 *Overview of the number of rotor transits (total and mean number per hour for day and night), number of observation hours for both turbines when operating and non-operating. The 'Day/Night transit Ratio shows the mean number of rotor transits per hour during daytime relative to nighttime. A ratio below 1 indicates that transit rates are lower during the day compared to the night. *These numbers include the barn swallow event.*

Day or Night	N hour	N transits	Mean rotor transits/hour	Day/Night rotor transit ratio
day	4279	193 / (592)*	0.0451 / (0.1383)*	0.5589 / (1.7138)*
night	5379	434	0.0807	

4.2.1 Relationship between number of rotor transits and turbine operational status

To compare the number of transits in relation to the operational status of the turbine we classified rotor speeds equal to or exceeding 2 rpm as operational, whereas speeds below 2 rpm are considered non-operational. Out of the total of 627 transits (excluding the barn swallow event), only 45 occurred while the rotor was operational and 582 while it was non-operational. However, these numbers must be interpreted in the context of the corresponding duration of rotor operation and non-operation. The mean number of transits per hour and operational status are provided in Table 4-4.

When turbines were not operating, the transit rate was 0.1552 per hour: about 20 times higher than when the rotor was in motion (and 34 times higher when including the barn swallow event). When turbines were operating the transit rates per hour dropped to 0.0076. In other words, we would expect a rotor transit about every 132 hours (or every 5 and a half days) when rotors are active, whereas at non-active turbines, we would expect a transit every 6 hours, highlighting the effect of operational status. This effect of operational status was about twice as high during the night than during day (see Table 4-6).

A comparison of transit rates between day and night shows that during non-operational time periods more transits occurred during the night, while during turbine operational times more transits were recorded during the day (see Table 4-6).

Table 4-4 *Overview of the rotor transit rates (transits per hour) in relation to the turbine operating status (i.e. y = ≥ 2 rpm, n = < 2 rpm). In addition, the total number of observation hours, rotor transits, mean MTR during observation hours and the ratio of the transit rate during non-operation relative to operation are given. A ratio greater than 1 indicates that transits are more frequent when the rotor is not operating. *These numbers include the barn swallow event.*

Operating	N hour	N transits	Mean MTR	Mean rotor transits/hour	Non-operating/operating rotor transit ratio
n	3753	582 / (981)*	173.7 / (173.8)*	0.1552 / (0.2614)*	20.37 / (34.31)*
y	5907	45	159.6	0.0076	

Table 4-5 *Overview of the rotor transit rates (transits per hour) in relation to the turbines operating status (i.e. y = ≥ 2 rpm, n = < 2 rpm), separately for day and night. For details see caption of Table 4-4. *These numbers include the barn swallow event.*

Day or Night	Operating	N hour	N transits	Mean MTR	Mean rotor transits/hour	Non-operating/Operating rotor transit ratio
day	n	1437	168 / (567)*	222.6 / (222.8)*	0.1167 / (0.3940)*	13.27 / (44.79)*
day	y	2842	25	175.4	0.0088	
night	n	2314	414	143.0	0.1789	27.42
night	y	3065	20	144.8	0.0065	

4.2.2 Relationship between rotor transits and migration intensity at rotor height

Given the rarity of transits, the number of transits per hour was zero in most cases when the turbine was operational and exceeded one in only four instances. An initial visual inspection of the data showed that during those four hours where more than one transit occurred, MTR values were rather low (see Figure 4-18). Also, when looking at the distribution of transits per date over the period of the study, no clear relationship with MTR per date was apparent (Figure 4-19, see also Figure A-1). Statistical analyses showed similar results.

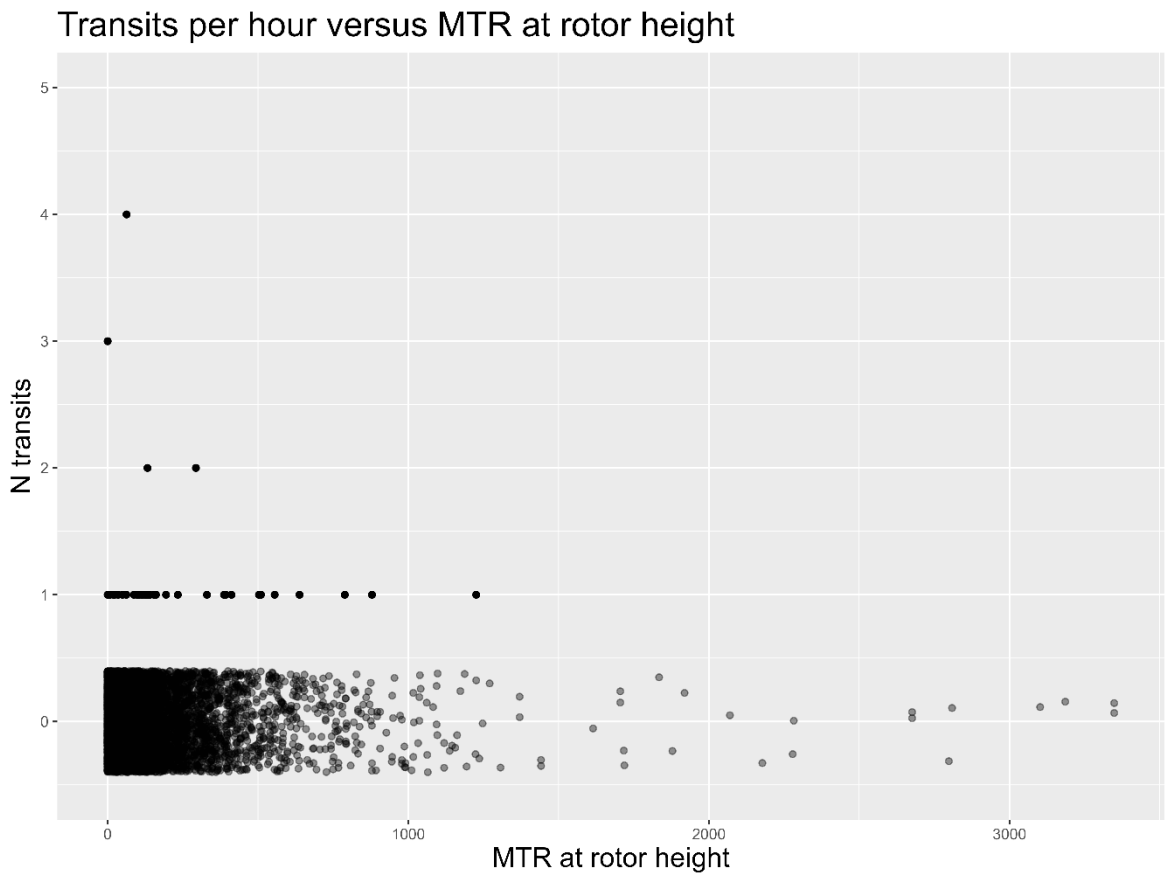

Figure 4-18 *Number of transits versus MTR at rotor height (25 – 180 m) for day and night combined. Note that when no transit occurred within an hour, we applied some jitter to the y-axis and reduced point opacity to enhance visual clarity. Consequently, points representing zero transits appear scattered around the zero line.*

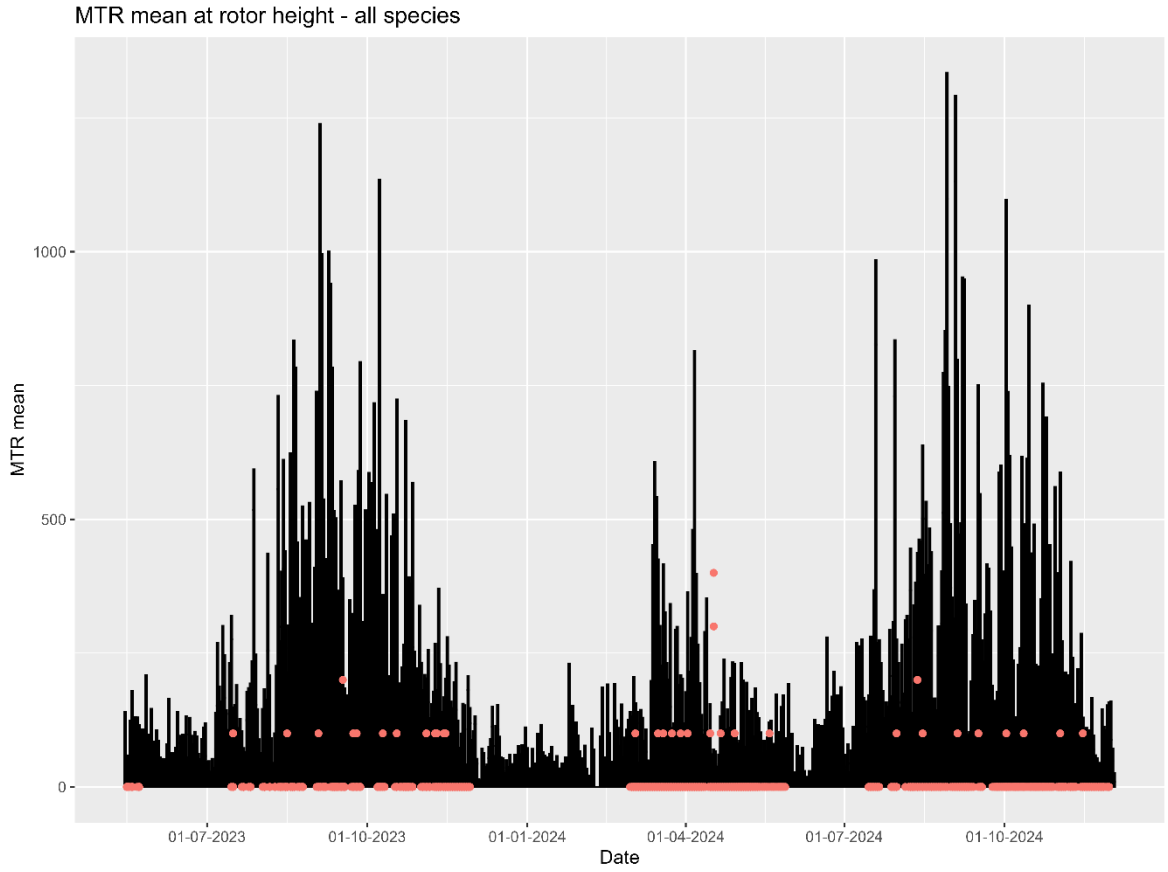

Figure 4-19 *MTR at rotor height for day and night combined with superimposed transits counts. (Transits counts were multiplied by 100 to make them visual i.e. at y=100 red dots indicate 1 transit and at y=200 red dots indicate 2 transits etc.) Note, red dots on y =0 indicates measurements with zero transits.*

To test the hypothesis that rotor transits correlate linearly with the number of birds flying at rotor height, we first used simple non-parametric Kendall's rank correlation tests.

Table 4-6 *Kendall's rank correlation test for testing the rank correlation between transits and MTR at rotor height for day and night separately. Only transits which occurred when turbines were active (rpm ≥ 2) were used for this analysis. Kendall's 'tau' indicates the strength of the correlation from 0 to 1 with small number indicating low correlation.*

Day or night	z-value	p-value	tau
day	1.82	0.069	0.029
night	1.70	0.089	0.026

Although both for day and night the p-values where low (yet statistically non-significant), the *tau* values clearly showed that the strength of the correlation was close to zero. In other words, according to the rank correlation test, the effect of MTR on the number of rotor transits was negligible (Table 4-6).

The binomial GLM showed similar results (see Table 4-7). The model output indicated no difference in transit rate between the two turbines and a non-significant trend of a lower probability of transits

during the day compared to the night. Transits during the day were independent of MTR at rotor height. A marginal significant interaction term of MTR and 'DayOrNight' indicated a slight positive effect of MTR on the likelihood of transits during the night (p-value = 0.056). However, the 'McFadden' (pseudo-) R^2-value of only 0.016 indicates that similar to the Kendall's rank correlation test, only a very small part of the variance is explained by the model. Thus, while there might be a marginal significant correlation between transits and MTR at rotor height during the night, this correlation is very weak and MTR at rotor height is therefore not a suitable predictor of rotor transits and consequently of collision risk.

Table 4-7 *Model output for generalized linear model with binomial family and 'logit' link function. Depending variable was transits (yes/no) within one hour. Explanatory variables are indicated in column 'fixed effects', the reference level of factorial variables is indicated. Camera effort was used as an offset in the model.*

Fixed effects	Estmate (SE)	z value	p-value
Intercept	-5.858 (0.313)	-18.724	
MTR	<0.001 (<0.001)	0.889	0.374
Turbine ID [Iterra]	-0.112 (0.331)	-0.338	0.736
Day or Night [night]	-0.501 (0.412)	-1.216	0.224
MTR all classes × Day or Night [night]	0.002 (<0.001)	1.908	0.056

4.2.3 Weather dependency of rotor transits

The Bayesian GAM examining the effect of weather and other additional explanatory variables on rotor transits showed mixed results. As indicated by the MCMC interval plots (Figure 4-20), the following variables affected the occurrence of transits as the 90 % CI of the posteriors did not overlap with zero:

- temperature (**day**, higher temperature less transits)
- precipitation (**day**, more precipitation less transits)
- CWC (**day**, more wind less transits)
- visibility (**night**, higher visibility more transits)
- MTR at rotor height (**night**, higher MTR more transits)
- rotor rotation speed (**day** and **night**, faster rotor rotation less transits, potentially larger effect at night), please note that in this dataset only observations are included when the rotor was active. Thus, the influence of rotor speed here is explained by the range of rpm ≥ 2 to max. rotation speed.

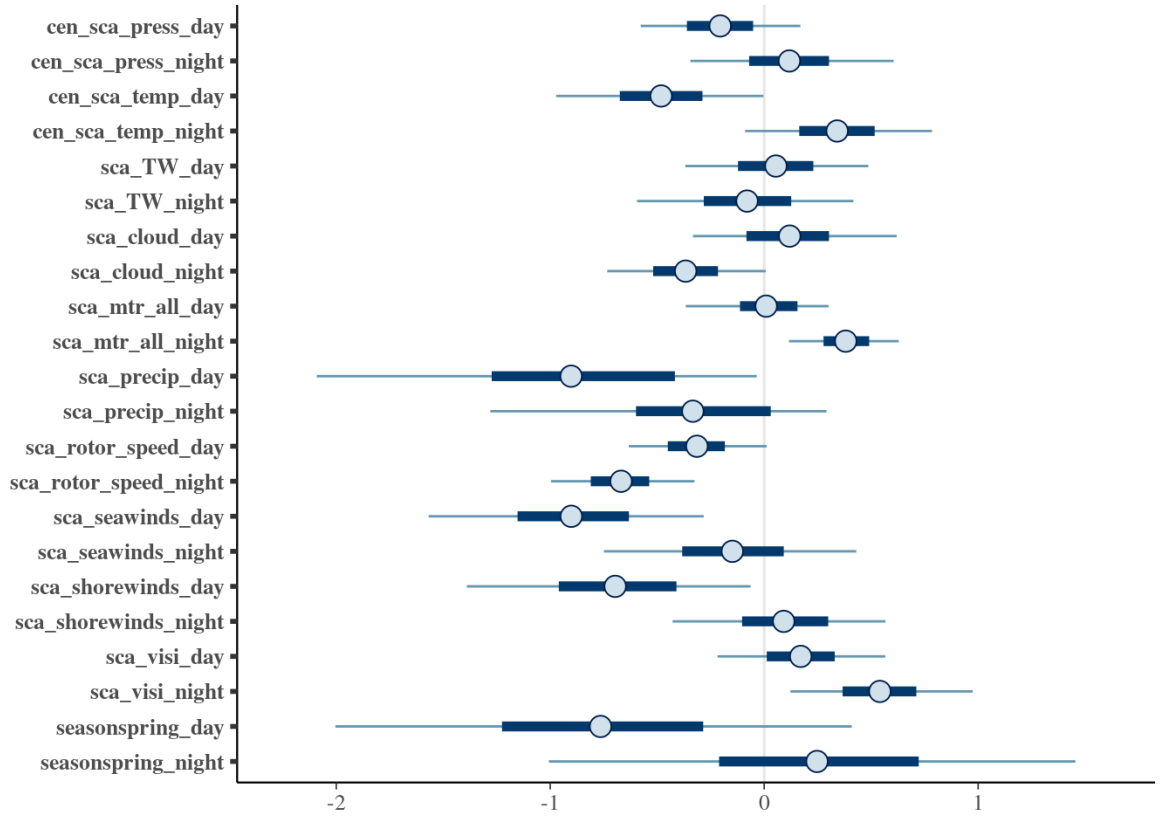

Figure 4-20 MCMC-interval plot of both day and night models for influences of weather variables, rotor speed and MTR at rotor height on the likelihood of transits. Note that day and night models were separately run, however, variables are ordered so that they are shown in day/night pairs for easier comparison. Note also that, since scaling was applied within each day/night subset, a direct comparison of the relative effect size of those variables on this plot is possible.

For seeing the effect size on the original scale of the data please see figures in the appendix (Figure A-3 to Figure A-11).

However, both the LOO (Leave-one-out) approach and the Bayesian R^2 values indicated that the model explained only a minor proportion of the variance in the rotor transit data. LOO shows the improvement of an extended model in comparison to the base model. The large SEs of the model differences found in these comparisons (Table 4-8 and Table 4-9) indicated that all explanatory variables included in the extended model versions did not contribute much to explain the variance in the data. This is confirmed by the Bayesian R^2-values which were 0.019 for model on day data and 0.041 for the night ones (see the appendix A).

Table 4-8 LOO comparison of Bayesian models for daytime transits when rpm ≥ 2 and its influence by weather parameter, rotor speed and MTR at rotor height. Elpd_diff = Expected Log Predictive Density Difference. SE_diff = Standard Error of the difference.

Model	elpd_diff	se_diff
mb_wind_TW_CW_abs	0.0	0.0
mb_wind_TW_shore_sea	-0.9	0.3
mb_base	-2.6	2.9
mb_date	-3.4	2.8
mb_wind_all	-3.5	3.1
mb_large	-3.8	3.0
mb_date_circadian	-4.2	2.9
mb_large_shore_sea	-4.5	2.9
mb_wind_TW_CW	-5.2	3.1
mb_wind_TW_CW_season	-6.6	3.1

Table 4-9 LOO comparison of Bayesian models for nighttime transits when rpm ≥ 2 and its influence by weather parameter, rotor speed and MTR at rotor height.

Model	elpd_diff	se_diff
mb_large	0.0	0.0
mb_large_shore_sea	-0.4	1.1
mb_date	-2.4	5.9
mb_date_circadian	-2.7	5.9
mb_wind_all	-3.0	5.1
mb_base	-3.5	6.5
mb_wind_TW_CW_abs	-3.6	5.4
mb_wind_TW_CW	-3.8	6.0
mb_wind_TW_shore_sea	-4.4	5.9
mb_wind_TW_CW_season	-5.0	6.4

4.3 Avoidance rate

4.3.1 Calculation based on number of rotor transits

Overall, the average avoidance rates, as calculated based on rotor transits, and the MTR at rotor height, across all bird species groups (see chapter 3.7.7) were very high with some variation between day and night, and, particularly between periods when turbines were active versus inactive. Differences between the two turbines for which rotor transits were recorded by camera systems, however, were low, indicating that the concrete location of the turbines was not important (Table 4-10).

When turbines were active, the avoidance rate during the night (0.9987) was slightly higher than during the day (0.9986) and considerably higher than estimated earlier (see chapter 5). With

respect to the proportion of birds not avoiding the rotor plane (1-avoidance rate), the ratio between night and day was 0.9412 indicating a slightly (about 6 %) increased probability of rotor transits during the day for a given number of birds aloft.

Table 4-10 *Avoidance rate while rotors were active (i.e. rpm ≥ 2). The table shows the estimated avoidance rate based on the number of 'expected transits' and 'actual transits'. 'Expected' transits were calculated from number of radar signals at rotor height corrected for the rotor area assuming no avoidance. 'Actual transits' are transits observed with AVES-Camera in the rotor area. 'Transits corrected' is number of actual transits corrected for camera downtime and expected number of transits missed due to birds colliding with the rotor and hence could not cross it. Avoidance rates are calculated form the ratio of 'expected' and 'actual' transits or 'transits corrected' accordingly.*

Turbine ID	Day or night	Transits expected	Transits actual	Transits corrected	Avoidance rate
A2	night	8255.8	11	12.73	0.9985
A2	day	10816.4	11	13.15	0.9988
A4	night	11063.3	9	11.30	0.9990
A4	day	11238.8	14	16.95	0.9985
Turbines combined	night	19319.2	20	24.03	0.9987
Turbines combined	day	22055.2	25	30.10	0.9986

The average avoidance rates for times when the turbines were inactive (rpm < 2) were markedly lower compared to active turbines but still high (day: 0.9847, night: 0.9660; see Table 4-11). Interestingly, the avoidance rate during the night was considerably lower than during the day in this case. This was also indicted when considering the ratio of non-avoidance between night and day: the probability of birds flying without avoidance response through the rotor during the night was more than twice as high as during the day when rotors were idle (ratio 2.22).

Table 4-11 *Avoidance rate while rotors were inactive (i.e. rpm < 2). The table shows the estimated avoidance rate based on the number of 'expected transits' and 'actual transits'. For details please see Table 4-10.*

Turbine ID	Day or Night	Transits expected	Transits actual	Transits corrected	Avoidance rate
A2	night	10478.3	271	313.77	0.9701
A2	day	9052.4	78	93.26	0.9897
A4	night	4645.5	141	176.97	0.9619
A4	day	5652.8	95	114.99	0.9797
Turbines combined	night	15123.8	412	490.74	0.9660
Turbines combined	day	14705.2	173	208.25	0.9847

4.3.2 Calculation based on number of fatalities

The predicted collision rate based on MTR data at rotor height and with avoidance rate set to 0 was 57889.2 [CI 43289.1 - 73762.7]. The estimated number of collision victims found during 'Post Construction Fatality Monitoring' was 99.7. [CI:55 -168] (see chapter 4.5).

Using mean results of PCFM (=99.7) and the mean CRM collision estimate (=57889.2 fatalities), resulted in a calculated avoidance rate of = 0.9983. The estimate ranged from 0.9961 when applying the lower CI of CRMs and the upper CI of fatalities to 0.9993 when using the upper CI of CRMs and the lower CI of fatalities.

4.4 Band collision risk models

With the help of stochastic CRMs and applying the avoidance rates determined in this study (approx. 0.998, see chapter 4.3), we estimated a mean of 76.6 (95 %-CI: 57.3 - 97.6; Table 4-12) collision victims for the study period for all five wind turbines combined. During daytime the sum was 40.59 and during night 36.01 collisions. The estimates per turbine were similar but for one turbine per year which showed considerably lower numbers (see Figure 4-21; 'A6' in 2023 and 'iTerra' in 2024), which was caused by the long periods these were non-operative due to maintenance.

In comparison, when applying an avoidance rate of 0.98 (e.g. SCHULZ ET AL. 2014; POTIEK ET AL. 2021), the total number of collision victims was estimated at 1157.6, with an avoidance rate of 0.9562, the conservative rate reported by Schulz et al 2014, the estimate increased to 2535.2 collision fatalities (Table 4-12). This corresponds to a 15-fold and 33-fold increase compared to the number of collision victims estimated with the avoidance rate determined in this study, respectively.

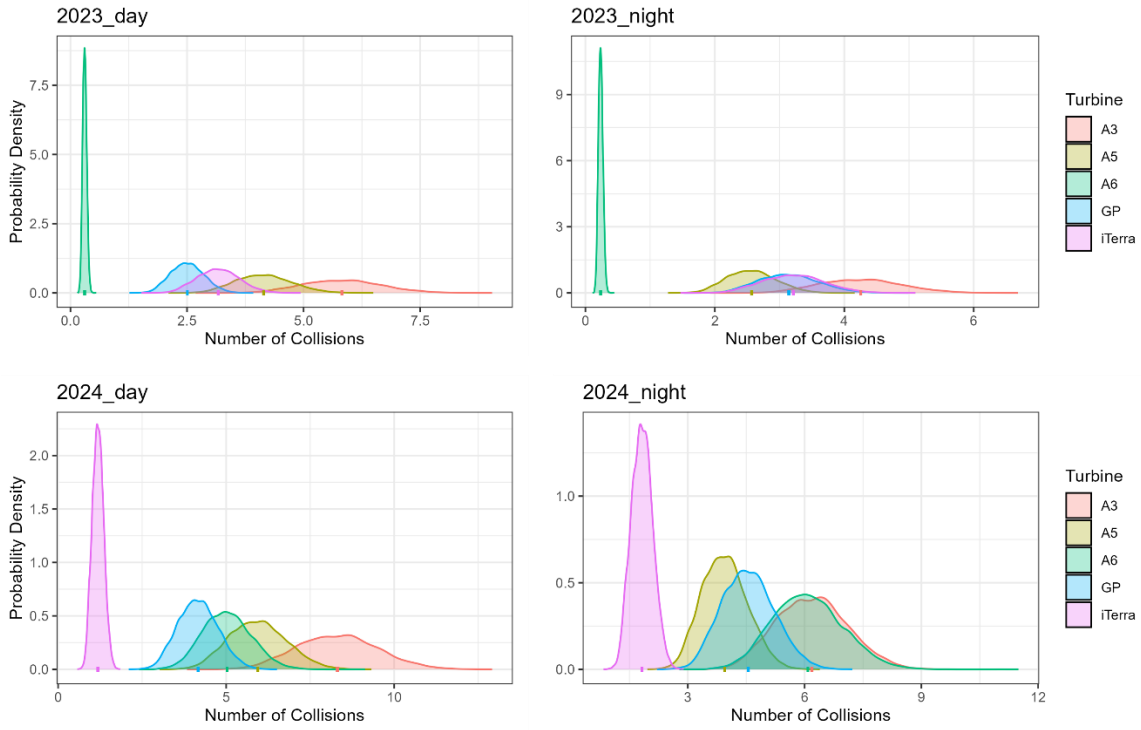

Figure 4-21 *The figure shows the calculated collisions per year and season. The collision numbers are plotted on the x-axis, the mean values are indicated by the small lines on the x-axis ('ticks') in the colour of the corresponding scenarios. The y-axis shows the probability density and thus indicates the probability of a given mean number of collisions. The width of the bell curve indicates the variance. Turbines with AVES cameras installed are spelled out (i.e.: 'GP' and 'iTerra'). Please note that 'A6' and 'iTerra' were not operating for extended periods, which resulted in narrow density curves close to zero.*

Table 4-12 Summary table of estimated collisions over the period of study duration based on stochastic CRMs for three different scenarios. The three scenarios differ in the assumed avoidance rate where the first row shows results for the rates as found in the present study (day=0.9986; night=0.9987), the second row for the 'standard' rate of 0.98 and the last row for the lower rate as found in Schulz et al 2014 (= 0.9562).

Avoidance rate	Mean collisions	SD	Median	Lower CI	Upper CI
0.9987 (empirical avoidance rate, this study)	76.6	10.5	76.6	57.3	97.6
0.980 (SCHULZ ET AL. 2014; POTIEK ET AL. 2021)	1157.8	158.6	1157.6	865.8	1475.3
0.9562 (SCHULZ ET AL. 2014)	2535.5	347.3	2535.2	1896.1	3230.8

4.5 Post Construction Fatality Monitoring (PCFM)

4.5.1 Estimating carcass dispersion (dwp)

An overview of the number of carcasses found (total 16 carcasses), date, respective turbine and species level, where possible, is provided in Table 4-13.

Table 4-13 Information on carcasses found during PCFM during the whole study period. Each row resembles one collision victim. In total 16 carcasses were found. Rows with light blue background indicate collision victims found within the main bird migration periods. Bold fonts indicate migrating passerines that at least partially migrate during the night.

Species	Date	Turbine /search area
Duck unidentified	03/06/2023	A05-03
Oystercatcher	08/06/2023	A03-03
Common Buzzard	13/06/2023	A02-11
Carrion Crow	18/06/2023	A05-02
Black-headed Gull	03/07/2023	A03-03
Black-headed Gull	12/08/2023	A03-01
Black-headed Gull	27/08/2023	A05-01
Great Tit	26/09/2023	A03-01
House Sparrow	21/10/2023	A02-05
Song Thrush	14/01/2024	A04-04
Starling	04/03/2024	A05-01
Starling	19/03/2024	A03-01
Wood Pigeon	28/05/2024	A04-01
Wood Pigeon	27/07/2024	A03-01
Common Buzzard	05/10/2024	A03-03
Kestrel	25/10/2024	A04-04

For the estimation of the density weighted proportion (dwp) of carcass distribution around the turbine we chose to use the Maxwell-Boltzmann distribution, although it scored higher ΔAICc value compared to other candidate distributions (Table 4-14). This was done because it provided higher,

more realistic predicted proportions of carcasses falling within a 150 m radius of turbine masts, while the other candidate distributions predicted substantially lower proportions (see Figure 4-22).

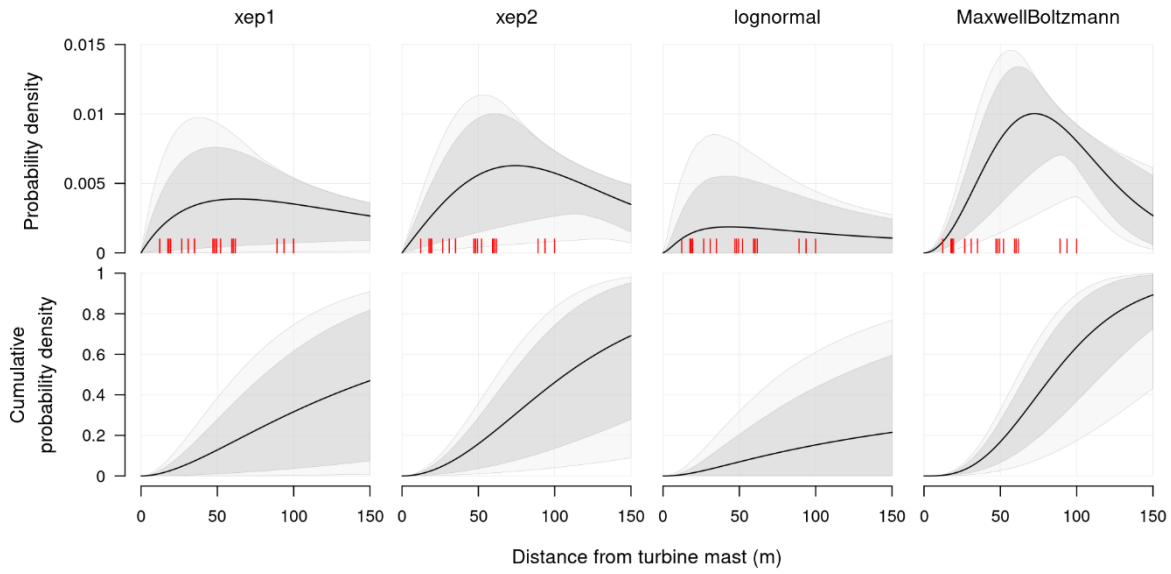

Figure 4-22 *Fitted distributions of carcass distances from turbine masts using the dwp package. 'xep1', 'xep2', 'lognormal' and 'MaxwellBoltzmann' were the best candidate models for the distribution function. Top row, probability density functions for the distribution of carcass distances; bottom row, cumulative probability density functions. The black lines are the mean predictions, while the light and dark grey envelopes represent the 95 % and 80 % confidence intervals, respectively. Red ticks represent the observed distances for the 20 carcasses kept in the dataset for fit with dwp.*

However, since the Maxwell-Boltzmann distribution parameters *a* simulated by dwp nonetheless contained some high values resulting in a large proportion of birds predicted to fall far from the masts, we decided to apply a conservative threshold for the allowed proportion of carcasses falling far away: we chose an initial truncation threshold for the Maxwell-Boltzmann distribution parameter *a* so that no more than 50 % of birds could fall beyond 150 m radius (Figure 4-23). This means that we truncated the distribution of *a* values provided by dwp at 97.52, the value corresponding to 50 % of birds falling beyond 150 m from the masts. We used a mixture of Gaussians to approximate this truncated distribution of *a* (using the mclust package) to be able to use it as a prior for the Stan model.

Since that prior was still very permissive in terms of proportion of carcasses allowed to fall far from the masts, we used carcass dispersion results estimated in a comparable study conducted by BioConsult SH in which modelling carcass dispersion was easier due to more homogenous search areas and applied a correction factor to account for differences in turbine height. Thus, we determined the threshold radius below which we expected 95 % of carcasses to fall at 156.7 m.

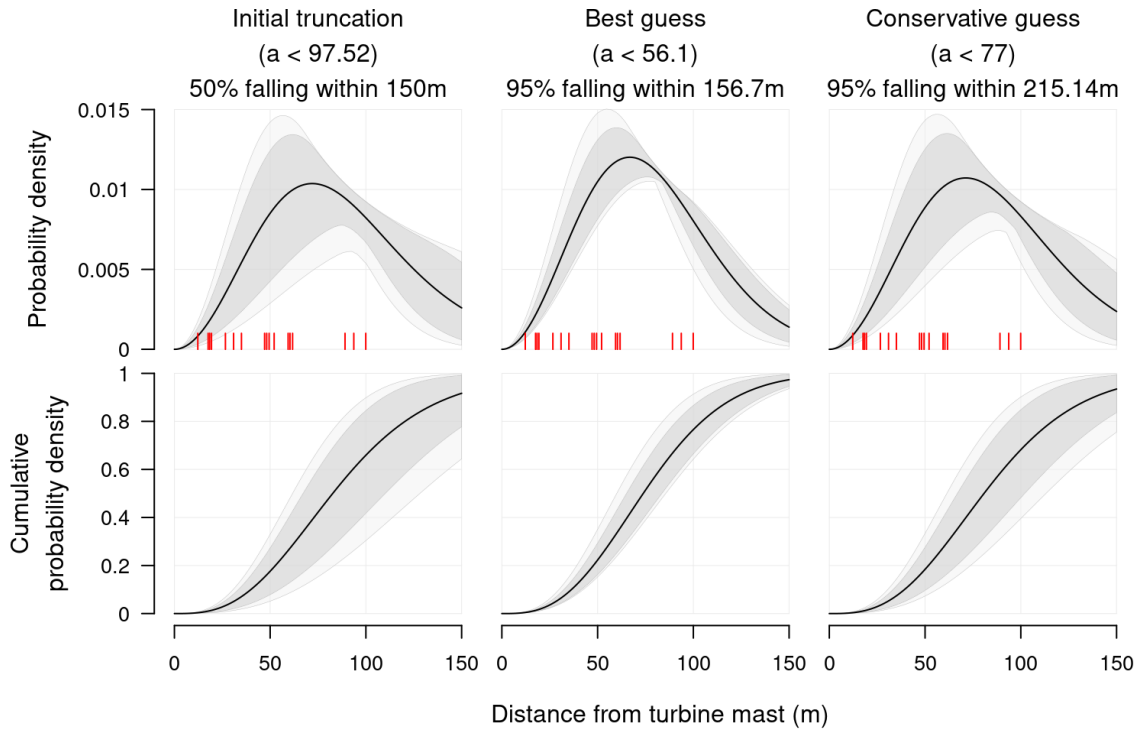

Figure 4-23 *Priors for Maxwell-Boltzmann distributions representing carcass dispersion distances used in the fatality model, using the a parameter distributions based on the dwp fit in the previous figure above. Initial truncation, using a prior distribution for a obtained from a mixture of Gaussians fitted on the dwp output after applying a threshold on a so that at least 50 % of carcasses would be expected to fall within 150 m; Best guess, using a prior distribution for a after applying to the initial truncation distribution a threshold on a so that at least 95 % of carcasses would be expected to fall within 156.7 m; Conservative guess, using a prior distribution for a after applying to the initial truncation distribution a threshold on a so that at least 95 % of carcasses would be expected to fall within 215.14 m. Legend for black lines, grey envelopes, and red ticks is as for the figure above. Final MCMC runs for the fatality model were performed using the best guess prior or the Conservative guess prior.*

Table 4-14 *Scores of distribution models fitted with dwp. See the dwp documentation (Table 6 in Dalthorp et al. (2022)) for the precise description of each model based on their name (left column). Selection criteria are (0/1 indicate failure/success for a given model): 'extensible', the distribution function predicts a finite number of carcasses outside the searched areas; 'rtail' and 'ltail', the distribution function does not predict too many carcasses too far from or too close to the turbine mast (threshold-based); 'aicc', the ΔAICc value relative to the model with lowest AICc is < 10; 'hin', the model is not affected by any highly influential point. The last column indicates the ΔAICc value relative to the model with lowest AICc.*

Candidate	Extensible	rtail	ltail	aicc	hin	deltaAICc
xep1	1	0	1	1	1	0.605
xep2	1	0	1	1	1	1.510
lognormal	1	0	1	1	1	1.890
MaxwellBoltzmann	1	0	1	1	1	7.570

4.5.2 Estimating carcass persistence

Carcass persistence trials allowed to determine how long carcasses stay in the field before they are not detectable anymore. We used the GenEst package to estimate the persistence. Multiple models using different distributions families were compared (Table 4-15) and the model with the best fit was used as prior knowledge in the final fatality estimates (see Methods). Depending on the carcass size the persistence differed (see Figure 4-24).

Table 4-15 Summary of model fits for carcass persistence. The location and scale formula columns indicate whether the model included an effect of size class (~ size category) or not (~ 1) for that parameter. Note that the exponential model does not have a scale parameter.

Distribution	Location formula	Scale formula	AICc	ΔAICc
weibull	l ~ 1	s ~ 1	270.16	0.00
loglogistic	l ~ 1	s ~ 1	270.37	0.21
lognormal	l ~ 1	s ~ 1	270.93	0.77
weibull	l ~ size_category	s ~ 1	271.49	1.33
loglogistic	l ~ size_category	s ~ 1	271.79	1.63
exponential	l ~ 1	NULL	272.02	1.86
lognormal	l ~ size_category	s ~ 1	272.30	2.14
exponential	l ~ size_category	NULL	272.81	2.65
weibull	l ~ 1	s ~ size_category	273.03	2.87
loglogistic	l ~ 1	s ~ size_category	274.20	4.04
lognormal	l ~ 1	s ~ size_category	274.60	4.44
weibull	l ~ size_category	s ~ size_category	275.78	5.62
loglogistic	l ~ size_category	s ~ size_category	276.11	5.95
lognormal	l ~ size_category	s ~ size_category	276.54	6.38

Based on the model comparison table above (Table 4-15), we chose to use a model with an exponential distribution and with an effect of size class on the location parameter because (i) among the models which retained an effect of the size class covariate, that model had one of the smallest ΔAICc values compared to the model with the lowest AICc (ΔAICc=2.65) and (ii) the other models using distributions with both a location and a scale parameter had only a slightly lower AICc value than the exponential model (e.g. ΔAICc=1.33 for the model using a Weibull distribution with an effect of the size category covariate) indicating no significant increase in its explanatory power.

We then used the GenEst::rcp() function to generate plausible values from that chosen model for the location parameter of the exponential persistence function, for each size class. Finally, we approximated the distribution of those plausible values provided by GenEst by using log-normal distributions (one per size class), that were then used as priors in the fatality model.

Generally, estimated persistence was high. After five days (i.e. the standard interval of collision fatality searches in this study), about 80 %, 85 % and 90 % of small, medium-sized and large birds were still present, respectively. After 20 days, presence varied between approx. 40 % - 65 % for the different size classes (see Figure 4-24).

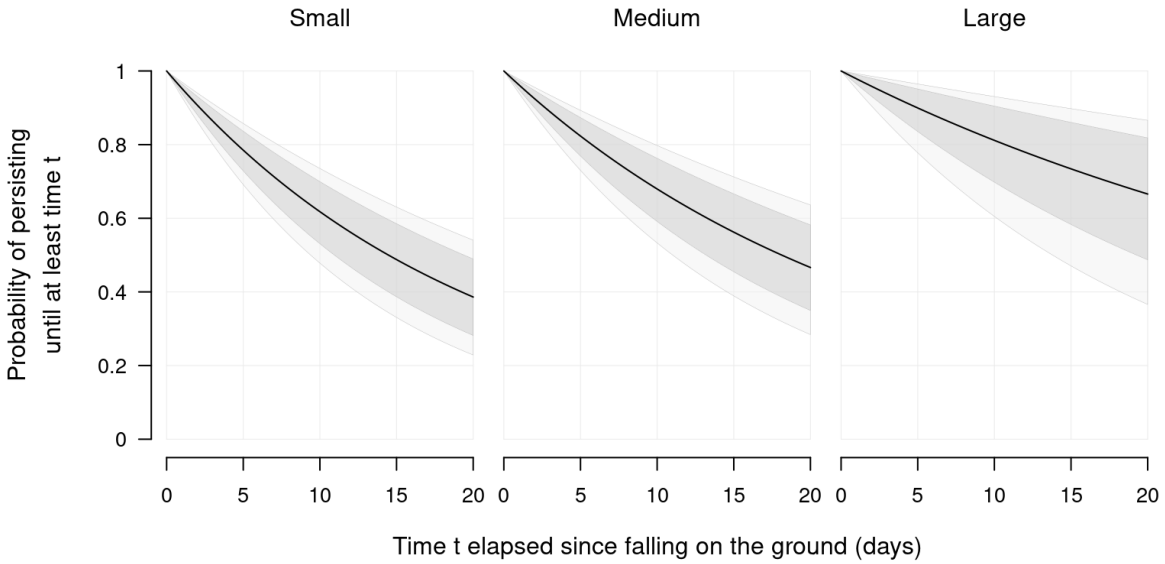

Figure 4-24 Carcass persistence predicted from the selected model (exponential distribution with effect of size class). The black lines are the mean predictions, while the light and dark grey envelopes represent the 95 % and 80 % confidence intervals, respectively.

4.5.3 Estimating search efficiency (GenEst)

The estimated mean search efficiency per carcass size category and visibility condition ranged from 0.31 (small carcass size and sufficient visibility) to 0.91 (large carcass size and very good visibility. For the whole range of efficiency values used in the final fatality estimate model see Figure 4-25.

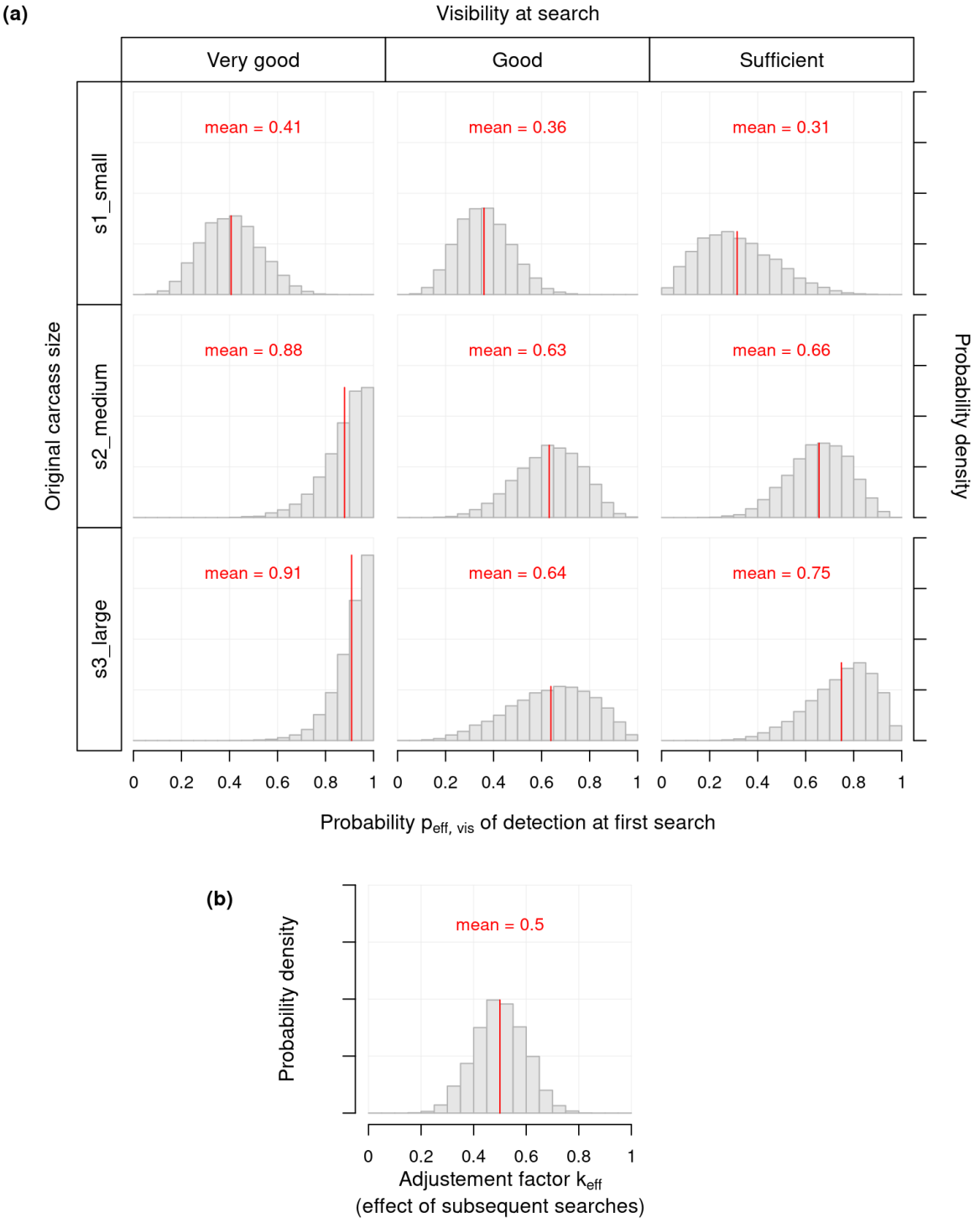

Figure 4-25 *Priors used in the fatality model for parameters affecting searcher efficiency $p_{eff,vis}$ and k_{eff}. (a) Priors on $p_{eff,vis}$, one prior per size class and per visibility level. Those priors are obtained by fitting a detection model on the field trial data with GenEst. (b) Prior on k_{eff}, based on literature including tutorials and simulated datasets. The red vertical lines show the mean values for each prior distribution.*

4.5.4 Fatality model

The mean estimation of base fatality rate *lambda_0* for times when rotor speed was > 2 rpm ranged from 0.0178 for small birds to 0.0245 for large birds. Notably, for medium-sized birds the estimate was lowest with 0.0101 (see Table 4-16 for full range of CIs).

Table 4-16 Lambda_0, the base fatality rate in birds/turbine/day, when rotor speed > 2 rpm.

Bird size class	2.5 %	10 %	Median	Mean	90 %	97.5 %
small	0.0034	0.0059	0.0150	0.0178	0.0326	0.0500
medium	0.0027	0.0043	0.0090	0.0101	0.0172	0.0236
large	0.0113	0.0144	0.0231	0.0245	0.0364	0.0450

The overall probability of detecting a collision victim at the wind farm over the study period per size class of the bird was estimated by the parameter '*P_Detect*'. These values integrate among others the search efficiency per visibility condition, carcass persistence, and the probability of the carcass falling within the searched area. Mean values for *P_Detect* ranged from 0.094 for small birds to 0.260 to large birds (see Table 4-17 for the whole range of CIs).

Table 4-17 P_Detect, overall probability of detection of a collision victim killed at the wind farm over the study period.

Bird size class	2.5 %	10 %	Median	Mean	90 %	97.5 %
small	0.0499	0.0621	0.090	0.0935	0.128	0.154
medium	0.1440	0.1630	0.206	0.2070	0.254	0.283
large	0.1700	0.1980	0.258	0.2600	0.326	0.363

Finally, the number of estimated fatalities per size class over the period of the study ranged from 18.9 for medium-sized birds to 47.0 for large birds (Table 4-18). Noticeably, passerine birds fall into the size class of small and medium-sized birds and constitute a large part of the total population flying in and through the wind farm (see chapter 4.1.1), however, the combined mean estimate of these two classes is 52.8 and thus not much higher than the estimate for large birds (47.0).

The mean estimate for the total number of fatalities for all size classes together over the whole period of the study at all five turbines was 99.7, 95 % CI ranged from 55 to 168 (see Table 4-18).

Table 4-18 Number of fatalities per size class over the study period.

Bird size class	2.5%	10%	median	mean	90%	97.5%
small	7	11	28	33.9	62	93
medium	6	8	17	18.9	31	43
large	24	29	44	47.0	69	85
total	55	66	96	99.7	137	168

4.5.5 Fatality estimates in relation to total population

Based on the MTR data for the altitude range from 25 - 1025 m, we estimated that a total number of 4236841 birds flew through and over the wind farm (assuming a width of the windfarm of 1.2km perpendicular to the main migration direction). In this calculation, one radar signal is counted as one bird regardless of whether it relates to separate individuals or multiple passages of same birds.

With the equation:

$$Percent\_population = n\_carcass / sum\_flights * 100$$

we estimate that 0.0018 % of all bird passages through the area of wind warm resulted in a collision with one of the turbines. Separate calculations for day and nighttime resulted in 0.0020 % and 0.0016 % of the population, for day and night, respectively. When repeating the same calculation with the upper 95 %-CI of the PCFM fatality estimate (168 collision victims, Table 4-18), the percentage of collisions increases to 0.004 %. Please note that in the latter case we cannot distinguish between day- and nighttime collision victims.

4.6 Bird calls

The accuracy of the AI was considered good enough for further analysis for a total of 23 species (Table A-9, n calls = 112359). Of these 23 species six belong to the order *Passeriformes* (i.e. passerines; n calls = 4882).

The species composition of nocturnal calls in spring was dominated by Blackbirds (44 %). Other commonly recorded species were Northern Lapwings, Mallards and different species of geese but also the Song Thrush was recorded frequently (Figure 4-26). During autumn the most dominant species was the Barnacle Goose with 24 % followed by four passerine species: Redwing, Robin Blackbird and Song thrush (12 %, 11 %, 7 %, 5 % respectively) (Figure 4-27). Together these four passerines accounted for about one-third of the total number of nocturnal calls in autumn.

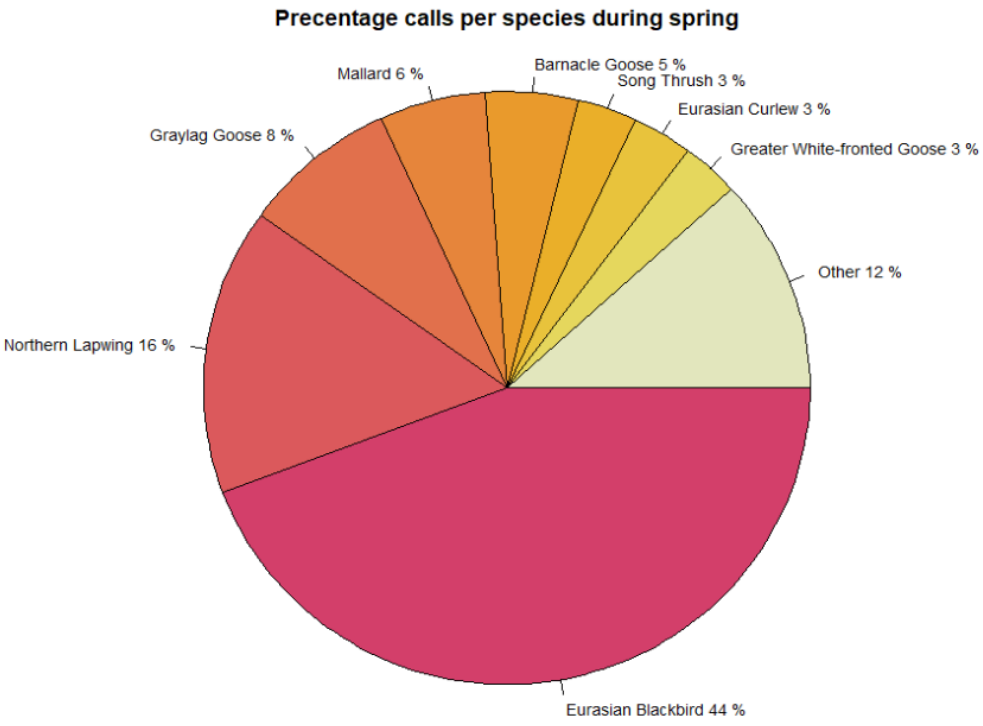

Figure 4-26 *Calls spring. Pie chart of percentages of nocturnal calls for most dominant species during the night. Subset of species is based on AI species identification for which the AI's accuracy was deemed to be high enough. Species which made less than 3 % of total calls were lumped together under the index 'rest'.*

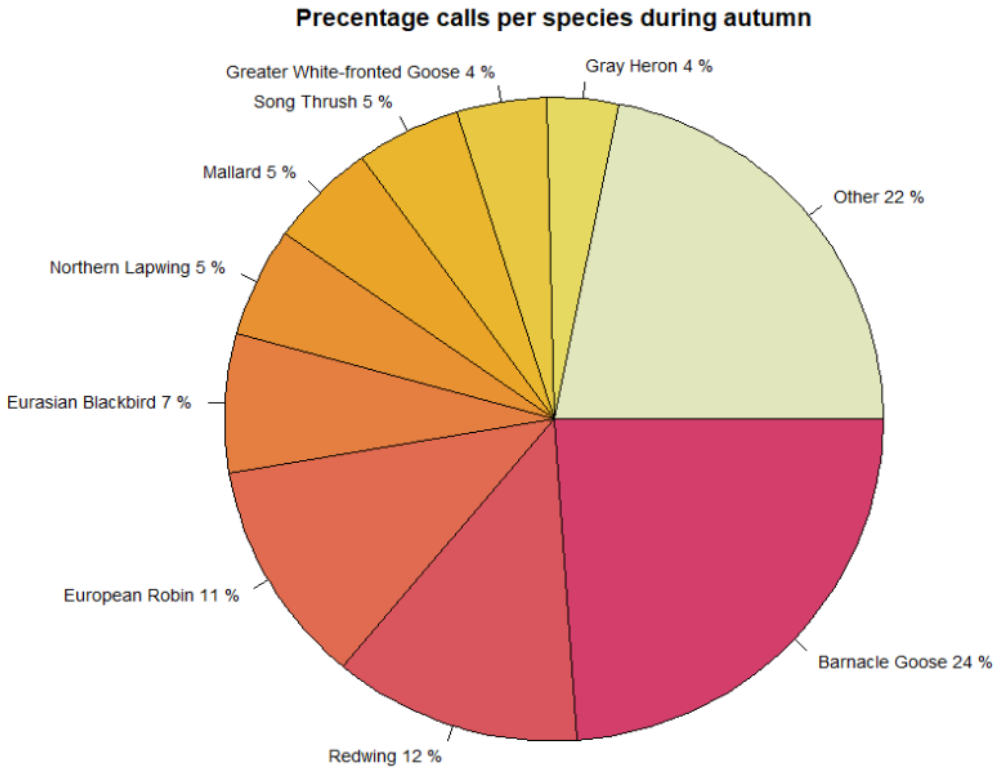

Figure 4-27 Calls autumn. Pie chart of percentages of nocturnal calls for most dominant species during the night. Subset of species is based on AI species identification for which the AI's accuracy was deemed to be high enough. Species which made less than 4 % of total calls were lumped together under the index 'rest'.

Calls per species were also plotted against Julian day to illustrate the annual temporal pattern. As expected, in the beginning of the year and during summertime less calls were recorded in comparison to the migration seasons reflecting the higher number of birds in the area during that time. Noticeable are the high number of Blackbird calls during the end of spring migration, which most likely are related to local breeding birds rather than Blackbird migration activity which typically occurs earlier in spring. During the autumn season high numbers of geese calls dominated the spectrum which are also likely to stem to a considerable part from locally resting and wintering birds (Figure 4-28 and Figure 4-29).

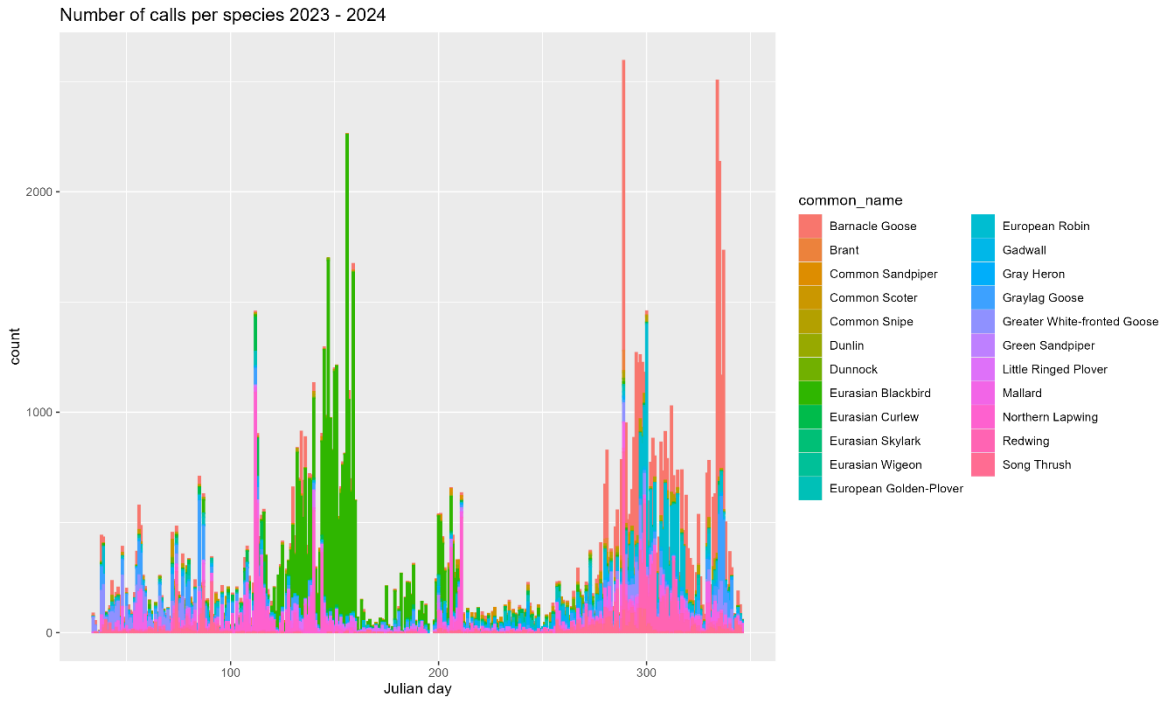

Figure 4-28 Number of calls per species over the course of seasons during nighttime. Here all 23 species with high enough accuracy as given by the AI are plotted.

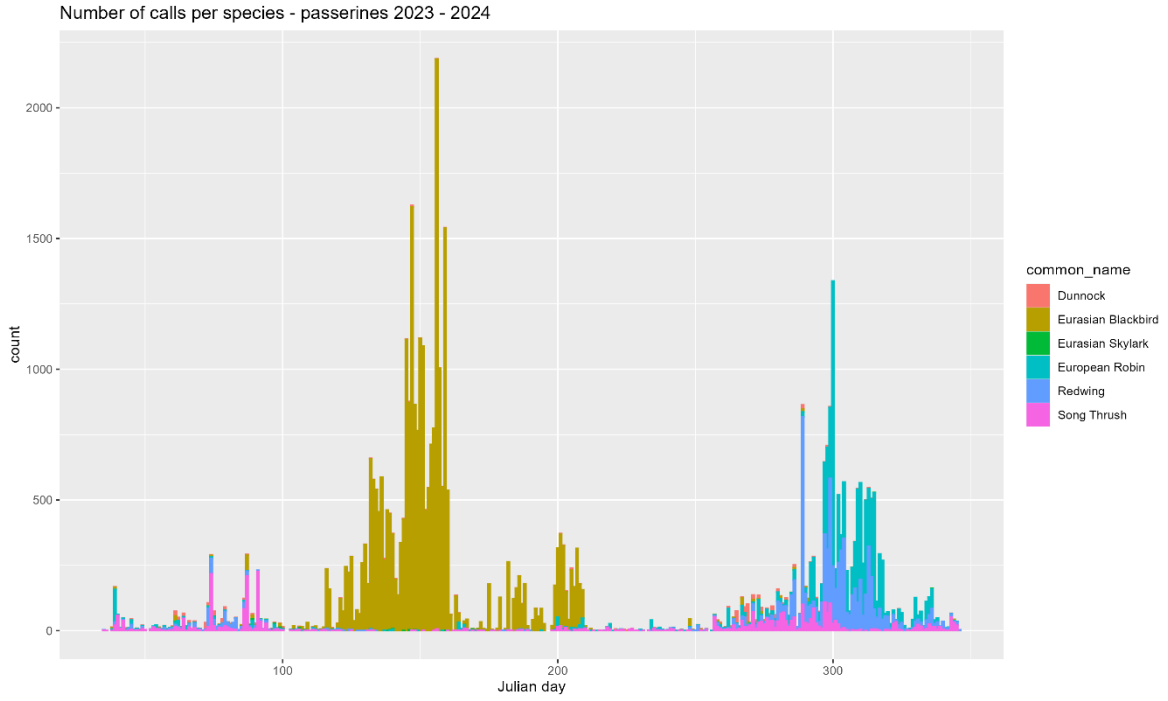

Figure 4-29 Number of calls of passerine species over the course of seasons during nighttime. All six species of passerine with high enough accuracy as given by the AI are plotted.

5 DISCUSSION

In this study we applied both innovative and established methods to evaluate the collision risk particularly of nocturnal bird migration at a coastal wind farm with the aim to allow conclusions about the collision risk of these birds at offshore wind turbines.

A specialised bird radar recorded data on MTR and FHD for four migration periods at the study site and contributed data to empirically determine avoidance rates and the magnitude of fatalities. The BirdScan MR1 radar we deployed can be regarded as a state-of-the-art ornithological radar which has been validated by the scientific community (LIECHTI ET AL. 2018; NILSSON ET AL. 2018; SCHMID ET AL. 2019), has widely been used in quantitative studies and has even been utilized for validating weather radar measurements (JIMENEZ ET AL. 2024).

The novel AI-driven camera systems we deployed were specifically developed to detect rotor transits of birds and bats during both day and night. The design of the system allowed us to collect representative data on rotor transits as they monitored i) a substantial proportion of the rotor plane and the area leeward of the rotor (50 %) at all times, independently of wind direction and associated turbine orientation, ii) equally covered areas above and below the nacelle, and iii) recorded rotor transits up to the whole length of the rotors. Although AI development was not finalised before the start of the data collection period and post-analyses of stored video sequences required large computational capacities and, hence, delayed analysis of video data, the total number of days (305) and nights (547) analysed for rotor transits resulted in a comprehensive and robust data set. In addition, the technical availability of the cameras was very high reducing data gaps and necessary correction of data to a minimum.

Nonetheless, rotor transits of birds can be regarded as rare events with the total number recorded in this study amounting to only 45 (when turbines were operational). This emphasises the need for a high data acquisition effort to collect a sufficiently large data set on transits for statistically robust conclusions.

Finally, we conducted intensive collision fatality searches to independently estimate the actual number of collision victims and facilitate a comparison with and validation of the Band collision risk model. We implemented a high frequency of searches, and a narrow transect design to maximise the probability of finding also small-sized collision victims such as passerine birds and thus minimise uncertainty due to large correction factors. In addition, we performed comprehensive search efficiency as well as carcass persistence trials to ensure robust estimation of these important parameters. Moreover, we applied most recent Bayesian developments of modelling collision fatalities integrating data on size-dependent and visibility-dependent efficiency and persistence together with the probability of carcasses falling within the search areas. We expanded the existing approach by allowing the models to account for temporal variation in visibility conditions of search plots which can potentially have large effects on model outcomes. Overall, this approach resulted in reliable estimation of collision fatalities at the study site with relatively low confidence intervals.

Migration intensity and flight height distribution

Radar data on MTR and FHD revealed patterns that can be regarded as typical for bird migration in the geographical region of the study site. Both the temporal pattern of increased but intermittent

bird migration during spring (with peaks in March/April) and autumn (maxima in September/October) and the absolute values of MTR fell within the range reported in previous studies in coastal and offshore areas in northern Germany and adjacent areas (KRIJGSVELD ET AL. 2009; FEBI 2013; WELCKER ET AL. 2017; WELCKER 2019; BSH 2025). Maximum MTR values tended to be comparatively high which could be related to differences in radar technology applied in different studies (LIECHTI ET AL. 2018; WELCKER 2021) but may also indicate that high-intensity bird migration occurs at the study site.

Similarly, FHDs recorded during all four migration periods corresponded well with earlier studies in coastal and offshore areas (KEMP ET AL. 2013; WELCKER ET AL. 2017; BRUDERER ET AL. 2018; WELCKER & VILELA 2020; BRADARIĆ ET AL. 2024a). Although FHDs varied to a varying degree between spring and autumn as well as between day and night, in all circumstances the highest proportion of birds flew within the lowest altitude bands comprising the rotor area of the wind turbines. This implies that the collision risk of migrating birds was not principally reduced due to a preference of flight altitudes above the rotor height. This applies particularly to nocturnal migration as movements of local birds that often fly at lower altitudes primarily occur during the day.

In line with previous studies, bird call data comprised high proportions of species known to constitute a substantial part of nocturnal bird migration in the region such as the Robin and different species of thrushes. Also, the radar data suggested that a considerable proportion of nocturnal bird movements were related to passerines and other small birds. If these species would incur a particularly high collision risk, we would expect collision fatalities to be dominated by these species. However, this was not the case. Of the 16 detected collision victims, only starlings are considered as partly nocturnally migrating while a song thrush which is considered a typical nocturnal migrant was found during winter (see Table 4-13 for a list of all collision victims found).

Transit rates and migration traffic rates

The low absolute numbers of rotor transits recorded at the two turbines equipped with camera systems (988 and 45 with inactive and active rotors, respectively) generally translated into low transit rates per hour. As indicated by these absolute numbers, there was a remarkable difference in transit rates depending on the operational status of the rotors. When turbines were active, about 20 times lower transit rates were recorded suggesting that birds perceive the rotating blades and avoid them to a larger extend than when they are idle. Consequently, data on rotor transits at inactive turbines cannot be used as an indicator of collision risk, and, hence, are also not suitable for estimating the efficiency of turbine curtailment as a collision mitigation measure.

We observed nearly twice as many transits per time unit at night compared to daytime. This occurred even though the average MTR at night was not higher than during the day on the dates we analysed. Instead, the increased transit rate at night was primarily driven by a reduced avoidance rate during nighttime when the turbines were not operating (i.e., rotor speed < 2 rpm). When the turbines were active, the difference in transit rates between day and night was reversed. However, the absolute number of transits with active rotors was very low in both cases—25 during the day and 20 at night. Given these small numbers, a change of just one or two transits more at night, and one or two transits less per day would be sufficient to eliminate the observed pattern, suggesting that this effect may be subject to stochastic variation. In contrast, when turbines were not

operating a much higher number of transits occurred, and the observed pattern of increased transit rates at night —approximately 1.5 times higher than during the day—appeared to be more robust.

One of the most striking findings of the present study was that the number of transits depended only weakly—if at all—on the MTR at rotor height. As no transits can occur without traffic, a basic low correlation is naturally expected. Nonetheless, our study clearly shows that MTR may not be a good predictor of rotor transits. Thus, an increase in MTR does not necessarily result in a proportional increase in the number of transits and, thus, collision rate. Apparently, other factors may be more important in determining transit rates. Most notably and as described above, there is a strong correlation between transit rates and the operational status or rotation speed of the turbine. The data clearly showed that transit rates were significantly higher when the rotor was stationary or rotating slowly (less than 2 rpm). Even when the turbine was operational—defined here as having a rotor speed of 2 rpm or higher—a negative relationship was observed: the likelihood of rotor transits decreased as rotor speed increased. This negative association was evident during both day and night, but the effect was considerably more pronounced during nighttime hours.

This result implies that during periods of high flux rates of birds the rate of rotor transits, and, consequently, the rate of collisions is not necessarily increased. As has been shown in chapter 4.1.3 and as demonstrated by a suit of previous studies, the magnitude of nocturnal bird migration heavily depends on prevailing weather with high migration intensities predominantly occurring during periods of favourable conditions. This includes e.g. supportive wind conditions, good visibility and no precipitation. Although the proportion of birds flying at low altitudes increases with adverse weather (chapter 4.1.3), in situations with favourable weather and high migration activity, on average still the largest proportion of bird movements occur in the altitude range of the rotors. However, birds seem to perceive the turbines and rotating blades sufficiently well to avoid them keeping collision risk also at high migration intensities low.

These conclusions have important repercussions for mitigation measures implementing turbine curtailment during time periods of high migration intensities at rotor height. These measures imply a positive relationship between the probability of bird collisions and flux rates. However, as the likelihood of birds passing through the rotor seems independent of concomitant migration intensity, as suggested by our results, these measures are likely to be ineffective.

It needs to be noted though, that contrasting evidence exists from a coastal wind farm in The Netherlands (Eemshaven). In a trial implementing turbine curtailment at a subset of turbines during 10 nights with expected high nocturnal migration intensities, collision victims of nocturnally migrating birds were only found at turbines that remained operational (KLOP & BRENNINKMEIJER 2020, see also KLEYHEEG-HARTMAN et al. 2025). Although this does not necessarily indicate a positive relationship between MTR and the number of collisions, it suggests potential effectiveness of curtailment. Clearly, more research is needed to determine how local differences may affect the collision risk of nocturnal bird migration.

Transit rates and weather

In addition to the minor relationship with MTR, the occurrence of rotor transits was only weakly predicted by weather conditions. Still worthwhile to mention and contrary to our initial hypothesis, transits were more likely to occur under favourable weather conditions — specifically when

visibility was high and both precipitation and crosswind levels were low. However, these findings should be interpreted with caution, as the models capturing these effects explained only a small proportion of the variance in the data (R^2-value of 0.019 for the model on day data and 0.041 for the night (see appendix).

Given the rarity and potentially high randomness of transit events, a substantially larger sample size would be required to improve the statistical power of the models and to more reliably identify which environmental factors may contribute to systematic patterns. It also seems possible that the probability of rotor transits depends on factors or interactions of factors not considered in this study. Further research is needed to determine under which conditions or circumstances birds neglect to show an avoidance response and thus incur a higher risk of collision.

Avoidance rate

We applied two methods to calculate the avoidance rate. The first method was based on the actual number of collisions fatalities found during the PCFM, compared to the expected number of collisions predicted by the CRMs under the assumption of zero avoidance. This method was suggested by BAND (2012) as the preferred way to derive avoidance rates to be used in the Band CRM and is independent of the rotor transits recorded by the camera systems. Because carcasses found in the field could not be linked to either daytime or nighttime collisions, we could only derive an overall avoidance rate. This overall rate was 0.9983, ranging from 0.9961 (based on the lower CI of the CRMs) to 0.9993 (based on the upper CI of fatalities from the PCFM).

With the second method, we were able to calculate avoidance rates by directly recording transit rates through the rotor plane using camera systems and quantifying the MTR at rotor height using a specialised bird radar. The avoidance rate calculated by this method represents the factor by which the expected number of rotor transits obtained by radar MTR data and assuming no avoidance response, has to be corrected to derive the actual number of rotor transits as recorded by the cameras. With 0.9987 for night and 0.9986 for daytime, respectively, these avoidance rate estimates fell well within the range of the results of the first method.

The good correspondence between the avoidance rates obtained with and without usage of the camera data lends further credibility to the performance of the camera systems and suggests that only few rotor transits might have been missed.

Furthermore, both methods used in this study resulted in avoidance rates substantially higher than previously assumed. In comparison, an avoidance rate of 0.980, including passerines, is recommended by some authors as a precautionary approach in cases where no site-specific data are available (MACLEAN ET AL. 2009; POTIEK ET AL. 2021). This rate is frequently used as a default in Band CRMs, with the understanding that it is likely conservative and tends to overestimate collision rates.

Avoidance rates are often regarded at three spatial scales: macro-avoidance (avoidance of the whole wind farm area), meso-avoidance (avoidance of turbine rows/turbines within wind farms) and micro-avoidance (last second avoidance of the rotor-swept area or single rotor blades). Overall avoidance rates usually integrate the response of the birds at all spatial scales.

Particularly for nocturnal passerine migration it is unknown at which distance to turbines birds may start to alter their flight behaviour. Our radar was placed about 650 m outside the wind farm. Even though we regard it as unlikely that a relevant proportion of nocturnally migrating songbirds responded at larger distances, our estimates of avoidance rates may not fully integrate macro-avoidance and therefore represent a conservative estimate. Likewise, at the micro scale birds may actively avoid single rotor blades while still passing through the rotor plane. Such behaviour was recorded in some instances also on the video footage in our study. However, as this behaviour could not be quantified (only parts of the rotor blades were within the field of view of the cameras), it is also not incorporated in the estimates of avoidance rates resulting in further potential underestimation.

Particularly for nocturnal migration information on avoidance rates is scarce. A study employing a similar approach but using different camera and radar technologies estimated avoidance rates at an offshore site (SCHULZ ET AL. 2014). Their estimates ranged between 0.9562 and 0.9803 and thus were substantially lower than our estimate at 0.9987. This discrepancy may be due to differences in the technical setup, especially the less advanced technology available at that time. Notably, the deployed cameras had a substantially narrower field of view and presumably lower detection rates due to inferior sensors and a lack of AI detection. Furthermore, one camera without distance estimation capabilities was mounted on the nacelle facing upwards only. An additional camera at the turbine base monitored areas outside the immediate rotor-swept area. Given that flight intensity is not evenly distributed across the vertical span of the rotor—as shown in FHD data—this setup is likely to introduce systematic bias.

Avoidance rate and turbine operational status

Although overall avoidance rates differ significantly between Schulz et al. (2014) and those found in the present study, they are comparatively similar during periods when the turbines are active. A much greater difference emerged under conditions when the rotor was idling or stationary. In both studies, the number of transits increased considerably when the turbines were inactive.

As reported in chapter 4.2, the nighttime avoidance rate at our study site dropped from 0.9987 to 0.9660, making transits over 26 times more likely under inactive rotor conditions, yet still quite rare. In contrast, Schulz et al. (2014) reported an avoidance rate of 0.407 when rotors were inactive, resulting in a much greater increase in transit rates. The relative increase in transit probabilities (1-avoidance rate) in the study by Schulz et al. (2014) was 13.5 times higher compared to our results. The reason for this considerable discrepancy remains speculative.

In our study, the difference in avoidance rates between active and inactive rotors was more pronounced during the night indicating that rotor status had a greater effect on the avoidance response of birds during the night. While the high avoidance rates at active turbines suggest that birds are able to recognise the turbines in time to respond appropriately, perception of inactive turbines at night might be more restricted. As it seems likely that the sounds produced by the rotating blades contributes significantly to the perception of the turbines by the birds, the lack of this clue at inactive rotors may at least partly explain reduced avoidance at night. This notion is also supported by the fact that rotor transits decreased and avoidance increased with increasing rotor speed and, thus, presumably increased noise levels.

In addition to acoustic cues, the stronger air turbulence associated with increasing rotor speed may also play a role. Since these turbulences primarily occur in the wake behind the rotor blades, it remains uncertain to what extent they are perceptible to birds. It might be that birds approaching the rotor from behind can use this as an additional cue.

The smaller drop of avoidance rates between active and inactive turbines during daytime remains more speculative. As visual clues may play a more prominent role during daytime, diurnally active birds may be able to recognise idling or stationary rotor blades and the corresponding reduced need to respond by avoidance. This could for instance been observed during the documented 'barn swallow event' when several swallows were actively foraging in the immediate rotor area and resting on the stationary rotor blade but avoided the area at once the rotors started to rotate again. Thus, increased avoidance during active rotors may be caused by risk averse behaviour of the birds, as birds judge transits between faster moving blades as too risky. Alternatively, an increased rotation speed might lead to motion smear (see e.g. MAY ET AL. 2020) making it difficult for birds to assess the threat. In contrast to the general view that motion smear may lead to a lower probability of an avoidance response and thus to a higher collision risk, it may also lead birds to avoiding the rotor plane as they cannot fully perceive all details of the situation.

Collision fatalities

The results of the fatality surveys indicated a relatively low number of collision victims. An estimated total of 99.7 fatalities of all bird species (95 % CI: 55–168) were estimated across the study period at the five monitored wind turbines. This corresponds to a mean of 12.9 collision fatalities per year and turbine.

Based on the species composition of carcasses found in the field, the risk for nocturnally migrating passerine birds appeared to be very low. Only two Starlings found during the fatality searches can be regarded as at least a partially nocturnally migrating passerine. Even after accounting for lower detection probabilities—due to reduced search efficiency and shorter carcass persistence for small birds—the absolute risk remained lower than for larger birds (33.9 *versus* 47.0 carcasses). The estimated total number of carcasses for small and medium-sized birds, to which passerines are counted based on their size, was 33.9 (small birds) and 18.9 (medium-sized birds), respectively. The sum of those numbers (52.8) was still not considerably larger than that for large birds. Also, baseline mortality rates (λ) were similar across size classes (small birds: $\lambda = 0.018$; medium-sized birds $\lambda = 0.010$, large birds: $\lambda = 0.025$) with confidence intervals for all three size classes overlapping substantially. Nonetheless, small birds occurred in much higher absolute numbers than large birds, making their relative fatality numbers small in proportion. According to bird radar data, small bird species—such as passerines and swift-type migrants—accounted for up to 85 % of radar signals at night. Similarly, the nocturnal bird call data showed that passerines made up a large proportion of all recorded calls.

These results confirm earlier findings suggesting that nocturnally migrating birds do not incur a high collision risk at wind farms but, in comparison to diurnally active bird species, may rather be able to avoid collisions more effectively (KRIJGSVELD et al. 2009, GRÜNKORN et al. 2016, WELCKER et al. 2017; but see also KLEYHEEG-HARTMAN et al. 2025). With the currently available data, the reasons for this discrepancy remain uncertain. A possible explanation may be related to behavioural differences between nocturnally migrating and diurnally active birds. While during migration, birds need to concentrate on navigation including the avoidance of obstacles when flying at low altitudes,

diurnally active birds are engaged in a variety of activities that may at least partly divert their attention and impair their capabilities to perceive fast moving objects. On the other hand, several diurnally active species found during the collision fatality searches in our study can to some degree also be active at night. Although the cameras were not designed to systematically detect collisions directly, one of two nocturnal collisions recorded involved an individual identified as possibly a small gull. This may suggest that although nocturnally migrating birds seem not to incur a high collision risk, collisions of predominantly day-active species may still occur at night.

Comparison of results of Band Collision risk models and fatality searches

To estimate collision fatalities independently of PCFM, we ran stochastic SOSS Band models, giving us the opportunity to compare and validate estimates derived by these methods. We were able to implement Band models eliminating the most prominent sources of uncertainty associated with Band CRMs (CHAMBERLAIN ET AL. 2006; MASDEN 2015; MASDEN & COOK 2016; WELCKER & VILELA 2019). Most importantly, we applied avoidance rates empirically determined by radar and camera data in our study and confirmed by a separate calculation based on PCFM independently of camera data. As this parameter has a paramount impact on model outcome (see also chapter 4.3.2), a precise estimate of the avoidance rate is crucial in obtaining realistic fatality estimates. Furthermore, we quantified MTR and FHD during day and nighttime directly at the study site minimising uncertainty of estimating expected rotor transits.

The Band model calculates monthly collision rates taking into account rotor downtime (e.g. due to low wind or maintenance) as well as mean rotor rotation speeds and pitch angles. As these data were kindly provided by turbine operators, we could integrate turbine-specific information on all these parameters further decreasing uncertainty in modelled outcome. As these parameters together with turbine dimensions (e.g. rotor diameter and hub-height) differ between the five turbines included in our study, we ran CRM for each of the turbines separately and finally summed up estimated collision to get the estimate for the whole wind farm for the duration of the study.

All together this large and exhaustive data collection allowed an adequate estimation of expected collisions. Indeed, the results based on CRMs applying avoidance rates determined in this study match to a very high degree with estimates derived by the post construction fatality monitoring (76.59 [95 %-CI: 57.3 - 97.6] *versus* 99.7 [95 %-CI: 55 - 168]). This strong overlap in the estimates of two independent methods is reassuring and their consistency supports each other's reliability. However, this logic could follow a circular argument if both methods shared a common, biased data source. This was not the case as the only common source of information was the turbine operational data, i.e. the rotor speed and corresponding turbine downtime.

While a change in turbine downtime would lead to systematic changes in the estimation of the expected collisions in the CRM, in PCFM this effect is buffered since the same downtime data is used both to estimate the fatality rate *lambda_0* and to predict the number of fatalities. Thus, the estimated fatality rate *lambda_0* would increase while the predicted number of fatalities, which depends on the product between the estimated fatality rate and the provided turbine uptime, would be expected to change little overall. Irrespective, we see no reason to distrust the turbine data, which are simple metrics that do not require complex data processing other than calculating the monthly percentage of rotor speed above 2 rpm.

Uncertainty of estimates

For a thorough comparison we need to consider the CIs of the different methods. While the mean estimates closely match and the 95 %-CIs overlap completely, the upper CI of the PCFM estimate (168) and the lower CI of the CRM estimate (57.3) still vary considerably leaving room for substantial variation between methods. 'CIs' are derived by different mathematical approaches in both methods. In case of the CRMs, 'confidence intervals' are calculated which are more precisely 'percentile intervals' capturing the central 95 % of the distribution based on resampling procedures. The 'CI' of the Bayesian MCMC intervals of PCFM represent more precisely 'central intervals' where the upper and lower tails of posterior distributions are cut off to get the remaining e.g. 95 %. Common for both methods is that these CIs are based on true distributions, unlike in frequentist statistics. This means that, in cases such as ours in which the distributions roughly follow a normal distribution, the closer values within the CI are to the mean estimate, the higher their credibility (compare KRUSCHKE 2015b). Thus, even with larger datasets resulting in reduced CIs it seems unlikely that significant differences in the estimation of fatalities between the methods would occur.

In general, the PFCM method showed larger uncertainty in the estimate (credible intervals were larger). This uncertainty is caused by the rigorous error propagation of the Bayesian approach used to analyse the PCFM data. Here, several different sources of uncertainty are possible and included in this estimate leading to potentially large CI for this method: (i) uncertainty in searcher efficiency and its dependence on bird size and visibility conditions, (ii) uncertainty of persistence time of carcasses, and (iii) uncertainty due to a fraction of carcasses falling outside the search areas. Due to rigorous error propagation, the results of the PCFM are expected to be very robust, making them suitable as a way of 'ground truthing'. On the other hand, underlying calculations of CRMs are likely to underestimate the uncertainty of model outcomes as uncertainty associated with input parameters are not comprehensively captured and integrated into its final estimate (such as daily changes in FHD, MTR within month, or differences of species). Thus, it is not surprising that the 95 %-CI range of the CRMs (57.3 - 97.6) exceeded the 95-CI of the PCFM (55 - 168).

Nonetheless, the estimated mean of collisions by CRM (76.6) was about 25 % lower than that by PCFM (99.7). This difference in estimated collision victims might be explained by multiple factors:

- Missed rotor transits by the camera systems: Missed transits would lead to a decrease in the estimated avoidance rate and hence to an increased estimation of collision victims by the CRM. However, the AI models of the AVES system were applied with confidence levels that resulted in no false negatives in comparison to manual review by experts at the cost of a high false positive rate. While it is unrealistic that detection by AI models was perfect and we assume that only few false negatives occurred, the lower estimate by CRM may at least partly be related to rotor transits missed by the camera systems.

- Not all carcasses found in the field may have been caused by collision with rotor blades: While we followed the suggestions of the PFCM Handbook (INTERNATIONAL FINANCE CORPORATION 2023) in assigning carcasses and feathers found in the field as to being a collision victim or not, causes of death could not be determined in the vast majority of cases. Thus, some of the carcasses found might not have been killed by the turbines but may have been related to natural or other non-wind-farm related causes. Thus,

slight overestimation of collision fatalities by PCFM through misassignment of carcasses as collision victims cannot be dismissed. To avoid this potential source of error, the 'baseline' mortality would have to be determined in the field adding substantially to the already high effort of fatality searches.

- Potential collision of birds with non-operational turbines: The Band model assumes no collision risk during periods in which the turbines are not active. Band himself pointed out that this is a simplification and that in nature birds may collide with non-moving anthropogenic structures (BAND 2012). However, he regarded this risk to be minor and for simplicity it was not incorporated in the CRM. Consequently, if some carcasses found during the fatality searches were birds colliding with inactive turbines this would lead to a higher collision estimate in PCFM but not in CRM.

Thus, there are some plausible reasons why on the one hand CRM may have underestimated the actual number of collision and on the other hand reasons why the PCFM methods may have overestimated the actual number of collisions. However, it seems likely that eliminating these potential sources of error would lead to further improved correspondence of estimates rather than greater divergence and, thus, the good accordance between the estimates of the two independent methods seems to be robust.

Validation of Band Collision risk models

Given the similarity in estimates of the BAND model, using the avoidance rates found in this study, and the PCFM method, this seems to validate the 'inner' part of the BAND model concerning the purely mathematical calculation of the 'single transit risk'. In the BAND model the number of transits is calculated from the MTR at rotor height and the FHD, and the avoidance rates. These parameters have been determined directly in our study by state-of-the-art technology. The single transit risk then depends on the birds' size and flight speed and on turbine parameters such as rotation speed, blade pitch and profile, and rotor diameter. For all turbine parameters we had either accurate measurements or good estimates. Bird data was taken from literature of average bird species during night and day separately based on the species composition found in our study. We assumed that variation in e.g. bird parameters would cancel out due to the large sample size involved.

Consequently, we are confident that valid data and good approximations have been used in the models. Thus, any strong deviance of the estimates by the BAND model from the PCFM estimates would most likely have been caused by a miscalculation of the single transit risk of the BAND model itself. Since the correspondence between the estimates was very high, we conclude the mathematical derivation of the single transits risk seems to be realistic – at least on average.

Furthermore, comparison of CRM outputs using different avoidance rates, e.g. earlier estimates for nocturnal bird migration (Schulz et al. 2014) emphasises the fact that inaccurate assumptions about avoidance behaviour may lead to vast overestimation of the actual collision risk. Although assuming an avoidance rate of 0.9802 or 0.9987 may at first sight seem negligible, it yet led to a difference of more than one order of magnitude in collision estimates. As mentioned above, the high consistency between collision estimates derived by PCFM and CRMs suggests that high avoidance rates determined in our study, particularly for nocturnal migration, are realistic and corroborates previous studies suggesting a relatively low collision risk of nocturnally migrating birds at wind farms.

Transferring our results to an offshore environment

Generally, we found good agreement of bird migration characteristics, especially related to nocturnal bird movements, between our coastal study site and data available for offshore locations in the German EEZ and adjacent areas (KRIJGSVELD ET AL. 2009; FEBI 2013; WELCKER ET AL. 2017; BRUDERER ET AL. 2018; WELCKER 2019; BRADARIĆ ET AL. 2020, 2024a; BSH 2025). This included temporal patterns, mean MTR values and flight height distributions indicating a preference for flight movements at low altitude. Additionally, in line with information from offshore studies, nocturnal bird migration at our study site was dominated by passerines and comprised similar species as indicated by radar and bird call data, respectively (SCHULZ ET AL. 2013, 2014; WELCKER & VILELA 2018; BSH 2025). As expected, weather dependency of bird migration at the study site was also similar to patterns reported for offshore areas (WELCKER & VILELA 2019; BRADARIĆ ET AL. 2024b). As it also seems reasonable to assume that nocturnal migrants respond similarly to wind turbines both on- and offshore, we regard results of this study relating to nocturnal bird migration to be generally transferable to offshore locations. Transferability may be reduced for diurnal bird movements primarily due to the fact that considerable differences in species composition can be expected between our coastal study site and offshore locations.

Furthermore, turbine size may affect the transferability of results. Given that larger turbines encompass a greater risk zone and have larger blades, it may reduce the bird's ability to avoid them. On the other hand, larger blades might increase the turbines visibility, counter-acting the potential negative effect of a greater risk zone. Also, light conditions, both background lighting and illumination of turbines, particularly at the base of the tower of offshore wind turbines, may differ between onshore and offshore potentially contributing to differences in bird behaviour.

For nocturnal bird migration, one crucial difference between on- and offshore areas may reduce transferability of results during specific situations. While at onshore locations passerine species and other landbirds may interrupt migration activity and alight at any time, this is not possible offshore.

This may particularly be important when birds face deteriorating weather conditions e.g. when approaching a bad weather front. Onshore, they may simply land, seek shelter and wait for better conditions. Offshore, they do not have this possibility and are forced to continue their flight. As shown in our study and supported by others (KEMP ET AL. 2013; BRADARIĆ ET AL. 2024a) a first response of most birds when facing adverse weather conditions is to decrease their flight height. Consequently, during these specific circumstances when nocturnally migrating birds are forced to continue their flight activity, they may incur an increased collision risk. Although evidence for offshore wind farms is still lacking, increased collision risk has been reported for other offshore anthropogenic infrastructures (RUSSELL 2005; AUMÜLLER ET AL. 2011). Situations in which bird migration triggered by favourable weather conditions early at night faces adverse weather while at sea can be regarded as rather rare events (LENSINK ET AL. 1999; WELCKER & VILELA 2019). Yet, when collision risk proves to be increased implementing mitigation measures in these circumstances may be highly effective.

We recommend conducting similar studies as presented here at offshore wind farms to confirm or refute the transferability of the results of our study to the offshore environment.

Conclusions

Applying novel AI-based camera technology, we found that rotor transits are infrequent events also during nights with high migration intensities. As rotor transits and, thus, the potential number of collisions was found to be only weakly correlated with MTR, mitigation measures such as turbine curtailment during time periods of increased flux rates are likely to be ineffective.

Empirically determined avoidance rates, particularly during the night, were substantially higher than previously estimated. Applying these avoidance rates in stochastic Band models resulted in an estimated number of collision victims congruent to fatality numbers independently estimated by PCFM. This lends credibility to the avoidance rates determined by state-of-the-art radar and camera technology and suggests that Band CRMs fed with realistic avoidance rates and appropriate site-specific turbine and bird data result in realistic collision fatality estimates.

In agreement with earlier studies, our results support the notion that in the vast majority of situations nocturnally migrating birds effectively avoid collisions and the overall collision risk in relation to the total amount of birds passing a wind farm at night is very low.

Although predicting collision risk based solely on MTR and FHD seems not possible and corresponding mitigation measures are likely to prove ineffectual, additional data from offshore locations are needed to rule out the possibility of an increased collision risk in situations when bird migration meets adverse weather conditions at sea.

6 LITERATURE

Alerstam, T. (1990) Bird Migration. publ. Cambridge University Press, Cambridge (GBR), New York (USA), Melbourne (AUS), pp. 420.

Aumüller, R., K. Boos, S. Freienstein, K. Hill & R. Hill (2011) Beschreibung eines Vogelschlagereignisses und seiner Ursachen an einer Forschungsplattform in der Deutschen Bucht. Vogelwarte (vol. 49), pp. 9–16.

Avitec Research GbR (ed.) (2014) Testfeldforschung zum Vogelzug am Offshore-Pilotpark *alpha ventus* und Auswertung der kontinuierlich auf FINO1 erhobenen Daten zum Vogelzug der Jahre 2008 bis 2012 im Rahmen des Forschungsprojektes "Ökologische Begleitforschung am Offshore-Testfeldvorhaben *alpha ventus* zur Evaluierung des Standarduntersuchungskonzeptes des BSH (StUKplus). (auts. Hill, R., K. Hill, R. Aumüller, K. Boos & S. Freienstein). no. FKZ 0327689A/Avitec1 und Avitec 2, StUKplus-Endbericht, Osterholz-Scharmbeck (DEU), Im Auftragdes Bundesamts für Seeschifffahrt und Hydrographie (BSH), p. 255.

Band, B. (2012) Using a collision risk model to assess bird collision risks for offshore wind farms. Final Report, The Nunnery, Thetford (GBR), p. 62.

Van Belle, J., J. Shamoun-Baranes, E. Van Loon & W. Bouten (2007) An operational model predicting autumn bird migration intensities for flight safety. Journal of Applied Ecology (4, vol. 44), pp. 864–874.

Bourne, W. R. P. (1980) The midnight descent, dawn ascent and re-orientation of land birds migrating across the North Sea in autumn. Ibis (4, vol. 122), pp. 536–540.

Brabant, R., N. Vanermen, E. W. M. Stienen & S. Degraer (2015) Towards a cumulative collision risk assessment of local and migrating birds in North Sea offshore wind farms. Hydrobiologia (1, vol. 756), pp. 63–74.

Bradarić, M. (2022) On the radar: Weather, bird migration and aeroconservation over the North Sea. PhD Thesis, Universiteit van Amsterdam.

Bradarić, M., W. Bouten, R. C. Fijn, K. L. Krijgsveld & J. Shamoun-Baranes (2020) Winds at departure shape seasonal patterns of nocturnal bird migration over the North Sea. Journal of Avian Biology (10, vol. 51).

Bradarić, M., B. Kranstauber, W. Bouten, H. Van Gasteren & J. S. Baranes (2024a) Drivers of flight altitude during nocturnal bird migration over the North Sea and implications for offshore wind energy. Conservation Science and Practice (4, vol. 6), p. e13114.

Bradarić, M., B. Kranstauber, W. Bouten & J. Shamoun-Baranes (2024b) Forecasting nocturnal bird migration for dynamic aeroconservation: The value of short-term datasets. Journal of Applied Ecology (6, vol. 61), pp. 1147–1158.

Bruderer, B. & F. Liechti (1998) Flight behaviour of nocturnally migrating birds in coastal areas - crossing or coasting. Journal of Avian Biology (4, vol. 29), pp. 499–507.

Bruderer, B., D. Peter & F. Korner-Nievergelt (2018) Vertical distribution of bird migration between the Baltic Sea and the Sahara. Journal of Ornithology (2, vol. 159), pp. 315–336.

BSH (2013) Standard - Untersuchung der Auswirkungen von Offshore-Windenergieanlagen auf die Meeresumwelt (StUK 4). Ergänzung zum Schutzgut Benthos, gemäß StUK4. (ed. Bundesamt für Naturschutz). Hamburg & Rostock (DEU).

BSH (2025) Umweltbericht zum Flächenentwicklungsplan 2025 für die deutsche Nordsee. no. BSH-Nummer 7608, Hamburg (DEU).

Bürkner P (2017). “brms: An R Package for Bayesian Multilevel Models Using Stan.” Journal of Statistical Software, 80(1), 1–28. doi:10.18637/jss.v080.i01.

Caneco, B., G. Humphries, A. S. C. P. Cook & E. Masden (2022) Estimating bird collisions at offshore windfarms with stochLAB.

Chamberlain, D. E., M. R. Rehfisch, A. D. Fox, M. Desholm & S. J. Anthony (2006) The effect of avoidance rates on bird mortality predictions made by wind turbine collision risk models. Ibis (s1, vol. 148), pp. 198–202.

Crainiceanu, C. M., D. Ruppert & M. P. Wand (2005) Bayesian Analysis for Penalized Spline Regression Using WinBUGS. Journal of Statistical Software (vol. 14), pp. 1–24.

Croll, D. A., A. A. Ellis, J. Adams, A. S. C. P. Cook, S. Garthe, M. W. Goodale, C. S. Hall, E. Hazen, B. S. Keitt, E. C. Kelsey, J. B. Leirness, D. E. Lyons, M. W. McKown, A. Potiek, K. R. Searle, F. H. Soudijn, R. C. Rockwood, B. R. Tershy, M. Tinker, E. A. VanderWerf, K. A. Williams, L. Young & K. Zilliacus (2022) Framework for assessing and mitigating the impacts of offshore wind energy development on marine birds. Biological Conservation (109795, vol. 276).

Dalthorp, D. & M. Huso (2023) dwp: Density-Weighted Proportion.

Dalthorp, D., M. Huso & D. Dail (2017) Evidence of Absence (v2.0) Software User Guide. no. 1055, U.S. Geological Survey Data Series, p. 109.

Dalthorp, D., M. Huso, M. Dalthorp & J. Mintz (2023a) Accounting for the Fraction of Carcasses outside the Searched Area and the Estimation of Bird and Bat Fatalities at Wind Energy Facilities. arXiv.

Dalthorp, D., L. Madsen, M. M. Huso, P. A. Rabie, R. Wolpert, J. Studyvin, J. Simonis & J. Mintz (2018) GenEst statistical models—A generalized estimator of mortality. no. 7-A2, in Techniques and Methods, p. 13.

Dalthorp, D., J. Simonis, L. Madsen, M. Huso, P. Rabie, J. Mintz, R. Wolpert, J. Studyvin & F. Korner-Nievergelt (2023b) GenEst: Generalized Mortality Estimator.

Van Doren, B. M. & K. G. Horton (2018) A continental system for forecasting bird migration. Science (6407, vol. 361), pp. 1115–1118.

Drewitt, A. L. & R. H. W. Langston (2008) Collision effects of wind-power generators and other obstacles on birds. Annals of the New York Academy of Sciences (vol. 1134), pp. 233–266.

Erni, B., F. Liechti, L. G. Underhill & B. Bruderer (2002) Wind and rain govern the intensity of nocturnal bird migration in central Europe - a log-linear regression analysis. Ardea (1, vol. 90), pp. 155–166.

FEBI (2013) Fehmarnbelt Fixed Link EIA. Bird Investigations in Fehmarnbelt – Baseline. Volume II. Waterbirds in Fehmarnbelt. no. E3TR0011.

Gelman, A., B. Goodrich, J. Gabry & A. Vehtari (2019) R-squared for Bayesian Regression Models. The American Statistician (3, vol. 73), pp. 307–309.

Gould, E., H. S. Fraser, T. H. Parker, S. Nakagawa, S. C. Griffith, P. A. Vesk, F. Fidler, D. G. Hamilton, R. N. Abbey-Lee, J. K. Abbott, L. A. Aguirre, C. Alcaraz, I. Aloni, D. Altschul, K. Arekar, J. W. Atkins, J. Atkinson, C. M. Baker, M. Barrett, K. Bell, S. K. Bello, I. Beltrán, B. J. Berauer, M. G. Bertram, P. D. Billman, C. K. Blake, S. Blake, L. Bliard, A. Bonisoli-Alquati, T. Bonnet, C. N. M. Bordes, A. P. H. Bose, T. Botterill-James, M. A. Boyd, S. A. Boyle, T. Bradfer-Lawrence, J. Bradham, J. A. Brand, M. I. Brengdahl, M. Bulla, L. Bussière, E. Camerlenghi, S. E. Campbell, L. L. F. Campos, A. Caravaggi, P. Cardoso, C. J. W. Carroll, T. A. Catanach, X. Chen, H. Y. J. Chik, E. S. Choy, A. P. Christie, A. Chuang, A. J. Chunco, B. L. Clark, A. Contina, G. A. Covernton, M. P. Cox, K. A. Cressman, M. Crotti, C. D. Crouch, P. B. D'Amelio, A. A. De Sousa, T. F. Döbert, R. Dobler, A. J. Dobson, T. S. Doherty, S. M. Drobniak, A. G. Duffy, A. B. Duncan, R. P. Dunn, J. Dunning, T. Dutta, L. Eberhart-Hertel, J. A. Elmore, M. M. Elsherif, H. M. English, D. C. Ensminger, U. R. Ernst, S. M. Ferguson, E. Fernandez-Juricic, T. Ferreira-Arruda, J. Fieberg, E. A. Finch, E. A. Fiorenza, D. N. Fisher, A. Fontaine, W. Forstmeier, Y. Fourcade, G. S. Frank, C. A. Freund, E. Fuentes-Lillo, S. L. Gandy, D. G. Gannon, A. I. García-Cervigón, A. C. Garretson, X. Ge, W. L. Geary, C. Géron, M. Gilles, A. Girndt, D. Gliksman, H. B. Goldspiel, D. G. E. Gomes, M. K. Good, S. C. Goslee, J. S. Gosnell, E. M. Grames, P. Gratton, N. M. Grebe, S. M. Greenler, M. Griffioen, D. M. Griffith, F. J. Griffith, J. J. Grossman, A. Güncan, S. Haesen, J. G. Hagan, H. A. Hager, J. P. Harris, N. D. Harrison, S. S. Hasnain, J. C. Havird, A. J. Heaton, M. L. Herrera-Chaustre, T. J. Howard, B.-Y. Hsu, F. Iannarilli, E. C. Iranzo, E. N. K. Iverson, S. O. Jimoh, D. H. Johnson, M. Johnsson, J. Jorna, T. Jucker, M. Jung, I. Kačergytė, O. Kaltz, A. Ke, C. D. Kelly, K. Keogan, F. W. Keppeler, A. K. Killion, D. Kim, D. P. Kochan, P. Korsten, S. Kothari, J. Kuppler, J. M. Kusch, M. Lagisz, K. M. Lalla, D. J. Larkin, C. L. Larson, K. S. Lauck, M. E. Lauterbur, A. Law, D.-J. Léandri-Breton, J. J. Lembrechts, K. L'Herpiniere, E.

J. P. Lievens, D. O. De Lima, S. Lindsay, M. Luquet, R. MacLeod, K. H. Macphie, K. Magellan, M. M. Mair, L. E. Malm, S. Mammola, C. P. Mandeville, M. Manhart, L. M. Manrique-Garzon, E. Mäntylä, P. Marchand, B. M. Marshall, C. A. Martin, D. A. Martin, J. M. Martin, A. R. Martinig, E. S. McCallum, M. McCauley, S. M. McNew, S. J. Meiners, T. Merkling, M. Michelangeli, M. Moiron, B. Moreira, J. Mortensen, B. Mos, T. O. Muraina, P. W. Murphy, L. Nelli, P. Niemelä, J. Nightingale, G. Nilsonne, S. Nolazco, S. S. Nooten, J. L. Novotny, A. B. Olin, C. L. Organ, K. L. Ostevik, F. X. Palacio, M. Paquet, D. J. Parker, D. J. Pascall, V. J. Pasquarella, J. H. Paterson, A. Payo-Payo, K. M. Pedersen, G. Perez, K. I. Perry, P. Pottier, M. J. Proulx, R. Proulx, J. L. Pruett, V. Ramananjato, F. T. Randimbiarison, O. H. Razafindratsima, D. J. Rennison, F. Riva, S. Riyahi, M. J. Roast, F. P. Rocha, D. G. Roche, C. Román-Palacios, M. S. Rosenberg, J. Ross, F. E. Rowland, D. Rugemalila, A. L. Russell, S. Ruuskanen, P. Saccone, A. Sadeh, S. M. Salazar, K. Sales, P. Salmón, A. Sánchez-Tójar, L. P. Santos, F. Santostefano, H. T. Schilling, M. Schmidt, T. Schmoll, A. C. Schneider, A. E. Schrock, J. Schroeder, N. Schtickzelle, N. L. Schultz, D. A. Scott, M. P. Scroggie, J. T. Shapiro, N. Sharma, C. L. Shearer, D. Simón, M. I. Sitvarin, F. L. Skupien, H. L. Slinn, G. P. Smith, J. A. Smith, R. Sollmann, K. S. Whitney, S. M. Still, E. F. Stuber, G. F. Sutton, B. Swallow, C. C. Taff, E. Takola, A. J. Tanentzap, R. Tarjuelo, R. J. Telford, C. J. Thawley, H. Thierry, J. Thomson, S. Tidau, E. M. Tompkins, C. M. Tortorelli, A. Trlica, B. R. Turnell, L. Urban, S. Van de Vondel, J. E. M. Van der Wal, J. Van Eeckhoven, F. Van Oordt, K. M. Vanderwel, M. C. Vanderwel, K. J. Vanderwolf, J. Vélez, D. C. Vergara-Florez, B. C. Verrelli, M. V. Vieira, N. Villamil, V. Vitali, J. Vollering, J. Walker, X. J. Walker, J. A. Walter, P. Waryszak, R. J. Weaver, R. E. M. Wedegärtner, D. L. Weller, S. Whelan, R. L. White, D. W. Wolfson, A. Wood, S. W. Yanco, J. D. L. Yen, C. Youngflesh, G. Zilio, C. Zimmer, G. M. Zimmerman & R. A. Zitomer (2025) Same data, different analysts: variation in effect sizes due to analytical decisions in ecology and evolutionary biology. BMC biology (1, vol. 23), p. 35.

Grünkorn, T., J. Blew, T. Coppack, O. Krüger, G. Nehls, A. Potiek, M. Reichenbach, J. Von Rönn, H. Timmermann & S. Weitekamp (2016) Ermittlung der Kollisionsraten von (Greif-)Vögeln und Schaffung planungsbezogener Grundlagen für die Prognose und Bewertung des Kollisionsrisikos durch Windenergieanlagen (PROGRESS). Schlussbericht zum durch das Bundesministerium für Wirtschaft und Energie (BMWi) im Rahmen des 6. Energieforschungsprogrammes der Bundesregierung geförderten Verbundvorhaben PROGRESS, FKZ 0325300A-D. p. 332.

Hartig, F. (2024) DHARMa: Residual Diagnostics for Hierarchical (Multi-Level / Mixed) Regression Models. Abstract.

Hüppop, O., J. Dierschke, K. M. Exo, E. Fredrich & R. Hill (2006) Bird migration studies and potential collision risk with offshore wind turbines. Ibis (vol. 148), pp. 90–109.

Hüppop, O. & G. Hilgerloh (2012) Flight call rates of migrating thrushes: effects of wind conditions, humidity and time of day at an illuminated offshore platform. Journal of Avian Biology (1, vol. 43), pp. 85–90.

Hüppop, O., R. Hill, K. Hüppop & F. Jachmann (2009) Auswirkungen auf den Vogelzug - Begleitforschung im Offshore-Bereich auf Forschungsplattformen in der Nordsee (FINOBIRD). Abschlussbericht, Helgoland (DEU), p. 278.

Hüppop, O., K. Hüppop, J. Dierschke & R. Hill (2016) Bird collisions at an offshore platform in the North Sea. Bird Study (vol. 63), pp. 73–82.

International Finance Corporation (ed.) (2023) Post-construction bird and bat fatality monitoring for onshore wind energy facilities in emerging market countries. Washington D.C. (USA).

Jimenez, M. F., B. Haest, A. Khalighifar, A. L. Abbott, A. Feuka, A. Liu & K. G. Horton (2024) Quantifying range-and topographical biases in weather surveillance radar measures of migratory bird activity. Remote Sensing in Ecology and Conservation.

Kemp, M. U., J. Shamoun-Baranes, A. M. Dokter, E. Loon & W. Bouten (2013) The influence of weather on the flight altitude of nocturnal migrants in mid-latitudes. Ibis (4, vol. 155), pp. 734–749.

Krijgsveld, K. L., K. Akershoek, F. Schenk, F. Dijk & S. Dirksen (2009) Collision risk of birds with modern large wind turbines. Ardea (3, vol. 97), pp. 357–366.

Krijgsveld, K. L., R. C. Fijn, M. Japink, P. W. Van Horssen, C. Heunks, M. P. Collier, M. J. M. Poot, D. Beuker & S. Dirksen (2011) Effect studies Offshore Wind Farm Egmond aan Zee - Final report on fluxes, flight altitudes and behaviour of flying birds. Final Report, Culemborg (NDL), p. 328.

Kruschke, J. K. (2015a) Doing Bayesian Data Analysis. A Tutorial with R, JAGS, and Stan. ED. 2nd Edition, publ. Academic Press.

Kruschke, J. K. (ed.) (2015b) Chapter 11 - Null Hypothesis Significance Testing. (aut. Kruschke, J. K.). in Doing Bayesian Data Analysis (Second Edition), publ. Academic Press, Boston, pp. 297–333.

Lensink, R., D. A. Jonkers, M. Leopold, H. Schekkerman & S. Dirksen (1999) Falls of migrant birds, an analysis of current knowledge. Culemborg, Bureau Waardenburg, 1999. Report 99.55, 117 pp.

Liechti, F., J. Aschwanden, J. Blew, M. Boos, R. Brabant, A. M. Dokter, V. Kosarev, M. Lukach, M. Maruri, M. Reyniers & Others (2018) Cross-calibration of different radar systems for monitoring nocturnal bird migration across Europe and the Near East. Ecography (vol. 42), pp. 1–12.

Lindén, A. & S. Maentyniemi (2011) Using the negative binomial distribution to model overdispersion in ecological count data. Ecology (7, vol. 92), pp. 1414–1421.

De Lucas, M., G. F. E. Janss & M. Ferrer (eds.) (2007) Trapped within the corridor of the southern North Sea: The potential impact of Offshore Wind Farms on Seabirds. (auts. Stienen, E. W. M., J. Van Waeyenberge, E. Kuijken & J. Seys). in Birds and wind farms: risk assessment and mitigation, publ. Quercus, Madrid (ESP), pp. 71–80.

Maclean, I. M. D., L. J. Wright, D. A. Showler & M. M. Rehfisch (2009) A review of assessment methodologies for offshore windfarms. British Trust for Ornithology Report Commssioned by Cowrie Ltd.

Makowski, D., Wiernik, B. M., Patil, I., Lüdecke, D., & Ben-Shachar, M. S. (2022). correlation: Methods for correlation analysis (0.8.3) [R package].

Masden, E. (2015) Developing an avian collision risk model to incorporate variability and uncertainty. Thurso (GBR), p. 26.

Masden, E. A. & A. S. C. P. Cook (2016) Avian collision risk models for wind energy impact assessments. Environmental Impact Assessment Review (vol. 56), pp. 43–49.

May, R., T. Nygård, U. Falkdalen, J. Åström, Ø. Hamre & B. G. Stokke (2020) Paint it black: Efficacy of increased wind turbine rotor blade visibility to reduce avian fatalities. Ecology and Evolution (vol. 10), pp. 8927–8935.

McElreath, R. (2019) Statistical Rethinking: A Bayesian Course with Examples in R and STAN. ED. 2. Ed., publ. CRC Press, Boca Raton (USA), pp. 601.

Newton, I. (2023) The Migration Ecology of Birds (2nd ed.). publ. Academic Press.

Nilsson, C., A. M. Dokter, B. Schmid, M. Scacco, L. Verlinden, J. Bäckman, G. Haase, G. Dell'Omo, J. W. Chapman, H. Leijnse & F. Liechti (2018) Field validation of radar systems for monitoring bird migration. Journal of Applied Ecology (6, vol. 55), pp. 2552–2564.

Nilsson, C., A. M. Dokter, L. Verlinden, J. Shamoun-Baranes, B. Schmid, P. Desmet, S. Bauer, J. Chapman, J. A. Alves, P. M. Stepanian, N. Sapir, C. Wainwright, M. Boos, A. Górska, M. H. M. Menz, P. Rodrigues, H. Leijnse, P. Zehtindjiev, R. Brabant, G. Haase, N. Weisshaupt, M. Ciach & F. Liechti (2019) Revealing patterns of nocturnal migration using the European weather radar network. Ecography (5, vol. 42), pp. 876–886.

Nussbaumer, R., S. Bauer, L. Benoit, G. Mariethoz, F. Liechti & B. Schmid (2021) Quantifying year-round nocturnal bird migration with a fluid dynamics model. Journal of the Royal Society Interface (20210194, vol. 18).

Nussbaumer, R., B. Schmid, S. Bauer & F. Liechti (2022) Favorable winds speed up bird migration in spring but not in autumn. Ecology and Evolution (e9146, vol. 12).

Potiek, A., J. J. Leemans, R. P. Middelveld & A. Gyimesi (2021) Cumulative impact assessment of collisions with existing and planned offshore wind turbines in the southern North Sea. Analysis of additional mortality using collision rate modelling and impact assessment based on population modelling for the KEC 4.0. no. Rapportnr. 21-205, Culemborg (NLD).

R Core Team (2022) R: A language and environment for statistical computing, R version 4.2.2.

Roy, A., T. Désert, V. Delcourt, C. Bon & B. Schmid (2025) Enhanced forecasting of bird nocturnal migration intensity in relation to previous days and synoptic weather patterns. International Journal of Biometeorology.

Russell, R. W. (2005) Interactions between migrating birds and offshore oil and gas platforms in the northern Gulf of Mexico. no. OCS Study MMS 2005-009, Final Report, New Orleans (USA).

Schekler, I., Y. Levi & N. Sapir (2024) Contrasting seasonal responses to wind in migrating songbirds on a globally important flyway. Proceedings of the Royal Society B: Biological Sciences (2027, vol. 291), p. 20240875.

Schmaljohann, H., F. Liechti, E. Bächler, T. Steuri & B. Bruderer (2008) Quantification of bird migration by radar – a detection probability problem. Ibis (2, vol. 150), pp. 342–355.

Schmid, B., S. Zaugg, S. C. Votier, J. W. Chapman, M. Boos & F. Liechti (2019) Size matters in quantitative radar monitoring of animal migration: estimating monitored volume from wingbeat frequency. Ecography (5, vol. 42), pp. 931–941.

Schulz, A., T. Dittman & T. Coppack (2014) Erfassung von Ausweichbewegungen von Zugvögeln mittels Pencil Beam Radar und Erfassung von Vogelkollisionen mit Hilfe des Systems VARS. StUKplus Schlussbericht. Schlussbericht, Rostock (DEU), Im Auftrag des Bundesamts für Seeschifffahrt und Hydrographie (BSH), p. 89.

Schulz, A., T. Dittmann, A. Weidauer, M. Kilian, T. Löffler, V. Röhrbein & K. Schleicher (2013) Weiterentwicklung der Technik für Langzeituntersuchungen der Vögel mittels Radar und automatischer Kamerabeobachtung am Standort FINO 2 und Durchfühung von Langzeitmessungen am Standort für den Zeitraum 2010 bis 2012. Abschlussbericht, Neu Brodersdorf (DEU), Teilprojekt Vogelzug. Bestandteil des Forschungsvorhabens “Betrieb für Forschungsplattform FINO 2” (BMU; FKZ 0329905D), p. 103.

Scottish Natural Heritage (ed.) (2000) Windfarms and Birds: Calculating a theoretical collision risk assuming no avoiding action.

Sivula, T., M. Magnusson, A. A. Matamoros & A. Vehtari (2025) Uncertainty in Bayesian Leave-One-Out Cross-Validation Based Model Comparison. Bayesian Analysis (1, vol. 1), arXiv:2008.10296 [stat].

Skov, H., S. Heinänen, T. Norman, R. Ward, S. Méndez-Roldán & I. Ellis (2018) ORJIP Bird Collision and Avoidance Study. Final Report, London (GBR), p. 247.

Vehtari, A., J. Gabry, M. Magnusson, Y. Yao, P.-C. Bürkner, T. Paananen, A. Gelman, B. Goodrich, J. Piironen, B. Nicenboim & L. Lindgren (2024) loo: Efficient leave-one-out cross-validation and WAIC for Bayesian models.

Welcker, J. (2019) Patterns of nocturnal bird migration in the German North and Baltic Seas. ProBIRD report 2. Husum (DEU), p. 70.

Welcker, J. (2021) Vergleichbarkeit verschiedener Radarsysteme zur Erfassung des Vogelzugs. Husum, Im Auftrag des Bundesamts für Naturschutz, p. 42.

Welcker, J., M. Liesenjohann, J. Blew, G. Nehls & T. Grünkorn (2017) Nocturnal migrants do not incur higher collision risk at wind turbines than diurnally active species. Ibis (2, vol. 159), pp. 366–373.

Welcker, J. & R. Vilela (2018) Analysis of bird flight calls from the German North and Baltic Seas. Final Report. Husum, p. 128.

Welcker, J. & R. Vilela (2019) Weather-dependence of nocturnal bird migration and cumulative collision risk at offshore wind farms in the German North and Baltic Seas. Technical report, Husum (DEU), p. 70.

Welcker, J. & R. Vilela (2020) ProBIRD - Prognose des regionalen und lokalen Vogelzugs und des kumulativen Vogelschlagrisikos an Offshore-Windenergieanlagen. Endbericht, Husum (DEU), p. 70.

Wood, S. N. (ed.) (2017) Generalized additive models. An intoduction with R. publ. CRC Press, Boca Raton (USA).

Zehnder, S., F. Liechti, B. Trösch & B. Bruderer (2001) Gibt es topographie-unabhängigen Nachtzug über den Alpen? Der Ornithologische Beobachter (vol. 98), pp. 215–222.

Zuur, A. F., E. N. Ieno, N. J. Walker, A. A. Saveliev & G. M. Smith (2009) Mixed effects models and extensions in ecology with R. in Statistics for Biology and Health, publ. Springer, New York, NY (USA), pp. 574.

7 ACKNOWLEDGEMENTS

We would like to express our gratitude to Windtestfeld-Nord GmbH for their support and collaboration. We also thank the turbine operators GP Joule Windpark Südermarsch GmbH & Co. KG and iTerra Wind GmbH & Co. KG for access to their wind turbines and support during installation and maintenance of the camera systems as well as to Ulf Schröder who kindly allowed us to install the radar on his property. We further acknowledge the operators of the weather station (Pavana Wind) for providing valuable data, and we extend our gratitude to four external reviewers for their constructive comments which helped greatly to improve this report.

A APPENDIX

A.1 Cameras

Table A-1 Overview of the number of days and nights camera data was analysed for rotor transits per month.

Month	Day		Night	
	Turbine GPJoule	Turbine IterraWind	Turbine GPJoule	Turbine IterraWind
May-23	3	3	3	3
Jul-23	3	3	3	3
Aug-23	9	9	9	9
Sep-23	12	12	12	12
Oct-23	12	12	12	12
Nov-23	12	12	23	23
Mar-24	9	31	30	31
Apr-24	9	27	28	28
May-24	9	14	31	24
Jul-24	17	3	17	17
Aug-24	9	9	30	31
Sep-24	9	9	24	24
Oct-24	12	12	30	30
Nov-24	12	12	25	23
total	**137**	**168**	**277**	**270**

A.2 Transits

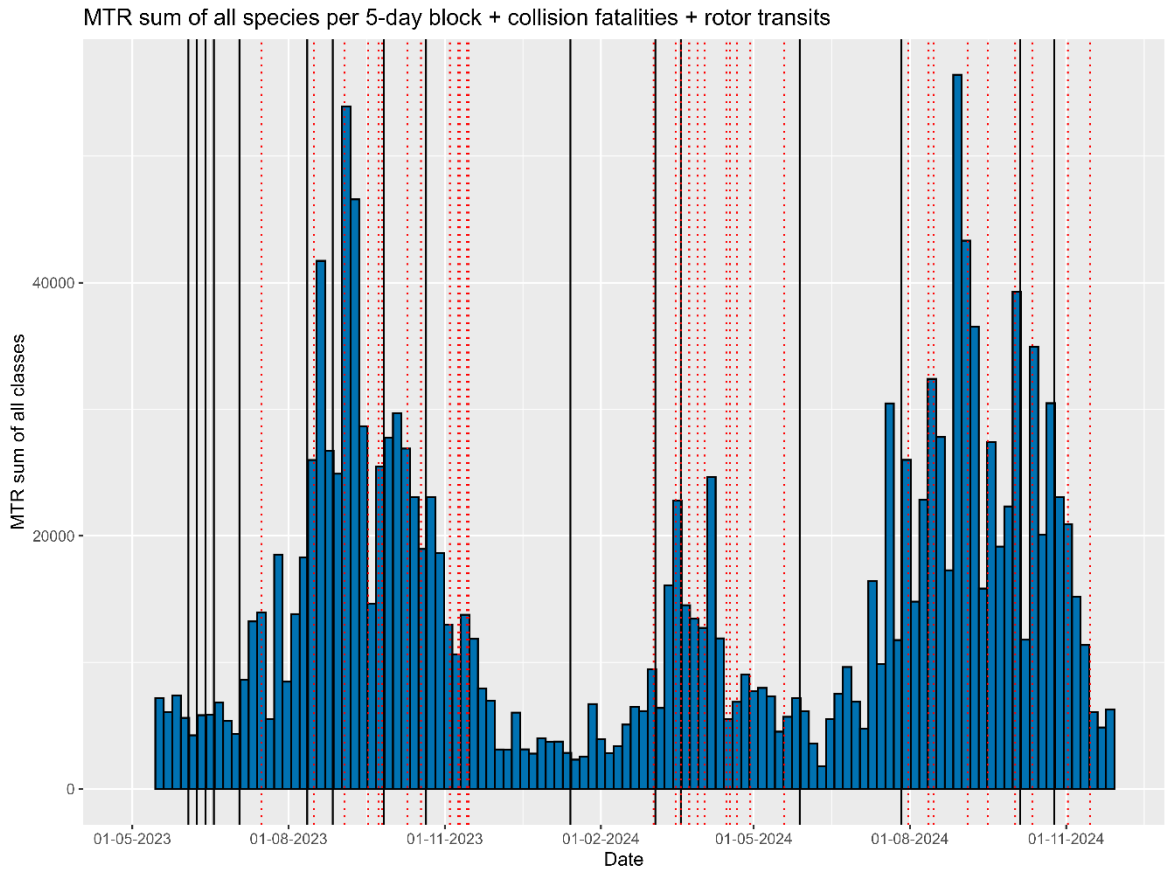

Figure A-1 *Temporal relationships among three datasets: the MTR at rotor height aggregated over 5-day intervals corresponding to the carcass search periods (solid blue bars); carcasses detected during the searches (solid black vertical lines) and rotor transits recorded during turbine operation (rpm ≥ 2 dotted red vertical lines).*

Table A-2 *Single rotor transits risk as calculated in SOSS Band model for the given two turbines and for day and night species represented by dove and redwing accordingly.*

Turb_Id	Day Or night	Single transit risk
iTerra	night	0.06117728
iTerra	day	0.07149246
GP_Joule	night	0.07728854
GP_Joule	day	0.08905901

Table A-3 *R^2 values for Bayesian models on rotor transits in relation to weather parameters.*

Model	Bayesian R^2		
	Median	CI 2.5 %	CI 97.5 %
night	0.041	0.012	0.114
day	0.019	0.007	0.056

Table A-4 *Table gives absolute numbers of transits through the rotor for given turbine, day or night and operating status (i.e. y = ≥ 2 rpm, n = < 2 rpm). Last column gives the mean per hour (i.e. number of transits / observation effort). Results are given excluding the 'barn swallow event' (see main text for more details).*

Turbine ID	Day or night	Operating	Sum transits	Mean no. transits / hour
A2	day	n	79	0.0943
A2	day	y	11	0.0072
A2	night	n	271	0.1918
A2	night	y	11	0.0086
A4	day	n	89	0.1486
A4	day	y	14	0.0106
A4	night	n	143	0.1587
A4	night	y	9	0.0050

Table A-5 *Overview of the total number of observation hours per turbine ID the number of transits (total and mean per hour), for dates on which transits were analysed. The table also includes the turbines operating status (i.e. y = ≥ 2 rpm, n = < 2 rpm) and the mean MTR, all during daytime and nighttime. *These numbers include a single outlier event with 399 rotor transits caused by barn swallows on 17 September 2023.*

Turbine ID	Operating	N hour	N rotor transits	Mean N rotor transits/hour	Mean MTR
A2	n	2251	350	0.1555	179.4
A2	y	2801	22	0.0079	143.8
A4	n	1502	232 / (631)*	0.1547 / (0.4201)*	165.2
A4	y	3106	23	0.0074	173.9

Table A-6 *Overview of the total number of observation hours for each turbine separately in relation to the turbines operating status (i.e. y = ≥ 2 rpm, n = < 2 rpm). The non-operating/operating rotor transits shows the mean number of transits per hour during non-operation, relative to operational periods. A value greater than 1 indicates that transits are substantially more frequent when the rotor is not operating. *These numbers include the `barn swallow event'. For details see text in 4.1.*

Turbine ID	Operating	N hour	N transits	Mean MTR (day and night)	Mean rotor transits/hour	Non-operating/Operating rotor transit ratio
A4	n	1502	232 / (631)*	165.5	0.1545 / (0.4201)*	20.859 / (56.733) *
A4	y	3106	23	173.9	0.0074	
A2	n	2251	350	179.4	0.1555	19.796
A2	y	2801	22	143.7	0.0079	

Table A-7 *Overview of the total number of observation hours for each turbine and day and night separately in relation to the turbines operating status (i.e. y = ≥ 2 rpm, n = < 2 rpm). The non-operating/operating rotor transits shows the mean number of transits per hour during non-operation, relative to operational periods. A value greater than 1 indicates that transits are substantially more frequent when the rotor is not operating. *These numbers include the `barn swallow event'. For details see text in 4.1.*

Day or night	Operating	N hour		N transits		Mean MTR (day or night)		Mean rotor transits/hour		Non-operating / Operating rotor transit ratio	
		A4	A2	A4	A2	A4	A2	A4	A2	A4	A2
day	n	599/ (601)*	838	89 / (488)*	79	224.8	221.3	0.1486 / (0.8120)*	0.0953	13.977 / (76.384)*	13.070
day	y	1.317	1.525	14	11	206.1	148.7	0.0106	0.0084		
night	n	901	1.413	143	271	125.3	154.1	0.1587	0.2170	31.549	22.248
night	y	1.789	1.276	9	11	149.8	137.7	0.0050	0.0096		

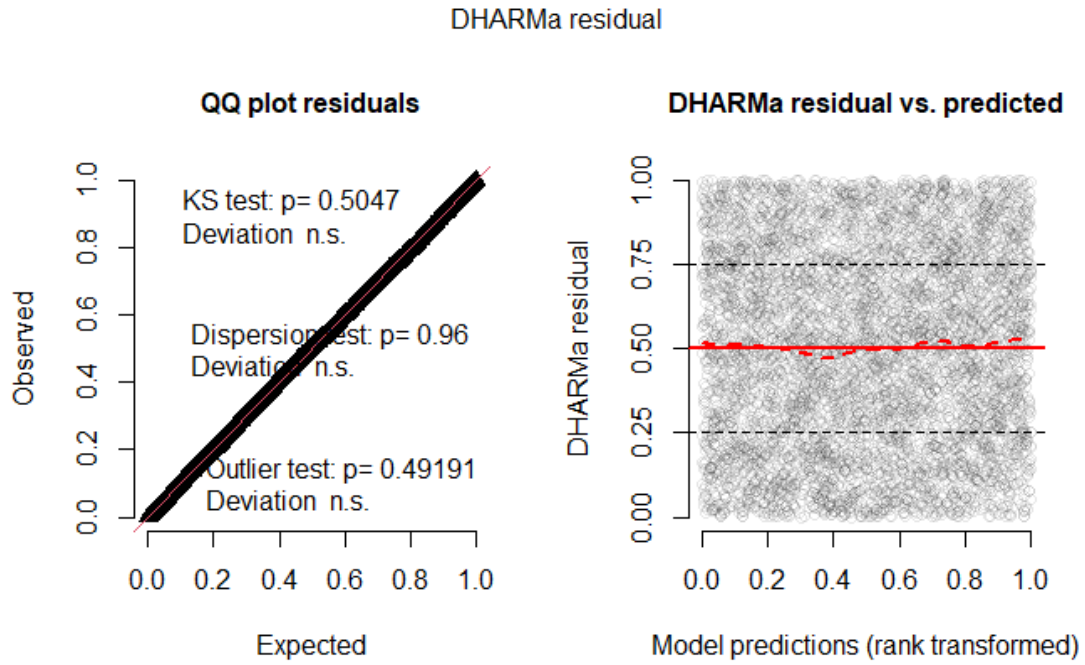

Figure A-2 *Diagnostic plots for binomial GLM of transits ~ MTR at rotor height. Non-significant results highlights in the left column show that there is not deviation from expected distribution (Kolmogorov-Smirnov test), no overdispersion, and no outlier present. On the right-hand side, the horizontal red line indicates that there is no systematic deviation of the residuals.*

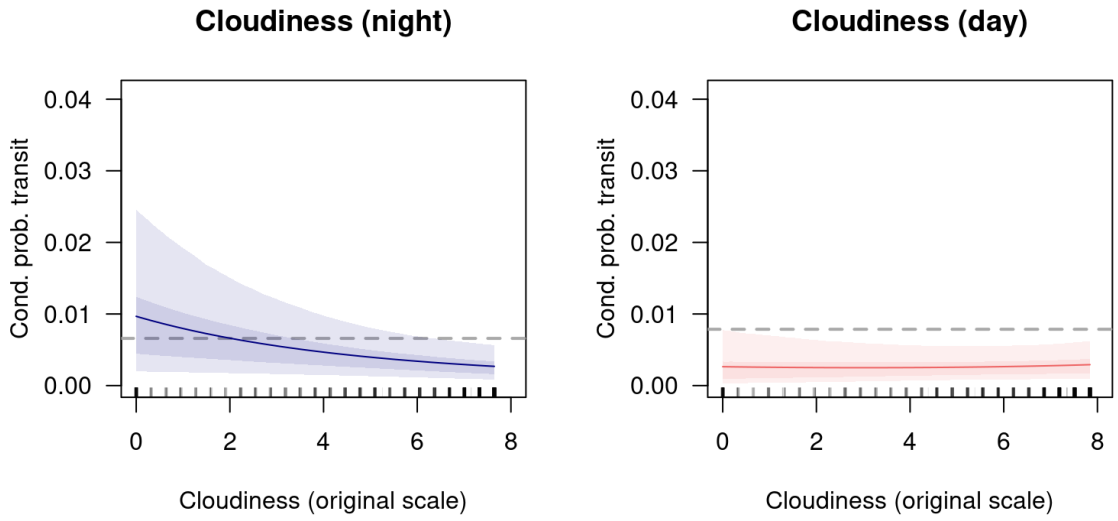

Figure A-3 *Estimated effect of cloudiness on transit probability. On the y-axis is the conditional probability of having at least one transit within one hour. Note that in the plots below the y-scale is the same, so that they are more easily comparable.*

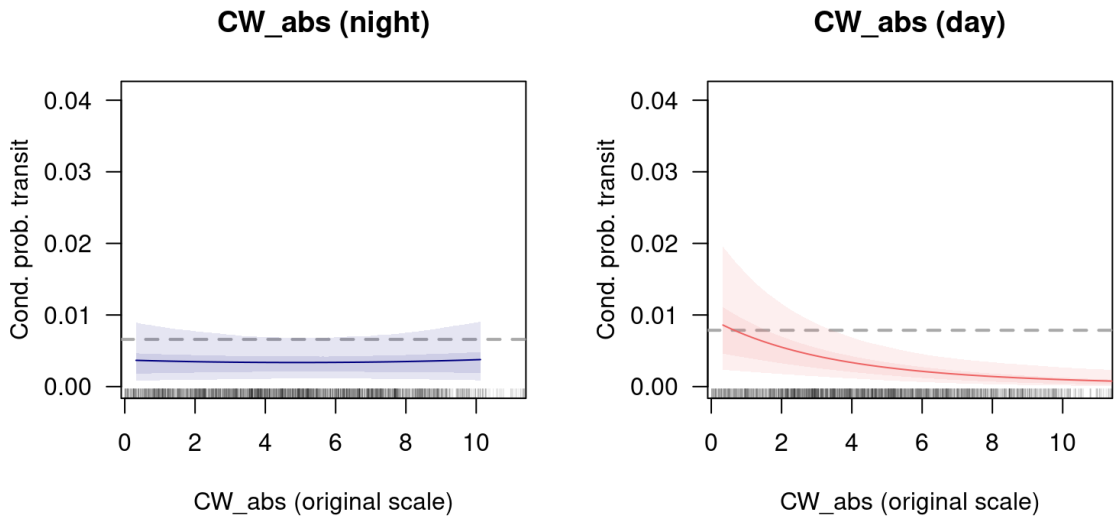

Figure A-4 *Estimated effect of crosswind on transit probability. On the y-axis is the conditional probability of having at least one transit within one hour. Note that in the plots below the y scale is the same, so that they are more easily comparable.*

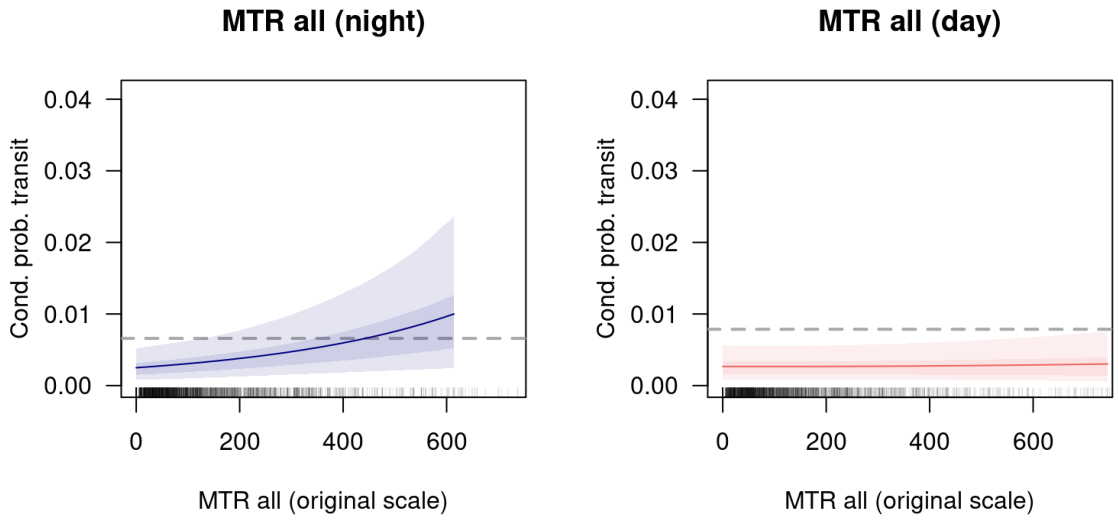

Figure A-5 *Estimated effect of MTR (at rotor height) on transit probability. On the y-axis is the conditional probability of having at least one transit within one hour. Note that in the plots below the y scale is the same, so that they are more easily comparable.*

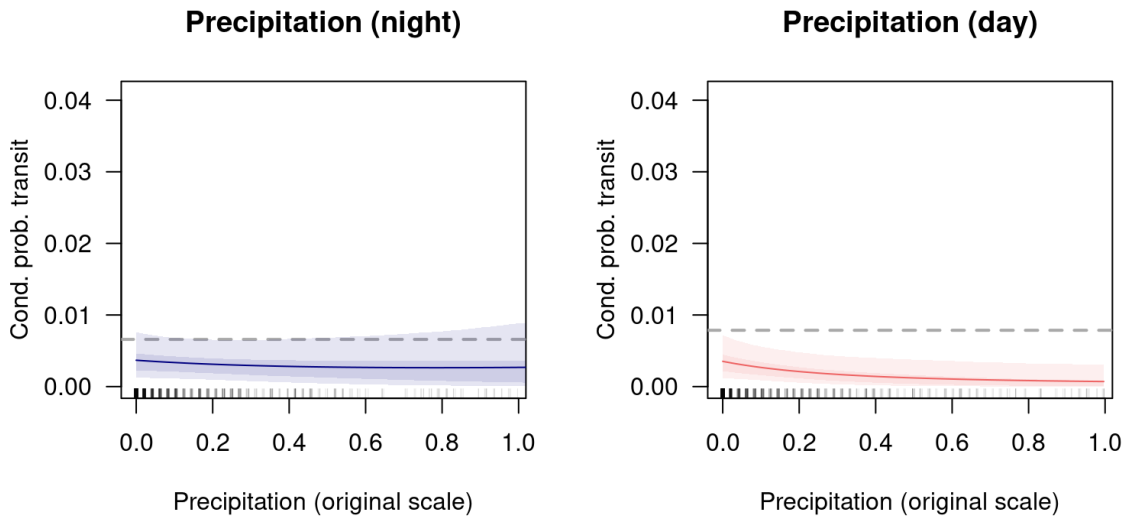

Figure A-6 *Estimated effect of Precipitation on transit probability. On the y-axis is the conditional probability of having at least one transit within one hour. Note that in the plots below the y scale is the same, so that they are more easily comparable.*

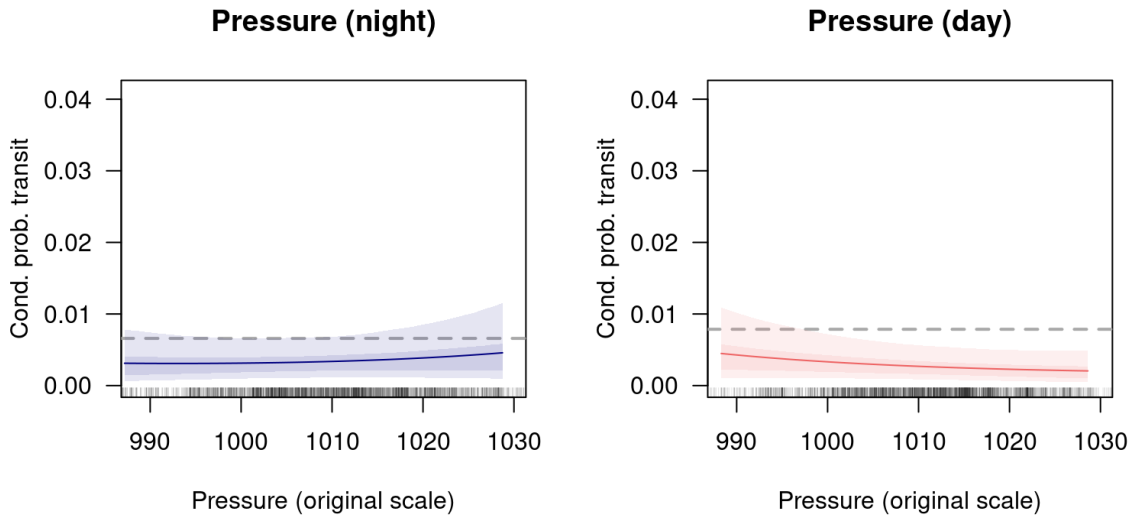

Figure A-7 *Estimated effect of atmospheric pressure on transit probability. On the y-axis is the conditional probability of having at least one transit within one hour. Note that in the plots below the y-scale is the same, so that they are more easily comparable.*

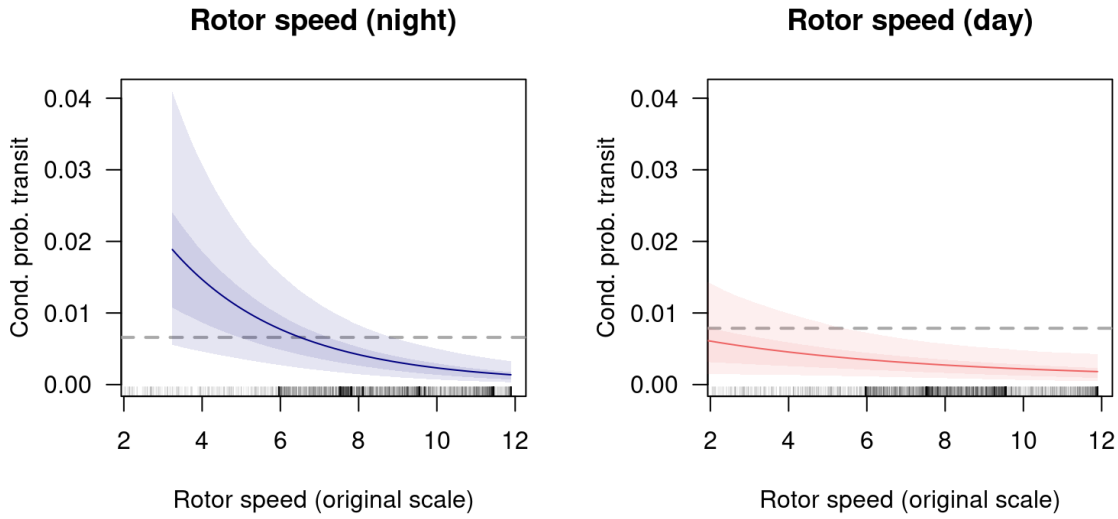

Figure A-8 *Estimated effect of rotor speed (rpm) on transit probability. On the y-axis is the conditional probability of having at least one transit within one hour. Note that in the plots below the y-scale is the same, so that they are more easily comparable.*

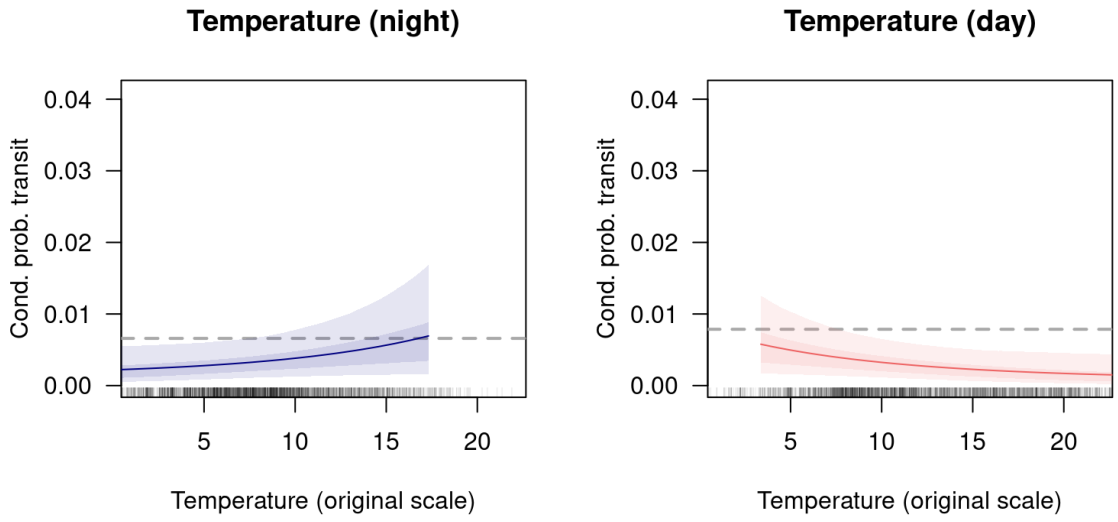

Figure A-9 *Estimated effect of temperature (in C°) on transit probability. On the y axis is the conditional probability of having at least one transit within one hour. Note that in the plots below the y-scale is the same, so that they are more easily comparable.*

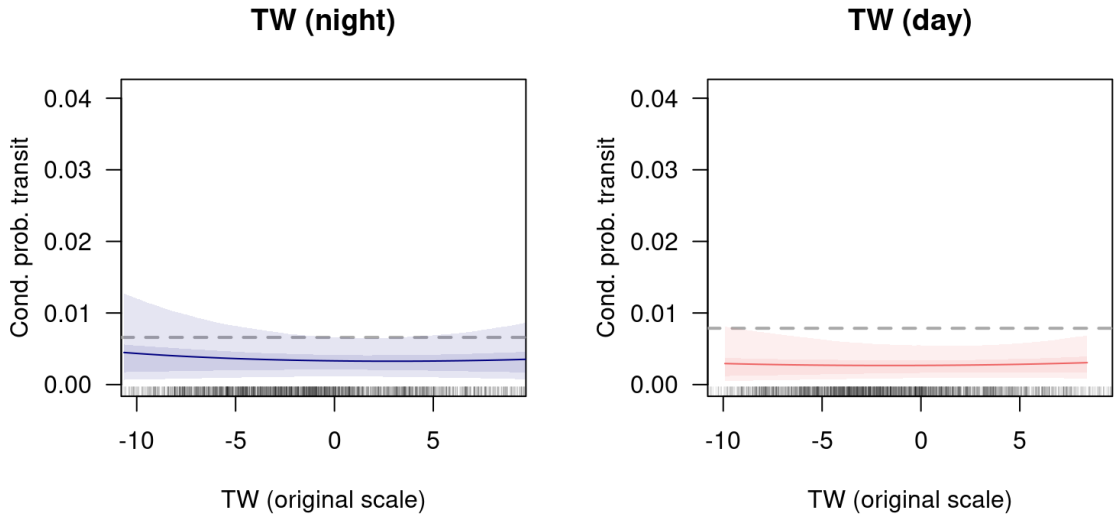

Figure A-10 *Estimated effect of tailwind on transit probability. On the y-axis is the conditional probability of having at least one transit within one hour. Note that in the plots below the y scale is the same, so that they are more easily comparable.*

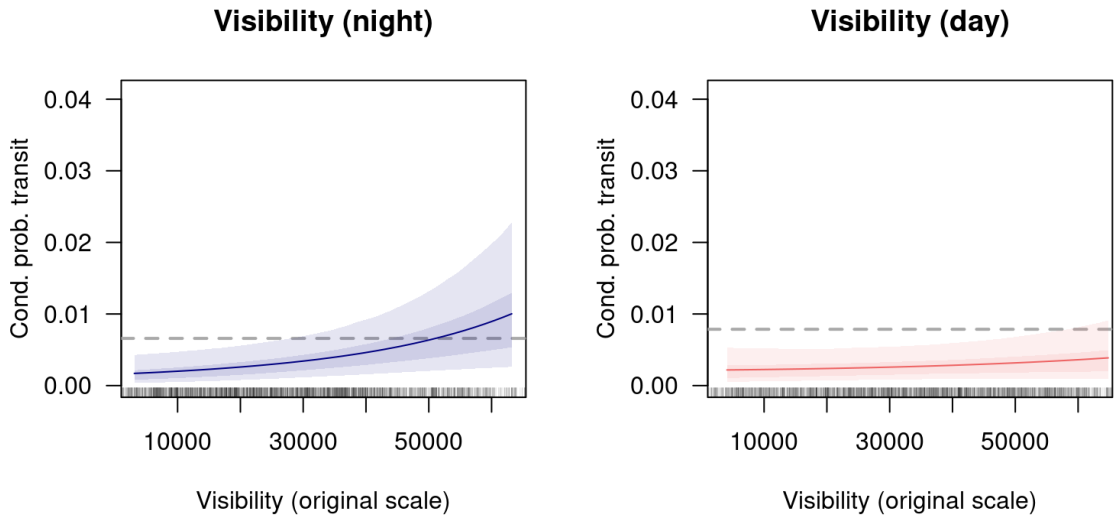

Figure A-11 *Estimated effect of visibility (m) on transit probability. On the y axis is the conditional probability of having at least one transit within one hour. Note that in the plots below the y-scale is the same, so that they are more easily comparable.*

A.3 Calls

Table A-8 List of species with at least 10 calls as identified by human expert.

Species	Total number of calls
Barnacle Goose	3586
Brant	173
Canada Goose	11
Common Ringed Plover	10
Common Sandpiper	29
Common Scoter	17
Common Shelduck	56
Common Snipe	486
Dunlin	48
Dunnock	52
Eurasian Blackbird	66
Eurasian Coot	13
Eurasian Curlew	117
Eurasian Moorhen	16
Eurasian Oystercatcher	66
Eurasian Skylark	36
Eurasian Wigeon	45
Eurasian Wren	235
European Golden-Plover	418
European Robin	807
Gadwall	1926
Gray Heron	252
Graylag Goose	345
Greater White-fronted Goose	2313
Green Sandpiper	316
Little Ringed Plover	472
Mallard	170
Northern Lapwing	661
Redwing	1564
Sedge Warbler	20
Song Thrush	1004
bird sp.	113
duck sp.	112
goose sp.	76
shorebird sp.	22

Table A-9 *Table of species subset used in call analyses. Names are given in common names and confidence level shows which minimum confidence level of the AI tools was use for filtering the data for that species. This list is a subset of the list in Table A-8 as not for all species a sufficient accuracy of the AI was reached.*

Species	Confidence Level
Barnacle Goose	0.65
Brant	0.70
Common Sandpiper	0.75
Common Scoter	0.75
Common Snipe	0.70
Dunlin	0.65
Dunnock	0.60
Eurasian Blackbird	0.90
Eurasian Curlew	0.85
Eurasian Skylark	0.70
Eurasian Wigeon	0.75
European Golden-Plover	0.65
European Robin	0.55
Gadwall	0.45
Gray Heron	0.65
Graylag Goose	0.75
Greater White-fronted Goose	0.65
Green Sandpiper	0.75
Little Ringed Plover	0.60
Mallard	0.90
Northern Lapwing	0.35
Redwing	0.55
Song Thrush	0.70

A.4 Master thesis

The Master thesis by Friedja Mehnert can be found on the following pages.

Effects of weather on migration intensity and flight height distribution of nocturnally migrating birds in Northern Germany

by

Friedja Mehnert

born on

19th May 1998

A thesis submitted for the degree of Master of Science in Biology

Department of Behavioural Biology

University of Hamburg

June 2025

Supervisors: Prof. Dr. Jutta Schneider [1] & Dr. Jannis Liedtke [2]

[1] *Zoological Institute and Museum, Department of Biology, University of Hamburg, Martin-Luther-King Platz 3, 20146 Hamburg, Germany.*

[2] *BioConsult SH GmbH & Co. KG, Schoböller Straße 36, 25813 Husum, Germany.*

Eidesstattliche Versicherung

Hiermit erkläre ich, Friedja Mehnert, an Eides statt, dass ich die vorliegende Arbeit selbst verfasst und keine anderen als die angegebenen Quellen und Hilfsmittel benutzt habe.

Sofern im Zuge der Erstellung der vorliegenden Abschlussarbeit gKI-basierte elektronische Hilfsmittel verwendet wurden, versichere ich, dass meine eigene Leistung im Vordergrund stand und dass eine vollständige Dokumentation aller verwendeten Hilfsmittel gemäß der Guten wissenschaftlichen Praxis vorliegt. Ich trage die Verantwortung für eventuell durch die gKI generierte fehlerhafte oder verzerrte Inhalte, fehlerhafte Referenzen, Verstöße gegen das Datenschutz- und Urheberrecht oder Plagiate.

In der hier vorliegenden Arbeit habe ich generative-Künstliche-Intelligenz-Systeme (gKI-Systeme) wie folgt genutzt[1]:

- ☐ Gar nicht
- ☐ Bei der Ideenfindung
- ☐ Bei der Erstellung der Gliederung
- ☐ Zum Erstellen einzelner Passagen, insgesamt im Umfang von ___ % am gesamten Text
- ☐ Zur Entwicklung von Software-Quelltexten
- ☐ Zur Optimierung oder Umstrukturierung von Software-Quelltexten
- ☐ zum Korrekturlesen oder Optimieren
- ☒ Weiteres, nämlich:

  Im Rahmen meiner Arbeit habe ich KI (insbesondere ChatGPT) unterstützend eingesetzt. Dabei diente sie vorrangig der statistischen Analyse meiner Daten bei der Verwendung der Software „RStudio“. Insbesondere habe ich die KI bei der Behebung von Fehlermeldungen sowie bei der Erstellung von Grafiken verwendet. Darüber hinaus kam sie in begrenztem Umfang auch bei der Literaturrecherche zum Einsatz.

03.06.2025 F. Mehnert

Hamburg, den Unterschrift

[1] Mehre Kreuze möglich. Bei Punkt 4 bitte Prozentangabe ergänzen. Beim letzten Punkt bitte näher beschreiben.

Abstract

Twice a year, billions of passerines embark on great journeys between breeding and wintering grounds. Their migratory behaviour is strongly shaped by the atmospheric conditions encountered on route. In recent years the lower atmosphere (i.e. troposphere) - a critical habitat for migratory birds – has been increasingly designated as space for wind energy development, and as a result aerial wildlife flying in lower altitudes face the risk of fatally colliding with wind turbines. Understanding the atmospheric conditions under which migratory birds intensively use this airspace is crucial in effectively reducing human-wildlife conflicts.

In order to evaluate the effects of weather parameters on migration traffic rates (MTR) and flight altitude distributions of nocturnally migrating passerines, we analysed two years of vertical-looking radar (BirdScan MR1) data from the German North Sea coast. Particular focus was given to factors influencing low-altitude flights (25–180 m), in correspondence to local wind turbine heights. As anticipated, our findings revealed that among meteorological variables wind was a key driver of passerine migration intensity, although with different seasonal repercussions: crosswind significantly reduced MTR during spring, while tailwind drastically increased MTR in autumn. Additionally, we found that warmer temperatures favoured migration intensity during both seasons. Regarding the mean flight height and the proportion of migrants within the “risk altitude” we observed no relevant differences between spring (304.64 m; 33.21 %) and autumn (300.72 m; 32.65 %) seasons. While we observed an overall preference for low-altitude flight in both seasons, spring and autumn migrants, respectively, were affected differently by atmospheric conditions. For the first time in this region, our research revealed that Δ barometric pressure, i.e. the change compared to the previous night, was the main predictor for the likelihood of low-altitude flight in both seasons: elevated pressure increased the probability of rotor-height flight in spring, whereas the opposite trend emerged in autumn. During spring, migrants lowered their flight altitudes under strong crosswinds. Contrastingly, during autumn particularly tailwinds influenced the flight height choice and increased wind assistance led to elevated flight heights. Overall, the migration intensity and flight altitudes of nocturnally migrating passerines in response to environmental conditions seem to reflect a compromise between multiple season-specific adaptive pressures. Our findings enable a more detailed understanding of passerine migration at the German North Sea coast and help to better assess the factors influencing low-altitude flight, providing valuable insight for future conservation efforts regarding wind turbine curtailment strategies aiming to reduce the collision risk of birds.

Zusammenfassung

Jedes Jahr unternehmen Millionen von Singvögeln (Passeriformes) weite Wanderungen zwischen ihren Brut- und Überwinterungsgebieten, wobei ihr Zugverhalten maßgeblich von atmosphärischen Bedingungen beeinflusst wird. Der bodennahe Teil der Troposphäre, der ein wichtiges Habitat für Zugvögel darstellt, wird im Zuge der Energiewende zunehmend für die Windenergienutzung erschlossen, wobei Windenergieanlagen ein Kollisionsrisiko für Zugvögel darstellen. Um Mensch-Wildtier-Konflikte zu minimieren, ist ein umfassendes Verständnis der lokalen atmosphärischen Bedingungen, unter welchen Zugvögel diesen Luftraum vermehrt nutzen von zentraler Bedeutung. Zur Untersuchung der Einflüsse meteorologischer Parameter auf das nächtliche Zugaufkommen (Migration Traffic Rate, MTR) sowie auf die Verteilung der Flughöhen nächtlich ziehender Singvögel wurden zwei Jahre vertikaler Radarmessungen (BirdScan MR1) an der deutschen Nordseeküste analysiert. Dabei lag ein besonderer Fokus auf den Wetterparametern, die Flüge in „Risikohöhe“ (25–180 m) beeinflussten. Unter den meteorologischen Variablen erwies sich der Wind wie erwartet als ein zentraler Treiber der Zugintensität, wobei sich saisonal unterschiedliche Effekte zeigten: im Frühjahr wurde das Zugaufkommen signifikant von Seitenwind reduziert, wohingegen Rückenwind im Herbst zu einem deutlichen Anstieg der MTR führte. Zudem begünstigten höhere Temperaturen die Zugintensität in beiden Jahreszeiten.

Bezüglich der mittleren Flughöhe sowie des Anteils ziehender Vögel innerhalb der „Risikohöhe“ zeigten sich keine signifikanten Unterschiede zwischen Frühjahr (304,64 m; 33,21 %) und Herbst (300,72 m; 32,65 %). In beiden Zugperioden wurde eine allgemeine Präferenz für Flüge in niedrigeren Höhen festgestellt, der Einfluss atmosphärischer Bedingungen auf die Flughöhenwahl variierte jedoch zwischen dem Frühjahrs- und Herbstzug. Erstmals konnte für diese Region gezeigt werden, dass die Veränderung des Luftdrucks im Vergleich zur vorherigen Nacht (Δ Luftdruck) einen maßgeblichen Einfluss auf die Flughöhe der Zugvögel hatte: Im Frühjahr erhöhte ein ansteigender Luftdruck die Wahrscheinlichkeit für Flüge in kritischer Höhe, während im Herbst ein gegenteiliger Zusammenhang bestand. Während im Frühling die Singvögel ihre Flughöhe zusätzlich unter starkem Seitenwind reduzierten, beeinflusste im Herbst insbesondere Rückenwind die Flughöhenwahl: Eine stärkere Windunterstützung ging hier mit höheren Fluglagen einher. Unsere Ergebnisse liefern wertvolle Hinweise auf saisonal unterschiedliche Verhaltensanpassungen nächtlich ziehender Singvögel an die vorherrschenden Wetterbedingungen. Zudem tragen die Ergebnisse zu einem vertieften Verständnis der Zugstrategien von Singvögeln an der deutschen Nordseeküste bei

und unterstreichen die Notwendigkeit, saisonale Unterschiede bei der Umsetzung von Umweltschutzstrategien in Bezug auf Windkraftanlagen zu berücksichtigen.

List of abbreviations

a.g.l.	Above ground level
a.s.l.	Above sea level
CI	Credible interval
CWC	Crosswind component [m/s]
DWD	Deutscher Wetterdienst (German Meteorological Service)
ELPD	Expected log predictive density
FHD	Flight height distribution
FMCW	Frequency modulated continuous wave (radar)
GAM	Generalised additive model
LOO	Leave-One-Out cross-validation
MCMC	Markov-Chain-Monte-Carlo
MTR	Migration traffic rate [birds km^{-1} h^{-1}]
PPC	Posterior predictive check
SPO	Sankt Peter-Ording
TWC	Tailwind component [m/s]
UTC	Universal Time Coordinated

List of contents

Introduction

Twice a year, billions of birds (e.g. Hahn et al. 2009, Van Doren & Horton 2018, Nussbaumer et al. 2021) migrate vast distances between breeding and wintering sites, passing through landscapes and airspaces increasingly transformed by human activities. These biannual journeys typically follow a north-south axis, with most migratory birds spending the non-breeding period in lower latitudes compared to their breeding season (Newton 2023, p. 2). This large-scale seasonal movement allows birds to exploit geographically distinct regions that offer optimal ecological conditions - such as abundant food resources, favourable climate and reduced predation pressure - at different times of the year, thereby maximising both survival and reproductive success (Newton 2008). Governed by atmospheric conditions, particularly wind (e.g. Shamoun-Baranes et al. 2017, Manola et al. 2020), through natural selection over generations of migratory birds optimal migratory routes have evolved (Kranstauber et al. 2015). These well-established pathways used by migratory avian species throughout their annual cycle are termed “flyways” (Kirby et al. 2008, Hahn et al. 2009, BirdLife International 2010, last viewed 25.05.2025). One of the most prominent flyways, the East Atlantic Flyway (BirdLife International 2010, last viewed 25.05.2025), extends from Canada and central Siberia to wintering grounds in Western Europe and West Africa. The German North Sea basin and its coast lie within the East Atlantic Flyway and serve as key migratory corridors for many avian species (e.g. Hahn et al. 2009, Hüppop et al. 2016). Of the nocturnally migrating birds, passerines (Order: Passeriformes, Linnaeus 1758), in particular thrushes (*Turdus* spp., see Hüppop et al. 2016), account for up to 95% of the nocturnally migrating birds in Northern Germany (Hahn et al. 2009). As large bodies of water constitute a geographical barrier particularly for long-distance migrants (Åkesson & Sandberg 1999), near-shore habitats serve as important stopover sites to rest and refuel, before or after crossing barriers (Newton 2008) such as the North Sea basin. Due to the rapid expansion of wind energy infrastructure both on- and offshore (Global Offshore Renewables Map, last viewed 13.03.25), this barrier effect has become more severe in recent years. While wind farms are widely regarded as one of the most promising strategies to meet Europe’s decarbonisation targets (European Commission 2020), they also pose significant threats to aerial wildlife through collision risk, habitat alteration and displacement effects (e.g. Drewit 2006, Hüppop et al. 2006, Drewitt & Langston 2008, Perold et al. 2020, Lloyd et al. 2023). Although estimates of fatal avian collisions with wind turbines vary greatly (e.g. Drewitt 2006, Erickson et al. 2014, Thaxter et al. 2017, Allison et al. 2019, Welcker & Vilela 2019), volant animals such as bats and birds are at risk (e.g. Schuster et al.

2015, Lloyd et al. 2023) and these effects are expected to become even more pronounced in the future with continued wind farm development.

Bird migration is a highly dynamic phenomenon, with nightly and seasonal variations in migration intensity and flight altitude, which are strongly influenced by atmospheric conditions (Lack 1960, Able 1970, Richardson 1990, Alerstam 2011, Bruderer et al. 2018, Newton 2023). Variations in weather conditions can significantly affect the energetic cost of flight and, consequently, migratory success (Newton 2008). Wind has been consistently identified as the dominant factor shaping nocturnal migratory behaviour, with supportive tailwinds facilitating long-distance flights and adverse headwinds often leading to delayed departures or overall reduced migratory activity (e.g. Richardson 1990, Liechti 2006, Alerstam 2011, Horton et al. 2016a). Furthermore, migratory birds have been observed to actively select altitudes that minimize energetic costs and maximize directional efficiency (Horton et al. 2016a, Newton 2023). Within the stratified layers of the troposphere, altitude choice is guided by varying atmospheric conditions, including wind regimes, temperature gradients, and oxygen availability (Bruderer et al. 2018, Rohli et al. 2024). Thus, birds must navigate a series of trade-offs, as elevating the flight height is associated with greater energetic costs (Newton 2023) yet may facilitate more efficient overall migration if atmospheric conditions further up offer stronger support. In mid-latitudes such as Northern Europe, prevailing westerly winds (i.e. winds coming from the west, Rohli et al. 2024) - which typically strengthen with altitude (Pennycuick 2008) - can hinder southwest-oriented autumn migration. Consequently, nocturnal avian migration has been observed to occur at lower altitudes in autumn than in spring to avoid energetically expensive westerly winds in higher altitudes (North Sea: Welcker & Vilela 2019, Bradarić et al. 2024, Netherlands: Kemp et al. 2013, Review: Bruderer et al. 2018). Radar studies in the Netherlands (Dokter et al. 2013, Kemp et al. 2013) and over the North Sea (Bradarić et al. 2024) demonstrated that birds chose altitudes with increased tailwind support in both migration seasons but only elevated to altitudes where they first encounter supportive winds (Kemp et al. 2013). Furthermore, temperature plays an important role, with birds showing a preference for elevated heights under increased temperature when migrating over land (e.g. Kemp et al. 2013) and generally decreasing flight altitude under lower air temperature (Shamoun-Baranes et al. 2006, Galtbalt et al. 2021). Additionally, migrants tend to fly lower under overcast and rainy conditions (e.g. Bruderer et al. 2018, Newton 2023) but have also been observed to elevate their flight height, cruising above cloud layers (Eastwood 1967, Newton 2023).

While inclining barometric pressure - usually associated with moderate winds, clear skies and no precipitation - has been shown to increase migration intensities (Richardson 1990, Welcker

& Vilela 2019), not a lot is known regarding its impact on the flight height choice of birds. In general, the relationship between nocturnal migratory behaviour and weather conditions, at times with focus on collision risk with wind turbines (e.g. Bradarić et al. 2024), is well studied over the North Sea using weather or marine radars (e.g. Eastwood 1967, Lack 1960, Hüppop et al. 2006, Fijn et al. 2015, Welcker & Vilela 2019). However, due to the technical limitations of conventional radar systems, there remains a knowledge gap concerning the specific (meteorological) factors that influence the flight behaviour of passerines within rotor-swept altitudes - an airspace particularly relevant for assessing collision risk with wind turbines. As weather conditions in coastal landscapes are shaped by complex interactions between land and sea masses, birds are faced with different migratory decisions over inland, coastal or offshore regions (Åkesson 1993, Bruderer & Liechti 1998). Thus, it remains unclear to what extent offshore findings apply to nearshore and coastal regions. Therefore, in order to effectively implement locally adapted conservation strategies - such as curtailment of turbine operations during high-risk periods - it is pivotal to understand local patterns of bird's migration and the environmental factors influencing those patterns. Crucially, seeing as the atmosphere is a vertically stratified system the meteorological conditions driving overall migration intensity may differ from those affecting flight altitude selection (Newton 2008). Consequently, migration intensity and the vertical distribution of migrants must be treated as distinct, albeit interrelated, responses to weather conditions. Disentangling these patterns is essential to determine under which conditions the risk of turbine collision is highest for passerines in coastal Northern Germany.

To address this knowledge gap, our approach distinguishes between two key components of migration dynamics: (a) the overall intensity of migration, measured as migration traffic rates (MTR), and (b) the vertical distribution of migrants, with a particular focus on low-altitude flights (≤ 180 m), corresponding to the rotor heights of local wind turbines. We hypothesize that low-altitude flight increases under unfavourable weather conditions - such as crosswinds, cloud cover, and low temperatures - potentially reflecting a strategy to remain prepared for landing if conditions deteriorate or to avoid even worse conditions at greater heights (Newton 2008). Furthermore, we anticipate that seasonal differences in selective pressures will modulate the effects of weather on flight behaviour. Specifically, we expect that the pressure for early arrival and territory establishment in spring (Kokko et al. 1999) may promote riskier flights under less favourable conditions. Whereas in autumn, at least two aspects may lead to a different pattern: i) the presence of inexperienced juvenile migrants may lead to more conservative flight strategies, favouring lower altitudes when conditions are suboptimal and ii) early arrival in

wintering grounds is probably less important as there is less competition for the best nesting site and consequently the birds can afford to wait for more favourable weather conditions en route. Our study specifically aims to answer the following research questions: i) Which meteorological variables primarily influence nocturnal migration traffic rates? ii) How do these variables influence the fraction of low-altitude migration across four migratory seasons? To address these questions, we analysed two years of vertical-looking radar data collected in the coastal town Husum, northern Germany, using a BirdScan MR1 system (manufacturer: Swiss Birdradar Solution AG, Winterthur, Switzerland) capable of quantifying nocturnal flight activity and altitude distributions. Its valuable ability to distinguish between broader avian groups based on wingbeat signatures allows us to specifically investigate passerines - the dominant group of nocturnal migrants over northern Germany - and to draw ecologically meaningful conclusions regarding their flight behaviour and collision risk in response to weather conditions.

Materials and methods

This study evaluates the influence of weather variables, time of year and proportion of night on the nocturnal passerine migration density with particular focus on the vertical profile of bird densities. The overarching goal is twofold: a) describe the nocturnal migration pattern and its weather dependency at a near shore location in north Germany and b) to investigate the conditions influencing the likelihood of nocturnally migrating passerines flying at risk hight, i.e. at rotor hight of wind turbines. This study constitutes a part of the “VolZug” project studied by BioConsult SH GmbH & Co. KG (Husum, Germany), commissioned by the “Bundverband Windenergie Offshore e.V.” (BWO).

Radar data

Radar data were collected using a frequency modulated continuous-wave radar (FMCW) (BirdScan MR1, manufacturer: Swiss Birdradar Solution AG, Winterthur, Switzerland) which was positioned on the Windtestfeld-Nord GmbH (last visited 21.03.2025) in the Südermarsch in close vicinity to Husum, Germany (54.4572°, 9.0408°). The operating period of the radar spans over two entire years (4 migration periods), from the 23.02.2023 to 03.12.2024. The BirdScan radar is able to automatically discern between basic classification groups of aerial fauna such as birds, bats and insects as well as non-biological objects (e.g. drones) (BirdScan MR1, last viewed 21.01.2025). Bird echoes are further subdivided into passerine, wader and swift types and large birds by the characteristics of their wing-flapping pattern. This study only

focusses on passerine migration; other types of aerial fauna were therefore omitted from further analyses. A passerine-type bird is detected by the radar due to the flap-bounding type of flight (Fig. 1), consisting of short bursts of wing beating and short pauses in between where the wings are pulled towards the body (e.g. Brown 1963). When working with radar data, a long-standing challenge for ornithologists has been identifying and removing contamination of radar data by e.g. precipitation and anomalous propagation (e.g. Dokter et al. 2011, Van Doren & Horton 2018, Nussbaumer et al. 2021). Fortunately, for this study elimination of contaminated radar data had been done beforehand by the manufacturer, Swiss Birdradar Solution AG.

Figure 1: Micro-doppler signature of a passerine-type bird, as detected by the BirdScan radar (With thanks to FaunaScan MR2 for permission to use this image, last visited 21.01.2025)

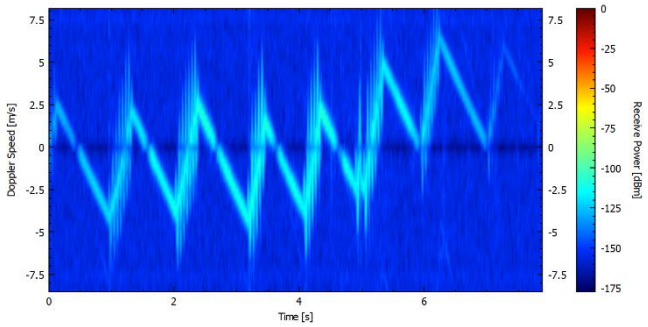

The number of birds aloft is commonly quantified using the migration traffic rate (MTR). MTR is defined as the number of birds that cross a theoretical 1 km transect perpendicular to the direction of movement during one hour (Swiss-Birdradar, last visited 29.01.2025). Radar data obtained by the BirdScan and used for this study includes hourly MTR (birds km^{-1} h^{-1}) as well as the vertical profile of bird density. Due to technical implications, the radar is unable to accurately detect echoes within the first 25 m a.g.l. Migration intensity was measured within altitude intervals ("bins") of 50 m (i.e. 25 - 75 m, 75 – 125 m etc.), ranging from 25 m a.g.l. to 1025 m a.g.l. For the analysis of the proportion of MTR at risk height, we used radar data between 25 - 180 m a.g.l. (altitude bin size of 155 m, average altitude per chunk 102.5 m). The upper altitude limit was set at 180 m, corresponding to the height of the upper rotor tip of turbines at a wind farm near the radar location. MTR signals between 25 and 180 meters were therefore considered to be within the 'at-risk' flight height range. As we only used nightly radar data for our analysis, the day/night classification was adopted from the SwissRadar dataset, where the "civil twilight" (i.e. when the sun is 6 ° below the horizon) was used as the border between day and night.

Descriptive analyses of MTR and FHD

All data analyses were conducted using R version 4.4.2 (R Core Team, 2024). To investigate temporal patterns in the migratory behaviour of passerines passing through Husum, differences in migration traffic rate (MTR) and flight height distribution (FHD) between spring and autumn were analysed and visualised using the "*ggplot2"* package (v. 3.5.1; Wickham, 2016).

Nocturnal variation in migration intensity was explored using violin plots (Fig. 3), while heatmaps (Fig. 5) were generated to illustrate that nocturnal migration intensity varies simultaneously with time of night and flight altitude.

Meteorological data

For "windrose" plots of combined directional and wind speed data, the package "*clifro*" (v. 3.2.5; Seers & Shears 2015) was used (Appendix, Fig S1 – S3). To combine multiple plots in one figure, package "*patchwork*" (v. 1.3.0; Pedersen 2024) was applied.

Meteorological parameters were measured on the Windtestfeld-Nord GmbH (Husum, Germany) by a weather station run by Pavana GmbH (Husum, Germany). Unfortunately, meteorological measurements were discontinued from August 2024 onwards and are therefore not available for the entirety of the studied period. To have comparable weather measurements for the regression analyses of all four migratory seasons studied, publicly available local hourly meteorological data of the German Meteorological Service (Deutscher Wetterdienst, DWD) were used (downloaded from opendata.dwd.de, last visited on 07.01.2025). Based on literature review of previous nocturnal (passerine) migration studies, eight weather parameters were downloaded and used for the analyses (listed in Table 2). Weather data was initially loaded into R Studio, faulty data was removed, and the time format was adjusted to YMD-HMS to facilitate merging of radar and weather data at a later stage.

The DWD station geographically closest to the study area is located in Hattstedt (54.527°, 9.043°; 9 km distance to study area), however not all relevant parameters are recorded at that station. Consequently, the data of a total of five meteorological stations nearest to the study area were used as described below. Details regarding the different meteorological stations used are summarised in Table 1. Cloud coverage was recorded in oktas, ranging from 0 (completely clear sky) to 8 (full overcast).

Pearson correlations

Using the R package „*correlation*" (v. 0.8.5; Makowski et al. 2022), Pearson correlations between Pavana GmbH weather data and data from the local DWD stations were performed. The goal was to individually assess the best substitute for local weather parameters which were not measured at the turbines themselves. Additionally, the average between different DWD stations for each parameter was used for the correlation analysis. However, some for this study relevant parameters were not measured by Pavana GmbH (relative humidity, cloudiness, visibility) and thus no Pearson correlation could be performed to find the best single substitute DWD station. Consequently, we decided on using the respective DWD mean for relative humidity, cloudiness and visibility (Tab. 2).

To avoid multicollinearity and ensure stable regression estimates in the subsequent analyses, the correlation between explanatory variables was examined. Variables with a correlation coefficient $r \geq 0.7$ were considered highly correlated. In such cases, one of the correlated variables was excluded from further analysis to prevent potential issues with model instability (O'Brien 2007). Relative humidity and visibility were the only parameters correlating with a $r > 0.7$. As we were interested in a possible association between visibility and migratory behaviour of passerines, relative humidity was henceforth omitted from further analysis (Tab. 2).

Table 1: Summary of DWD stations used for collection of meteorological data.

Name of town	DWD Station ID	Altitude a.s.l. (m)	Coordinates
Hattstedt	7298	4	54.527, 9.043
Erfde	1266	18	54.299, 9.316
Leck	2907	7	54.7903, 8.9514
Sankt Peter-Ording (SPO)	4393	5	54.3279, 8.6031
Schleswig	4466	47	54.528, 9.549

Table 2: Meteorological parameters used for the regression analyses and their DWD sources. Where available, R^2 coefficients of Pearson correlations with local turbine weather data are depicted as well.

Parameters	Unit	Meteorological stations used	R^2
Precipitation	mm	Mean of Hattstedt, Erfde, Leck, Schleswig, SPO	0.71
Temperature	°C	Mean of Hattstedt, Erfde, Leck, Schleswig, SPO	0.99
Wind speed	m/s	Mean of Leck, Schleswig, SPO	0.95
Wind direction	°	Mean of Leck, Schleswig, SPO	0.90
Barometric pressure	hPa	Mean of Leck, Schleswig, SPO	0.99
Cloudiness	oktas	Mean of Leck, Schleswig, SPO	NA
Visibility	m	Mean of Leck, Schleswig, SPO	NA

Wind data analysis

Wind is among the main environmental factors governing migration intensity and flight height distribution of passerines, where supporting tailwind increases and strong cross- or sidewinds hinder migration. Calculating the flow-assistance a bird encounters during migration, offers a commonly applied method (e.g. Kemp et al. 2012, Nilsson et al. 2019, Schekler et al. 2024) to simplify the complex effects of the two flow components (i.e. its speed and direction) into a

single variable (Kemp et al. 2012). This allows quantitative comparisons between flow-conditions. When assessing the potential influence of wind-assistance on migratory birds, two repeatedly discussed flow components are the tailwinds (TWC (m/s)) along a preferred migration direction and the crosswinds (CWC (m/s)) perpendicular to the preferred migration direction. Here the TWC and CWC were calculated following Kemp et al. (2012), Nilsson et al. (2019) and Schekler et al. (2024):

$$TWC = s * \cos(\alpha_{wind} - \alpha_{migration})$$
$$CWC = s * \sin(\alpha_{wind} - \alpha_{migration})$$

Where s = wind speed (m/s), α_{wind} = wind direction (rad) and $\alpha_{migration}$ = flight direction (rad). This equation implicitly assumes that wind blowing in the direction of the mean track direction is beneficial (Liechti 2006, Chapman et al. 2011, 2016, Kemp et al. 2012). Positive TWC values correspond to supportive winds (tailwind), negative TWC values correspond to headwinds. For this study only absolute CWC values were used, disregarding the direction of which the side wind blew from. Hence, high CWC values correspond to increased side wind (from either left or right in relation to flight direction) compared to low CWC values. Wind direction was provided in degrees (°) and was defined as the direction the wind is blowing from. The birds flight direction (i.e. direction migrants are flying from) was derived from the radar echoes for the spring and autumn migration periods respectively, and was defined as:

Spring: $\alpha_{migration} = 220° = 3.840$ rad
Autumn: $\alpha_{migration} = 30° = 0.524$ rad

All directional wind data was converted from degrees to radians (multiplied by π/180), for further trigonometric calculations.

Preprocessing of explanatory variables

Scaling and centering

Prior to modelling, weather variables were scaled and centered. To allow for simplified interpretation and comparison of the estimated coefficients in terms of effect size on the response variable, all variables were scaled by dividing the given original variable by its standard deviation. This results in variables with a standard deviation of one. An exception was made for atmospheric pressure, which was additionally centered prior to scaling by subtracting the mean value from each observation. As a result, the zero value of the centered variable corresponds to the mean of the original variable. Since pressure is the only variable where the value 0 (hPa) is not biologically meaningful, centering the variable allows for a clear

interpretation of the models' intercept. This approach allows for a direct comparison of the estimated effect sizes of explanatory variables, enabling us to determine which variables affect the response variable the strongest.

Delta (Δ) variables

Changes in weather conditions compared to the previous day have been shown to impact MTR (Newton 2008, Nilsson et al. 2019, Benjumea et al. 2024, but see Schekler et al. 2024). Thus, the relative change to the proceeding night was calculated for precipitation, pressure, temperature and both the tailwind and crosswind component (TWC, CWC). To allow for meaningful Δ variables and to ensure that the changes in weather conditions were represented consistently across all variables, the Δ variables were calculated after scaling and centering.

Seasonal data

In line with the methodology employed in several other studies and considering the unique characteristics of the two migration seasons - such as bird composition, timing, migration routes, and meteorological conditions - we performed separate analyses for the spring and autumn datasets. To directly compare the effect sizes of explanatory variables between seasons, the dataset was split into migratory seasons post-scaling and -centering. Date and length of seasons was defined according to the initial radar (MTR) data structure and beginning and end of migratory seasons were matched to the respective local initiation of migration by the passerines. Spring for both study years was defined as a time frame from 10th of March to 31st of May. For autumn the time frame was set from 15th July to 30th November.

Final explanatory variables

The meteorological parameters chosen as explanatory variables for the regression analyses were precipitation, Δ precipitation, pressure, Δ pressure, air temperature, Δ air temperature, cloudiness, visibility, TWC, Δ TWC, CWC and Δ CWC. In addition to the atmospheric parameters, three variables accounting for temporal patterns in migration intensity were included in the analyses. To capture phenological patterns within the four migration periods studied, the "*lubridate"* package (v. 1.9.3; Grolemund & Wickham 2011) was used to calculate fractionised Julian date ("ydate"). The study year ("year") was used as an additional temporal variable to account for interannual variations. Migration intensities are known to systematically vary throughout the course of the night (e.g. Newton 2008). To account for circadian MTR patterns, a "proportion of the night" variable was calculated for each hourly observation. Eventually, the radar data and pre-processed meteorological data were combined. The final

dataset used for regression analyses only included nightly data, predefined by Swiss Birdradar Solution AG as the time between sunset and sunrise (UTC +1, summer: UTC + 2).

Regression analyses

As the relationship between the predictors and the response variables was assumed to be non-linear, generalised additive models (GAMs) were chosen to estimate the impact of weather variables on the MTR and the fraction of passerines flying at risk height. GAMs offer a high degree of flexibility in modelling such non-linear relationships, while also providing a straightforward and interpretable representation of the effects of individual variables (Wood 2017). Compared to traditional linear models, GAMs are better suited to capture and visualize complex non-linear patterns within the data.

Model fitting

Bayesian models were fitted using the "*brms*" package (v. 2.22.0; Bürkner 2017). The GAMs were separately constructed for two response variables, to determine the effects of temporal, phenological and meteorological explanatory parameter on:

(i) the nocturnal MTR throughout the migratory seasons up to 1025 m

(ii) MTR at risk zone: the proportion of MTR occurring within the height of the wind turbines, i.e. the "risk zone" (defined here as 25 – 180 m a.g.l).

Both GAMs were fitted for the two migratory seasons, separately. Thus, a total of four GAMs were constructed, each with a total of 15 parameters chosen as explanatory variables. For models with total MTR as response variable, a negative binomial distribution family with a log link function was employed to account for heterogenous and over-dispersed count data (as an alternative to a Poisson distribution). The negative binomial distribution was chosen due to its flexibility in modelling count data with no upper bound and with greater variance than mean, which is a common characteristic of ecological data (Lindén & Mäntyniemi 2011). To allow for the overdispersion parameter of the negative binomial distribution to vary with date, a "shape" function for the smoothed effect of "ydate" was added to the model.

Models with the proportion of MTR at risk height as response variable were treated as a beta binomial distribution family with a logit link function. Beta-binomial distributions are typically used to model over-dispersed count data with an upper bound, where the variance exceeds the mean, making them ideal for situations with variability in proportions as are measured in this study. As was done with the negative binomial model, a "phi" parameter for the effect of "ydate" was added to the beta-binomial models, to allow for the overdispersion parameter to vary with date, resulting in more accurate predictive abilities. Both types of models were also fit with smoothing splines for the temporal effects such as Julian date and proportion of night.

Smoothing splines are often used in regression analyses to capture non-linear trends and patterns in time-series data without overfitting the models to the data. With the large amount of data used in this study, priors have a neglectable influence on the posterior distribution of the model output. Thus, the default priors of the "*brms*" package were used instead of individually defining priors for each explanatory variable. For the final run of models, a total of 4 chains with 5000 iterations (including 2500 warm-up iterations) was specified. The models fitted for this study, use a stochastic sampling process known as Markov-Chain-Monte-Carlo (MCMC) for the estimation of posterior probability distributions. To facilitate convergence of chains and reduce faulty so-called divergent transitions, for all four GAMs values "adapt_delta" and "max_treedepth" were increased to 0.95 and 15, respectively.

Model validation

To assess the quality of alternative models and to compare predictive abilities of different models for the same seasons the so-called "leave-one-out" (LOO) cross-validation approach was employed using the package "*loo*" (v. 2.8.0; Vehtari 2024). Compared models only differed in k-values used for the smoothing splines of "ydate" and "ProportionOfNight". The set of explanatory variables were the same for all alternative models. The model with the best predictive abilities for the respective data base, was chosen based on the differences in expected log predictive density (ELPD) and the corresponding standard error. According to the authors of the package, if the difference in ELPD values exceeds four-times (or larger) the size of its estimated standard error, that implies a relevant difference in predictive abilities between tested models (Sivula et al. 2020). Based on the LOO evaluation, a total of four models were picked. One model per migratory season for the general relationship between weather parameters and migration intensity (MTR), and one model per migratory season for the weather-dependency of birds flying at low altitudes, i.e. in the risk height. To prevent overfitting the models to the data and putting a disproportionate amount of weight on date as an explanatory variable, the lowest k-values for the smoothing parameters of date were chosen, which did not result in significantly worse predictive abilities of the models according to LOO. For models with total MTR as response variable, for the smoothed effect of date k = 30 was used for both seasons. K-values for proportion of night differed among seasons, for spring k = 5 and for autumn k = 7 was used. K = 10 resulted in the best fit for the "shape" function of the negative binomial models for both seasons. For the risk zone models, i.e. beta binomial models, k = 10 was used for the smoothed effect of date for both seasons. Again, k-values for proportion of night differed among seasons, for spring k = 5 and for autumn k = 7 was used. K-values for the "phi" function also varied between seasons: k = 10 (spring) and k = 5 (autumn).

Additionally, posterior predictive checks (PPCs) were conducted to compare model fits. PPCs are a commonly applied method to evaluate the model's predictive accuracy and identify potential misspecifications, by comparing simulated (bird count) data from the posterior predictive distribution to the observed data. PPCs for all four models are attached in the appendix (Fig. S5 & S6).

Model output interpretation

Model outputs were visualised using the "*bayesplot*" package (v. 1.11.1; Gabry 2024) and "*posterior*" package (v. 1.6.0; Bürkner et al. 2024). The function "mcmc_intervals" was exploited to plot central posterior uncertainty interval (i.e. credible intervals, CI) estimates from MCMC draws. These MCMC intervals (Fig. 6 & 10) were computed to summarize the sizes and directions of the effects of the explanatory variables on the respective response variable. For the "year" categorical variable, year 2023 was used as the intercept in the models and thus the MCMC analyses estimated the effect of year 2024 relative to year 2023 (Fig. 6 & 10). To quantify the (conditional) effect of different explanatory variables on the focal response variable, the amplitude of fold-change on the expected passerine count was calculated for each model output, using the function "posterior_epred" (Fig. 8 & 9). The "expected" bird count refers to the expected value of the posterior predictive distributions when drawing samples from the predicted negative binomial responses. These predictions of expected bird counts are based on the respective explanatory variable of interest and are conditional on the mean values for the other explanatory variables. To avoid outlier influence, extreme values were removed by only keeping the central 95 % interval. The fold-changes are then calculated as the ratio between the maximum and minimum mean value of the predicted response. Fold-changes thus indicate the maximum effect size a focal variable, or the combination of several variables, exerts on the response variable on an average day (i.e. middle of the season, middle of the night, mean weather values). Consequently, the fold-changes allow to make quantitative statements such as "tailwind can lead up to a 7-fold increase in MTR on an average day in autumn".

Fold-changes were also calculated for the risk zone models but seeing as the probability of a bird flying in the risk zone rather than count data was modelled as the response variable, fold-changes were calculated for change of the odd-ratios of the probability of flying low. (If the probability of being in the risk zone is p, then the odd-ratios are calculated by $p/1 - p$.). Thus, fold-changes for the risk zone models imply magnitude of fold-changes of the odds-ratios of flying in the risk zone on an average day (Fig. 12 & 13). The corresponding effect on p will depend on the values of all the other explanatory variables. Fold-change calculations were

performed for each MCMC iteration, resulting in a full posterior distribution of the magnitude of fold-change for each explanatory variable.

The function “conditional_effects” was used to display the conditional effects of relevant predictors on the response variables, as well as for the smoothed effects of “ydate” and “proportion of night”. The conditional effect plots will draw the predicted response when the focal variable varies, while keeping the other variables fixed at their mean values. Thus, they allow to visualize the shape of the effect of a focal variable. By default, the mean was used for the continuous weather variables, and the reference category was used for factor variables such as “year”. Again, the year 2023 was used as the reference for conditional effects. Conditional plots were created for the smoothed effects of date and proportion of night variables (Fig. 7 & 11), as well as the top three most influential explanatory variables per model which are attached in the appendix (Fig. S7 & S8). The magnitude of fold-change gives similar information, but only considering the “expected” response and after having removed extreme outliers (here "expected" is used in the statistical meaning of "average").

Results

Meteorological data

According to the Köppen-Geiger climate classification system, the study area in Husum, Northern Germany, has a Cfb climate type (Köppen & Geiger 1968/Beck et al. 2023). This temperate (maritime) climate is characterised by mild winters and cool summers.

Table 3 summarizes the mean and standard deviation values for all meteorological explanatory variables used autumn and spring data for the two studied years are combined respectively. Hourly mean precipitation was 0.11 ± 0.35 mm in spring and 0.16 ± 0.51 mm in autumn (Tab. 3). Air temperature was slightly lower during spring (7.48 ± 3.85 °C) than autumn (10.92 ± 5.05 °C). Similarly, cloud coverage was slightly lower in spring (5.97 ± 2.78 oktas) compared to autumn (6.08 ± 2.54 oktas). Barometric pressure only displayed minor differences across seasons: 1010.01 ± 10.42 hPa (spring) and 1009.56 ± 11.48 hPa (autumn). Average hourly visibility was 29171.23 ± 16737.76 m (spring) and 28048.42 ± 15321.17 m (autumn) (Tab. 3). Windrose-figures S1 – S3 (appendix) provide an overview of the atmospheric wind conditions in spring and autumn, respectively. These figures depict both wind speed and direction. In both season, winds blew predominantly from the south and south-south-west respectively (spring: 179.27 ± 87.77 °, autumn: 192.92 ± 75.28, Tab. 3). Average wind speed was 4.18 ± 1.93 m/s (spring) and 3.88 ± 2.04 m/s (autumn) (Tab. 3). In summary, wind conditions were generally more supportive of the north-easterly movement of spring migration than the south-westerly

movement of autumn migration. Contrastingly, tail- and crosswind conditions (i.e. combination of directional wind and wind speed) were slightly more favourable for autumn migrants (Tab. 3). During spring, mean hourly TWC was -0.14 ± 3.41 m/s, mean CWC was 2.55 ± 1.77 m/s. In autumn, mean TWC was 0.03 ± 3.06 m/s, mean CWC was 2.50 ± 1.91 m/s. For additional information regarding the underlying meteorological data used for this study, tables S1 – S3 (appendix) depict mean, median, minimum and maximum values of all the weather parameters, independently for each of the four seasons studied.

Table 3: Mean and standard deviations (sd) of explanatory meteorological variables used for the regression analyses. Both studied spring (green) and autumn (grey) seasons are summarised for this table.

		Spring		Autumn	
Variable	**Unit**	**Hourly Mean**	**sd**	**Hourly Mean**	**sd**
Precipitation	mm	0.11	0.35	0.16	0.51
Delta precipitation	mm	0.003	0.51	0.00	0.72
Cloudiness	Out of 8	5.97	2.78	6.08	2.54
Temperature	°C	7.48	3.85	10.92	5.05
Delta temperature	°C	0.15	2.77	-0.18	2.84
Barometric pressure	hPa	1010.01	10.42	1009.56	11.48
Delta pressure	hPa	0.19	7.31	0.07	7.44
Visibility	m	29171.23	16737.76	28048.42	15321.17
Wind speed	m/s	4.18	1.93	3.88	2.04
Wind direction	°	179.27	87.77	192.92	75.28
TWC	m/s	-0.14	3.41	0.03	3.06
Delta TWC	m/s	0.06	3.42	-0.02	3.20
CWC	m/s	2.55	1.77	2.50	1.91
Delta CWC	m/s	-0.01	2.21	-0.01	2.48

Overview of passerine migration in Husum 2023 - 2024

For this analysis, a total of 82 nights during the spring seasons and a total of 138 nights during the autumn seasons were used (Tab. 4). Initially, results regarding the migration traffic intensity are listed, followed by description of the flight height distribution of migrating passerines.

MTR – migration traffic rate

To visually compare diurnal and nocturnal migration traffic rates of passerines, figure 2 depicts the summed MTR per night and day across the four studied seasons. As anticipated, the mean

MTR of nocturnally migrating passerines showed quantitative differences for spring and autumn seasons respectively (Tab. 4, Fig. 2). Both intra- and interseasonally, considerable temporal variations in migration intensity were observed (Fig. 2 depicts stacked bar of day/night comparison of passerine MTR). The seasonal sum of migrants reached more than double the amount in autumn compared to spring. Between-year differences of summed MTR were neglectable for autumn seasons, while spring of 2024 showed a reduction of ~22.000 migrants compared to the previous year (Tab. 4). During the spring seasons there are two peaks in the migration intensities around mid-March and mid-April, these peaks being more pronounced during spring of 2024 (Fig. 2a). In the fall seasons, migration peaked during October (Fig. 2b) with particularly one night standing out as the night with overall highest MTR within the first half of October, during both years respectively. In 2023, the nights with the highest MTR were the 21$^{st\ of}$ March (18171.35 n/km/h) in spring and the 7th of October (54346.55 n/km/h) in autumn (Tab. S4). Similar patterns but with an overall decrease in MTR was observed for 2024: highest nocturnal MTR was observed on 14th of March (15307.11 n/km/h) in spring and on the 2nd of October (45681.76 n/km/h) in autumn (Tab. S4). Overall, higher migration rates were observed during both autumn seasons compared to the spring seasons, with slightly higher migration rates for spring seasons in 2023 and autumn seasons in 2024.

Figure 3 shows violin plots illustrating the MTR of passerines during the course of the night given as proportions of the night (from zero to one). A comparison between seasons reveals that migration activity peaked earlier in the night during autumn than in spring. In autumn (Fig. 3b), the highest median MTR occurred during the first quarter of the night (20 – 30 %), followed by a steady decline as the night progressed. In contrast, spring migration (Fig. 3a) showed a gradual increase in activity toward the middle of the night, with a slight decrease thereafter. Notably, more birds migrated in the hours immediately before sunrise than in the hours following the sunset in spring, with the highest median MTR observed between 60% and 70% of the night.

Table 4: Summary of migration traffic rates MTR (n/km/h) over the study period. All values except for the seasonal sum refer to the hourly MTR values.

Year	Seasons	N (Nights)	Seasonal sum	Mean	Q1	Median	Q3
2023	Spring	82	232445.924	363.197	60.60	153.040	439.76
	Autumn	138	499886.908	361.713	65.52	159.685	356.67
2024	Spring	82	210068.962	317.805	80.45	193.819	431.71
	Autumn	138	499964.957	357.373	59.12	155.239	381.17

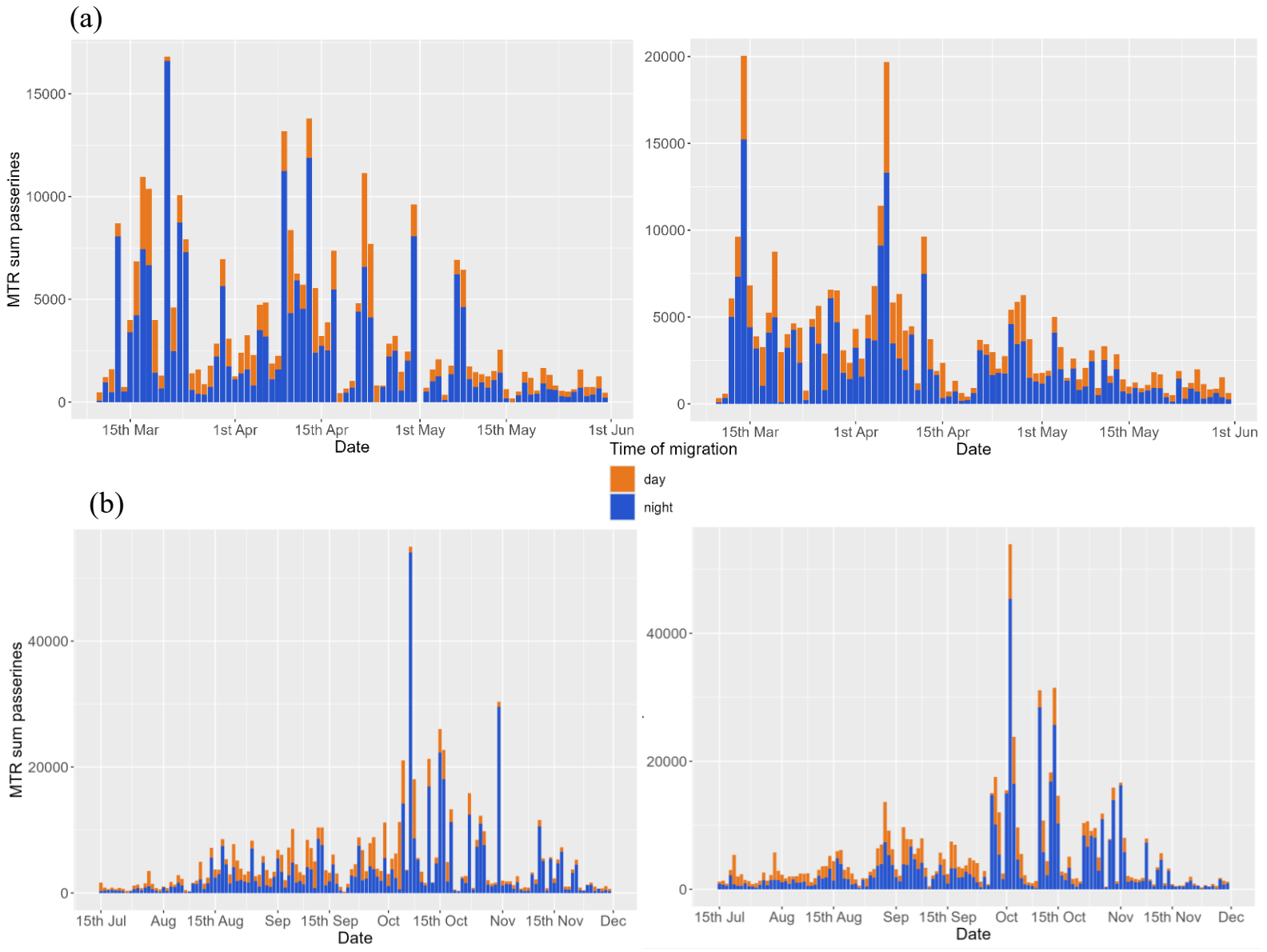

Figure 2: Stacked bar showing summed MTR (n/km/h) of migrating passerines for (a) spring and (b) autumn seasons of 2023 (left side) and 2024 (right side). Bars depict summed MTR of single nights (dark blue) and days (orange).

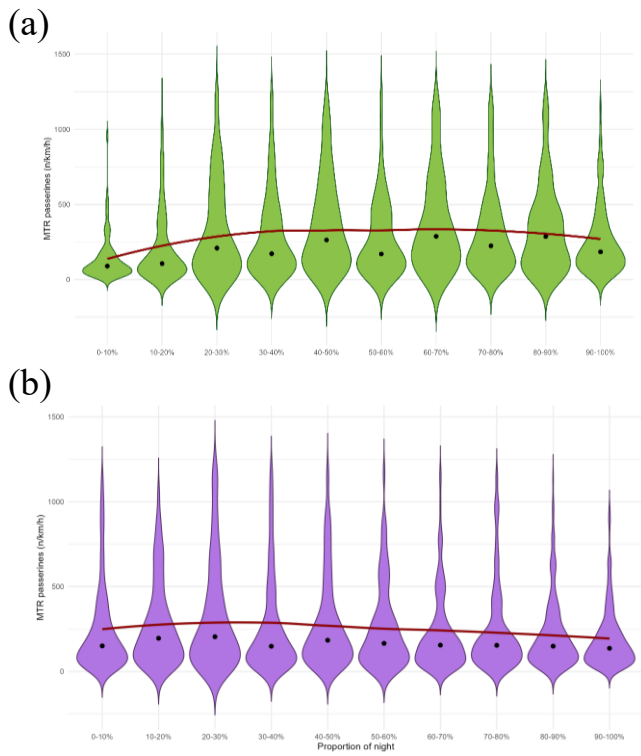

Figure 3: Violin plots depicting the distribution of the central 90 % of passerine MTR in relation to the proportion of night for (a) spring and (b) autumn seasons. The width of each violin represents the density of observations within each night group. Black dots indicate the median MTR per group. The red line represents a smoothed LOESS trend illustrating overall changes in MTR across the night.

FHD – flight height distribution (25 – 1025 m)

Henceforth, any data regarding altitude and height will be understood as height above ground level (a.g.l.), unless stated otherwise.

Figure 4 shows the vertical distribution of studied passerines for all four migratory seasons. During both the spring and autumn seasons of 2023 and 2024, the flight height distribution of nocturnally migrating birds as well as the mean flight height exhibited similar patterns. Across all seasons the altitude distribution follows the typical positively skewed pattern observed in passerine FHD, where the frequency of observations decreases with increasing altitude, peaking at intermediate heights in the lowest third of the altitude range (Fig. 4). This suggests that passerines tend to favour a lower altitude for their nocturnal flight, avoiding both extreme low and high altitudes.

During spring of 2023 and during both fall seasons, highest migration rates occurred within the second lowest altitude bin (75 – 125 m, Fig. 4a & b). In spring of 2024 the height-range where most passerines passed through was slightly elevated, between 125 – 175 m (Fig. 4a). Both migratory seasons expressed slight interannual variations regarding mean flight height. For the spring seasons, the mean flight height slightly decreased from study year 2023 (314.00 m) to 2024 (295.78 m). Contrastingly, for the autumn seasons, the mean flight height slightly increased from 2023 (295.28 m) to 2024 (305.65 m). However, mean flight height always ranged above maximum local wind turbine height (i.e. 180 m). Within the studied altitude range

of 25 – 1025 m, throughout both spring seasons 90 % of nocturnal migrants flew below ~ 580 m (Fig. 4a, grey intercept). During the autumn seasons 90 % of migrants flew below 525 m (2023) and 560 m (2024) respectively (Fig 4b, grey intercept). Comparing the quantity of migrants flying within the "risk zone height" (altitude between 25 – 180 m) showed no obvious seasonal differences. Throughout all four seasons, about a third of nocturnal migrants travelled through the risk zone (2023: spring = 32.12 %, autumn = 32.29 %; 2024: spring = 34.30 %, autumn = 33.01 %) (Fig. 4, red borders).

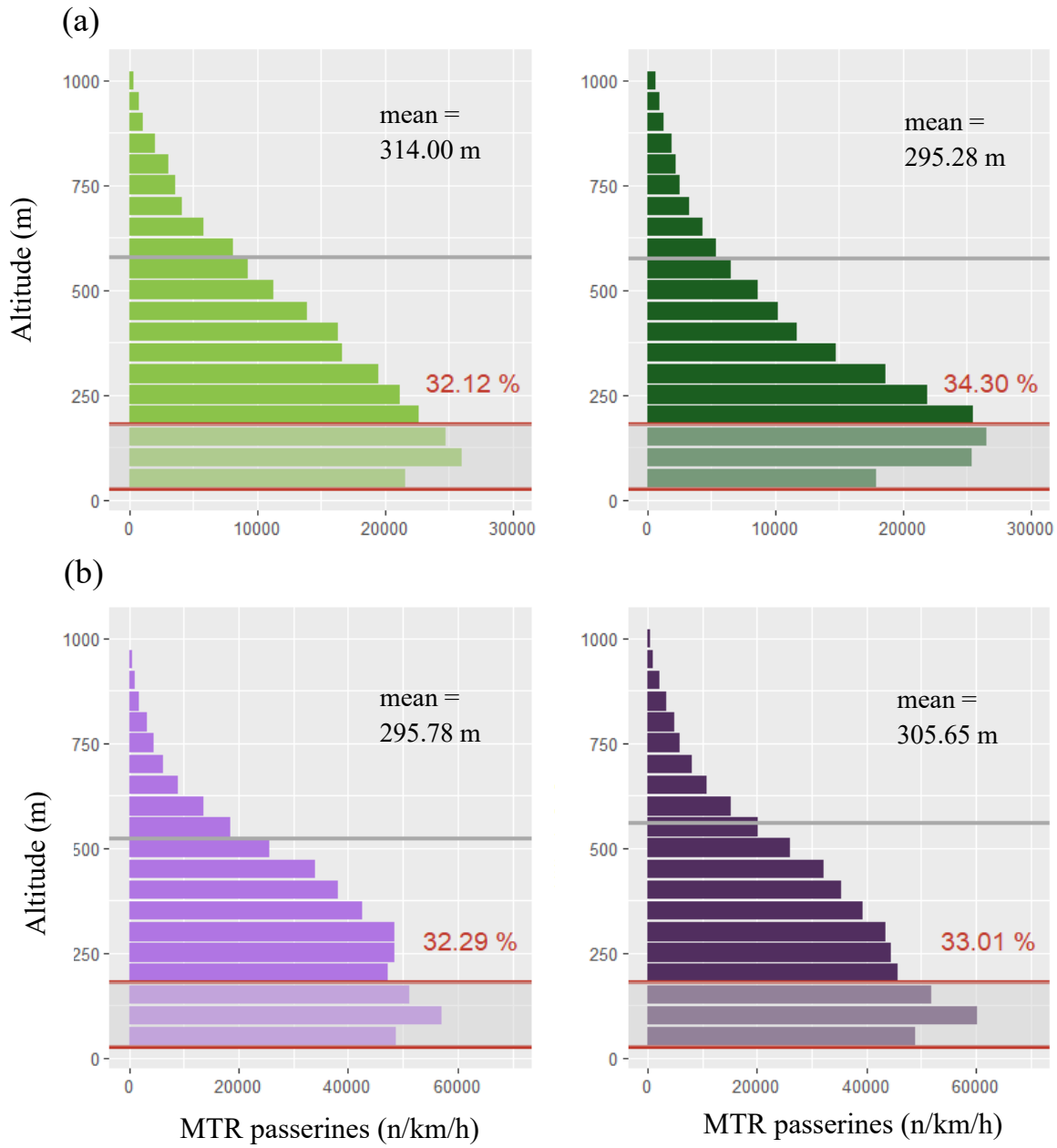

Figure 4: Flight height distribution of passerines for (a) spring and (b) autumn migratory seasons of 2023 (left: light green, light purple) and 2024 (right: dark green, dark purple). The grey y-intercepts indicate the threshold-height under which 90% of passerines were passing through the radar. The "risk zone", i.e. 25 – 180 m, is bordered by red lines and red values indicate percentage of migrants within the risk zone.

Fig. 5 represents heatmaps further elucidating the relationship between flight altitude and MTR of passerines migrating through Northern Germany across different portions of the night. The x-axis represents the proportion of the night (from sunset to sunrise), divided into time bins, while the y-axis shows average flight altitude (in meters). Passerine flight height distribution (FHD) exhibited clear nocturnal variation, with distinct seasonal patterns.

In both spring and autumn, the majority of the migratory activity occurred within the lower half of the studied altitude range. During spring, peak migration intensity at altitudes considered within the risk zone was observed around the middle of the night (50%, Fig. 5a). In contrast, autumn migration was characterised by elevated activity at risk altitudes both shortly after sunset (10%) and near the end of the night (100%). Towards the end of the night during fall, migration activity showed a very strong (yellow) peak in the second altitude bin (average height 100 m, Fig. 5b).

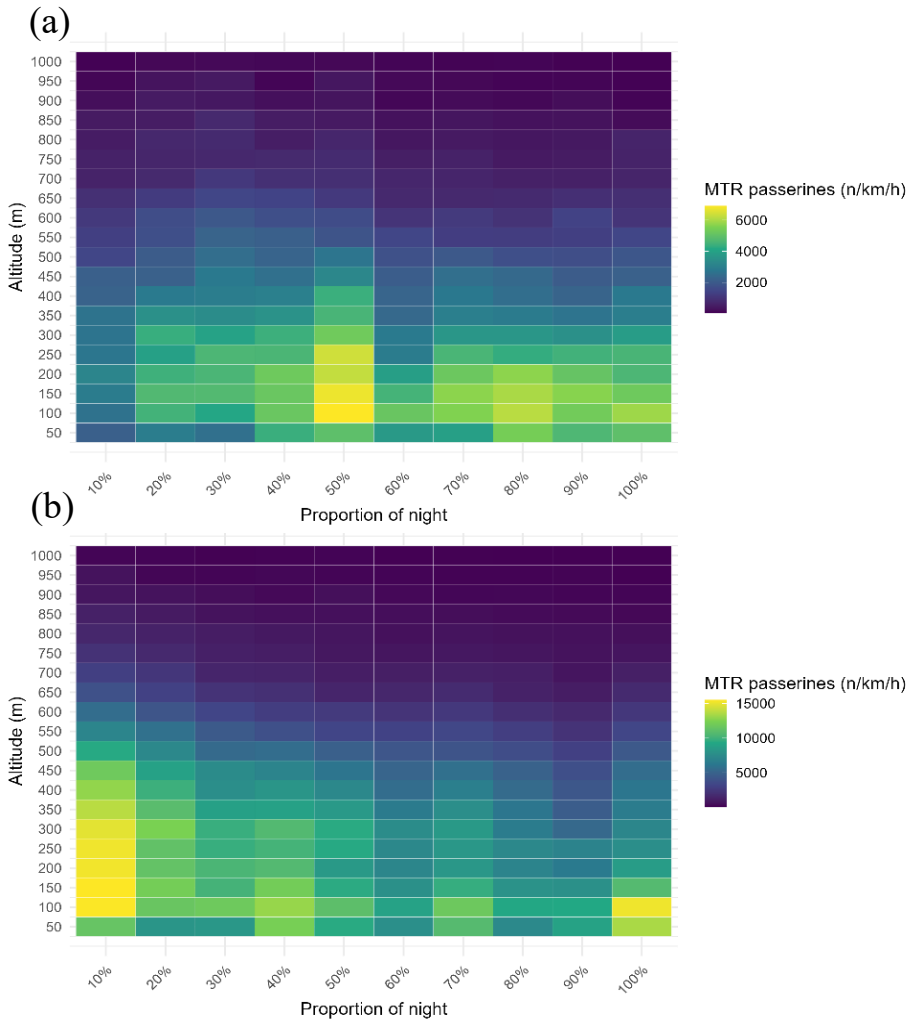

Figure 5: Heatmaps showing the relationship between flight altitude and MTR of passerines across different portions of the night for (a) spring and (b) autumn season respectively. Colour intensity reflects MTR values (n/km/h), with darker (blue) shades indicating higher migration activity. The y-axis illustrates the average altitude for each 50 m bin (i.e. 25 – 75 m = 50 m).

Statistical analyses

In the following section, results for both response variables i) MTR over the entire altitude range and ii) proportion of MTR in the risk zone, will be listed separately, starting with i). Spring and autumn models will be collectively considered for both model types.

Effects of explanatory variables on MTR (25 – 1025 m)

MCMC intervals

In a Bayesian framework, MCMC intervals are a standard tool for indicating the effect size of explanatory variables. Posterior uncertainty intervals of the explanatory variables used are portrayed in Figure 6. The points depict posterior medians, the thick segments show the 50% credible intervals, the thinner outer lines indicate the 90% credible intervals. The x-axis is read as the effect size of variables, with negative values indicating negative association between respective variable and passerine MTR. The y-axis lists the explanatory variables. Variables, where the median or CI values cross the grey x-intercept, appear to have no significant effect on the response variable according to the model output. Comparing the MCMC intervals for spring and autumn (Fig. 6a and b), at first glance the credible intervals for autumn seem a lot narrower. As the values were scaled (and centered) before splitting the data into spring and autumn seasons (see material and methods section), this allows for a direct comparison between the seasonal data. Thus, looking at the x-axis scale explains this apparent difference between the credible intervals. For spring the x-axis runs from approximately -0.5 to 0.5, for autumn some variables have overall greater impact on MTR and the x-axis runs from -0.7 to 0.8. In spring, variables with positive association with passerine MTR (listed from most influential to least, i.e. from right to left) are temperature, Δ temperature, TWC, Δ TWC and Δ CWC (Fig. 6a). Increase in both temperature and tailwind as well as increase in both components compared to the previous night (delta values) results in rising migration traffic rates. Additionally, Δ CWC positively correlates with MTR during spring. Variables negatively impacting MTR in spring are CWC, year 2024, pressure, visibility, precipitation and Δ pressure. No significant influence on MTR is exerted by Δ precipitation and cloudiness. During autumn, variables exerting positive influence on passerine MTR are (from right to left) TWC, Δ pressure, temperature, visibility, Δ CWC and pressure (Fig. 6b). Variables negatively impacting MTR in autumn are Δ temperature, CWC, year 2024, precipitation. No significant change in MTR during autumn has been observed for Δ precipitation, cloudiness and Δ TWC. Overall, both Δ precipitation and cloudiness did not seem to significantly impact passerine migration during both migratory seasons (Fig. 6).

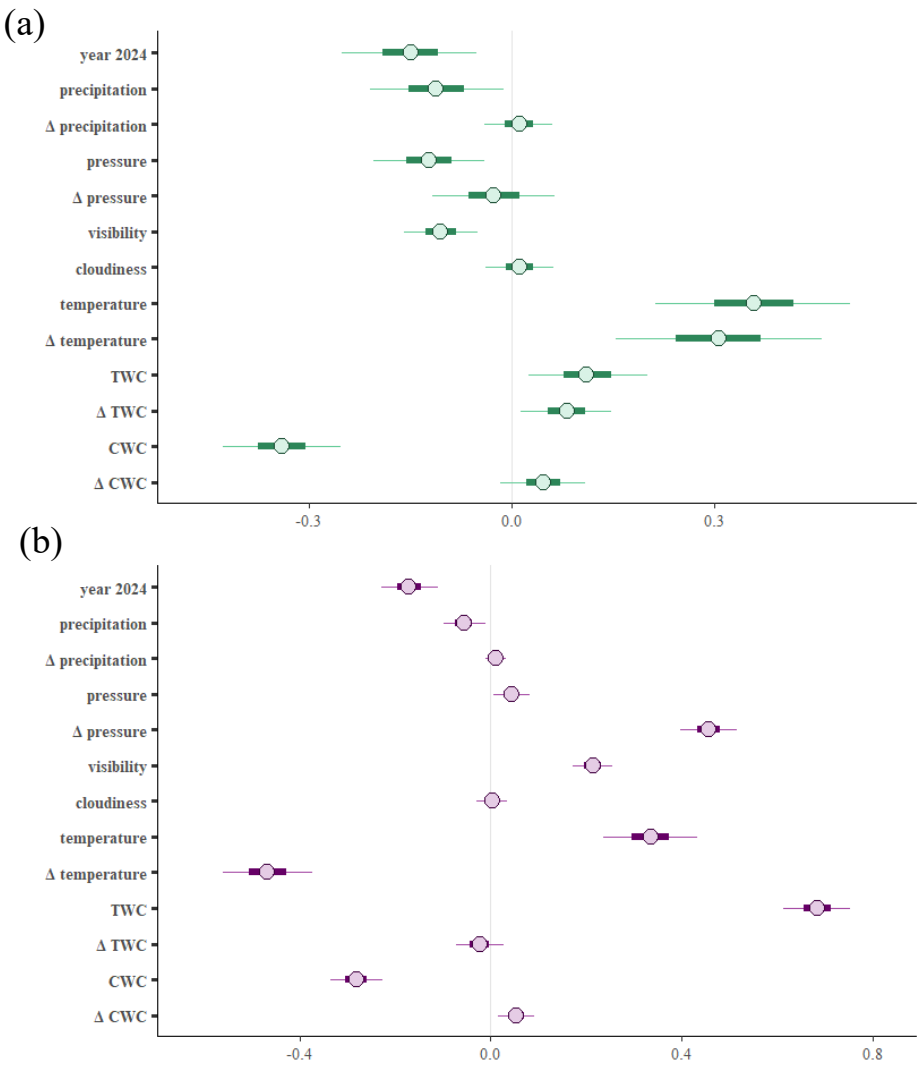

Figure 6: MCMC intervals for (a) spring and (b) autumn models with MTR (n/km/h) as response variable. Posterior medians are depicted as light blue points. Thick dark blue segments indicate 50% CIs, thin segments indicate 90% CIs. Positive values on the x-axis correspond to positive associations with the MTR and vice versa.

Conditional effects

Figure 7 illustrates the conditional effects (for an explanation see material and methods section) of time of night ("ProportionOfNight") and Julian day ("ydate") on the migration traffic rate of passerines across both migration periods. In spring, the influence of time of night gradually increased after sunset and reached a distinct peak around the middle of the night (Fig. 7a). After the peak, the effect slightly declined, though it remained stronger just before sunrise than it was shortly after sunset. During autumn, the peak occurred earlier, within the first quarter of the night (Fig. 7b). The effect then gradually decreases with a slight uptick again right before sunrise. Similar to the spring season, the influence of nighttime during autumn was also somewhat stronger toward sunrise than immediately after sunset.

The influence of date as an explanatory variable for the MTR also showed distinct patterns in spring (Fig. 7c) and autumn (Fig. 7d). In spring, the effect was strongest at the very beginning of the migratory period, around day 76 (March 17th), between approximately day 102 and 105

(April 12th to 15th), and again around day 128 (May 8th). After May 8th, the influence of date declined rapidly (Fig. 7c). In contrast, during autumn, the effect of date was more concentrated within a few weeks, although again scales of the x-axis differ between seasons corresponding to the respective lengths (see Tab. 4). It gradually increased and peaked in the second half of the migratory season, around day 288 (October 15th). Overall, the strongest influence of date on MTR in autumn was observed between day 275 and 320 (October 2nd to November 16th) (Fig. 7d).

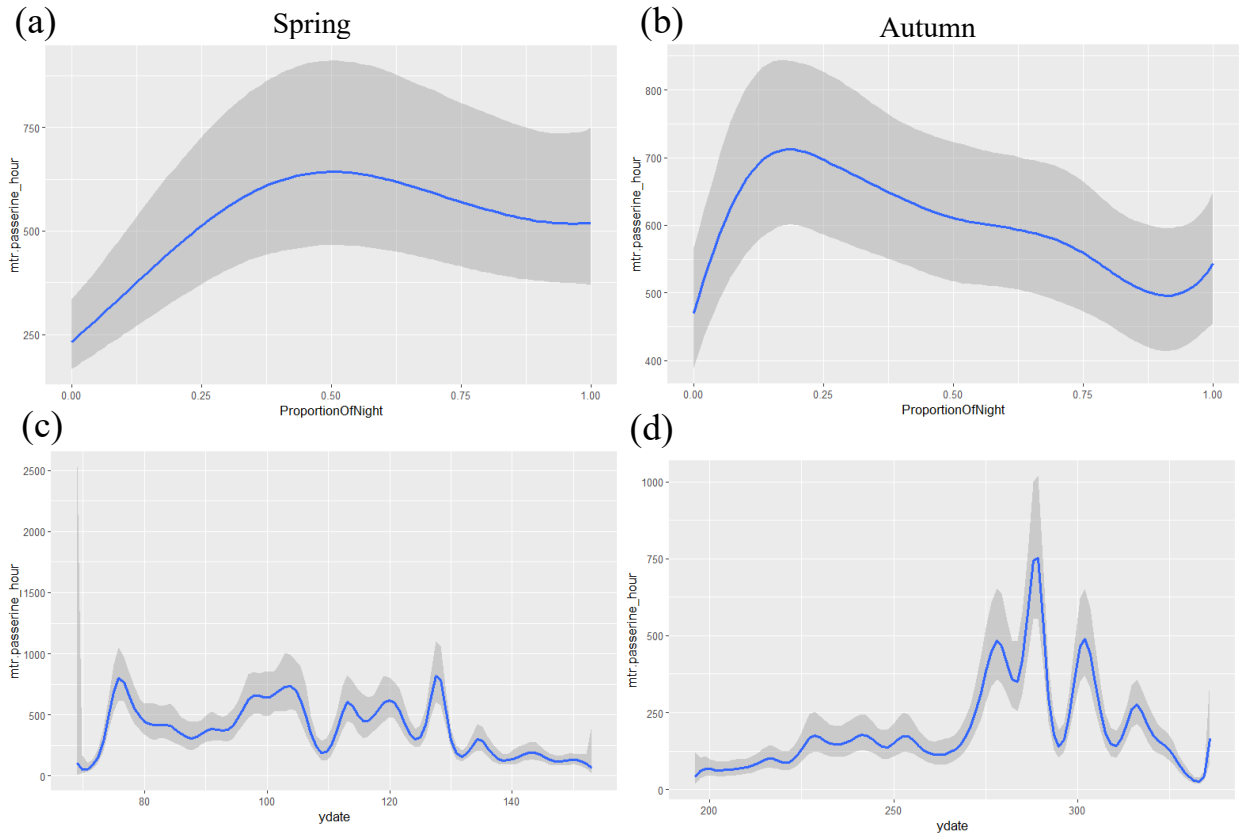

Figure 7: Conditional effect plots for the explanatory variables time of night (a, b) and Julian day (c, d) on the MTR as the response variable. Left plots illustrate the spring seasons, the right plots depict autumn season. The y-axis illustrates the migration traffic rate (MTR, n/km/h) of passerines. The blue line represents the median of the predicted response; the grey ribbon illustrates the 95% prediction interval.

Magnitude fold change in expected bird counts

Additionally, figures 8 and 9 show the magnitude of fold change in expected passerine counts per (set of) explanatory weather variable, i.e. the means of the negative binomial distributions. The same figures including temporal variables are attached in the appendix (Fig. S7). Again, credible intervals are depicted as thick (50%) and thinner (90%) outer lines. The dashed grey x-intercept at 1 depicts no fold change in bird numbers aloft. Seeing as the MCMC-intervals

provide information on the effect direction and relative effect size, they do not allow for a straightforward quantification of the effect of an explanatory variable on the response variable. Fold change is a commonly used effect size to quantify the relative change in one variable in response to a change in another. In the following paragraph, resulting median fold change in bird counts, i.e. effect size of individual explanatory variables, will be referred to in numerical values without units (see table 5 & 6). Corresponding means and 95% CIs referenced in below are summarised in table 5 & 6. Seeing as a fold change of 1 means no change in expected bird counts, for the 2.5% CIs a minimum of 1.01 was chosen as the threshold for exerting an effect on bird counts. All variables below the threshold (i.e 2.5% confidence interval includes 1.00) result in a neglectable change of MTR and thus are interpreted as non-relevant for further discussion.

Combined, all explanatory variables tested with the models ("all_vars") had an overall greater impact on the fold change in bird counts during autumn (56.55) than during spring (35.84, Fig. 8 & 9, Tab. 5 & 6). For both migratory seasons, day of year is the temporal variable which explained the biggest differences in MTR throughout the seasons (spring: 12.28, autumn: 20.14). Proportion of night had an increased impact on bird counts in spring (2.77, Tab. 5) than in autumn (1.54, table 6).

Combined weather variables

Combination of all the weather variables had the overall second highest effect on the expected bird count in both seasons, with a fold change of 7.71 (spring) and 18.93 (autumn). According to the generalised additive models, combined wind variables (i.e. cross- (CWC, Δ CWC) and tailwind components (TWC, Δ TWC)) explained most of the differences in observed bird counts among all weather parameters, for both seasons respectively (Fig. 8 & 9). However, the fold change in expected bird counts during autumn (7.50) was more than double the magnitude of fold change during spring (3.50). In spring, overall air temperature (Δ temperature and temperature) resulted in the second highest magnitude of fold change in expected bird counts (3.13, Fig. 8). Combined pressure variables resulted in a 1.65-fold change of expected bird counts, followed by combined precipitation variables (1.24).

For autumn migration, combined barometric pressure led to a maximum of a 3.89-fold change in expected bird counts, followed by overall temperature with a 2.82-fold change of passerine counts (Tab. 6). Again, combined precipitation had the weakest effect for combined variables during autumn (1.16, Fig. 9).

Single weather variables

Starting off with spring, CWC was the explanatory variable with the biggest (negative) impact on MTR (2.93), according to the magnitude of fold change in the expected passerine counts (Fig. 8, Tab. 5). Second most important explanatory variable for spring migration was air temperature, with a maximum fold change of 2.34. Similarly, maximum Δ temperature led to a fold change of 1.73. Both, barometric pressure and visibility negatively correlated with estimated bird count with a magnitude of 1.56-fold and 1.46-fold change of expected bird counts, respectively. Further, Δ pressure (1.13) and precipitation (1.22) show a negative effect on the MTR, however it should be mentioned that for both variables the CI 2.5% is barely above 1.00 (see table X) and thus the effects must be interpreted with caution. The same applies for the following wind variables exerting a slight positive influence on spring MTR: TWC (1.47), Δ TWC (1.36) and Δ CWC (1.23).

During autumn, TWC (7.12) had the largest (positive) impact on expected passerine counts among single explanatory variables, followed by Δ barometric pressure (3.64) and temperature (2.76) (Fig. 9, Tab. 6). Contrastingly, an increase in air temperature compared to the previous night (Δ temperature), led to a 2.29-fold decrease in MTR. While maximum present-night CWC led to a decreasing number of migrating birds by a 2.51-fold change, contrastingly Δ CWC minimally increased bird count by 1.31. Further, visibility positively correlated with estimated bird counts, max visibility resulting in a 1.99-fold change. Both pressure (1.19) and precipitation (1.15) only had a minimal impact on the autumn MTR, positively and negatively, respectively.

Overall, both Δ precipitation and cloudiness had a negligible association with expected bird counts during both migratory seasons (Fig. 8 & 9, Tab. 5 & 6). Moreover, Δ TWC showed negligible influence on passerine MTR during autumn. Altogether, both, increased side wind component (CWC) and precipitation, reduce number of migratory birds aloft in both seasons. Air temperature, increased tail wind (TWC) and change in CWC compared to previous night seemed to increase MTR in both seasons.

*Table 5: Median and corresponding CI 2.5% and 97.5% values for the magnitude of fold change in expected bird counts during **spring**. Light orange background indicated negative association with passerine MTR and refers to the MCMC interval results. Bold variables depict the three most influential (single) explanatory variables.*

MTR - Spring			
Variable	Median	CI 2.5%	CI 97.5%
Year	1.16	1.03	1.31
year_date	12.28	7.86	20.22
Night	2.77	2.34	3.31
Precipitation	1.22	1.02	1.49
Δ Precipitation	1.10	1.00	1.38
Pressure	1.56	1.10	2.23
Δ Pressure	1.13	1.01	1.47
Visibility	1.46	1.15	1.84
Cloudiness	1.07	1.00	1.25
Temperature	**2.34**	**1.54**	**3.53**
Δ Temperature	**1.73**	**1.24**	**2.41**
TWC	1.47	1.05	2.11
Δ TWC	1.36	1.04	1.84
CWC	**2.93**	**2.12**	**4.07**
Δ CWC	1.23	1.01	1.68
All precipitation	1.24	1.06	1.48
All pressure	1.65	1.21	2.29
All temperature	3.13	2.29	4.27
All wind	3.50	2.74	4.49
All weather	7.71	6.01	9.85
All variables	35.84	24.69	51.71

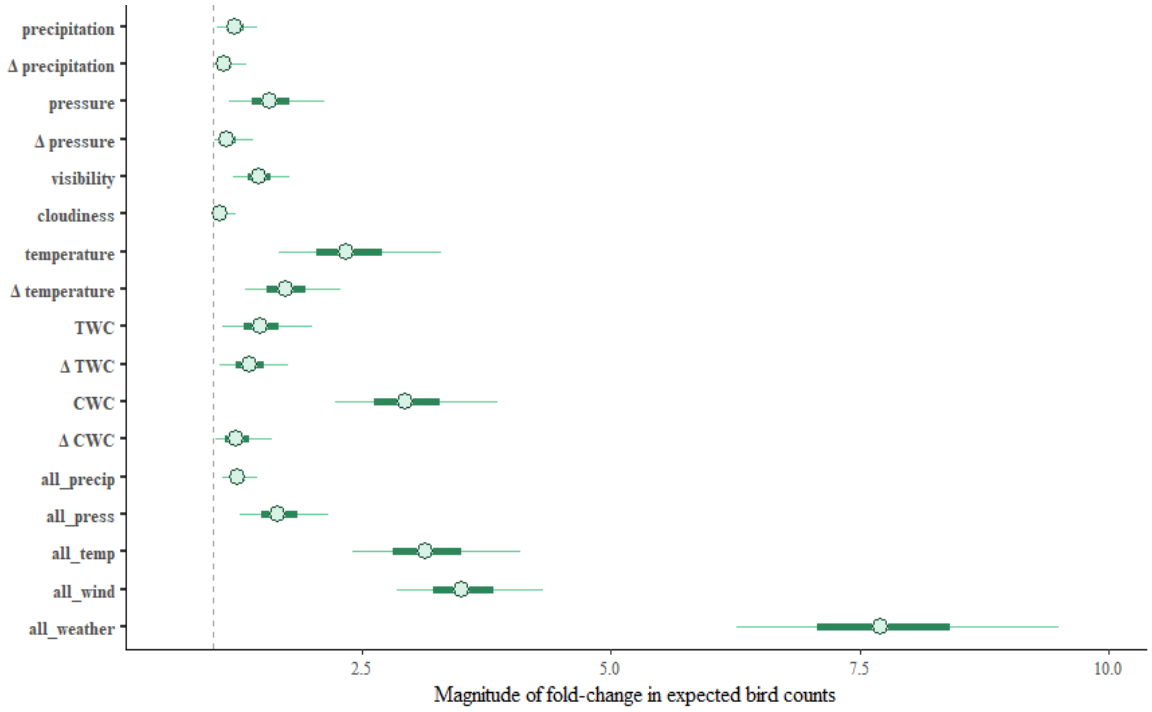

*Figure 8: Magnitude of fold-change in expected bird counts, per (set of) explanatory variable for **spring**. Dashed x-intercept at 1 depicts no fold-change. Thick dark glue segments represent the 50% CIs, thin segments represent the 90% CI.*

*Table 6: Median and corresponding CI 2.5% and 97.5% values for the magnitude of fold change in expected bird counts during **autumn**. Light orange background indicated negative association with passerine MTR and refers to the MCMC interval results. Bold variables depict the three most influential (single) explanatory variables.*

MTR - Autumn			
Variable	Median	CI 2.5%	CI 97.5%
Year	1.19	1.10	1.27
year_date	20.14	15.01	26.95
Night	1.54	1.37	1.74
Precipitation	1.15	1.02	1.30
Δ Precipitation	1.07	1.00	1.24
Pressure	1.19	1.02	1.44
Δ Pressure	**3.64**	**2.97**	**4.44**
Visibility	1.99	1.69	2.33
Cloudiness	1.04	1.00	1.14
Temperature	**2.76**	**1.94**	**3.90**
Δ Temperature	2.29	1.88	2.80
TWC	**7.12**	**5.59**	**9.01**
Δ TWC	1.10	1.00	1.35
CWC	2.51	2.02	3.09
Δ CWC	1.31	1.05	1.64
All precipitation	1.16	1.04	1.30
All pressure	3.89	3.22	4.70
All temperature	2.82	2.11	3.81
All wind	7.50	6.17	9.14
All weather	18.93	15.70	22.91
All variables	56.55	45.78	69.92

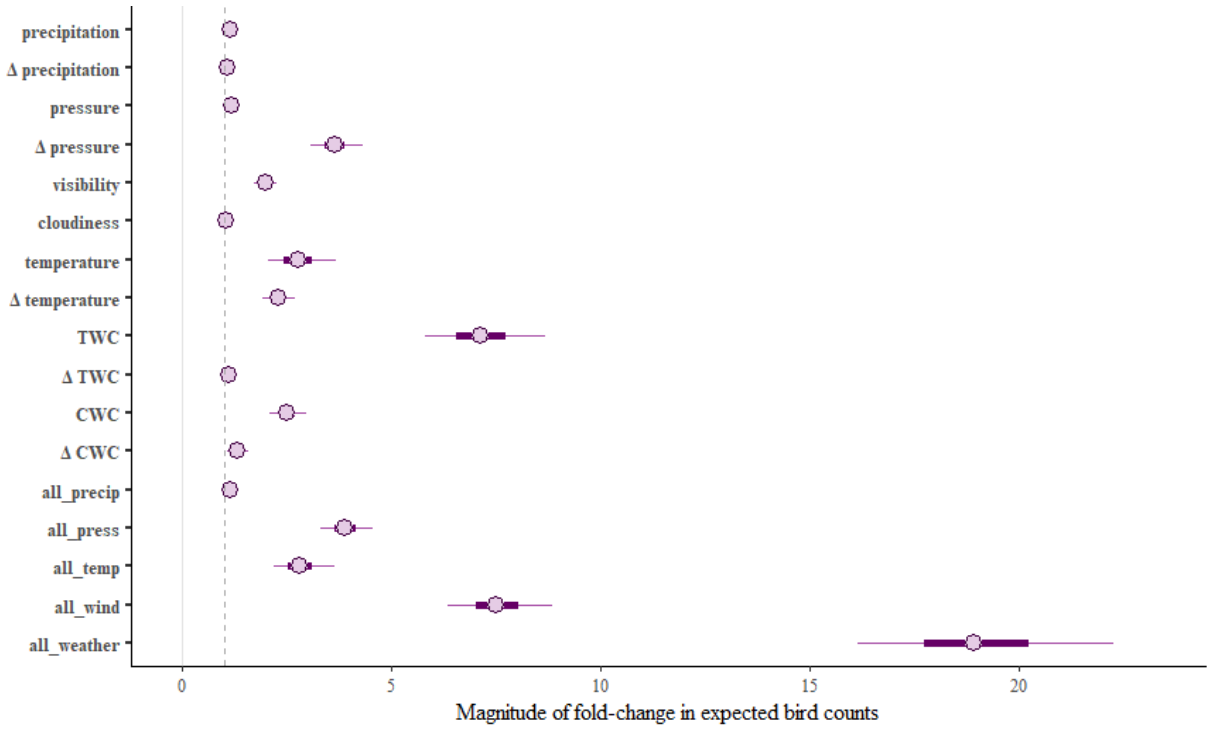

*Figure 9: Magnitude of fold-change in expected bird counts, per (set of) explanatory variable for **autumn**. Dashed x-intercept at 1 depicts no fold-change. Thick dark glue segments represent the 50% CIs, thin segments represent the 90% CI.*

Effects of explanatory variables on proportion of birds in risk height

MCMC intervals

Posterior uncertainty intervals of the explanatory variables used are portrayed in Figure 10a & b. Description of the figures can be found in the previous explanation of MCMC intervals for passerine migration intensity (p. 21).

During spring, variables exerting a positive influence on the probability of flying in the risk zone (i.e. between 25 – 180 m) according to the MCMC intervals are (listed from most to least influential) Δ pressure, CWC, precipitation, TWC, temperature and pressure (Fig. 10a). Δ temperature, year 2024, Δ precipitation and Δ TWC seem to negatively impact the probability of flying in risk altitudes. Variables with no apparent influence on probability of flying in risk altitudes during spring are visibility and cloudiness (Fig. 10a). For the autumn seasons, Δ temperature seems to be the most influential variable positively impacting the probability of flying at risk height, followed by CWC, temperature and year 2024 (Fig. 10b). While increasing

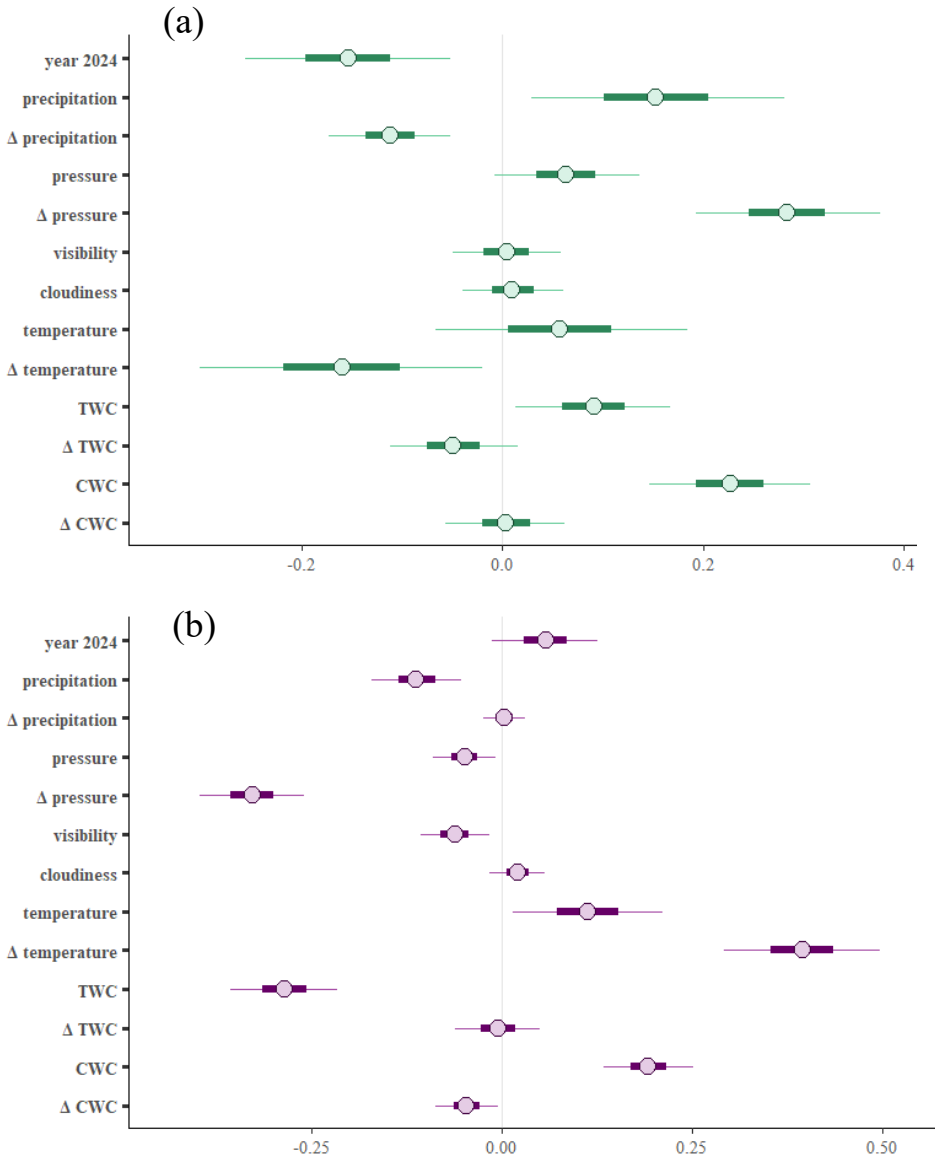

Figure 10: MCMC intervals for (a) spring and (b) autumn models with the probability of flying in the risk zone as the response variable. Posterior medians are depicted as light blue points. Thick dark blue segments indicate 50% CIs, thin segments indicate 90% CIs. Positive values on the x-axis correspond to positive associations with the low-flight probability and vice versa.

the number of passerines flying at low heights during spring, contrastingly Δ pressure, TWC, precipitation and pressure seem to reduce the probability of flying at low heights during autumn. Additionally, increased visibility and Δ CWC resulted in less passerines passing through the risk height. During autumn, parameters Δ precipitation, cloudiness and Δ TWC exerted no influence on the probability of flying low.

Altogether, cloudiness did not influence the flight height of passerines nor the general migration traffic rate during neither migratory season (Fig. 10a & b).

Conditional effects

Figure 11 shows the conditional effects of time of night ("ProportionOfNight") and Julian day ("year_date") on the probability of passerines flying at risk altitude during both migration periods. The effect of time of night followed a similar pattern during spring (Fig. 11a) and autumn (Fig. 11b), with only minor variation throughout the course of the night. During spring, the effect slightly increased towards the second half of the night and dropped minimally just before sunrise, without a distinct peak of the effect. In autumn, the effect initially declined after

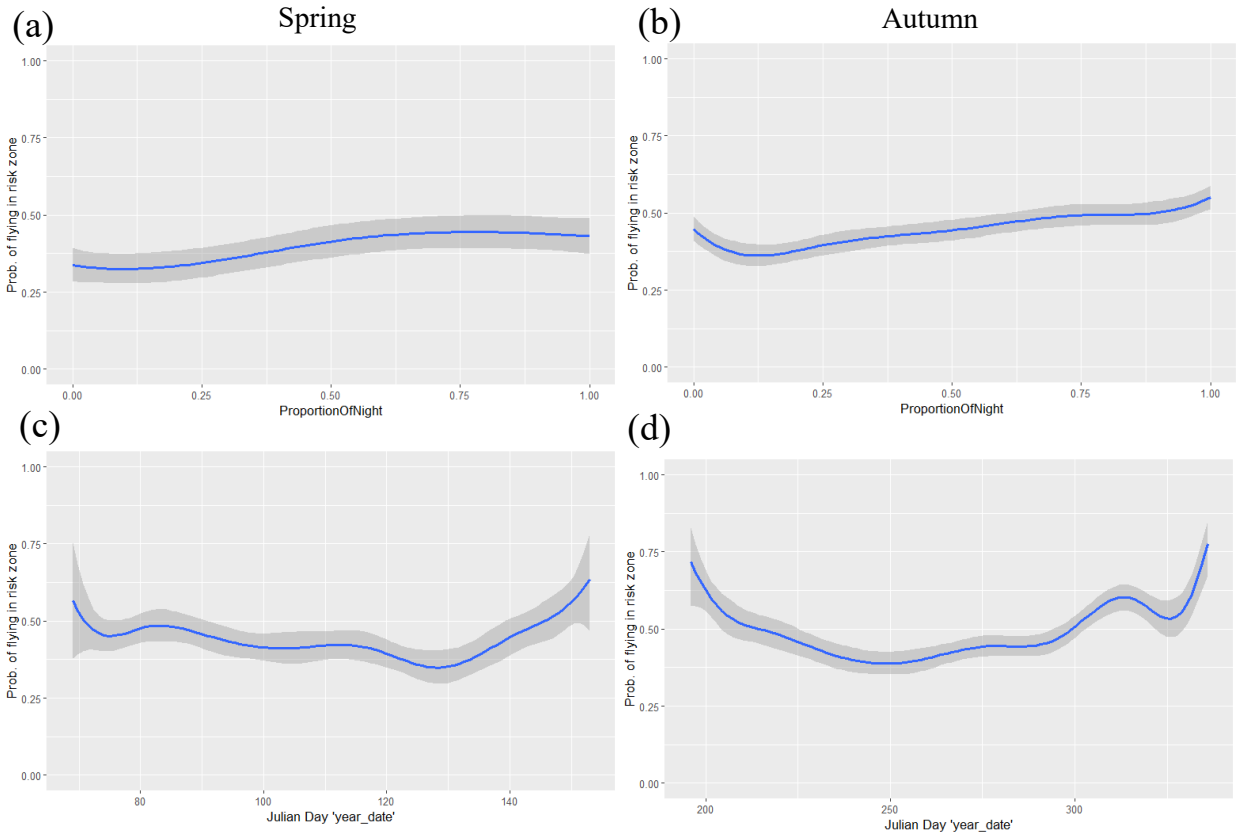

Figure 11: Conditional effect plots for the explanatory variables time of night (a, b) and Julian day (c, d) on the "probability of flying at risk heights" as the response variable. Left plots illustrate the spring seasons, the right plots depict autumn season. The y-axis illustrates the migration traffic rate (MTR, n/km/h) of passerines. The blue line represents the median of the predicted response, the grey ribbon illustrates the 95% prediction interval.

sunset but then gradually rose toward the end of the night. The main difference between the two seasons lies in the stronger effect observed shortly before sunrise in autumn compared to spring. The effect of date also showed a similar pattern during spring (Fig. 11c) and autumn (Fig. 11d), in that the effect was strongest at the edges of the migratory periods. For both seasons the effect was slightly increased towards sunrise rather than sunset. In spring, the effect of date on the probability of flying at risk height was least pronounced in the second half of the season, around day 128 (May 8th). In autumn the lowest effect of date on the probability of flying at risk altitudes was observed within the first half of the season, round day 250 (September 7th).

Magnitude fold change in expected bird counts

Figures 12 and 13 depict the magnitude of fold change in odds-ratios of the probability of flying in the risk zone, per (set of) explanatory weather variable. The same figures including temporal variables are attached in the appendix (Fig. S8). The figure set-up has been explained previously for the MTR models (p. 23). Corresponding means and 95% CIs referenced below are summarised in tables 7 and 8.

As for the previous set of models, all explanatory variables combined ("all_vars") had an overall greater impact on the fold change in the odds-ratios during autumn (10.41) than during spring (5.89) (Fig. 12 &13, Tab. 7 & 8). However, "all_vars" impacted the passerine MTR approximately five times more than it impacted the probability of flying in the risk zone (Tab. 7 & 8). Among the temporal explanatory variables, day of year ("year_date") explained the biggest differences in MTR throughout the seasons (spring: 2.53, autumn: 3.26), followed by the proportion of night ("night") for both seasons (spring: 1.73, autumn: 2.16).

Combined weather variables

As for the MTR models, combination of all weather variables ("all_weather", table 7 & 8) had the largest explanatory potential for the probability of flying in the risk zone among combined variables. Combined pressure variables had the second highest impact on low altitude flights for both seasons (spring: 2.64, autumn: 2.72), followed by combined wind (spring: 2.20, autumn: 2.56). Combined temperature variables almost impacted low altitude flight twice as much during autumn (2.43) than during spring (1.37). Combined precipitation however had a similar slight influence on low passerine flight for both seasons (spring: 1.41, autumn: 1.26).

Single weather variables

Among single weather variables, Δ pressure had the greatest (positive) impact on low passerine flight during spring (2.24), followed by CWC which induced a maximum of a 1.96-fold increase of the odd-ratios of flying low (Fig. 12, Tab. 7). Further explanatory variables positively increasing the odds-ratio during spring are TWC (1.37), precipitation (1.30), pressure (1.26),

temperature (1.17) and Δ CWC (1.11). However, seeing as the respective CI 2.5% values for those variables are all below 1.04, the potential impact those variables have on the response variable should be taken with caution (see Table 7). Curiously, all variables negatively impacting the odds-ratio are Δ variables: Δ precipitation (1.62), Δ temperature (1.33) and Δ TWC (1.21). Again, Δ temperature and Δ TWC should be carefully considered as impacting the response variable, as the CI 2.5% values are 1.03 and 1.01 respectively (Tab. 7).

Interestingly in autumn, Δ pressure (2.48) also seems to be the (single) explanatory variable exerting the greatest influence on the odds-ratio of flying in the risk zone (Fig. 13, Tab. 8). In contrast to spring however, an increase in Δ pressure results in decreasing number of low-flying migrants. TWC (2.23) had the second greatest (negative) repercussion on the odds-ratios. Increase in variables Δ CWC (1.26), precipitation (1.23), pressure (1.22) and visibility (1.22) also resulted in declining numbers of migrants in the risk zone (Tab. 8). Δ Temperature had the largest positive impact, inducing a maximum 2.01-fold change of the odd-ratios, followed by CWC (1.86) and temperature (1.40).

Cloudiness had no influence on the response variable during both migratory seasons. During spring, visibility also had negligible influence on the odds-ratios (Fig 12, Tab. 7). Additionally, Δ TWC exerted no influence on the odds-ratios in autumn (Fig. 13, Tab. 8).

*Table 7: Median and corresponding CI 2.5% and 97.5% values for the magnitude of fold change in odds-ratios of the probability of flying in the risk zone, during **spring**. Light orange background indicates negative association with low-altitude flight and refers to the MCMC interval results. Bold variables depict the three most influential (single) explanatory variables.*

Risk zone - Spring			
Variable	Median	CI 2.5%	CI 97.5%
Year	1.17	1.04	1.32
year_date	2.53	1.89	3.45
Night	1.73	1.47	2.05
Precipitation	1.30	1.03	1.68
Δ Precipitation	**1.62**	**1.18**	**2.21**
Pressure	1.26	1.01	1.77
Δ Pressure	**2.24**	**1.65**	**3.06**
Visibility	1.08	1.00	1.31
Cloudiness	1.07	1.00	1.25
Temperature	1.17	1.01	1.61
Δ Temperature	1.33	1.03	1.80
TWC	1.37	1.03	1.89
Δ TWC	1.21	1.01	1.62
CWC	**1.96**	**1.47**	**2.62**
Δ CWC	1.11	1.01	1.43
All precipitation	1.41	1.15	1.75
All pressure	2.64	1.93	3.61
All temperature	1.37	1.08	1.80
All wind	2.20	1.72	2.85
All weather	4.28	3.36	5.49
All variables	5.89	4.73	7.43

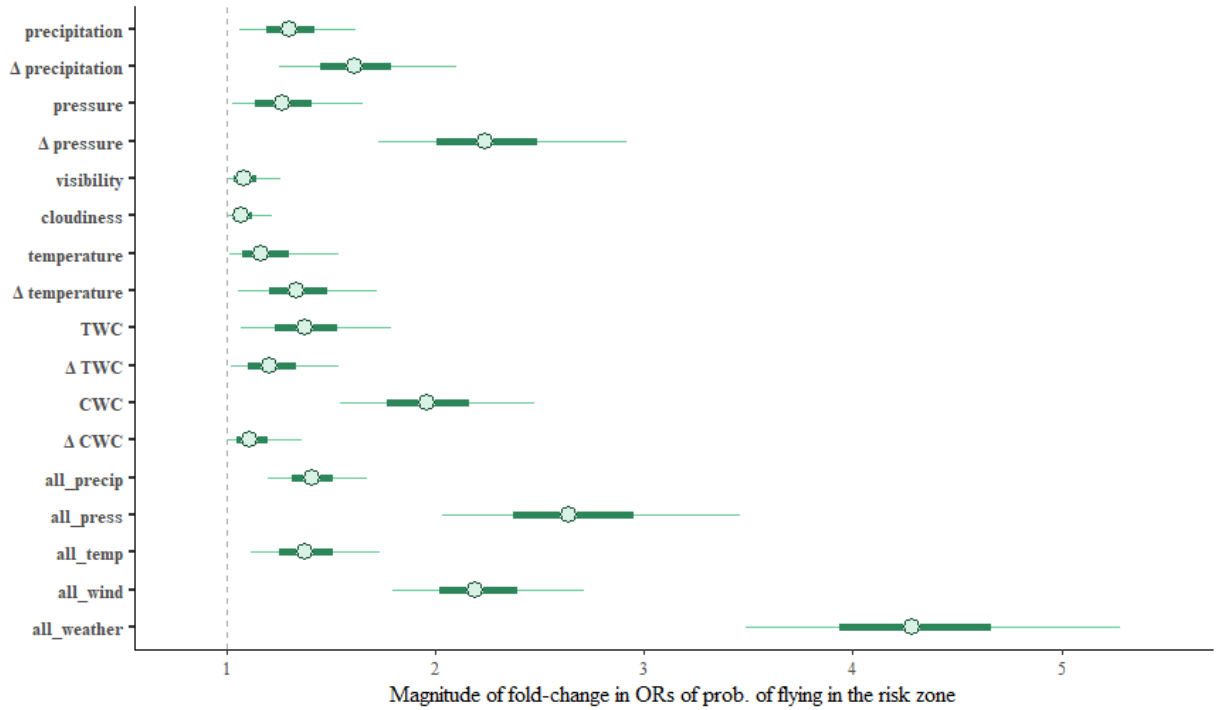

*Figure 12: Magnitude of fold-change in the odds-ratios (ORs) of the probability of flying in the risk zone, per (set of) explanatory variable for **spring**. Dashed x-intercept at 1 depicts no fold-change. Thick dark green segments represent the 50% CIs, thin segments represent the 90% CI.*

*Table 8: Median and corresponding CI 2.5% and 97.5% values for the magnitude of fold change in odds-ratios of the probability of flying in the risk zone, during **autumn**. Light orange background indicates negative association with low-altitude flight and refers to the MCMC interval results. Bold variables depict the three most influential (single) explanatory variables.*

Risk zone - Autumn			
Variable	Median	CI 2.5%	CI 97.5%
Year	1.06	1.00	1.15
year_date	3.26	2.46	4.40
Night	2.16	1.83	2.56
Precipitation	1.23	1.08	1.40
Δ Precipitation	1.06	1.00	1.23
Pressure	1.22	1.02	1.49
Δ Pressure	**2.48**	**1.97**	**3.10**
Visibility	1.22	1.03	1.45
Cloudiness	1.07	1.00	1.22
Temperature	1.40	1.03	2.00
Δ Temperature	**2.01**	**1.62**	**2.50**
TWC	**2.23**	**1.77**	**2.84**
Δ TWC	1.09	1.00	1.32
CWC	1.86	1.48	2.32
Δ CWC	1.26	1.02	1.59
All precipitation	1.26	1.12	1.43
All pressure	2.72	2.20	3.36
All temperature	2.43	1.91	3.16
All wind	2.56	2.09	3.13
All weather	7.07	5.84	8.58
All variables	10.41	8.69	12.52

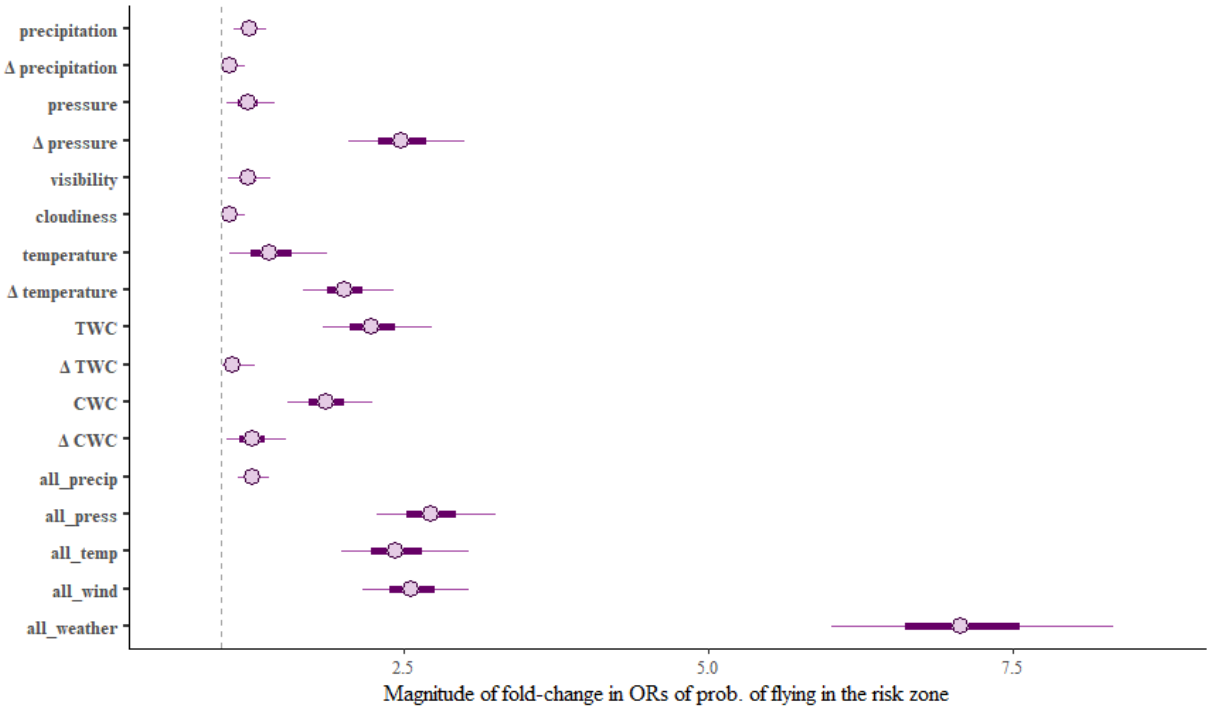

*Figure 13: Magnitude of fold-change in the odds-ratios (ORs) of the probability of flying in the risk zone, per (set of) explanatory variable for **autumn**. Dashed x-intercept at 1 depicts no fold-change. Thick dark purple segments represent the 50% CIs, thin segments represent the 90% CI.*

Discussion

The aim of this study was to determine the varying degrees of the influence of meteorological parameters on migration intensity of nocturnal passerines, with particular focus on environmental predictors for low-altitude flight where migrants are faced with increased collision risk with wind turbines. The foundation of this study was constituted by radar data collected over four migration seasons (spring and autumn of 2023 and 2024) near the North Sea coastline in Northern Germany, Husum.

MTR - Migration traffic rate (birds/h/km)

In line with our hypothesis and previous research, we demonstrate overall wind conditions to be the main meteorological predictor for nocturnal passerine migration intensity during both migratory seasons ("all wind", Tab. 5 & 6). Furthermore, we found temperature to increase MTR during both seasons, and Δ pressure, i.e. the change in barometric pressure compared to the previous day, to strongly influence migratory decisions during autumn.

Among the wind assistance parameters, increased tailwind was positively associated with MTR during both seasons, while increased sidewind generally declined numbers of birds aloft (Fig. 6). Overall, the impact of tailwind support on the migration intensity was higher during autumn than spring, with tailwind conditions (TWC) being the single most influential weather variable during fall migration. Winds in central Europe are generally less supportive for fall migration (e.g. Kemp et al. 2010, Nussbaumer et al. 2022; reflected in our wind data, see Fig. S1 – S3), as the prevailing west and southwest winds are experienced as head- or crosswinds by birds migrating south-westwards. Additionally, both frequency and speed of tailwinds over central Europe have increased during the last 40 years (Gordo 2007), further facilitating advantageous wind regimes during spring and unfavourable wind conditions during fall migration. Combination of these factors may partly explain why autumn migrants are more dependent on supportive tailwind conditions in mid-latitudes for the migratory progression than spring migrants, with passerines mainly exploiting nights with positive wind assistance during their fall journey. This observed correlation corroborates what was previously recorded for the relationship between wind and nocturnally migrating passerines (e.g. Richardson 1990, Bruderer & Liechti 1998, Åkesson & Hedenström 2000, Ernie et al. 2002, 2005, Liechti 2006, Alerstam 2011, Brust et al. 2019, Benjumea et al. 2024). Strong headwinds have been shown to weaken a migrant's propensity to take off (e.g. Werber & Sapir 2025) and can greatly affect the energetic cost of migration (Lack 1960, Liechti 2006, Gordo 2007), sometimes even promoting an accumulation of birds "outlasting" inclement weather ("Zugstau", coined by

Schüz 1952). Tailwind has further been proven to offer indispensable support to cover large geographic barriers (e.g. Kranstauber et al. 2015, 2023, Nilsson et al. 2019) such as the North Sea basin. Accordingly, our findings also support the "sit-and-wait" hypothesis of optimal migration (Liechti & Bruderer 1998, Kemp et al. 2010, Åkesson & Hedenström 2000), suggesting that the gain in flight distance under supportive wind outweighs the cost of waiting out less beneficial winds, particularly during autumn.

While tailwind was the main predictor for intense migration during fall, crosswind had the strongest (negative) effect among wind-assistance variables during spring migration (Fig. 8). Sidewinds not only increase energy expenditure during flight (e.g. Liechti 2006), but strong crosswinds may also cause migrants to be drifted off their intended route (Chapman et al. 2016), requiring birds to adjust their flight trajectories to maintain their intended migratory routes. Even though birds are incapable of predicting wind, migratory populations exhibit adaptive responses to wind drift, by either partially allowing drift, actively compensating for it (e.g. McLaren et al. 2012, Chapman et al. 2016, Horton et al. 2016b, Bruderer et al. 2024) or even increasing self-powered airspeed (Schekler et al. 2024). This behavioural flexibility of migratory animals is crucial in minimising energy expenditure and ensuring accurate navigation (e.g. Chapman et al. 2011, et al. 2016). As spring migration is often thought to be more time-sensitive due to the selective pressures related to breeding (e.g. Kokko 1999, Kappeler 2022), accurate navigation toward breeding grounds may be particularly crucial during spring to ensure the individual's fitness (Kokko 1999).

Interestingly, the relative change to the preceding night in the tested wind and precipitation parameters (Δ TWC, Δ CWC, Δ precipitation) was generally not of high biological relevance and had a much smaller impact on the MTR than the corresponding night-of-migration parameters, during both seasons. As anticipated, autumn migration was found to be additionally favoured by increase in Δ pressure, temperature and visibility and decreasing precipitation (Fig. 9), suggesting a selective preference for "favourable" weather conditions. Corroborating our findings, previous studies on passerines suggest that birds modify migratory behaviour in response to barometric pressure changes, particularly during autumn migration (Metcalfe et al. 2013, Chumra et al. 2020, Cooper et al. 2023). These results support the notion that birds prefer migrating under favourable weather conditions, as rising atmospheric pressure typically indicates the onset or approach of a high-pressure system. Such systems are characterised by subsiding air masses, which inhibit cloud formation and are typically associated with stable, fair-weather conditions.

During spring, air temperature and the change in air temperature had the strongest positive association with nocturnal migration activity of passerines (Fig. 6 & 8). Besides endogenous programs regulating birds annual cycles (e.g. Åkesson & Helm 2020, Kappeler 2022, p. 87), avifauna relies on exogenous cues for the initiation of the annual spring migration, and air temperature has been repeatedly shown to govern both, spring migration phenology (e.g. Richardson 1990, Gordo 2007, Kelly et al. 2016, Haest et al. 2018) and intensity (Richardson 1990, Kelly et al. 2016, Van Doren & Horton 2018, Gulson-Castillo et al. 2023). As competition for breeding opportunities favours early arrival at the breeding sites in spring (e.g. Kokko 1999, Nilsson et al. 2013), correlation between higher temperatures and increased migration activity during spring were anticipated.

Against our expectations, spring migration was reduced by increasing pressure and visibility. While this observation seems counterintuitive, it may be explained by a potential correlation between clear nights (i.e. increasing pressure and high visibility) and biotic or abiotic factors not considered in this study, that may negatively affect spring migration. Seeing as sidewind was found to strongly reduce spring migration activity in this study, clear nights might also be associated with intense winds perpendicular to the desired track direction, but more research has to be done to gain inside on the observed correlation.

Migration was found to be more evenly distributed throughout the night in spring, with maximum numbers observed in the middle of the night (Fig. 3a & 7a). On the other hand, fall migration shows a stronger peak earlier in the night and migration intensity declines in the second half of the night (Fig. 3b & 7b). These patterns are supported and discussed by previous research on passerines (e.g. Kranstauber et al. 2023, Werber & Sapir 2025). Spring migrants may have a higher incentive to speed up migration - due to the selective pressure related to breeding – and typically adopt a time-minimising approach on their annual journeys (e.g. Alerstam 2011). Consequently, during spring, passerines may use the entire night to progress northwards, leading to more evenly distributed migration fluxes throughout the night. On the contrary, more than twice the number of passerines migrated in autumn than in spring (Tab. 4, Fig. 2). As adult migrants are accompanied by their offspring, who undertake these long journeys for the first time, the inexperience of juvenile migrants may result in adjusted, energy-minimising behaviour, for example shorter flight periods (i.e. the decline of MTR in the second half of the night). What may further attribute to the observed differences in nocturnal migration patterns between spring and autumn may be the varying flight directions and geographic trajectories of passerines passing through the study area. In spring, most migrants passing through the study area travel in a north-easterly direction (~ 220° observed in our study area

but see Bradarić et al. 2020, 2024, Bruderer & Peter 2022), which often requires them to cross parts of the North Sea before reaching the mainland. Passerines typically initiate their nocturnal flight at dusk (e.g. Richardson 1990, Newton 2008) and therefore, it is likely that many individuals initiate their nocturnal flight from the Dutch coastline or the Frisian Islands, necessitating a longer overwater flight segment before reaching the region around Husum. Consequently, their arrival in the study area tends to occur later in the night. In contrast, during autumn migration, birds tend to fly in a more south-south-westerly direction (~30°; flight direction over Northern Europe: Nilsson et al. 2019, Bradarić et al. 2020, 2024, Bruderer & Peter 2022), following largely inland routes. In line with Kranstauber et al. (2023) reasoning, birds may stop immediately before crossing geographic barriers, such as the North Sea, to recover and avoid daytime crossing. As a result, a pronounced migration peak occurs early in the following suitable night (Fig. 7b), when the previously gathered birds initiate the crossing simultaneously. However, it should be noted that the observed local flight direction does not necessarily reflect the overall "true" track direction of the migration (e.g. Åkesson & Hedenström 2000). This is particularly relevant for our study area, as coastal areas tend to concentrate higher numbers of migrants (e.g. Horton et al. 2016a), likely because many species use topographical landmarks such as coastlines as orientational cues on their journey (Alerstam & Pettersson 1977, Åkesson 1993, Bruderer & Liechti 1998, Horton et al. 2016b, Brust et al. 2019, Kranstauber et al. 2023). Moreover, migratory species with different life-history characteristics have been observed to show different phenological and nocturnal patterns during migration (e.g. Benjumea et al. 2024). Disentangling species-specific effects of time of night and weather dependency should provide further clarification regarding the characteristics of bird migration in our study area.

Our findings further revealed that date had a stronger influence on nocturnal migration intensity than weather variables (single or combined, Tab. 5 & 6) in both seasons, with the effect being more pronounced during autumn. The relatively synchronised timing of spring migrants (e.g. Newton 2008, Alerstam 2011) may limit the explanatory power of date alone. In contrast the autumn migration period is typically more prolonged and less synchronised (e.g. Newton 2008, Alerstam 2011), involving not only experienced adults but also large numbers of juveniles migrating for the first time. Overall, the results suggest strong temporal variations between migratory seasons, with the more extended nature of autumn migration allowing date to emerge as an even stronger predictor of migratory activity.

FHD - Flight height distribution (25 – 1025 m)

What factors influence flight at risk height (< 180 m)?

Contrary to our expectations, no relevant differences in mean flight altitude were observed between the migratory seasons. Due to the vertical limitation of the radar used, this study focussed on altitudes between 25 – 1025 m above ground level (a.g.l.). Although the mean migration altitude of nocturnal passerines was approximately 300 m, their highest densities were consistently observed within the lowest two height bins (i.e. 75–175 m), as revealed by the full vertical distribution (Fig. 4). Numbers of migrants gradually decreased with inclining heights throughout all seasons studied (Fig. 4) and about a third of migrants travelled within the "risk altitude" range. Previous studies in the temperate zone revealed similar patterns of most intense migration activity at low levels and a pronounced decrease with height (e.g. Eastwood 1967, Bellrose 1971, Blokpoel & Burton 1975, Hüppop et al. 2006, Fijn et al. 2015). Nocturnal migrants have further been shown to prefer travelling through lower altitudes at coastal sites compared to inland sites (Horton et al. 2016a). Corroborating our findings and reviewing 40 years of radar migration studies regarding the vertical distribution of migratory birds, Bruderer et al. (2018) summarised that up to 30 % of nocturnal migration occurs within the lowest 200 m interval a.g.l., 50 % below 700 m and the 90% quantile reaching heights between 1400 and 2100 m. The remaining 10% of migrants are usually scattered up to about 4000 m above sea level (asl).

Several empirical studies have reached the conclusion that wind plays a fundamental role in the flight heights selected by nocturnally migrating birds, with migrants mostly selecting flight altitudes with maximum flow assistance, consequently minimising travel time and energy expenditure (e.g. Dokter et al. 2011, Schmaljohann et al. 2009, Kemp et al. 2013, Horton et al. 2016a, Bradarić et al. 2024, but see Bruderer et al. 2024). While wind assistance parameters did emerge as significant predictors of low-altitude flight in our study, they only exhibited the second strongest effect among weather variables across both seasons ("all wind" in Tab. 7 & 8). As anticipated, our results suggest that stronger crosswinds were associated with an increased likelihood of passerines flying within the risk-altitude range, but the effect was more pronounced in spring (Fig. 10, 12 & 13). Combination of the overall preference for lower altitudes observed in this study (mean height below 315 m across all seasons, Fig. 3) and a higher proportion of low-altitude migration under negative wind assistance, indicates that passerines may fly close to the ground to reduce the effect of overall hostile wind conditions (e.g. Alerstam 2011, Horton et al. 2016a), as wind speeds typically increase with altitude

(Pennycuick 2008, Bruderer et al. 2018). Moreover, maintaining a low flight altitude provides the opportunity to land quickly should environmental conditions worsen (Bruderer et al. 2018).

Kemp et al. (2013) studied the vertical distribution of nocturnally migrating avifauna in the Netherlands and found that improved tailwind increased the probability of elevating the flight heights, however birds depicted a general preference for low-altitude flight (~ 0.4 km) and concentrated around the lowest altitudes with acceptable wind conditions. While tailwinds facilitated migratory departure in both seasons (see MTR), its effect on flight altitude selection appeared to differ between the seasons. In autumn, favourable tailwinds were associated with a drastic decrease in the proportion of birds flying within the risk zone, suggesting that migrants ascend into higher altitudes when wind support allows for more efficient, energy-saving flight. This finding is consistent with the abovementioned notion that birds adopt an energy-minimising strategy during autumn migration (e.g. Newton 2008), likely due to the birds being accompanied by their inexperienced offspring as well as the generally less supportive wind patterns for southwest-oriented routes in Central Europe (Fig. S1 – S3, Kemp et al. 2010, Nussbaumer et al. 2022). In summary, the strong dependence on supportive winds during autumn migration was reflected in both, the significant increase in overall migration intensity (Fig. 6) and the decrease in low-altitude flights under tailwind conditions (Fig. 10).

Conversely, during spring, increased tailwind components were slightly positively associated with a higher proportion of migrants flying within the risk altitude range. While this might appear counterintuitive, it likely reflects a combination of seasonal and atmospheric dynamics. Tailwind typically acts as a strong departure cue, often prompting birds to initiate migration during the early hours of the night (e.g. Richardson 1990, Newton 2008), when the atmosphere is still thermally stable and vertically stratified (Pennycuick 2008). Under such conditions, vertical mixing is limited, and birds may remain within lower atmospheric layers, below temperature inversions or cloud bases. Additionally, maintaining lower altitudes may allow migrants to better optimize wind assistance or to retain visual contact with coastal landscape features that support orientation (e.g. Bruderer et al. 2018). Moreover, since wind direction and speed can substantially change with altitude (Pennycuick 2008), it is plausible that the tailwind component used in our analysis - measured at ~ 28 m above ground level (Tab. 1 & 2) - was only favourable for migration within these lower air layers. This vertical variability in wind conditions could therefore help explain the unexpectedly observed association between stronger tailwinds and increased low-altitude flight activity during spring. However, this association between supportive winds and reduced flight altitudes in spring was only marginally

pronounced (see Tab. 7), and its underlying mechanisms remain unclear. Further research would be valuable to further elucidate this pattern.

Curiously, among the meteorological variables Δ pressure exerted the strongest effect on the probability of flying at risk height, again with opposing effects between the two migratory seasons (Fig. 12 & 13). In line with our hypothesis, during autumn migration, rising Δ pressure resulted in a preference for higher flight altitudes of passerines. As described above, increasing atmospheric pressure is typically associated with the development of high-pressure systems, which leads to subsiding air masses and mostly stable weather conditions – conditions that are generally favourable for bird migration. Under such stable conditions, increasing flight altitudes may allow migrants to exploit more consistent and faster wind currents, while simultaneously benefiting from reduced turbulence (Pennycuick 2008). Correlational evidence suggests that a wide range of taxa - including insects (Pellegrino et al. 2013), mammals (Turbill 2008) and birds (Chmura et al. 2020, passerines: Cooper et al. 2023) - alter their behaviour in response to atmospheric pressure changes. Moreover, manipulative experiments on captive sparrows (*Zonotrichia* spp.) indicate that individuals not only respond to the weather changes associated with varying barometric pressure but are also capable of directly sensing pressure shifts and adjusting their behaviour accordingly (Breuner et al. 2013, Metcalfe et al. 2013). Consequently, when detecting rising barometric pressure during autumn, migratory birds may respond by increasing flight altitude to optimize their speed and energy efficiency, taking advantage of higher wind speeds commonly found at greater heights (Alerstam 2011, Horton et al. 2016a). Flying at higher altitudes can reduce frictional resistance due to lower air density (Pennycuick 2008), allowing birds to cover greater distances with the same amount of energy - a strategy that may be especially important for inexperienced juvenile migrants. While we observed that rising Δ pressure was associated with increased overall migratory activity in autumn (MTR, Fig. 6), it also corresponded with a reduced probability of low-altitude flights. This suggests that under conditions of increasing barometric pressure, birds not only initiate migration more readily but also ascend to higher altitudes and are therefore exposed to a lower risk of collision with wind turbines during this period.

In contrast to autumn, our findings for spring migration revealed that an increase in barometric pressure relative to the previous night led to a higher proportion of birds flying within the risk zone. At first glance this pattern may seem counterintuitive. However, it can likely be attributed to the atmospheric conditions that typically accompany high-pressure systems. As air descends within these systems, it heats up, frequently resulting in the formation of temperature inversions (Pennycuick 2008). These inversions can suppress vertical mixing and produce stable

atmospheric layers, often accompanied by a low cloud base that may act as a physical and visual barrier for ascending birds. The study area is frequently exposed to moist maritime air masses that promote persistent cloud formation throughout the year (see Tab. 3). This is supported by our meteorological dataset, which shows an average nightly cloud cover of approximately 6 oktas during both migration periods. The combination of thermally induced inversions and substantial cloud likely encourages migrants in spring to remain in lower air layers, beneath these stable atmospheric boundaries. Flying below the cloud base may facilitate visual orientation along coastal topography, a strategy well documented by previous studies (Able 1970, Alerstam & Pettersson 1977, Åkesson & Sandberg 1999, Horton et al. 2016b). Additionally, this behaviour may be reinforced by the previously discussed strong seasonal time constraints experienced by spring migrants, who are under pressure to reach the breeding grounds early to maximize their reproductive success (e.g. Kokko 1999). Under such conditions, birds during spring may prioritize timely departure and rapid route progression over energetically optimal flight altitudes, which may result in increased use of low-altitude airspace. In combination with the results regarding tailwind and increased low-altitude flight, it is likely that favourable wind assistance during spring may have predominantly occurred within lower atmospheric layers, thereby reinforcing the tendency of migrants to remain at low altitudes even under increasing barometric pressure conditions. Altogether, these findings reflect the seasonal trade-offs that migratory birds must navigate when selecting flight altitudes. Thus, in spring - in strong contrast to the patterns observed during autumn migration - the interaction between atmospheric structure in relation to elevated barometric pressure and time constraints appears to outweigh the benefits of higher-altitude flight.

Given that rising barometric pressure is typically accompanied by rising temperatures, one would expect similar responses to both explanatory variables. However, our results reveal contrasting effects of Δ pressure and Δ temperature on flight altitude selection (Fig. 10, Tab. 7 & 8). Previous research has shown that birds flying over land at mid-latitudes tend to avoid altitudes with colder air layers (Kemp et al. 2013). Early radar studies over the North Sea similarly suggest a “ceiling effect” of temperature, with birds ascending to heights just below the freezing level (Eastwood 1967, p. 222). In line with this, we observed a weak tendency of spring migrants to avoid colder air layers prevalent higher up, but elevating their flight height with increasing Δ temperature (Tab. 7). In contrast, during autumn, warmer temperatures relative to the previous night were associated with a markedly higher number of migrants flying lower, within the risk-altitude range. This positive correlation may reflect an increased migratory readiness observed under warm thermal conditions (as previously discussed in the

context of the MTR), without a simultaneous improvement in vertical flight conditions. Overall, it is hard to say whether the birds were reacting to pressure or temperature as such or to associated weather variables not captured in our data or analysis, particularly as the results for Δ temperature and Δ barometric air pressure showed contrasting effects. More study of apparent pressure and temperature responses in regard to flight height choice in coastal areas is needed before firm conclusions on this point can be drawn.

Against our expectation, visibility had no influence on flight altitude choice of spring migrants, but did lead autumn migrants to elevate their flight heights, potentially making use of unobscured flight with more favourable wind conditions. Conflicting results for precipitation during spring migration were observed: while increasing Δ precipitation induced low-altitude flight, precipitation alone was a strong predictor of elevated flight height (Tab. 7). Similarly, more birds flew at risk heights under rainy conditions in spring, while the opposite was true for fall migration.

Nevertheless, it should be mentioned that delta variables used in this study should be carefully considered, as they were calculated from hourly data and thus do not accurately reflect comparison of weather conditions between two nights, but rather between two hours, 24 hours apart. As atmospheric conditions such as precipitation or wind parameters are prone to rapidly shift at coastal sites, delta variables depicting changes in weather conditions on an hourly basis should be handled with caution. Variables used that typically do not show great hourly fluctuations are barometric pressure and air temperature. Using large-scale weather data for the calculation of delta variables as well as averaged nightly values - ideally originating from the migrants' departure sites - would likely provide clearer insights into the relationship between changes in weather variables and flight altitude selection during migration (e.g. Richardson 1990). Due to the spatiotemporal variations of meteorological parameters, the "local" weather likely correlates more if the wintering or stopover site is close to the study area, rather than further away.

Moreover, contrary to expectations and previous studies (e.g. Eastwood 1967, p. 217), cloud cover showed no biologically relevant effect as an explanatory variable, on either migratory intensity or flight altitude for neither migratory season. This may reflect the flexibility of nocturnally migrating passerines, which are capable of switching between multiple orientation mechanisms when celestial cues are obscured (Kappeler 2022, p. 80 - 83). Furthermore, we found flight decisions to be predominantly influenced by wind conditions, temperature and pressure changes, whereas cloudiness may play a more indirect or secondary role. Another

possible explanation stems from the fact that the variable used to quantify cloud cover in this study did not capture ecologically relevant aspects such as cloud base height or thickness of the cloud layer. These aspects may play a critical role in birds' decisions to initiate flight and in determining their chosen flight altitude, as nocturnal migrants have been found to elevate their flight height above cloud layers or even fly within clouds (e.g. Eastwood 1967, p. 217). Finally, as our study area is located in close vicinity to the North Sea coast, where overall average cloud coverage is typically higher compared to inland locations (also reflected in the meteorological dataset used, Tab. 3), limited seasonal variance in cloud cover may have further obscured potential effects.

Temporal variation of flight altitude

Among temporal variables, Julian day (i.e. day of year) had the largest effect on the likelihood of reducing flight altitude in both seasons, depicting similar patterns (Fig. 11 c & d) but exerting a stronger effect during fall (Tab. 7 & 8). The effect of date was most pronounced at the beginning and end of both migration seasons, where the probability to fly at risk height was increased. This pattern may be best explained by movements of local (non-migratory) birds, which likely account for a substantial proportion of overall bird activity during the seasonal edges. However, the effect of local birds might not be the only reason for the observed pattern. Bradarić et al. (2024) studied flight altitudes in the same region but offshore and observed distinct seasonal patterns of low-altitude migration, with day of year also showing a stronger influence on autumn migrants. In line with their discussion, seasonal variation in low-altitude migration may likely reflect differences in weather-driven migration phenology between short- and long-distance nocturnal migrants within the region. Temporal variations in the choice of flight altitude may thus be explained by the species composition of migrants travelling through Husum. Previous studies reveal that short-distance migrants in the regions tend to rely heavily on wind assistance during both spring and autumn, whereas long-distance migrants are more influenced by temperature and precipitation patterns in autumn (Haest et al. 2018, et al. 2019). The species composition of birds within the order of Passeriformes (Linnaeus 1758) migrating through central Europe is diverse, with typical long-distance migrants being the Grasshopper Warbler (*Locustella naevia*) or the Nightingale (*Luscinia megarhynchos*) (Berthold et al. 1998), whereas the Blackbird (*Turdus merula*) or the Eurasian Bullbinch (*Pyrrhula pyrrhula*) are among the short-distance migrants (Berthold et al. 1998). Variation in weather conditions encountered at differing areas of departure may thus influence altitude selection by shaping the atmospheric environment experienced during the migratory flight.

The effect of time of night did not greatly differ between seasons and showed almost constant patterns throughout the night (Fig. 11). In both seasons, however, the effect exhibited a slight increase during the second half of the night, which may reflect birds landing shortly before sunrise (e.g. Newton 2008). Nevertheless, this would also imply a corresponding peak earlier in the night as the birds initiate their nocturnal flight, which was not observed. Consequently, the effect of night may also be inhibited by movement of local birds, but no firm conclusions can be drawn.

In which season are migrants facing a higher collision risk?

Interestingly, a greater number of weather variables were positively associated with low-altitude flight during spring compared to autumn (Tab. 7 & 8). This suggests that spring migrants are more prone to flying in the collision-risk altitude range under a wide array of meteorological conditions. This pattern likely reflects the strong seasonal selective pressure associated with early arrival at breeding grounds during spring, prompting birds to initiate migration even under suboptimal vertical conditions. In contrast, the autumn migration appears to be more selective, with less weather parameters encouraging low-altitude flight and a higher occurrence of conditions inhibiting flight in the risk zone. While CWC led to increased probability of low-altitude flight in both seasons, crosswinds generally decreased number of migrants aloft in both seasons. Thus, we found CWC does not result in elevated collision risk regarding absolute numbers of migrants.

Moreover, when comparing variables that positively influenced both, migration intensity and the likelihood of flying at risk altitudes, temperature and TWC were positively associated with both response variables in spring. During autumn, only temperature showed a consistent positive effect on both, higher overall migration intensity and an increased occurrence of low-altitude flights. Therefore, according to our results the absolute number of migrants in the risk zone is highest under warm temperatures during both seasons and further elevated in spring under tailwind conditions.

Limitations and future direction

Some limitations should be considered when interpreting the results of this study. Due to the scope constraints of this master thesis, crosswind components were analysed as absolute values, without accounting for the specific direction of lateral wind. However, recent findings highlight the importance of crosswind direction in migratory decision-making: for instance, Werber and Sapir (2025) demonstrated that birds actively avoid drifting toward ecological barriers, such as the Mediterranean Sea, by landing when winds blow in unfavourable directions and

preferentially depart when winds are oriented away from such obstacles. Similar patterns have been reported in other studies (e.g. Horton et al. 2016b), emphasising the role of the direction of sidewind encountered in barrier-crossing strategies. Therefore, incorporating directional crosswind components may yield more insights into migratory behaviour and flight height choice in our study area.

Another key limitation - shared by comparable radar-based migration studies - is the underlying assumption that migratory birds exhibit consistent decision-making regarding flight altitude, regardless of temporal or spatial context. Since we assessed wind assistance based on an average migration direction per season for all passerine species, the effect of tail- and crosswind on migration intensity and choice of flight altitude may be potentially reduced in our findings. This generalisation overlooks inter- and intraspecific behavioural variability and may obscure species-specific or individual responses to tail- and crosswind conditions. Incorporating species-specific or individual track directions would likely enhance our understanding of the effects of wind support on flight altitude selection in nocturnally migrating passerines. Lastly, wind data in this study were obtained from a single near-surface level (~ 28 m a.s.l., see Tab. 1 & 2), rather than from vertically resolved atmospheric profiles. As a result, potential variation in wind conditions at flight-relevant altitudes could not be captured, further limiting the precision of wind effect estimates.

Conclusions

In this study, several variables were found to exert opposing effects on migratory behaviour between spring and autumn, reflecting the different ecological pressures shaping migration in each season. We found weather conditions to play a critical role in fine-tuning both departure decisions and flight altitudes of nocturnally migrating passerines. Our findings regarding the MTR of passerines are consistent with previous research, and although the isolated effect of precipitation on MTR appears minimal, the combined influence of multiple weather variables suggests a selective preference for “favourable” weather conditions. Passerines at coastal stopover sites, as discussed particularly along the German North Sea coast, may extend their stay until such optimal weather conditions arise. Further emphasising the importance of wind conditions in shaping migratory strategies, birds generally preferred strong tailwinds and avoided headwinds. With respect to flight altitude, our study provides the first evidence from this region that changes in atmospheric pressure significantly influence the probability of flying within altitudes associated with increased collision risk from wind turbines (25 - 180 m), with contrasting effects across seasons. These findings suggest that passerines can flexibly adjust their behaviour in response to dynamic atmospheric conditions such as barometric pressure and

wind. Overall, this work offers a detailed perspective on migratory decision-making at a mid-latitude coastal site. Understanding these behavioural adaptations are particularly valuable for informing more effective and targeted wind turbine curtailment strategies, helping to balance the need for renewable energy development with the protection of (declining, e.g. Both et al. 2006) migratory bird populations.

Acknowledgements

First and foremost, I would like to express my sincere gratitude to BioConsult SH GmbH & Co. KG, where I had the opportunity to conduct this master's thesis. I would also like to thank the BWO (Bundesverband Windenergie Offshore e.V) for providing access to the radar data that formed the foundation of this work. I am deeply grateful to Dr. Jannis Liedtke, my supervisor at BioConsult SH, for his continuous guidance and support throughout the entire process. His dedication and the time he generously invested in our discussions were invaluable to the development of this thesis. A heartfelt thank you goes to Matthieu Bruneaux, who patiently helped me understand and apply statistical concepts that were entirely new to me. Without his tireless explanations and support, I would probably still be working on the data analysis. I would also like to thank Prof. Dr. Jutta Schneider for kindly agreeing to supervise this thesis from the university's side, and for taking the time to review and provide valuable feedback on the final version before submission. And finally, a heartfelt thank you to my mom for lovingly proofreading the final version of this thesis and supporting me with her keen eye for grammar.

List of references

4C Offshore: Global Offshore Renewable Map. https://map.4coffshore.com/offshorewind/ (last viewed: 01.06.2025).

Able, K. P. (1970). A radar study of the altitude of nocturnal passerine migration. *Bird-banding*, *41*(4), 282-290.

Åkesson, S. (1993). Coastal migration and wind drift compensation in nocturnal passerine migrants. *Ornis Scandinavica*, 87-94.

Åkesson, S., & Sandberg, R. (1999). Ecological barriers and the flexible orientation system of migrating birds. In *Proc. 22 Int. Ornithol. Congr., Durban* (pp. 1005-1016).

Åkesson, S., & Hedenström, A. (2000). Wind selectivity of migratory flight departures in birds. *Behavioral Ecology and Sociobiology*, *47*, 140-144.

Åkesson, S., & Helm, B. (2020). Endogenous programs and flexibility in bird migration. *Frontiers in Ecology and Evolution*, *8*, 78.

Alberta, T., & Pettersson, S. G. (1977). Why do migrating birds fly along coastlines? *Journal of Theoretical Biology*, *65*(4), 699-712.

Alerstam, T. (2011). Optimal bird migration revisited. *Journal of Ornithology*, *152*(Suppl 1), 5-23.

Alerstam, T., & Lindström, Å. (1990). Optimal bird migration: the relative importance of time, energy, and safety. In *Bird migration: physiology and ecophysiology* (pp. 331-351). Berlin, Heidelberg: Springer Berlin Heidelberg.

Allison, T. D., Diffendorfer, J. E., Baerwald, E. F., Beston, J. A., Drake, D., Hale, A. M., ... & Winder, V. L. (2019). Impacts to wildlife of wind energy siting and operation in the United States. *Issues in Ecology*, *21*(1), 2-18.

Beck, H. E., McVicar, T. R., Vergopolan, N., Berg, A., Lutsko, N. J., Dufour, A., ... & Miralles, D. G. (2023). High-resolution (1 km) Köppen-Geiger maps for 1901–2099 based on constrained CMIP6 projections. *Scientific data*, *10*(1), 724.

Bellrose, F. C. (1971). The distribution of nocturnal migrants in the air space. *The Auk*, *88*(2), 397-424.

Benjumea, R., Astrain, C., Istúriz, A., Oria, P., Ibarrola, I., & del Mar Delgado, M. (2024). Weather conditions at different spatial and temporal scales influence avian post breeding migration patterns on route. *Journal of Zoology*, *323*(4), 305-316.

Berthold, P., Fiedler, W., Schlenker, R., & Querner, U. (1998). 25-year study of the population development of Central European songbirds: a general decline, most evident in long-distance migrants. *Naturwissenschaften*, *85*, 350-353.

BirdLife International (2010): The flyways concept can help coordinate global efforts to conserve migratory birds. https://datazone.birdlife.org/articles/the-flyways-concept-can-help-coordinate-global-efforts-to-conserve-migratory-birds (Last viewed: 01.06.2025).

Blokpoel, H., & Burton, J. (1975). Weather and height of nocturnal migration in eastcentral Alberta: a radar study. *Bird-Banding*, *46*(4), 311-328.

Both, C., Bouwhuis, S., Lessells, C. M., & Visser, M. E. (2006). Climate change and population declines in a long-distance migratory bird. *Nature*, *441*(7089), 81-83.

Bradarić, M., Bouten, W., Fijn, R. C., Krijgsveld, K. L., & Shamoun-Baranes, J. (2020).

Winds at departure shape seasonal patterns of nocturnal bird migration over the North Sea. *Journal of Avian Biology*, *51*(10).

Bradarić, M., Kranstauber, B., Bouten, W., van Gasteren, H., & Baranes, J. S. (2024). Drivers of flight altitude during nocturnal bird migration over the North Sea and implications for offshore wind energy. *Conservation Science and Practice*, *6*(4), e13114.

Breuner, C. W., Sprague, R. S., Patterson, S. H., & Woods, H. A. (2013). Environment, behavior and physiology: do birds use barometric pressure to predict storms?. *Journal of Experimental Biology*, *216*(11), 1982-1990.

Brown, R. H. J. (1963). The flight of birds. Biological Reviews, 38(4), 460-489.

Bruderer, B., & Liechti, F. (1998). Flight behaviour of nocturnally migrating birds in coastal areas: crossing or coasting. *Journal of Avian Biology*, 499-507.

Bruderer, B., Korner, P., & Peter, D. (2024). In-flight reactions of nocturnally migrating birds to winds. *Journal of Ornithology*, 1-18.

Bruderer, B., Peter, D., & Korner-Nievergelt, F. (2018). Vertical distribution of bird migration between the Baltic Sea and the Sahara. *Journal of Ornithology*, *159*(2), 315-336.

Bruderer, B., & Peter, D. (2022). Topography and wind moulding directions of autumn migration between Europe and the West African savannas. *Journal of Ornithology*, *163*(2), 357-371.

Brust, V., Michalik, B., & Hüppop, O. (2019). To cross or not to cross–thrushes at the German North Sea coast adapt flight and routing to wind conditions in autumn. *Movement ecology*, *7*, 1-10.

Bürkner, P. C. (2017). brms: An R package for Bayesian multilevel models using Stan. *Journal of statistical software*, *80*, 1-28.

Bürkner, P., Gabry, J., Kay, M., Vehtari, A. (2024). posterior: Tools for Working with Posterior Distributions. R package version 1.6.0, https://mc-stan.org/posterior/.

Chapman, J. W., Klaassen, R. H., Drake, V. A., Fossette, S., Hays, G. C., Metcalfe, J. D., ... & Alerstam, T. (2011). Animal orientation strategies for movement in flows. *Current Biology*, *21*(20), R861-R870.

Chapman, J. W., Nilsson, C., Lim, K. S., Bäckman, J., Reynolds, D. R., & Alerstam, T. (2016). Adaptive strategies in nocturnally migrating insects and songbirds: contrasting responses to wind. *Journal of Animal Ecology*, *85*(1), 115-124.

ChatGPT. https://chatgpt.com/ (last viewed: 22.05.2025).

Chmura, H. E., Krause, J. S., Pérez, J. H., Ramenofsky, M., & Wingfield, J. C. (2020). Autumn migratory departure is influenced by reproductive timing and weather in an Arctic passerine. *Journal of Ornithology*, *161*(3), 779-791.

Cooper, N. W., Dossman, B. C., Berrigan, L. E., Brown, J. M., Cormier, D. A., Bégin-Marchand, C., ... & Marra, P. P. (2023). Atmospheric pressure predicts probability of departure for migratory songbirds. *Movement Ecology*, *11*(1), 23.

Deutscher Wetterdienst: Klimadaten Deutschland (stündlich). https://opendata.dwd.de/climate_environment/CDC/observations_germany/climate/hourly/ (last viewed: 25.04.2025).

Dokter, A. M., Liechti, F., Stark, H., Delobbe, L., Tabary, P., & Holleman, I. (2011). Bird migration flight altitudes studied by a network of operational weather radars. *Journal of the Royal Society Interface*, *8*(54), 30-43.

Dokter, A. M., Shamoun-Baranes, J., Kemp, M. U., Tijm, S., & Holleman, I. (2013). High altitude bird migration at temperate latitudes: a synoptic perspective on wind assistance. *PloS one*, *8*(1), e52300.

Drewitt, A. L., & Langston, R. H. (2006). Assessing the impacts of wind farms on birds. *Ibis*, *148*, 29-42.

Eastwood, E. (1967). Radar ornithology. Methuen & Co Ltd., London. https://archive.org/details/radarornithology0000sire

Erickson, W. P., Wolfe, M. M., Bay, K. J., Johnson, D. H., & Gehring, J. L. (2014). A comprehensive analysis of small-passerine fatalities from collision with turbines at wind energy facilities. *PloS one*, *9*(9), e107491.

Erni, B., Liechti, F., & Bruderer, B. (2005). The role of wind in passerine autumn migration between Europe and Africa. *Behavioral Ecology*, *16*(4), 732-740.

Erni, B., Liechti, F., Underhill, L. G., & Bruderer, B. (2002). Wind and rain govern the intensity of nocturnal bird migration in Central Europe- a log-linear regression analysis. *Ardea*, *90*(1), 155-166.

Fijn, R. C., Krijgsveld, K. L., Poot, M. J., & Dirksen, S. (2015). Bird movements at rotor heights measured continuously with vertical radar at a Dutch offshore wind farm. *Ibis*, *157*(3), 558-566.

Gabry, J., Mahr, T. (2024). bayesplot: Plotting for Bayesian Models. R package version 1.11.1, https://mc-stan.org/bayesplot/.

Galtbalt, B., Lilleyman, A., Coleman, J. T., Cheng, C., Ma, Z., Rogers, D. I., ... & Klaassen, M. (2021). Far eastern curlew and whimbrel prefer flying low-wind support and good visibility appear only secondary factors in determining migratory flight altitude. *Movement ecology*, *9*, 1-12.

Gordo, O. (2007). Why are bird migration dates shifting? A review of weather and climate effects on avian migratory phenology. *Climate research*, *35*(1-2), 37-58.

Grolemund, G., Wickham, H. (2011). "Dates and Times Made Easy with lubridate." Journal of Statistical Software, 40(3), 1–25. https://www.jstatsoft.org/v40/i03/.

Gulson-Castillo, E. R., Van Doren, B. M., Bui, M. X., Horton, K. G., Li, J., Moldwin, M. B., ... & Winger, B. M. (2023). Space weather disrupts nocturnal bird migration. *Proceedings of the National Academy of Sciences*, *120*(42), e2306317120.

Haest, B., Hüppop, O., & Bairlein, F. (2018). The influence of weather on avian spring migration phenology: What, where and when?. *Global Change Biology*, *24*(12), 5769-5788.

Haest, B., Hüppop, O., van de Pol, M., & Bairlein, F. (2019). Autumn bird migration phenology: A potpourri of wind, precipitation and temperature effects. *Global Change Biology*, *25*(12), 4064-4080.

Hahn, S., Bauer, S., & Liechti, F. (2009). The natural link between Europe and Africa–2.1 billion birds on migration. *Oikos*, *118*(4), 624-626.

Horton, K. G., Van Doren, B. M., Stepanian, P. M., Farnsworth, A., & Kelly, J. F. (2016a). Where in the air? Aerial habitat use of nocturnally migrating birds. *Biology Letters*, *12*(11), 20160591.

Horton, K. G., Van Doren, B. M., Stepanian, P. M., Hochachka, W. M., Farnsworth, A., &

Kelly, J. F. (2016b). Nocturnally migrating songbirds drift when they can and compensate when they must. *Scientific reports*, *6*(1), 21249.

Hüppop, O., Dierschke, J., Exo, K. M., Fredrich, E., & Hill, R. (2006). Bird migration studies and potential collision risk with offshore wind turbines. *Ibis*, *148*, 90-109.

Hüppop, O., Hüppop, K., Dierschke, J., & Hill, R. (2016). Bird collisions at an offshore platform in the North Sea. *Bird Study, 63*(1), 73-82.

Kappeler, P. M. (2022). Orientation in time and space. In *Animal Behaviour: An Evolutionary Perspective* (pp. 69-91). Cham: Springer International Publishing.

Kelly, J. F., Horton, K. G., Stepanian, P. M., De Beurs, K. M., Fagin, T., Bridge, E. S., & Chilson, P. B. (2016). Novel measures of continental-scale avian migration phenology related to proximate environmental cues. Ecosphere, 7(9), e01434.

Kemp, M. U., Shamoun-Baranes, J., Dokter, A. M., van Loon, E., & Bouten, W. (2013). The influence of weather on the flight altitude of nocturnal migrants in mid-latitudes. *Ibis*, *155*(4), 734-749.

Kemp, M. U., Shamoun-Baranes, J., Van Gasteren, H., Bouten, W., & Van Loon, E. E. (2010). Can wind help explain seasonal differences in avian migration speed? *Journal of avian biology*, *41*(6), 672-677.

Kemp, M. U., Shamoun-Baranes, J., van Loon, E. E., McLaren, J. D., Dokter, A. M., & Bouten, W. (2012). Quantifying flow-assistance and implications for movement research. *Journal of theoretical biology, 308*, 56-67.

Kirby, J. S., Stattersfield, A. J., Butchart, S. H., Evans, M. I., Grimmett, R. F., Jones, V. R., ... & Newton, I. (2008). Key conservation issues for migratory land-and waterbird species on the world's major flyways. *Bird Conservation International*, *18*(S1), S49-S73.

Kokko, H. (1999). Competition for early arrival in migratory birds. *Journal of animal ecology*, *68*(5), 940-950.

Kranstauber, B., Weinzierl, R., Wikelski, M., & Safi, K. (2015). Global aerial flyways allow efficient travelling. *Ecology letters, 18*(12), 1338-1345.

Kranstauber, B., Bauer, S., & Shamoun-Baranes, J. (2023). Geographic barriers and season shape the nightly timing of avian migration. *Global Ecology and Biogeography*, *32*(11), 1928-1936.

Lack, D. (1960). The influence of weather on passerine migration. A review. *The Auk*, *77*(2), 171-209.

Liechti, F. (2006). Birds: blowin' by the wind? *Journal of Ornithology*, *147*, 202-211.

Liechti, F., & Bruderer, B. (1998). The relevance of wind for optimal migration theory. *Journal of Avian Biology*, 561-568.

Lindén, A., & Mäntyniemi, S. (2011). Using the negative binomial distribution to model overdispersion in ecological count data. *Ecology, 92*(7), 1414-1421.

Lloyd, J. D., Butryn, R., Pearman-Gillman, S., & Allison, T. D. (2023). Seasonal patterns of bird and bat collision fatalities at wind turbines. *Plos one, 18*(5), e0284778.

Makowski, D., Wiernik, B. M., Patil, I., Lüdecke, D., Ben-Shachar, M. S., & White, M. (2022). correlation: Methods for correlation analysis. https://CRAN.R-project.org/package=correlation.

Manola, I., Bradarić, M., Groenland, R., Fijn, R., Bouten, W., & Shamoun-Baranes, J. (2020).

Associations of synoptic weather conditions with nocturnal bird migration over the North Sea. *Frontiers in Ecology and Evolution*, *8*, 542438.

McLaren, J. D., Shamoun-Baranes, J., & Bouten, W. (2012). Wind selectivity and partial compensation for wind drift among nocturnally migrating passerines. *Behavioral Ecology, 23*(5), 1089-1101.

Metcalfe, J., Schmidt, K. L., Kerr, W. B., Guglielmo, C. G., & MacDougall-Shackleton, S. A. (2013). White-throated sparrows adjust behaviour in response to manipulations of barometric pressure and temperature. *Animal Behaviour*, *86*(6), 1285-1290.

Newton, I. (2008). *The migration ecology of birds* (Vol. 1). Elsevier

Newton, I. (2023). *The migration ecology of birds* (Vol. 2). Elsevier.

Nilsson, C., Dokter, A. M., Verlinden, L., Shamoun-Baranes, J., Schmid, B., Desmet, P., ... & Liechti, F. (2019). Revealing patterns of nocturnal migration using the European weather radar network. *Ecography, 42*(5), 876-886.

Nussbaumer, R., Bauer, S., Benoit, L., Mariethoz, G., Liechti, F., & Schmid, B. (2021). Quantifying year-round nocturnal bird migration with a fluid dynamics model. *Journal of the Royal Society Interface*, *18*(179), 20210194.

Nussbaumer, R., Schmid, B., Bauer, S., & Liechti, F. (2022). Favourable winds speed up bird migration in spring but not in autumn. *Ecology and evolution*, *12*(8), e9146.

O'brien, R. M. (2007). A caution regarding rules of thumb for variance inflation factors. *Quality & quantity, 41*, 673-690.

Pellegrino, A. C., Peñaflor, M. F. G. V., Nardi, C., Bezner-Kerr, W., Guglielmo, C. G., Bento, J. M. S., & McNeil, J. N. (2013). Weather forecasting by insects: modified sexual behaviour in response to atmospheric pressure changes. *PloS one*, *8*(10), e75004.

Pennycuick, C. J. (2008). *Modelling the flying bird* (Vol. 5). Elsevier.

Pedersen, T. (2024). patchwork: The Composer of Plots. R package version 1.3.0. https://CRAN.R-project.org/package=patchwork

Perold, V., Ralston-Paton, S., & Ryan, P. (2020). On a collision course? The large diversity of birds killed by wind turbines in South Africa. *Ostrich, 91*(3), 228-239.

Richardson, W. (1990). Timing of bird migration in relation to weather: updated review. *Bird migration: physiology and ecophysiology*, 78-101.

Rohli, R. V., Vega, A. J., & Henderson, K. G. (2024). The Basics of the Atmosphere. In *Atmospheric and Oceanic Circulation: An Explanation of Earth's Climate Patterns* (pp. 21-57). Cham: Springer Nature Switzerland.

Seers, B. M., & Shears, N. T. (2015). New Zealand's climate data in R—An introduction to clifro. *The University of Auckland, New Zealand. URL: http://stattech.wordpress.fos.auckland.ac.nz/2015-02-new-zealands-climate-data-in-r-an-introduction-to-clifro*.

Schekler, I., Levi, Y., & Sapir, N. (2024). Contrasting seasonal responses to wind in migrating songbirds on a globally important flyway. *Proceedings of the Royal Society B, 291*(2027), 20240875.

Schmaljohann, H., Liechti, F., & Bruderer, B. (2009). Trans-Sahara migrants select flight altitudes to minimize energy costs rather than water loss. *Behavioral ecology and sociobiology*, *63*, 1609-1619.

Schuster, E., Bulling, L., & Köppel, J. (2015). Consolidating the state of knowledge: a

synoptical review of wind energy's wildlife effects. *Environmental management*, *56*, 300-331.

Shamoun-Baranes, J., Liechti, F., & Vansteelant, W. M. (2017). Atmospheric conditions create freeways, detours and tailbacks for migrating birds. *Journal of Comparative Physiology A*, *203*, 509-529.

Shamoun-Baranes, J., van Gasteren, H., van Belle, J., Bouten, W., & Buurma, L. (2006). A comparative analysis of the influence of weather on the flight altitudes of birds. *American Meteorological Society, 87*, 47–61.

Sivula, T., Magnusson, M., Matamoros, A. A., & Vehtari, A. (2020). Uncertainty in Bayesian leave-one-out cross-validation based model comparison. *arXiv preprint arXiv:2008.10296*.

Swiss Birdradar Solution AG: FaunaScan MR2. https://swiss-birdradar.com/faunascan-mr2/ (last viewed: 01.06.2025).

Thaxter, C. B., Buchanan, G. M., Carr, J., Butchart, S. H., Newbold, T., Green, R. E., ... & Pearce-Higgins, J. W. (2017). Bird and bat species' global vulnerability to collision mortality at wind farms revealed through a trait-based assessment. *Proceedings of the Royal Society B: Biological Sciences, 284*(1862), 20170829.

Turbill, C. (2008). Winter activity of Australian tree-roosting bats: Influence of temperature and climatic patterns. *Journal of Zoology*, *276*(3), 285-290.

Van Doren, B. M., & Horton, K. G. (2018). A continental system for forecasting bird migration. *Science, 361*(6407), 1115-1118.

Vehtari, A., Gabry, J., Magnusson, M., Yao, Y., Bürkner, P. C., Paananen, T., & Gelman, A. (2015). loo: Efficient leave-one-out cross-validation and WAIC for Bayesian models. *CRAN: Contributed Packages.*

Welcker, J. & Vilela, R. 2019. Weather-dependence of nocturnal bird migration and cumulative collision risk at offshore wind farms in the German North and Baltic Seas. Technical report. BioConsult SH, Husum. 70 pp.

Werber, Y., & Sapir, N. (2025). Radar-measured passerine vertical speeds reveal a migratory switch near a major barrier. *iScience*.

Wickham, H. (2016). Toolbox. In *ggplot2: Elegant Graphics for Data Analysis* (pp. 33-74). Cham: Springer International Publishing.

Windtestfeld-Nord GmbH: Windtestfeld-Nord – Testfeld für Windkraftanlagen-Prototypen. https://www.windtestfeld-nord.de/de/ (last viewed: 19.04.2025).

Wood, S.N. (2017). Generalised Additive Models: An Introduction with R, Second Edition (2nd ed.). Chapman and Hall/CRC. https://doi.org/10.1201/9781315370279

List of figures

List of tables

Appendix

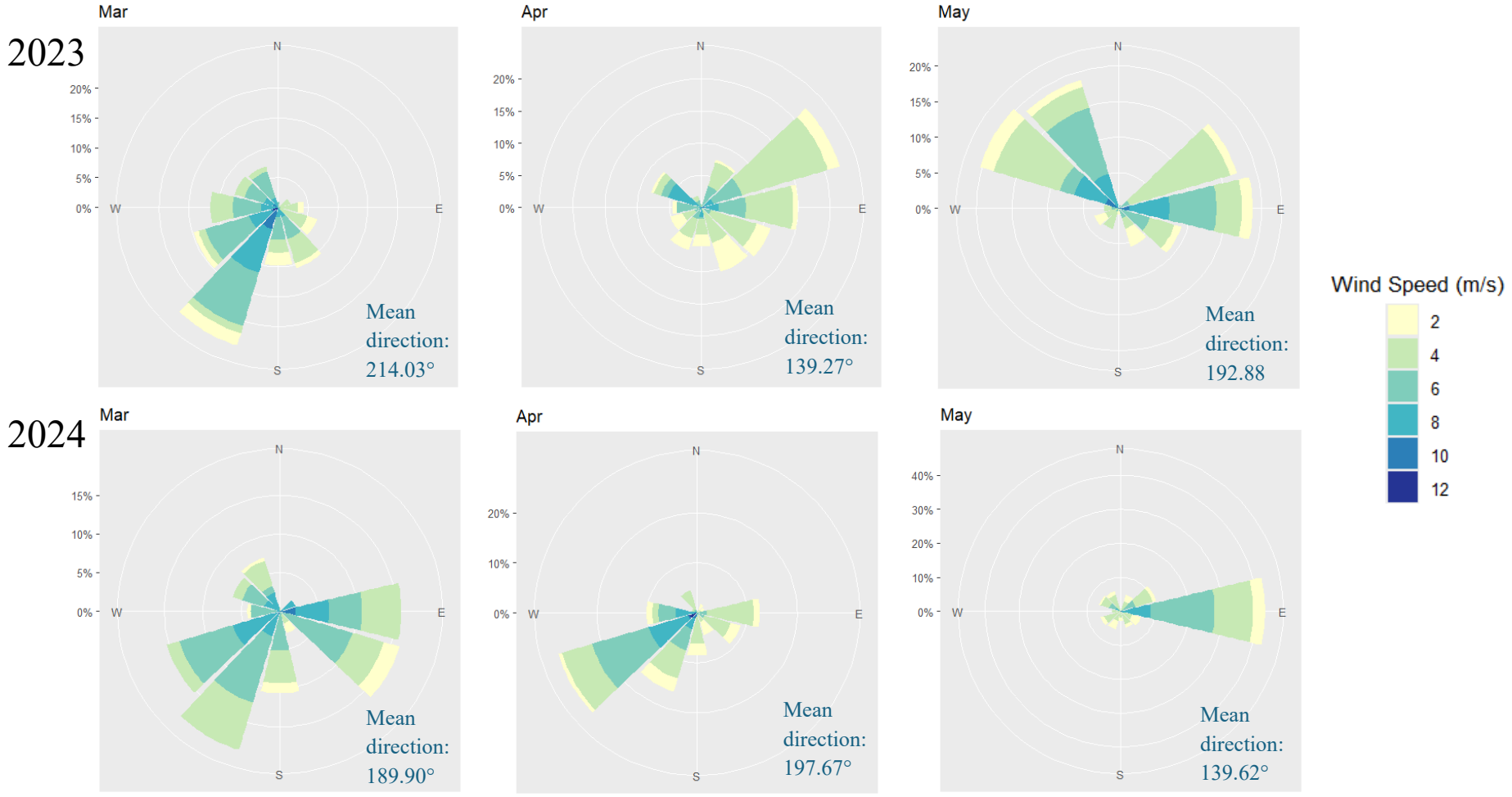

Figure S1: Windroses depicting both wind direction (i.e. direction the wind is coming from) and wind speed (yellow to blue) for spring migration periods of 2023 and 2024 in Husum, Germany. Mean wind direction of the month is noted on the respective figures. Data was downloaded from the opendata.dwd.de.

2023

Figure S2: Windroses depicting both wind direction (i.e. direction the wind is coming from) and wind speed (yellow to blue) for the autumn migration period of 2023 in Husum, Germany. Mean wind direction of the month is noted on the respective figures. Data was downloaded from the opendata.dwd.de.

2024

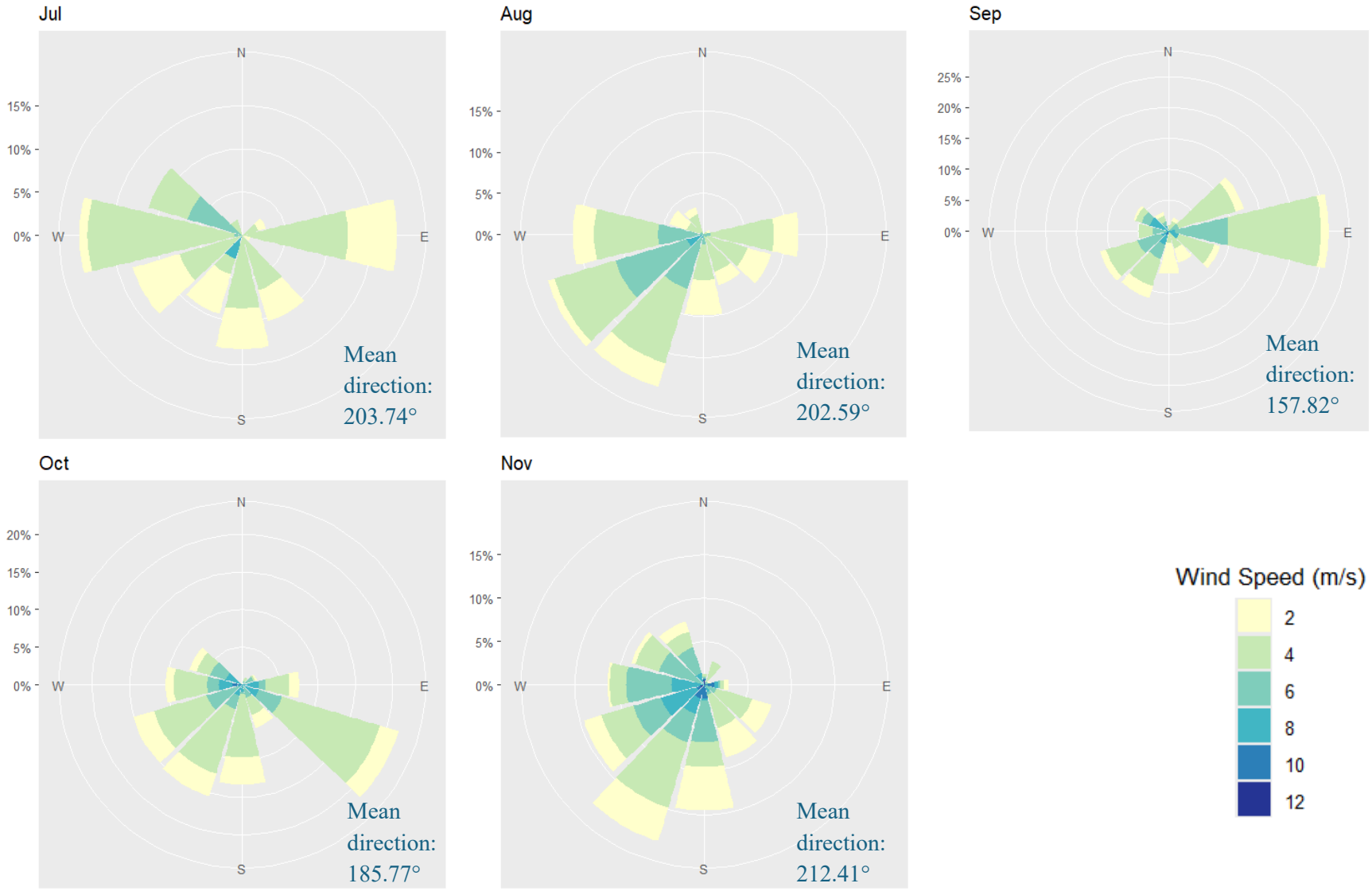

Figure S3: Windroses depicting both wind direction (i.e. direction the wind is coming from) and wind speed (yellow to blue) for the autumn migration period of 2024 in Husum, Germany. Mean wind direction of the month is noted on the respective figures. Data was downloaded from the opendata.dwd.de.

Table S1: Summarised hourly air temperature and precipitation for all four seasons studied. All data is calculated from mean values of 5 DWD stations: Hattstedt, Erfde, Leck, Schleswig and Sankt Peter-Ording (see table 2). For precipitation, the seasonal sum was calculated, as hourly rain data is less meaningful. Distinct migratory seasons are differentiated by green (spring) and grey (autumn) colouring.

		Temperature (°C)				Precipitation (mm)				
Year	Season	Min	Mean	Median	Max	Min	Mean	Median	Max	Sum
2023	Spring	-2.54	6.50	6.97	16.18	0	0.11	0	2.98	78.46
	Autumn	-11.06	10.72	11.36	20.76	0	0.21	0	5.06	290.27
2024	Spring	0.02	8.48	8.61	17.94	0	0.11	0	3.94	72.38
	Autumn	-2.36	10.83	11.14	22.52	0	0.12	0	9.30	170.92

Table S2: Summarised hourly visibility, cloudiness and barometric pressure (at ~20 m asl, see table 1 and 2) for all four seasons studied. All data was calculated from mean values of 3 DWD stations: Leck, Schleswig and Sankt Peter-Ording (see table 2). Cloudiness is depicted in a range from 0-8, 0 indicating no clouds, 8 indicating full cloud coverage. Distinct migratory seasons are differentiated by green (spring) and grey (autumn) colouring.

		Barometric pressure (hPa)				Visibility (m)				Cloudiness (0-8)			
Year	Season	Min	Mean	Median	Max	Min	Mean	Median	Max	Min	Mean	Median	Max
2023	Spring	980.1	1012.0	1013.5	1031.8	1177	29482	28782	70813	0	5.55	7.33	8
	Autumn	970.0	1005.6	1005.8	1026.7	860	28627	28130	67317	0	6.35	7.33	8
2024	Spring	982.5	1008.0	1008.1	1026.7	777	28858	28488	72437	0	6.39	7.67	8
	Autumn	981.1	1013.2	1013.5	1032.6	1577	27749	28187	67893	0	5.83	7.33	8

Table S3: Summarised hourly wind data and estimated flight direction of nocturnally migrating passerines. Wind data was calculated from mean values of 3 DWD stations: Leck, Schleswig and Sankt Peter-Ording (see table 2). Estimated flight direction was derived from the radar echoes.

Year	Seasons	Estimated flight direction (°)	Wind direction (°)				Wind speed (m/s)			
			Min	Mean	Median	Max	Min	Mean	Median	Max
2023	Spring	220	13.33	180.02	176.67	350.00	0.97	4.19	3.93	11.63
	Autumn	30	16.67	194.58	206.67	353.33	0.97	4.14	3.63	14.73
2024	Spring	220	20.00	178.51	193.33	350.00	0.93	4.17	3.98	10.73
	Autumn	30	10.00	191.7	200.00	356.7	0.80	3.61	3.20	11.03

Table S4: Top 5 high MTR nights across all altitude bins (25 – 1025 m) in descending order, for all four migratory seasons. MTR sums are rounded to full numbers for a simplified overview. MTRs are summed per night, with the civil twilight defining the border of day/night.

2023				2024			
Spring		Autumn		Spring		Autumn	
Date	Sum MTR	Date	Sum MTR	Date	Sum MTR	Date	Sum MTR
21st Mar	**18171**	**7th Oct**	**54347**	**14th Mar**	**15307**	**2nd Oct**	**45682**
13th Apr	11920	31st Oct	29759	6th Apr	13020	10th Oct	32385
9th Apr	11338	15th Oct	26332	5th Apr	9116	14th Oct	25313
22nd Apr	10209	16th Oct	18137	12th Apr	7533	27th Sep	17592
24th Mar	9939	12th Oct	16908	13th Mar	7415	13th Oct	16798

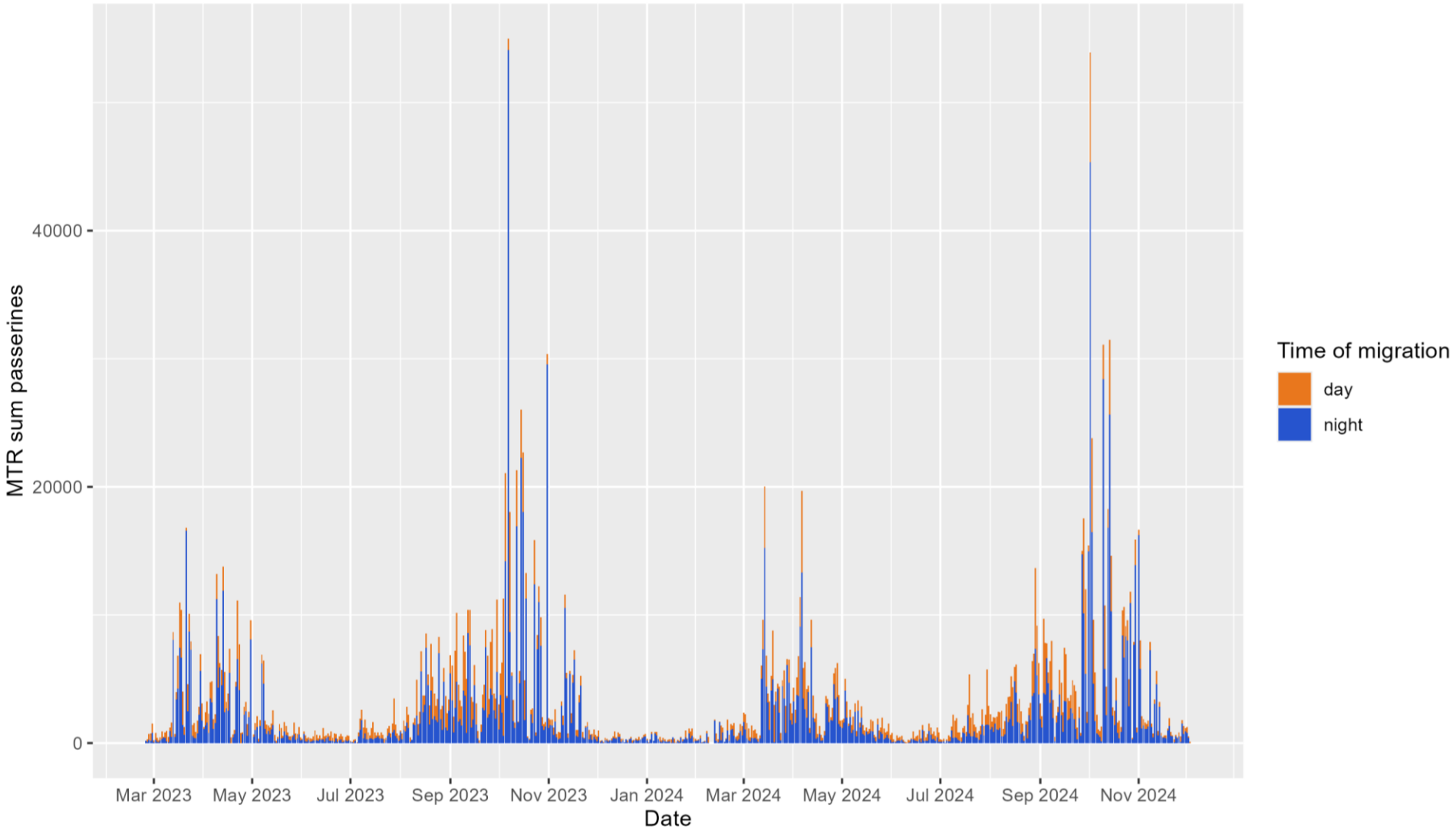

Figure S4: Stacked bar showing summed MTR (n/km/h) of passerines for the entire study period (four migratory seasons) in Husum, Germany. Bars depict summed MTR of single nights (dark blue) and days (orange).

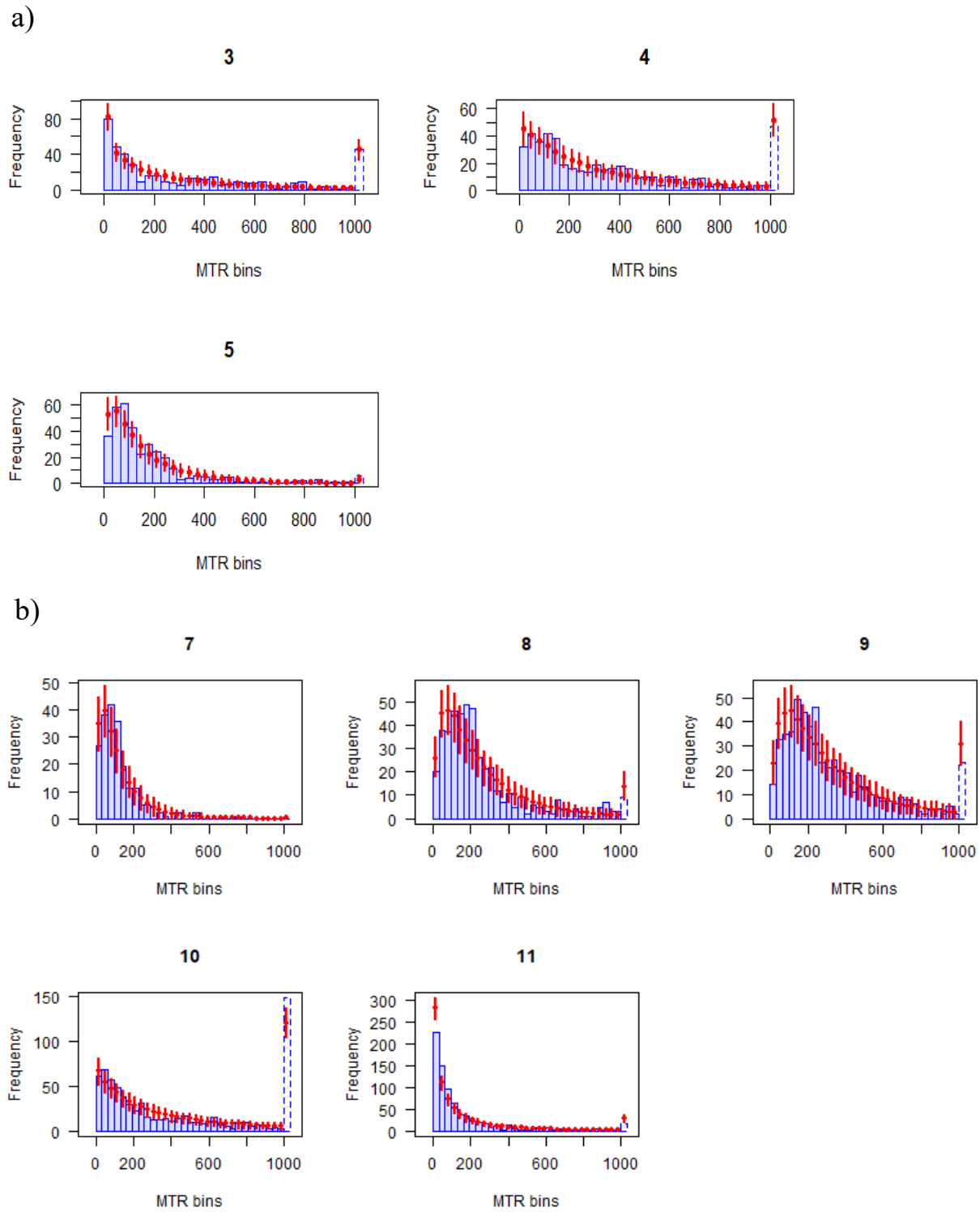

Figure S5: Posterior predictive checks for the (a) spring and (b) autumn models with MTR (n/km/h) as the response variable. The blue depicts the actual bird observations. For each bin, the red line indicates the 90% posterior interval from the model predictions, the red dot indicates the mean. In each plot, the rightmost bin (in dashed line) puts together all the counts above the previous bins.

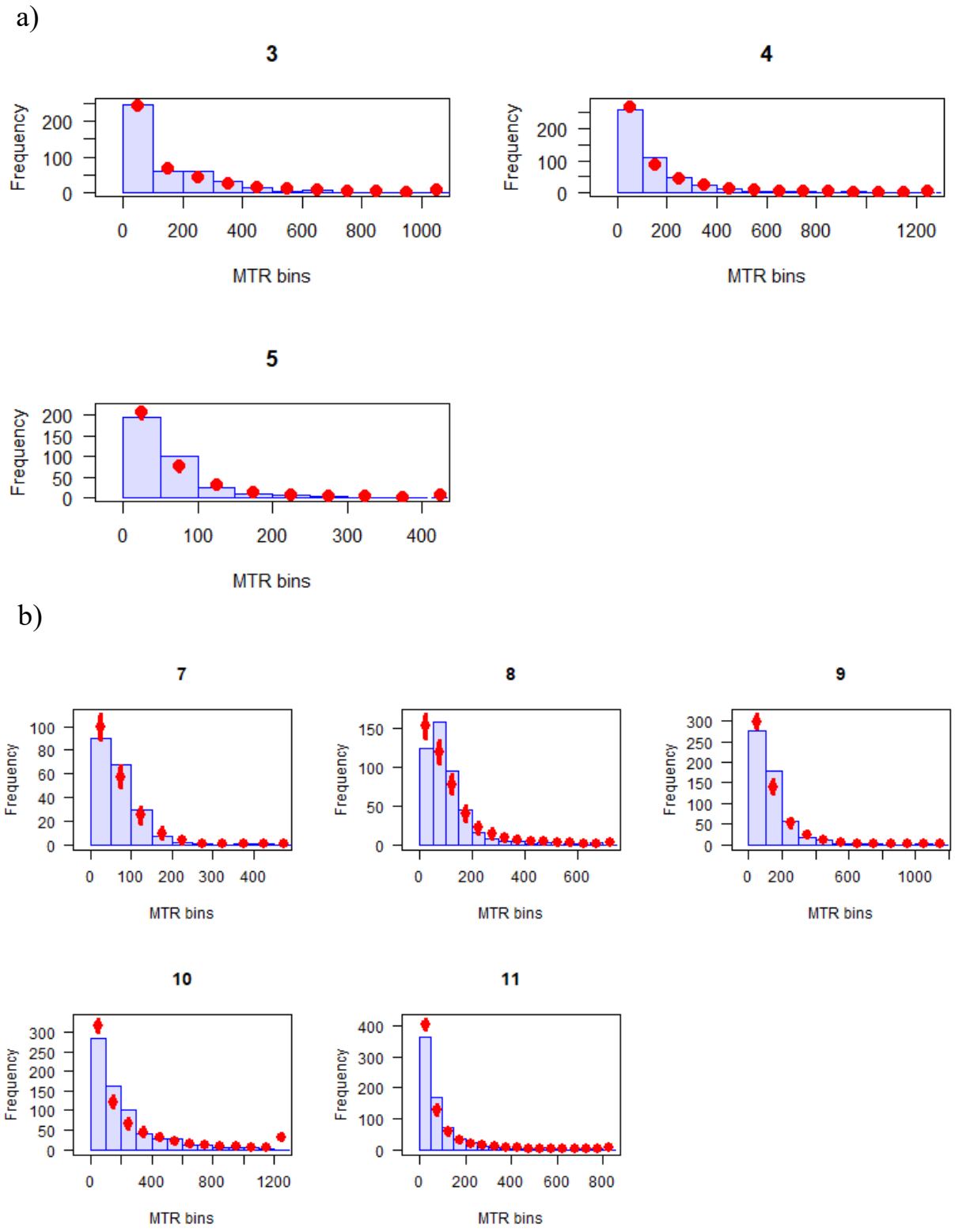

Figure S6: Posterior predictive checks for the (a) spring and (b) autumn models with the probability of flying in the risk zone as the response variable. The blue depicts the actual bird observations. For each bin, the red line indicates the 90% posterior interval from the model predictions, the red dot indicates the mean. In each plot, the rightmost bin (in dashed line) puts together all the counts above the previous bins.

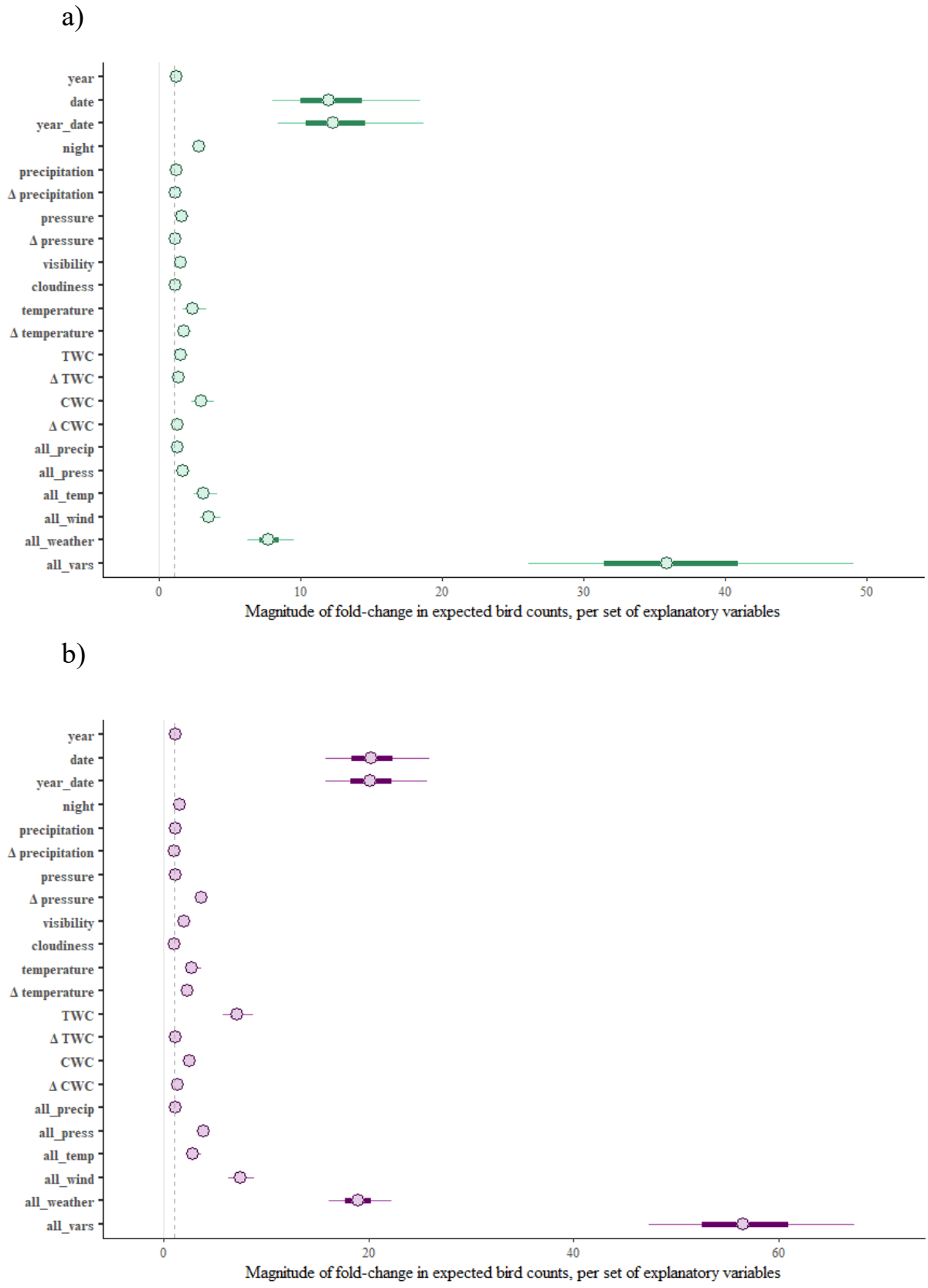

Figure S7: Magnitude of fold-change in expected bird counts, per (set of) explanatory variable for (a) spring and (b) autumn. Dashed x-intercept at 1 depicts no fold-change. Thick dark glue segments represent the 50% CIs, thin segments represent the 90% CI.

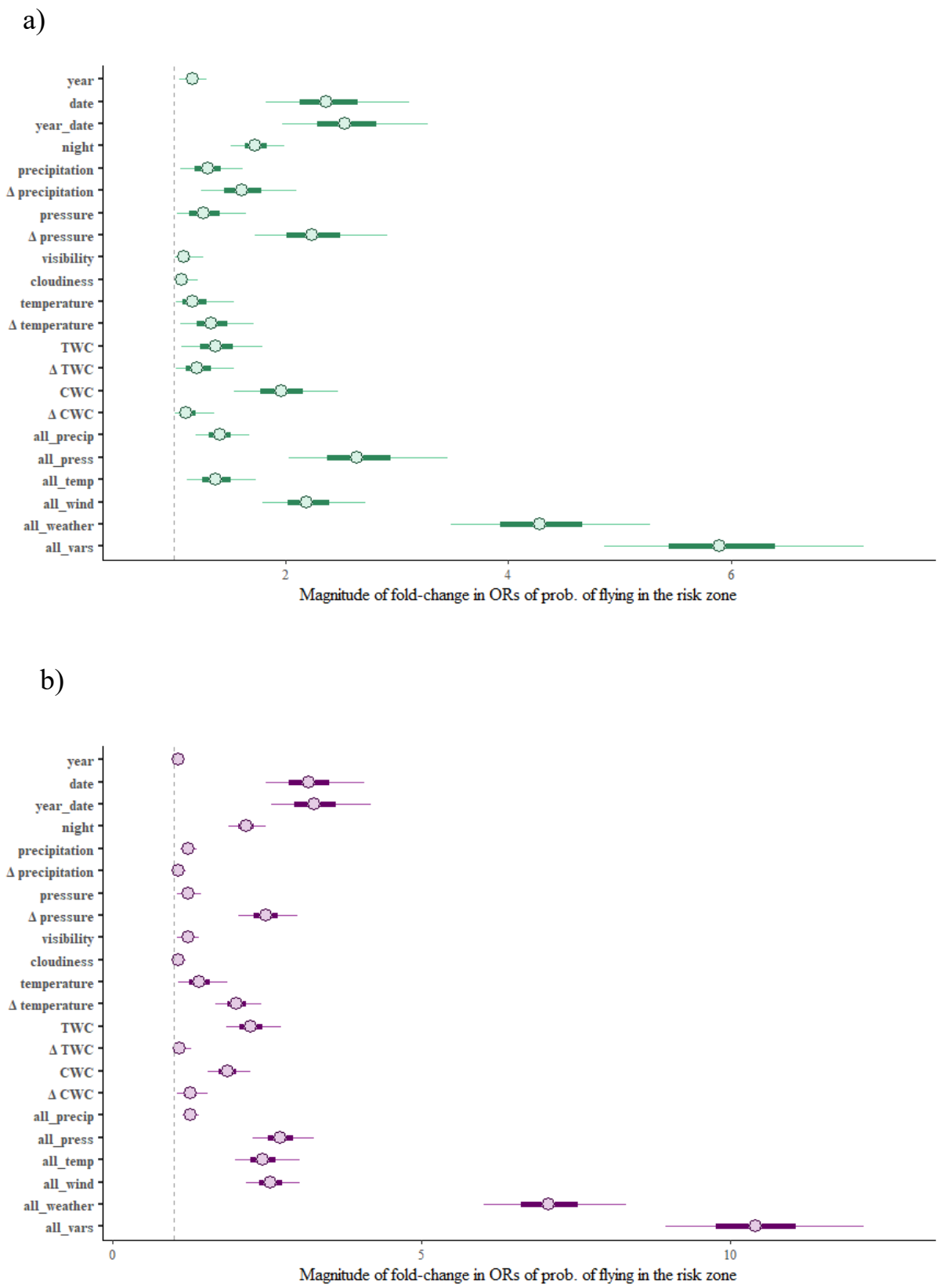

Figure S8: Magnitude of fold-change in the odd-ratios of flying in the risk zone, per (set of) explanatory variable for (a) spring and (b) autumn. Dashed x-intercept at 1 depicts no fold-change. Thick dark glue segments represent the 50% CIs, thin segments represent the 90% CI.

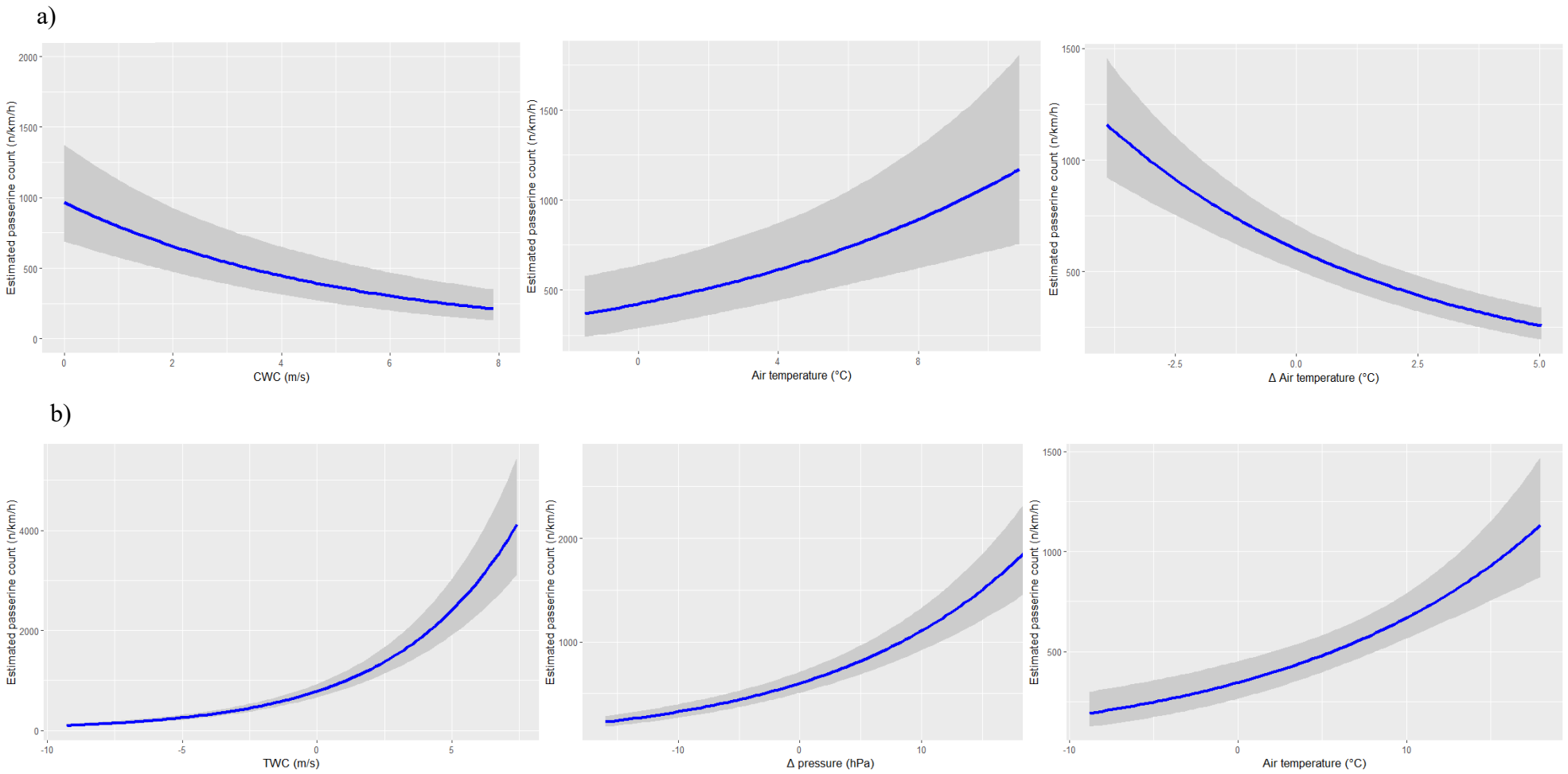

Figure S9: Plots depicting the conditional effects of the top three most influential (see Tab. 5 & 6) weather variables on the response variable (MTR, n/km/h) for (a) spring and (b) autumn models.

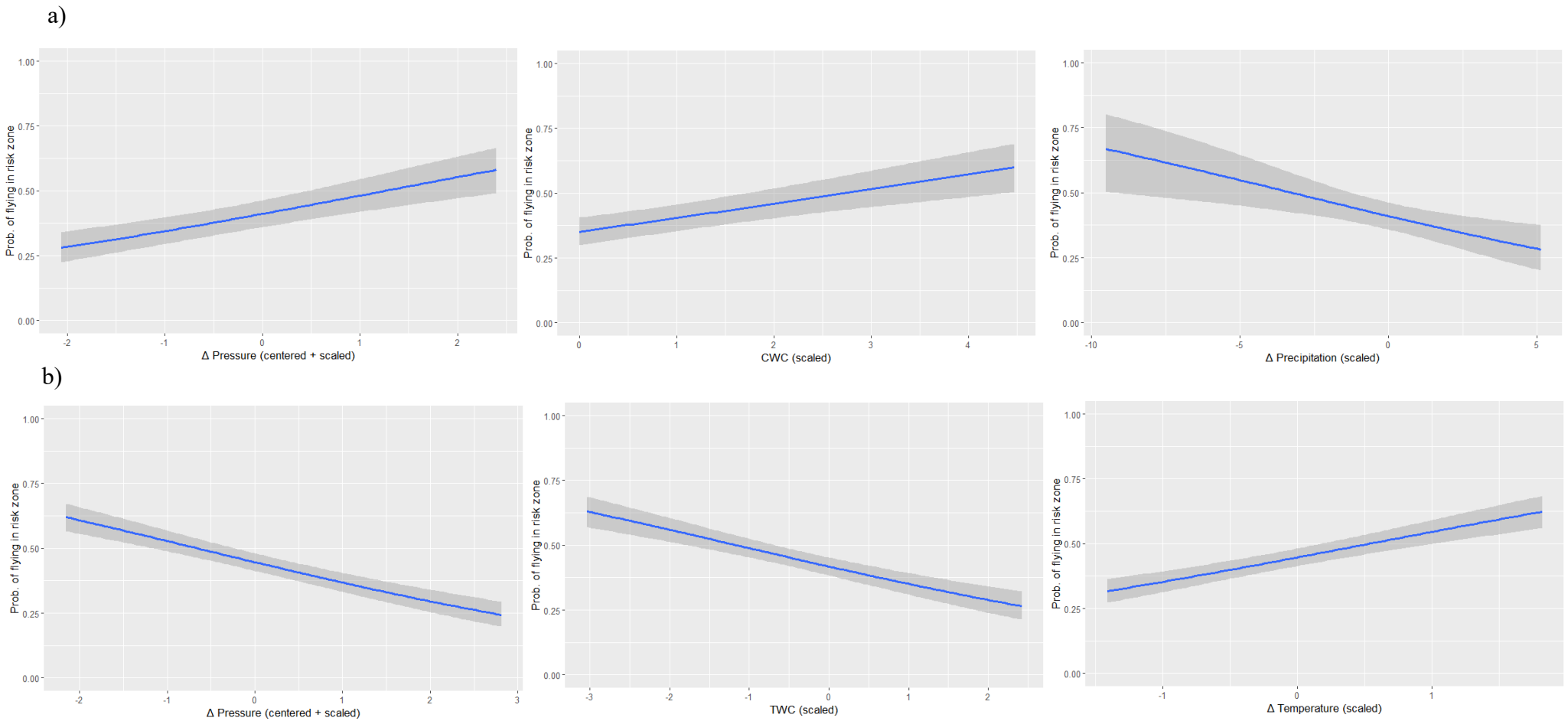

Figure S10: Plots depicting the conditional effects of the top three most influential (see Tab. 7 & 8) weather variables on the response variable (probability of flying in the risk zone) for (a) spring and (b) autumn models.

1.5 Ausfälle und Störungen

Das Radar ist blind während (starkem) Regen und kann keine Objekte aufzeichnen. Das Radar ist aufgrund von technischen Störungen bzw. Stromausfällen für kürzere Zeitabschnitte ausgefallen und zeichnete während dieser Zeitspanne keine Daten auf.

Von	Bis
18.04.2023 07:01 [UTC]	19.04.2023 06:15 [UTC]
24.04.2023 16:18 [UTC]	25.04.2023 08:57 [UTC]
01.05.2023 01:03 [UTC]	02.05.2023 08:52 [UTC]
08.02.2024 18:40 [UTC]	12.02.2024 13:50 [UTC]

Während sechs kurzen Zeitspannen (jeweils weniger als eine Stunde) wurde jeweils eine grosse Anzahl nicht biologische Objekte registriert, eine mögliche Ursache ist militärischer Chaff/Düppel. Objekte dieser Art werden teils fälschlicherweise als Vögel klassiert. Um einer Verfälschung der MTR zuvorzukommen, wurden diese Zeitspannen für die Analyse ausgeschlossen:

Von	Bis
07.03.2023 02:25 [UTC]	07.03.2023 03:00 [UTC]
13.07.2023 20:30 [UTC]	13.07.2023 22:30 [UTC]
08.11.2023 00:20 [UTC]	08.11.2023 00:40 [UTC]
25.01.2024 21:40 [UTC]	26.01.2024 00:20 [UTC]
26.01.2024 03:55 [UTC]	26.01.2024 04:10 [UTC]
09.04.2024 18:10 [UTC]	09.04.2024 19:00 [UTC]

Figure S11: Failures and disruptions of the radar recording. Provided by the manufacturer of the radar, Swiss Birdradar Solution AG Winterthur, Switzerland.